Durham E-Theses

The tribology of hard bearing surfaces for use in hip prostheses.

Susan Claire Scholes

THE TRIBOLOGY OF HARD BEARING SURFACES FOR USE
IN HIP PROSTHESES

Susan Claire Scholes B.Sc.

A thesis submitted for the degree of Doctor of Philosophy at the
University of Durham

Centre for Biomedical Engineering

School of Engineering

University of Durham

Science Laboratories

South Road

Durham

DH1 3LE

September 1999

1 2 APK 2000

Abstract

It is well documented that an important cause of osteolysis and subsequent loosening of replacement hip joints is polyethylene wear debris. To avoid this, interest has been renewed in metal-on-metal and ceramic-on-ceramic prostheses.

The intention of this thesis was to pursue a thorough investigation into the tribology of hard bearing surfaces. The friction and lubrication regimes of metal-on-metal joints (CoCrMo against itself) and ceramic-on-ceramic joints (Al_2O_3 against itself) were determined in a hip function simulator with various lubricants and compared with those for conventional metal-on-plastic joints (CoCrMo against ultra-high molecular weight polyethylene). The wear performance of different compositions of CoCrMo against itself were determined on a simple pin-on-plate reciprocating machine. A new pin-on-plate machine was designed, manufactured and validated to comply with the 1982 ASTM standard. This new machine had two axes of motion, reciprocating action and pin rotation. The wear performance of CoCrMo against itself was determined with and without the additional pin rotation.

The levels of friction factor and the corresponding lubrication modes encountered in all the material combinations tested depended on the type of lubricant used, whether it was carboxy methyl cellulose (CMC) fluids, silicone fluids, synovial fluid or bovine serum. Friction factor also depended on the concentration of bovine serum used. Protein was found to be attaching itself to the bearing surfaces and thus altering the lubrication mechanism and subsequently the friction. This was found to be most apparent in the ceramic-on-ceramic joints where the friction factor increased by at least one order of magnitude even with only a small amount of protein present. This was thought to be due to interfering of the fluid film lubrication mechanism.

High carbon CoCrMo against itself was found to be a better material in terms of wear than the low carbon CoCrMo against itself. The addition of rotational motion to the simple reciprocating pin-on-plate machine reduced the wear in metal-on-metal samples more closely to the values found clinically.

Acknowledgements

Declaration

The work contained in this thesis has not been submitted elsewhere for any other degree or qualification and, unless otherwise referenced, is all my own work.

Statement of copyright

Contents

List of Figures

List of Tables

Appendices

Notation

a	acceleration, contact area, distance to load at position 1
A	amplitude of motion
A_b	backward angle
ADC	analogue to digital converter
A_f	forward angle
A_i	angle at encoder position i
Al_2O_3	alumina
ANOVA	analysis of variance
a_t	true area of contact
A2	material A, tested on station 2
A3	material A, tested on station 3
b	distance to load at position 2
BS	bovine serum
BW	body weight
C	cup
c/c	ceramic-on-ceramic
CC	ceramic - control
CMC	carboxy methyl cellulose
CMM	coordinate measurement machine
CoCrMo	cobalt chrome molybdenum
CS	ceramic - serum
C_1, C_2	constants of integration
C1	material C, tested on station 1
C4	material C, tested on station 4
d	stroke length
D	diameter
DAC	digital to analogue converter
d_e	separation of two surfaces
E_c	elastic modulus of the acetabular cup
E_h	elastic modulus of the femoral head
ECD	equivalent circle diameter

EDTA	ethylenediaminetetra-acetic acid
EHL	elastohydrodynamic lubrication
E'	effective elastic modulus
f	frequency, friction factor ($f = T/R_h L$)
F	filtered, force, friction force
F_{adh}	frictional force due to adhesion
F_{def}	frictional force due to deformation
ffl	full fluid film lubrication
f_i	friction factor at encoder position i
H	head
h_i	inlet film thickness
$\overline{h_i}$	ratio of heights in a wedge
h_0	minimum film thickness
HS	heel strike
i	encoder position
I	second moment of area
k	ellipticity parameter, material specific wear coefficient
K	probability factor
L	distance to load on cantilever, length, load
L_b	backward load
L_f	forward load
L_i	load at encoder position i
M_A	moment at A
M_B	moment at B
MC	metal - control
micro-EHL	micro elastohydrodynamic lubrication
m/m	metal-on-metal
MNGC	multinucleated giant cell
m/p	metal-on-plastic
m_p	mass of the plate bed
m_r	mass of the pin and its holder
MS	metal - serum
N	normal load

p	material hardness
P	power
p_a	hardness of abrasive particle
PC	personal computer, plastic - control
PCA	porous coated anatomical
PMMA	polymethylmethacrylate
p_s	hardness of surface
PS	plastic - serum
PTFE	polytetraflouroethylene
$\overline{P_z}$	dimensionless load carrying capacity
P_1	load at position 1
P_2	load at position 2
r	radius
R	radius on the pin at which the point is referenced
R_a	average surface roughness
R_A	reaction force at A
R_B	reaction force at B
R_c	radius of the acetabular cup
R_h	radius of the femoral head
R_x	equivalent radius
S_a	average surface roughness
SDS-PAGE	sodium diodecyl sulphate - polyacrylamide gel electrophoresis
SEM	scanning electron microscope
SF	synovial fluid
Sim	simulator
SS	stainless steel
S_{sk}	skewness of a surface
S_q	root mean square surface roughness
S_{qc}	root mean square surface roughness of the acetabular cup
S_{qh}	root mean square surface roughness of the femoral head
S_{q1}	root mean square surface roughness of surface 1
S_{q2}	root mean square surface roughness of surface 2
t	time

T	frictional torque, torque
T_b	backward loading torque
T_f	forward loading torque
THR	total hip replacement
Ti	titanium
T_i	frictional torque at encoder position i
TKR	total knee replacement
TO	toe off
T_{rot}	period of pin rotation
T_{slid}	period of sliding motion
u	entraining velocity
u_c	sliding velocity of the acetabular cup
u_h	sliding velocity of the femoral head
u_i	entraining velocity at encoder position i
U	dimensionless speed parameter
UF	unfiltered
UHMWPE	ultra-high molecular weight polyethylene
v	deflection, velocity
v_{rot}	rotational velocity
v_{rotH}	horizontal component of rotational velocity
v_{rotV}	vertical component of rotational velocity
v_{slid}	sliding velocity
v_{slid0}	maximum sliding velocity
v_{totalH}	total horizontal component of velocity
v_{totalV}	total vertical component of velocity
v_0	maximum velocity of rotational motion
V	volumetric wear
W	dimensionless load parameter, load on cantilever
x	sliding distance
XLPE	cross linked polyethylene
XPS	X-ray photoelectron spectroscopy
x_0	maximum displacement (sliding)
$\dot{x}$	sliding velocity

y	distance across diameter
z	Sommerfeld number
z_i	Sommerfeld number at encoder position i
zirc	zirconia
α	amplitude of motion on simulator, angle of resultant velocity vector
β	amount of oscillation
β_0	maximum rotational displacement
$\dot{\beta}$	rotational velocity
$\dot{\beta}_0$	maximum rotational velocity
ϕ	diameter
γ	position of a particle with respect to 0x
η	viscosity of lubricant
λ	dimensionless surface separation parameter
μ	coefficient of friction
μ_b	coefficient of friction produced at the boundary lubricated asperity contact
μ_{dry}	coefficient of friction produced by contacting of the "dry" asperities
μ_{fl}	coefficient of friction produced by the shearing of the fluid film
v_c	Poisson's ratio of the acetabular cup
v_h	Poisson's ratio of the femoral head
θ	starting angle
σ	stress
σ_y	yield stress
σ^*	standard deviation of the peak asperity heights
τ	eccentricity torque
ω	angular velocity
ω_{rot}	rotational angular velocity
ω_{slid}	angular velocity of reciprocating motion

1. Introduction

Before the introduction of total joint arthroplasty as a solution for damaged joints, people with diseases such as osteoarthritis suffered a great deal of pain and discomfort. In many cases sufferers were confined to a wheelchair and relied on the care of others for what are normally considered as day-to-day living routines. Nowadays, with years of experience behind us, we can rely on this surgical technique to improve the lives of millions of people. However, with more and more people every year taking advantage of total hip replacement surgery, there are more hip arthroplasties performed on the younger patient. The longevity of these joints is therefore becoming increasingly important.

One of the most commonly used prosthetic hip systems is the Charnley low friction arthroplasty which incorporates a metal on ultra-high molecular weight polyethylene (UHMWPE) coupling. Currently, an artificial hip prosthesis can be expected to last on average up to fifteen years with failure due, in the majority of cases, to late aseptic loosening of the acetabular component (Wroblewski and Siney 1993, Callaghan *et al* 1998). This loosening is thought to be as a result of debris induced bone resorption (Howie *et al* 1988, Schmalzried *et al* 1992). As the femoral head articulates against the acetabular cup, wear takes place and produces, predominantly, UHMWPE wear particles. It has been suggested that it is the body's immunological response to this wear debris that causes osteolysis (Howie *et al* 1993). This bone resorption results in failure of the joint at the fixation interface.

It is now well accepted that this wear must be decreased in order to reduce bone resorption. One way of reducing this wear volume is to incorporate hard bearing surfaces such as metal-on-metal and ceramic-on-ceramic prostheses (Doorn *et al* 1996, Margevicius *et al* 1994, Palacios-Carvajal *et al* 1996). Early metal-on-metal joints (such as the McKee-Farrar prosthesis) were discarded in favour of the metal-on-UHMWPE prosthesis because of the high frictional torques produced by this large diameter bearing as well as poor stem design with subsequent failure (Müller 1995, Schmidt *et al* 1996, Amstutz and Grigoris 1996). Despite this high incidence

of failure, there have been a few reported cases of success after as much as twenty years of use (Jacobsson *et al* 1996, Schmalzried *et al* 1996). By designing these new generation metal-on-metal total hip prostheses to tighter tolerances using superior metal compositions it is thought that the long term survivorship of metal-on-metal implants can be further and more consistently improved.

2. Literature Review

2.1 Contact Area and Friction

It is well known from Hertzian contact theory that when a sphere is loaded against a plane, contact between the surfaces will occur over a circular area. This area, however, is the apparent contact area and the real area of contact will be somewhat smaller. The real area of contact is made up of several points of contact which occur at the interacting asperity tips of the two surfaces and is determined by the deformation of the material at these asperity tips.

Archard (1953) modelled the asperity contact for both a single area of contact and multiple areas of contact and derived relationships between contact area and load for both elastic and plastic contacting environments. He deduced that the most realistic model of asperity contact is where increasing the load increases both the size and number of contact areas. The single area of contact model consisted of a flat, nondeformable surface and a deformable spherical surface, from which he deduced that for elastic deformation, the true area of contact is proportional to the load to the power of 2/3. For plastic deformation, contact area is directly proportional to the load. For the multiple asperity model, where a perfectly flat nondeformable surface and a flat deformable surface containing a large number of spherical asperities come into contact, the area of contact due to elastic deformation was found to be proportional to the load to the power of 4/5 and that due to purely plastic deformation was found to be directly proportional to the load. These values are theoretical and when different values for the exponent are found experimentally it can be assumed that there is a combination of elastic and plastic asperity contacts. For metals, there is often some degree of elastic and plastic asperity contact. When the plasticity index of the metal (which depends on the Young's modulus, mean deviation of asperity heights, asperity tip radius and the plastic yield stress) exceeds some critical value the deformation will go from being elastic to plastic (Tabor

1981). For a value of plasticity index greater than about 1 most asperities will deform plastically, even under light loads (Hutchings 1992).

When sliding occurs, a frictional force is developed that is dependent on the contact of these asperities. Friction is defined as the resistance encountered by one body moving over another. Early work on friction was carried out by Leonardo da Vinci in the 1500's, Amontons in 1699 and Coulomb in 1785. The first two laws of friction, initially described by Leonardo da Vinci and rediscovered by Amontons in 1699 suggested that the friction force is proportional to the load ($F=\mu L$), where μ is termed the coefficient of friction and also that friction force is independent of the apparent area of contact. The third law, added by Coulomb in 1785 suggested that the friction force is independent of the sliding velocity. Most unlubricated metals obey the first and second laws, however, polymers do not. The third law added by Coulomb is not so well obeyed. These early workers envisaged that friction forces arose from mechanical interaction between the asperities.

Tabor (1981) discussed the three main elements involved in the frictional process as the true area of contact, the nature and strength of the interfacial bonds formed at the region of contact and the way in which the material around the contacting regions is sheared and ruptured during sliding. The Bowden and Tabor model assumes two separate sources of the frictional force, one source is due to the adhesion at the real areas of contact while the other is a deformation force needed to plough the asperities of the harder surface through the softer surface, i.e. $F=F_{adh}+F_{def}$. These will be considered separately however, in reality, these two mechanisms of friction are not mutually exclusive.

The adhesion term comes from the attractive forces at the asperity contact and is therefore material and environment specific. Metals form reasonably strong metallic bonds and for clean, like metal surfaces in contact, the bond across the interface is as strong as that within the bulk material, or perhaps stronger due to work hardening leading to a high friction force due to adhesion. Oxides and adsorbed films weaken the interfacial bond strength. The dry coefficient of friction for metal/metal contact is of the order of 0.3.

Ceramics have a lower adhesive friction component than metals due to the way in which they form bonds. The interatomic forces in ceramics are ionic and the bonding between one ceramic and another in contact is partly van der Waals forces and partly ionic. These interfacial bonds are weaker than the bonds within the bulk material and separation of the surfaces occurs at the interface with asperity contact more likely to be elastic. The dry coefficient of friction for ceramic/ceramic pairings is in the range of 0.25 to 0.8. Alumina (Al_2O_3) reacts with water (liquid or vapour) to form a hydrated surface layer which reduces the friction.

Contact between a polymer and a metal is predominantly elastic with a dry coefficient of friction between 0.1 and 0.5. The afore mentioned laws of friction are not applicable to this situation as polymers exhibit viscoelastic properties. At high loads, the asperities on the surface of the polymer deform elastically and can do so to such an extent that contact can be approximated to the single asperity contact model. Polymer chains are bonded by weak hydrogen bonds and van der Waals forces. When a polymer slides against a metal, often a transfer film of polymer is detectable on the metal counterface, subsequent interaction between the two will occur between the polymer and the transfer film of the polymer rather than the metal.

The introduction of a lubricant can substantially reduce the friction between surfaces. The following sections will discuss the fundamentals of lubrication theory.

2.2 Lubrication

Lubrication theory has been analysed for over a century. Work was done by both Tower and Petrov in the mid 1880's on the existence of lubricant films by pressure measurements within the lubricant and friction measurements respectively, both are discussed in Hamrock (1994). Using a reduced form of the Navier-Stokes equation along with the continuity equation, Reynolds (1886) produced his classical paper to define a second order differential equation for the pressure in a narrow wedge between bearing surfaces. The subsequent pressures allow very low friction as the

bearing surfaces are completely separated by the lubricant. This has come to be known as full fluid film lubrication and any friction developed is due solely to the shearing of the lubricant and is therefore largely dependent on the physical properties of the lubricant, namely the dynamic viscosity. Later work by Hardy and Doubleday (1922) helped the understanding of boundary lubrication with their findings of extremely thin films which adhere to the bearing surfaces and thus aid in the sliding contact. In boundary lubrication, the chemical composition of the lubricant and the bearing surfaces to which they may adhere are of great importance, with little or no influence from the viscosity of the lubricant.

Many advances in the understanding of lubrication have been made over the last half century. A more thorough understanding of the different mechanisms of full fluid film lubrication has been sought, along with the discovery of partial or mixed lubrication - the intermediate lubricating regime between boundary and full fluid film. As the name would suggest, mixed lubrication operates by incorporating both boundary and full fluid film regimes, therefore the load is carried by both the asperity contact and by the pressure generated by the shearing of the lubricant.

2.2.1 Full fluid film lubrication

Hydrodynamic lubrication is one form of full fluid film lubrication in which the relative motion of the bearing surfaces and the lubricant viscosity determine the fluid film and therefore the friction. The pressure developed within this system is sufficient to support a load and therefore separate the two bearing surfaces. This pressure can be achieved in three different ways; the converging wedge, squeeze film bearing and an externally pressurised bearing (hydrostatic bearing). For a positive pressure to be developed in the wedge, the lubricant film thickness must decrease with sliding direction. Squeeze films are produced when the load is transient and the pressure is generated by normal motion. The pressure is developed as the squeeze velocity is applied and the bearing surfaces approach each other. The already existing film takes a finite time to squeeze out of the system and thus the bearing is lubricated during the time of squeezing. In an externally pressurised bearing, the

pressure across the bearing due to fluid being pumped in supports the load. The load carrying capacity is independent of any possible entraining velocity and the lubricant properties.

Elastohydrodynamic lubrication (EHL) is another form of full fluid film lubrication. In this case the elastic deformation of the bearing surfaces become significant as the pressures generated in the lubricant are high compared with the elastic properties of the surfaces. The lubricant pressures cause deformations of the bearing surfaces to occur thus altering the geometry of the lubricating film by increasing the contact area and therefore becoming more conforming and subsequently modifying the pressure generated within the system. Hamrock (1994) described two types of EHL; hard and soft. Hard EHL relates to materials with high elastic moduli, such as metals and ceramics. The elastic deformation and the pressure-viscosity effects are equally important in this form of lubrication. Soft EHL relates to materials of low elastic modulus and, in such materials, the elastic deformations are large, even with low loads (Cudworth and Higginson, 1976). This form of lubrication is important in the analysis of the tribology of natural joints. Micro-elastohydrodynamic lubrication is a more localised form of EHL, in this case the asperities themselves can become more conforming.

2.2.2 Boundary lubrication

In boundary lubrication, the bearing surfaces are not separated by the lubricant and the load is carried by the asperity contacts. Thin surface films may form on the bearing surfaces through adsorption or chemical reaction and therefore the contact lubrication mechanism is dependent on the physical and chemical properties of these thin surface films. Although the friction in this case is less than for the unlubricated condition, it can still be approximately two orders of magnitude higher than for full fluid film lubrication. Due to the contacting of the asperities, the wear rate for boundary lubrication is also expected to be higher than for full fluid film lubrication.

There has been a lot of debate on the actual mechanisms of boundary lubrication. By the 1920's four main suggestions were put forward by various workers, this was discussed in a review paper by Spikes (1996a). Kingsbury (1903) suggested a boundary lubricating effect from an intensified viscosity of the fluid in the region of attraction of surface molecules. Wells and Southcombe (1920) suggested that better spreading of the lubricant was occurring on the surfaces. Deeley (1923) suggested a physiochemical union of the lubricant and the metallic surface, of more than one molecule thick and Hardy and Bircumshaw (1925) proposed the concept that two molecular layers were the lubricating film, with the plane of slip between them - this later became the well-known monolayer adsorption theory of boundary lubrication.

Spikes (1996a) measured the boundary film thickness using ultra-thin interferometry, in which films can be measured down to a thickness of 1 nm. He highlighted several mechanisms of boundary film formation. The more polar components of the lubricant selectively concentrated on the solid surfaces resulted in surface films of different viscosity to the bulk lubricant. The adsorption of monolayers onto the surfaces which continued to separate the surfaces even after motion was halted was another, while the formation of surface films several monolayers in thickness and the very rapid spreading of very thin films of lubricant on the solid surfaces was yet another. These findings therefore, have proven the significance of those suggestions made earlier in the century.

2.2.3 Mixed lubrication

Mixed lubrication occurs when the lubricant film is penetrated and some asperity contact occurs. This form of lubrication is therefore dependent on both the boundary lubricating properties of the thin surface films and the fluid film properties which in turn are dependent on the entraining velocity and viscosity of the lubricant. As the load is increased, or the entraining velocity or lubricant viscosity are decreased, a greater proportion of the load is carried by the asperity contacts as more penetration of the fluid film takes place. Therefore the transitions from full fluid film to mixed and mixed to boundary lubrication are not instantaneous but gradual.

Johnson *et al* (1972) developed a simple model of asperity contact in elastohydrodynamic lubrication to determine the transition from full fluid film lubrication to mixed lubrication and the relative effects of lubricant shearing and asperity contact on the friction in the latter regime. They combined the theory of Greenwood and Williamson (1966) of the contact of dry rough surfaces with the EHL theory of Dowson and Higginson. They found that the asperity pressure varied with the separation of the smooth surface from the mean height of the asperity peaks, d_e and that asperity pressure could be neglected at values of $d_e/\sigma^* > 3$. Where σ^* is the standard deviation of the peak asperity heights. This is the basis of the now well-known value of $\lambda > 3$ for the transition from mixed lubrication to full fluid film lubrication, where λ is defined below and is equivalent to d_e/σ^*. Further analysis of the contact time supported this value of 3.

$$\lambda = \frac{h_0}{\left(S_{q1}^2 + S_{q2}^2\right)^{0.5}} \qquad (2.1)$$

Where h_0 is the calculated minimum film thickness, S_{q1} and S_{q2} are the root mean square roughnesses of the two mating surfaces.

Spikes (1996b) reviewed the current state of understanding of mixed lubrication and specified the following assumptions, at $\lambda > 5$ the roughness had no effect on the film thickness, at $\lambda = 3$ no contact should be occurring but the roughness influences the film thickness, at $\lambda < 3$ the lubrication mode is mainly fluid film but with some asperity contact, at $\lambda = 0.5$ the lubrication is mainly mixed and at $\lambda < 0.5$ it can be assumed to be boundary lubrication. However, he pointed out that problems exist with λ values of less than 1 as it takes no account of the considerable effects of elastic and plastic deformations of the surfaces.

Tallian *et al* (1964) developed an electrical resistance technique to quantify the amount of asperity contact and showed how contact decreased with increasing λ values. Tallian (1972) looked at load sharing between the asperities and the fluid

film (like Johnson *et al* 1972) and found that at $\lambda=2$, 7% of the load was carried by asperities and at $\lambda=1$, 70% of the load was carried by asperity contact. However, he found this fraction to be lower if the asperities were allowed to deform elastically.

2.2.4 Stribeck plot

The transitions from boundary to mixed and mixed to full fluid film lubrication for bearing surfaces including human hip joints can be represented by a Stribeck plot initially described by Gümbel (Dowson 1993). Figure 2.1 shows an adaptation of the original Stribeck plot. The graph shows friction factor plotted against Sommerfeld number, z, which is a dimensionless parameter defined below:

$$z = \frac{\eta u R_h}{L} \qquad (2.2)$$

where u is the entraining velocity of the bearing surfaces (which is defined in Equation 2.3), η is the viscosity of the lubricant, R_h is the radius of the femoral head and L is the applied load.

$$u = \frac{u_h + u_c}{2} \qquad (2.3)$$

Where u_h is the sliding velocity of the femoral head and u_c is the sliding velocity of the acetabular cup.

Friction factor is used rather than the coefficient of friction originally suggested by Gümbel, because it takes into account the variation in frictional torque throughout the joint. Friction factor is defined below and can be taken to be of the same order as coefficient of friction (Unsworth 1978).

$$f = \frac{T}{R_h L} \qquad (2.4)$$

Where T is the frictional torque between the bearing surfaces, R_h is the femoral head radius and L is the applied load.

Figure 2.1 shows that a decreasing friction factor with increasing Sommerfeld number is indicative of the mixed lubrication regime whereas a rising friction factor with increasing Sommerfeld number indicates a full fluid film lubrication regime.
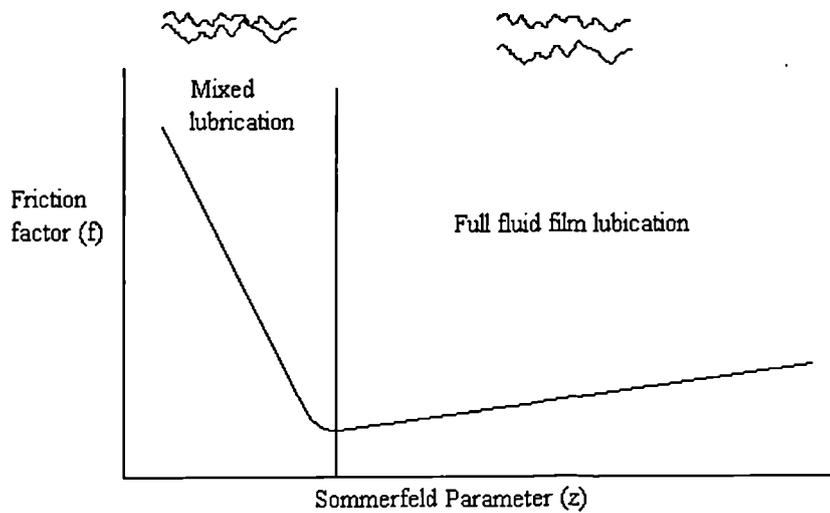
Figure 2.1: Idealised Stribeck plot

2.2.5 Theoretical film thickness

The minimum film thickness in an elliptical contact can be calculated from the theory of Hamrock and Dowson (1978) for materials of low elastic modulus:

$$\frac{h_0}{R_x} = 7.43\left(1 - 0.85e^{-0.31k}\right)U^{0.65}W^{-0.21} \tag{2.5}$$

where k is the ellipticity parameter, U is the dimensionless speed parameter and W is the dimensionless load parameter.

$$U = \frac{u\eta}{E'R_x}$$ (2.6)

$$W = \frac{L}{E'R_x^2}$$ (2.7)

Where u is the entraining velocity, η is the lubricant viscosity, E' is the effective elastic modulus, L is the applied load and R_x is the equivalent radius, defined below.

$$\frac{1}{R_x} = \frac{1}{R_h} - \frac{1}{R_c}$$ (2.8)

Where R_h is the radius of the head and R_c is the radius of the cup.

Effective elastic modulus:

$$\frac{1}{E'} = 0.5\left\{\left(\frac{1-\upsilon_h^2}{E_h}\right)+\left(\frac{1-\upsilon_c^2}{E_c}\right)\right\}$$ (2.9)

where υ_h and E_h are the Poisson's ratio and elastic modulus of the head respectively and υ_c and E_c are the Poisson's ratio and elastic modulus of the cup respectively.

For a point contact, such as in the hip, the ellipticity parameter, k, is equal to 1. Leading to the equation for minimum film thickness:

$$\frac{h_0}{R_x} = 2.798U^{0.65}W^{-0.21}$$ (2.10)

This equation is used as opposed to the film thickness equation for hard bearing surfaces because, as pointed out by Jin *et al* (1997), the deformation of the bearing surfaces is of far greater importance than the effect of pressure on viscosity.

Using the film thickness equation and the combined surface roughnesses of the bearing, the λ ratio can be determined. The λ value (from equation 2.1) and the experimental coefficient of friction can both give an indication of the mode of lubrication. However, the equation for minimum film thickness does not take into account the effect of the squeeze film that may develop under dynamic loading conditions.

2.3 Wear

Wear can be defined as the loss of material from a surface as a result of some mechanical action and is generally thought of as a harmful process though it is not necessarily so. There are four main types of wear according to the terminology suggested by Burwell and Strang (1952); adhesive wear, abrasive wear, fatigue wear and corrosion.

Adhesive wear is the most common form of wear and it occurs when asperities on opposing, sliding surfaces fuse together under high contact pressure, the junction work-hardens until the adhesion of the junction is stronger than the cohesion of the base material. This junction is then broken off within the base material during subsequent sliding, producing a wear particle, which can then subsequently become the source of third body abrasive wear. During sliding, there is a probability that the contact between the surfaces will be broken, not at the original interface, but within one of the bulk materials. This will result in a wear particle. In the case of a hard material sliding against a softer counterface, consideration of this wear particle formation would suggest that all of the breaks that did not occur at the original interface would take place within the softer material. This is due to the lower mechanical strength of the softer material compared with the harder and would result in wear particles of the softer material only. In most cases it is indeed true that more

particles are formed of the softer material, however, particles of the harder material can also be present suggesting an inconsistency within the harder material within which exist regions of low strength. When these regions of low strength coincide at a junction with local regions of high strength of the softer material, a wear particle of the harder material will be formed. Adhesive wear is the most important form of wear when considering two like metallic surfaces in sliding contact.

The theory for adhesive wear was proposed by Archard (1953) when he presented a simple model for wear particle production as one asperity slides over another making only two assumptions, one about the duration of the contact and another on the shape of the wear particle. Archard found that for the case of lump removal from contact areas formed by plastic deformation, the wear rate was proportional to the load but independent of the apparent area of contact. The wear model used extensively today is derived quite simply from Archard's model (Hutchings 1992) but was first introduced by Holm (1946) and is defined below:

$$V = \frac{KLx}{3p} \tag{2.11}$$

where V is the volumetric wear, K is the probability that a wear particle will be produced i.e. the probability factor, L is the applied load, x is the sliding distance and p is the material hardness. The factor 3 in this equation is a shape factor and is applicable in this case to the assumption of circular junctions and hemispherical adhesive wear particles. This factor, along with the hardness, is usually incorporated in the material specific wear coefficient, k, resulting in the following equation for adhesive wear (Lancaster, 1972):

$$V = kLx \tag{2.12}$$

The material specific dimensional wear coefficient, k, represents the volume of material removed by wear per unit sliding distance per unit normal load and is often referred to as the wear factor.

Rabinowicz (1965) also found that, for unlubricated contacts, the amount of adhesive wear was directly proportional to the load, the amount of wear was proportional to the sliding distance and the wear was inversely proportional to the hardness of the surface being worn away.

Abrasive wear occurs when the asperities of a rough surface, or a smooth surface containing hard particles, plough into the opposing softer surface. This wear results in a series of grooves, or scratches in the wear direction and is termed two body abrasive wear. Material expelled from these grooves may become wear particles. Also ductile materials such as metals may exhibit a harmful 'built-up-edge' due to this scratching, see Figure 2.2, which may result in a more severe asperity contact and therefore further abrasive wear. Abrasive wear of this type will not take place when the hard, sliding surface is perfectly smooth.

Built-up-edge   Abrasive asperity
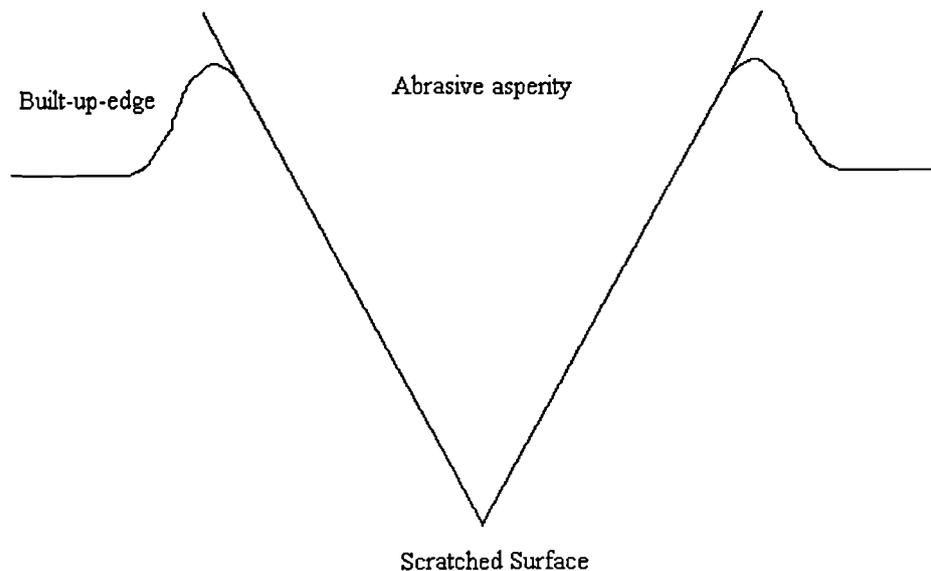
Scratched Surface

Figure 2.2: Schematic illustration of the 'built-up-edge' effect

Third body abrasive wear occurs when wear particles of a harder material are introduced into the bearing space and result in scratching of the softer surfaces, these particles may be due to work hardening of adhesive wear particles. Rabinowicz

(1965) discussed a simple model for abrasive wear in which the asperities on the hard surface were conical:

$$V = \frac{KLx}{p}$$ (2.13)

Where the constant, K depends on the fraction of displaced material actually removed and on the geometry of the abrasive particles. Equation 2.13 has the same form as Equation 2.12, the fundamental law of adhesive wear. Hutchings (1992) discussed how the hardness of the abrasive particles affected the severity of the wear. Particles of lower hardness than the surfaces caused less wear than harder particles. When the ratio of the hardness of the abrasive particle, p_a, to the hardness of the surface, p_s, was less than one, the wear rate became more sensitive to the hardness of the abrasive particle. Rabinowicz (1965) found that the wear factor due to third body abrasive wear was one order of magnitude lower than that of two body abrasive wear, this was attributed to the fact that the third body wear particles spent 90% of the time rolling and only 10% of the time sliding and abrading the surfaces. It was also found that with the additions of lubricating oils, the abrasive wear factor was doubled, this was thought to be due to the flushing action of the lubricant on the wear debris thus increasing the effectiveness of the abrading action.

Fatigue wear occurs when the material is stressed cyclically, even when operating well within the yield stress of the material. As the surfaces rub against each other, opposing asperities are repeatedly deformed inducing the formation of surface or subsurface cracks which may ultimately result in fatigue failure.

Although these wear mechanisms have been discussed separately, it is important to realise that these mechanisms do not generally operate independently and that particle detachment and debris formation is more often than not a result of two or more of the above processes operating either simultaneously or successively.

Wear by adhesion, abrasion and fatigue is only one form of classification. Lancaster (1990) described the need for a wear classification method based primarily on the

mechanisms by which particles are detached coupled with details on how specific geometrical arrangements then respond in producing debris. He described material specific wear mechanisms with two forms of wear for metals: severe and mild, then went on to describe the wear mechanisms in polymers separately as bulk deformation wear and interfacial wear.

Severe wear of metals is typically found at high loads and low sliding speeds. This type of wear obeys Archard's model for adhesive wear to a certain extent, however, other material parameters influence the wear such as crystal structure, toughness and ductility. Severe wear has two stages, small fragments of material are transferred to the counterface, the particles on the counterface experience work hardening leading to the transferred particles being stronger than the bulk material, therefore further transfer occurs at the weaker interface. This material is removed from the counterface as composite fragments containing fifty or so particles, probably when the bond between the conglomerate particle and the counterface is sufficiently weakened by the repeated cyclic loading.

In mild wear there is usually a transfer of metal fragments to a counterface, these fragments may then undergo back transfer, i.e. back to the original surface, oxidation of these fragments occurs with subsequent removal of the oxide layer by attrition. The rate of oxidation determines the rate of wear with the wear particles being mainly made up of the oxides. Any factor which affects the rate of oxidation will subsequently influence the transition from mild to severe wear, e.g. temperature, which in turn depends on sliding velocity and load.

Interfacial wear of polymers sliding against a smooth counterface arises due to adhesion between the surfaces and involves deformation only in the surface layers of the polymer. The most important process in this type of wear is adhesion, it involves the transfer of polymer to the counterface and subsequent removal as wear debris. The process is as follows: electrostatic forces (Van der Waals) attract the adhesion of the polymer to the counterface, this junction is stronger than that within the bulk polymer, therefore leading to failure within the bulk material leaving a transfer film of polymer on the counterface. These polymer chains may show orientation in the

direction of sliding which may lead to low wear. With repeated sliding the transfer layer will eventually become detached or back transfer to the polymer may occur. The introduction of a lubricant in the system may interfere with the transfer film formation and therefore effectively alter the wear.

Bulk deformation wear has been described as cohesive wear by other authors (Briscoe 1981, Hutchings 1992). There are three stages described by Lancaster (1990) for bulk deformation wear; the deformation by the penetration of indenting asperities, which is opposed by the material hardness, the relative motion between the contacting surfaces and the final detachment of a particle which may arise by a fatigue mechanism. These mechanisms are controlled by the cohesive strength or toughness of the polymer. Hutchings (1992) went on to discuss, in more detail, the effects of subsurface deformation due to the polymer sliding against the rough counterface asperities causing wear by either abrasion associated with the plastic deformation of the polymer or by fatigue crack growth in the deformed region. He suggested a level of counterface roughness for a transition from interfacial wear to cohesive wear of $R_a \sim 0.01$ - 1 μm.

Fisher (1994) discussed three processes of polymer wear, two of which he classed as surface wear processes which occurred less than 10 μm below the surface and were due to asperity interactions and one which was termed as a structural form of wear. Process 1, wear by microscopic counterface asperities, involved the sliding of a smooth counterface over a polymer. The microscopic asperities repeatedly deform the polymer surface both elastically and plastically with the generation of wear particles due to fatigue. For rougher counterfaces and larger asperities there may be more abrasive and cutting action. Process 2, macroscopic polymer asperity wear assumes, due to the scales, a perfectly smooth counterface. As the polymer is loaded, the macroscopic polymer asperities deform initially elastically, then plastically producing localised stress concentrations above the nominal contact stress and often above the yield stress of the polymer. With the addition of sliding, the inherent frictional force also increases the local stress concentrations. Under cyclic loading the polymer asperity is repeatedly deformed which may produce crack propagation and surface fatigue. Process 3, structural failure and wear, is associated with the

overall stress field which varies with time and spatially as the contact area or force vector may move over the polymer surface. On this large scale both the polymer and the counterface can be considered perfectly smooth with the stress field determined by the geometry of the contact, the load applied and the elastic moduli of the materials. In a number of geometrical configurations (non-conforming bearings) the structural stress field in the polymer can exceed the fatigue limit and yield stress of the polymer, under cyclic loading this can cause structural failure after only a few cycles.

Ceramics have a limited capacity for plastic flow and are brittle, therefore brittle fracture plays an important role in the wear of ceramics. Fracture typically takes place along the grain boundaries leading to the removal of individual grains. If a tangential force is applied, i.e. sliding, then the normal load required to initiate fracture reduces. Hutchings (1992) discussed the mild and severe wear forms of ceramics. If the orientation of the grains is correct, there may be brittle fracture coupled with predominantly plastic flow associated with the differences in crystallographic orientation of the grains. Mild wear is dominated by plastic flow or tribochemical reactions and is characterised by a low wear rate and smooth surfaces. In severe wear, higher wear rates are found and wear is dominated by brittle fracture. There is a linear dependence of wear on sliding distance and load and therefore this type of wear obeys the Archard equation.

Lubrication should reduce the incidence of asperity contact, reduce surface shear forces and therefore decrease the wear. Substances within the lubricant may, however, bind to the surfaces of the contacts (due to ionic bonding etc.) which may act to either increase or decrease the wear. The introduction of bovine serum in the pin on plate studies of polymer against metal can inhibit the transfer film formation and therefore influence the wear (McKellop 1981).

2.4 Tribology of natural hip joints

In order to understand the tribology of natural joints, it is important firstly to understand the joint loading and motion throughout each walking cycle. For this thesis it is necessary only to consider those within the hip joint. Paul (1966-67) combined records of movements of subjects marked at specific points taken with cine cameras with force plate measurements to determine the forces and relative motions of the thigh with the pelvis. He found that during a normal walking cycle, there were generally two load peaks during the transfer of support from one foot to the other, i.e. at heel strike and toe off. Corresponding to these two load peaks were periods of low relative hip joint velocities. From all his data he found the average of the peak values of load to be 3.39 times body weight. The walking cycle is now well established, it consists of four stages; heel strike, stance phase, toe off and the swing phase. At heel strike the loads on the hip joint are high and the velocity zero, during the stance phase the loads are low and the entraining velocity is high, at toe off the loads are again high and the velocities very low, however not as low as at heel strike, finally, during the swing phase of normal walking the load is low and the velocity high. These combinations of low load/high velocity and vice-versa are of extreme importance to the tribology of such joints.

It was Osborne Reynolds who, in 1886, was the first to recognise the relevance of full fluid film lubrication to the lubrication of animal joints, since then there has been much debate over the mode of lubrication of natural synovial joints.

Much of the earlier work on the lubrication of natural joints was performed on simple pendulum machines, where the joint formed the pivot of the pendulum and the mode of lubrication was determined by the decay in amplitude of oscillation of the pendulum. A linear decay indicated boundary lubrication while exponential decay indicated full fluid film lubrication. Using this type of machine, Charnley (1959) and Little *et al* (1969) both found the mode of lubrication to be boundary, however Jones (1936) found it to be hydrodynamic. Separate from the pendulum studies, Dintenfass (1963) and Tanner (1966) discussed the importance of deformation of the low elastic modulus cartilage in joint lubrication, thus

highlighting the significance of EHL. Dowson (1966-67) calculated the film thickness in the hip joint due to EHL and also squeeze film times, i.e. the time for the squeeze film to be diminished. He found these squeeze film times to be very long compared with the stance phase of the gait cycle. He therefore concluded that squeeze film action strongly resisted the tendency for the film to thin at the ends of the oscillatory motion, thus preserving the EHL film during heel strike and toe off but suggested that for prolonged periods of stance boundary lubrication would prevail. However, to determine whether the fluid film was sufficient to separate the bearing surfaces, Dowson and colleagues compared the calculated film thickness with the surface roughness of the cartilage. The value for the roughness of cartilage that was used was underestimated by 10^2 - 10^3 μm. This leads to an overestimation of the separation of the joint surfaces. Furthermore, due to the decrease in the separation once a load is applied, less time would be needed to reduce the film thickness to a level that would allow the cartilage surfaces to penetrate the fluid film and therefore contact. The theory of squeeze film assisted hydrodynamic action was also supported by the experiments performed by Fein (1966-67) in which he measured the film thickness between a convex lens and smooth PMMA flats after a period of loading.

Unsworth *et al* (1975a) shed some light on the discrepancy between the pendulum results of Charnley, Little and Jones. They theoretically worked through the calculations for pendulum motion and found the exponential component due to full fluid film lubrication to be very small and indeed, unmeasurable without sensitive equipment leading to data that could be misleading when determining lubrication modes. Not only that but such pendulum experiments using static loads result in a predisposition to boundary lubrication. They therefore developed a new machine in which they measured friction directly and determined that squeeze film, EHL and boundary lubrication all played their parts in the different stages of joint motion; with squeeze film at heel strike, EHL at stance, squeeze film and possibly boundary lubrication at toe off and full fluid film at the swing phase. These were also the findings of Dowson *et al* (1975).

A hip simulator which applied loads and motion similar to those found within physiological conditions was used in the experiments performed by O'Kelly *et al* (1978) from which they found full fluid film lubrication to be occurring due to the squeeze film mechanism. Higginson (1978) went on to calculate film thicknesses for rolling/sliding and squeeze films and found that rolling/sliding film thicknesses alone were not sufficient to separate the surfaces but under oscillatory loading the squeeze film mechanism could keep layers of healthy cartilage apart for about one second. He also suggested a relatively thick film could be entrained into the joint space during the swing phase.

A theoretical analysis by Dowson and Jin (1986) gave support to a new type of lubrication within synovial joints, micro-EHL. They found that locally generated pressures had the remarkable ability to 'smooth' the initially rough cartilage surfaces. The analysis yielded predictions of film thicknesses several times greater than previously thought with EHL referring to a λ ratio of one for the undeformed roughness increasing to nineteen for micro-EHL and therefore concluded micro-EHL to play a major role in joint lubrication. However, in this analysis the wavelength of cartilage was overestimated by 10^3. This leads to an overestimation of film thickness and therefore a slight overestimation when calculating the λ ratio. The effect of micro-EHL is, however, still apparent.

To summarise our present state of understanding of human joint lubrication: during the lightly loaded swing phase, a thick film of fluid is entrained between the cartilage surfaces (full fluid film). At heel strike the loads on the joint suddenly increase, here the thick film of fluid begins to squeeze out and the film thickness reduces (squeeze film), in normal walking these loads are only applied for about one tenth of a second and therefore the fluid film is maintained. The stance phase involves lower loads and high entraining velocities therefore promoting EHL. At toe off squeeze film comes into effect once more and during normal walking conditions will maintain the fluid film and prevent the cartilage from contacting. During periods of prolonged standing, an effective boundary lubricating film may be the only form of lubrication acting, however, once motion is resumed, a thick film of fluid will be entrained between the surfaces and the mode of lubrication will once again be full fluid film.

The human joint therefore mainly operates in the full fluid film lubricating regime with extremely low friction and wear, Unsworth *et al* (1975b).

2.5 Tribology of conventional artificial hip joints

2.5.1 Background

The healthy synovial joint is an exceptional natural bearing which provides low wear and low friction for many decades. Unfortunately diseases, such as osteoarthritis, or injury can destroy this natural bearing system. In osteoarthritis, substantial wear of the articular cartilage can result in pain and loss of function of the joint. As there is no cure for arthritis, the most effective way of alleviating this pain and regaining mobility is surgical replacement of the joint with a prosthesis.

During the earlier half of this century, many materials were used experimentally as bearing surfaces for joint replacement including ivory and glass. In 1946, acrylic femoral heads were introduced by Jean and Robert Judet for the treatment of various hip disorders. Prior to the 1960's, however, most hip replacements consisted of a metal femoral head and a metal acetabular cup, the metals being cobalt chrome molybdenum (CoCrMo) pairings, such as the McKee-Farrar prosthesis. It was the squeaking of one of the Judet acrylic prostheses which led Charnley to his belief of the important role of friction and lubrication in joint replacements, providing his basis for the low friction arthroplasty, for which he was famous. He believed that the surfaces chosen for the prosthesis should be self lubricating and therefore give low friction whether in the presence of a lubricant or not. The reasoning for this was based on another belief of Charnley's that synovial fluid was a specific lubricant for articular cartilage and would therefore not be a suitable lubricant with anything else. In 1958 he introduced the polytetrafluoroethylene (PTFE) acetabular cup and stainless steel system as this combination exhibited particularly low frictional resistance. However, this system had to be suspended in 1961 due to the excessive

wear of the PTFE component and subsequent loosening of the joint. Charnley introduced UHMWPE with a bearing diameter of 22 mm to reduce the frictional torque as a replacement for PTFE in 1962 and since then, although there have been many innovations regarding the strength and shape of the femoral stem, there has been little change to the bearing surfaces themselves.

2.5.2 Mechanical testing

Of the prosthetic hip systems available today, most incorporate a metal or ceramic femoral component with an UHMWPE acetabular cup, however there are still some surviving all metal prostheses. Since the introduction of Charnley's doomed PTFE acetabular cup there has been more emphasis on the mechanical testing of artificial joints prior to clinical trials. This testing has been mainly in the form of pendulum tests and simulator studies. Walker and Gold (1973) performed tests on new and explanted McKee-Farrar prostheses (CoCrMo/CoCrMo, 32 mm diameter) and on explanted Charnley joints (stainless steel on UHMWPE, 22 mm diameter) using a simulator with a dynamic loading cycle which measured the frictional torque at toe-off. They used pooled synovial fluid as the lubricant and found the coefficient of friction to be of the order of 0.15 and 0.05 for the all metal (both new and explanted) and metal-on-plastic joints respectively. The all metal prostheses were also tested with 0.35 percent solution of polyethylene oxide in Ringer's solution which was found to give coefficient of friction twice that lubricated with synovial fluid with much more surface damage evident. From their series of tests they concluded that "artificial joints seemed to display a boundary lubrication mechanism" although no attempt was made to quantify the exact lubrication mode by means of a Stribeck curve.

Walker (1971) used the same apparatus with pooled synovial fluid as the lubricant and determined the coefficient of friction for the all metal joint to be 0.08 and the metal-on-plastic joint to be about 0.02. He concluded the mode of lubrication for the all metal joint to be principally boundary with strongly adsorbed films from the

lubricant and for the metal-on-plastic joints to be mixed with some squeeze film action.

At this time the principal mode of failure was loosening of the acetabular component. One of the factors which was thought would influence this loosening was the frictional torque developed at the bearing surfaces. Andersson *et al* (1972) performed experiments to determine the static torque required to remove a well cemented socket from a cadaveric acetabulum and found that this torque would have to be in excess of 100 Nm for loosening to occur. However, if the cup is less well fixed, friction may play a more prominent role in prosthesis loosening and it must be pointed out that this work takes no account of the cyclic nature of the loading in the hip joint and therefore the possibility of fatigue failure.

Simon *et al* (1975) recognised the importance of friction developed at the start of motion which is usually significantly higher than dynamic friction. They tested a McKee-Farrar prosthesis and Charnley-Muller (metal-on-plastic) prosthesis in a hip joint simulator using serum, synovial fluid and veronate buffer as the lubricants. Loads between 222 N and 3336 N were applied with the simulator at rest for periods between 5 seconds and 8 hours. At the end of each preloading time, motion of the simulator was started and friction measurements were made. The friction was found to vary with preloading time for all types of prosthesis. Both synovial fluid and serum gave the same results, veronate buffer was a slightly poorer lubricant. As the premotion load was increased, the time required to get to the maximum friction value decreased, however, friction never increased by more than 90 percent of the dynamic friction and once the motion started the friction promptly dropped to the dynamic value. Therefore they concluded, like Andersson and co-workers, that a single application of frictional torque from a prosthesis would not be enough to loosen a joint. Again, however, they noted the possibility of fatigue failure at the cement-bone interface.

Tests on Charnley, Muller (CoCr/UHMWPE, 32 mm diameter) and McKee-Farrar joints were conducted on a pendulum machine with direct friction measurement by Unsworth *et al* (1975c). Static loads were compared with suddenly applied loads

and from this set of experiments, the authors were able to conclude squeeze film lubrication played an important role in the lubrication of all these joints. These results were confirmed by testing the joints dry. In the conclusions they stated "artificial joints have a coefficient of friction of between five and fifteen times that of normal human joints......even the worst of these artificial joints produced less frictional resistance than a joint severely affected by rheumatoid arthritis ($\mu = 0.4$)".

On the same pendulum machine, Unsworth (1976) performed experiments on both metal-on-metal and metal-on-plastic joints with silicone fluids of various viscosities as the lubricants, they were also tested dry. He found the coefficient of friction to be reduced when the joints were lubricated thus suggesting a dependence to some extent on fluid film lubrication. He also found a reducing coefficient of friction with increasing viscosity of lubricant suggesting a mixed lubrication regime.

O'Kelly *et al* (1977) used a hip simulator which applied dynamic loads and oscillatory motion to determine the lubrication mode of the Charnley joint when lubricated with silicone fluids. They again found that increasing the viscosity of the lubricant reduced the coefficient of friction (mixed lubrication) up to a viscosity of 0.5 Pa s where the rising coefficient of friction with increasing viscosity was indicative of full fluid film lubrication. They concluded that the Charnley joint operated in the mixed lubrication regime under physiological conditions.

The frictional characteristics of McKee-Farrar prostheses, Postel (CoCrMo/CoCrMo) prostheses and Charnley prostheses were compared in a pendulum with static and suddenly applied loads by Unsworth (1978). Degenerative synovial fluid and silicone fluids were used as the lubricants and the joints were also tested dry. Both types of all metal joint had the same diameters and clearance and therefore the same load bearing area when dry, resulting in the same dry friction. With static loading and degenerative synovial fluid as the lubricant, the all metal joints exhibited different friction factors to each other leading the author to believe that boundary lubrication could not be acting alone and therefore these joints were mixed lubricated. The all metal joints gave higher friction than the metal-on-plastic joints

0.25 cf. 0.05. Tests with static loads and suddenly applied loads on the Charnley joint clearly indicated some squeeze film action.

O'Kelly et al (1979) used a hip function simulator using silicone fluids, bovine synovial fluid, distilled water and Ringer's solution as lubricants with McKee-Farrar and Muller prostheses. They found that for physiological conditions, both joints operated in the mixed regime and when lubricated with bovine synovial fluid, a consistent reduction in coefficient of friction was obtained.

Work done by Gore et al (1981) on a dynamically loaded pendulum machine compared the frictional characteristics of McKee-Farrar, Charnley and Muller prostheses using distilled water and silicone fluids as the lubricants. The benefits on the friction factor of increasing the viscosity indicated a mixed lubrication regime and the combination of increased viscosity and suddenly applied loads demonstrated the squeeze film effect clearly.

A study of new and explanted metal-on-plastic and ceramic-on-plastic joints was carried out by Unsworth et al (1994) on a hip function simulator using carboxy methyl cellulose (CMC) solutions as the lubricants. Stribeck plots were produced and all joints were found to work in the mixed lubrication regime. There was no difference in friction factor between different head materials which was attributed to the fact that most of the friction in these combinations should result from solid shearing of the UHMWPE.

In a series of experiments by Hall et al (1994) and Hall et al (1997), new and explanted Charnley joints were found to operate in the mixed lubrication regime with an average friction factor of 0.04 ± 0.01 and 0.06 for new and explanted joints respectively.

Elfick et al (1998a) performed simulator experiments on 22 explanted and 2 unused non-cemented porous coated anatomical (PCA) joints. The explanted joints were not found to have significantly different friction factors to the new joints. Comparing these results with Hall et al (1997) they found that the PCA joints gave lower friction

than the explanted Charnley joints (0.025 cf. 0.04 at 0.01 Pa s). The higher friction in the Charnley joints was attributed to the ingression of cement into the joint.

A summary of the friction results found by the various workers is shown in Table 2.1. The previous research provides conclusive evidence that conventional hip prostheses operate in a mixed lubrication regime where some of the load is carried by the lubricant and some is carried by the contacting asperities. These contacts will inevitably result in wear particle production.

Reference	Joint description	Lubricant	Loading cycle	Machine	Friction factor
Walker and Gold (1973)	Charnley	Pooled synovial	Dynamic	Simulator	0.05
	McKee Farrar - new	Pooled synovial and Ringers			0.15
	- explanted				0.30
Walker (1971)	Metal/UHMWPE	Pooled synovial	Dynamic	Simulator	0.02
	Metal/metal				0.08
Unsworth et al (1975)	Metal/UHMWPE	Pooled synovial	Static and dynamic	Pendulum	0.05
	Metal/metal				0.2
Unsworth (1976)	Metal/UHMWPE	Pooled synovial	Dynamic	Pendulum	0.05
	Metal/metal				0.2
O'Kelly et al (1977)	Charnley	Silicone fluids	Dynamic	Simulator	0.02 - 0.08
Unsworth (1978)	Charnley	Synovial Fluid and Silicone fluids	Static and Dynamic	Pendulum	0.05
	McKee Farrar				0.25
O'Kelly et al (1979)	Charnley	Silicone fluids	Dynamic	Simulator	0.02 - 0.09
	McKee Farrar				0.1 - 0.4
Gore et al (1981)	Charnley	Water and Silicone fluids	Static and Dynamic	Pendulum	0.04
	McKee Farrar				0.1
Unsworth et al (1994)	Charnley - new	CMC fluids	Dynamic	Simulator	0.026 - 0.043
	- explanted				0.01 - 0.1
	28 mm Ø ceramic/UHMWPE				0.015 - 0.046
Hall et al (1994)	Metal/UHMWPE - new	CMC fluids	Dynamic	Simulator	0.02 - 0.05
	- explanted				0.01 - 0.15
Hall et al (1997)	Charnley - new	CMC fluids	Dynamic	Simulator	0.04
	- explanted				0.06
Elfick et al (1998a)	32 mm Ø PCA metal/UHMWPE - new	CMC fluids	Dynamic	Simulator	0.025
	- explanted				0.025
Saikko and Pfaff (1998)	Al_2O_3/Al_2O_3	Distilled water	Dynamic	Simulator	0.007

Table 2.1: Summary of friction results from various workers

2.5.3 Wear of conventional joints

The wear of conventional artificial hip joints has been studied *in vivo*, *ex vivo* and *in vitro* by many authors employing various methods. It was Charnley (1969) who first noted the tunnelling effect of the femoral head into the acetabular component in which a cylindrically shaped bore, having the same diameter as the femoral head, was worn into the socket. However, the direction of wear is never through the pole of the cup. The wear of artificial hip joints is usually characterised clinically by the penetration rate (rate of tunnelling of the femoral head into the acetabular component) and volumetric wear rate. The definition of wear rate from *in vitro* tests is more complex and less standardised. For those tests performed on a simulator which accurately matches the loading and motion patterns as experienced *in vivo* the wear can be measured in the form of penetration rates and volumetric wear rates. For studies using such apparatus as reciprocating pin-on-plate tests where the geometry of the prosthesis is not matched but contact stresses and sliding velocities can be matched as accurately as possible the wear factor, k, is used ($mm^3N^{-1}m^{-1}$). Clinical wear rates both *in vivo* and *ex vivo* have been determined by the use of radiographs. The linear wear is measured by comparing the latest radiograph with one performed shortly after implantation of the prosthesis. These radiographic analyses have been validated by comparing the wear rates determined from this method with the wear rates determined directly from volume measurements of the *ex vivo* (retrieval) studies. Errors encountered when using this technique can be in excess of 0.2 mm (Livermore *et al* 1990, Hall *et al* 1995). The main disadvantage of many of the retrieval studies is the lack of patient matched groups. When determining the effect a particular parameter has on the *in vivo* wear of a given prosthesis it is important to eliminate all other variables, as is common procedure in laboratory practice, however this seems to be neglected in many of the studies evaluating the wear of total hip replacements. Another fault in radiographic measurements is the neglected creep term which will account for some of the change in dimension of the acetabular component, however this has been shown to be a small percentage of the overall dimensional changes of most of the joints assessed in retrieval studies due to their long implant life (Elloy 1993).

The shadowgraph technique is commonly used to ascertain the wear of acetabular components. A mould is taken of the internal dimensions of the cup and then the outline of this mould is projected on to the screen of the shadowgraphic apparatus. The profile of the wear plane is then recorded. The penetration depth is determined by comparing the initial and final positions of the femoral head. The penetration angle is also recorded. The wear volume is then calculated by a theoretical formula.

Wroblewski and Siney (1992) studied the wear of the Charnley prosthesis in the young patient. The upper age limit at surgery was set arbitrarily at 51 years (range, 12-50 years) and the average follow up period was 10 years 4 months. Out of 1342 hips, they found that ten per cent were clinical failures, mostly due to loose acetabular components. The average penetration depth assessed radiologically for the whole group of patients was 0.11 mm/year with a correlation between penetration depth and incidence of socket migration.

Isaac et al (1992), using the shadowgraph technique, determined a mean penetration rate for Charnley joints of 0.21 mm/year (range, 0.005 to 0.6 mm/year) with a mean service life of 9 years with 92 per cent of failures associated with cup loosening. They found that no patients with a high penetration rate had a long service life.

Kabo et al (1993) measured the linear and volumetric wear in 60 retrieved joints both radiographically and directly by means of the shadowgraph technique. They found a good correlation between both methods of measurement of linear wear with the radiographic approach generally giving slightly lower values of wear than direct measurements. The average linear wear rate for the Charnley joint was 0.127 mm/year. The average volumetric wear rate was determined to be 25.9 mm^3/year.

Bankston et al (1993) studied the effects of femoral bearing material on the wear of 28 mm diameter joints in a patient matched series at a follow up period of 6.9 to 10.2 years. The linear wear rates were measured radiographically and found to be 0.06, 0.05 and 0.08 mm/year for stainless steel, CoCr alloy and titanium alloy respectively. The volumetric wear rates were 34.76, 33.72 and 46.14 mm^3/year respectively.

There was no significant difference between the wear rates for the different femoral bearing materials.

Cates *et al* (1993) found similar wear rates to the above for metal-backed and all polyethylene 28 mm diameter acetabular components. The linear wear rate was 0.107 and 0.078 mm/year for the metal-backed components and all polyethylene components respectively corresponding to volumetric wear rates of 66.13 and 48.22 mm^3/year, the difference being significant.

A study by Hall *et al* (1996) analysed 129 explanted Charnley sockets in which the wear was assessed using a shadowgraph. The median volume of wear produced at time of revision was 508 mm^3 with a linear wear rate of 0.2 mm/year and volumetric wear rate of 55 mm^3/year. The mean clinical wear factor was found to be 2.2×10^{-6} $mm^3 N^{-1} m^{-1}$ and is defined by Wallbridge and Dowson (1985). Analysis of further work by Hall *et al* (1998a) implicated a total wear volume to failure of about 550 mm^3, regardless of head size. Even further work has indicated that an accumulated UHMWPE wear volume threshold of about 640 mm^3 exists above which loosening of the joint will occur (Elfick *et al* 1998b).

Elfick *et al* (1998c) performed a study on the wear of 47 retrieved acetabular components from 32 mm diameter PCA joints using the shadowgraph technique. The mean age at primary surgery was 44 years and the mean implant period was 6.2 years. They found a mean penetration rate of 0.23 mm/year and the wear volume was calculated to be 551 mm^3 with a corresponding volumetric wear rate of 96 mm^3/year. The mean clinical wear factor, taking account of the expected number of cycles due to patient age and activity, was found to be 1.93×10^{-6} mm^3/Nm.

In a comparative study by Hall *et al* (1998b) the wear of 96 retrieved sockets was assessed radiographically. Two penetration depths were also recorded using the shadowgraph technique, one in the coronal plane and another in the wear plane. The wear measurements in the coronal plane corresponded to the penetration depth determined by the radiographic analysis. They found that the radiographic method gave lower wear than the shadowgraph measurement in the wear plane. They also

found a significant difference between the wear recorded in the coronal plane and that recorded in the wear plane. It was noted that a large discrepancy in the difference in wear between the two measurement techniques was attributable to the wear direction that is not recorded in the radiographic analysis.

The majority of retrieval studies have been performed on failed hip joints. Wroblewski et al (1992) radiographically determined the penetration rates of well fixed acetabular components and found the mean rate of penetration to be 0.022 mm/year, nine times less than in sockets revised for loosening. A study performed on 26 acetabular components obtained from well fixed implants at autopsy by Sychterz et al (1996) determined an average linear wear rate of 0.07 mm/year and mean volumetric wear rate of 39.8 mm^3/year.

Callaghan et al (1998) evaluated the wear of 93 Charnley total hip prostheses twenty to twenty five years after implantation. The patients were all less than fifty years old at the time of operation. Twenty nine per cent of the hips were revised, the majority of which for late aseptic loosening of the acetabular component. The average linear wear for all of the hips was 0.0928 mm/year corresponding to a volumetric wear rate of 104 mm^3/year. The higher wear rate relating to the joints implanted in the younger patient was reported on earlier (Wroblewski and Siney 1992).

Tables 2.2 and 2.3 summarise the wear results of metal-on-UHMWPE joints found by various workers using serial radiographs and the shadowgraph technique respectively.

Reference	Joint description	Method of measurement	Mean wear		
			Linear wear rate (mm/year)	Volumetric wear rate (mm³/year)	Wear factor (mm³/Nm)
Wroblewski and Siney (1992)	Charnley	Radiographic	0.11		
Wroblewski et al (1992)	Charnley - fixed cup, loose stem	Radiographic	0.022		
Kabo et al (1993)	Charnley - explanted	Radiographic	0.14	25.9	
Bankston et al (1993)	28 mm Ø	Radiographic			
	SS/UHMWPE		0.06	34.76	
	CoCr/UHMWPE		0.05	33.72	
	Ti/UHMWPE		0.08	46.14	
Cates et al (1993)	28 mm Ø	Radiographic			
	metal backed		0.107	66.13	
	non-metal backed		0.078	48.22	
Hernandez et al (1994)	28 mm Ø PCA	Radiographic			
	Cemented femoral		0.22	139	
	Uncemented femoral		0.15	92	
Callaghan et al (1998)	Charnley	Radiographic	0.0928	104	

Table 2.2: Summary of wear of metal-on-UHMWPE total hip joint replacements using serial radiographs

Reference	Joint description	Method of measurement	Mean wear		
			Linear wear rate (mm/year)	Volumetric wear rate (mm^3/year)	Wear factor (mm^3/Nm)
Isaac et al (1992)	Charnley - explanted	Shadowgraph	0.21		
Kabo et al (1993)	Charnley - explanted	Shadowgraph	0.127		
Hall et al (1996)	Charnley - explanted	Shadowgraph	0.2	55	2.2×10^{-6}
Sychterz (1996)	Various UHMWPE liners, both metal and ceramic heads - fixed at autopsy	Shadowgraph	0.07	39.8	
Elfick et al (1998c)	32 mm Ø PCA - explanted	Shadowgraph	0.23	96	1.93×10^{-6}
Hall et al (1998b)	Charnley - explanted	Shadowgraph	0.18	52	

Table 2.3: Summary of wear of metal-on-UHMWPE total hip joint replacements using the shadowgraph technique

The large range of wear rates found by the various workers in retrieved prostheses are not surprising due to the number of variables that can contribute to wear *in vivo*. These include patient-related variables such as age, weight, gender and activity level and variables related to the hip prosthesis including material combination, prosthesis design and also variables due to the implantation procedure such as cement technique. Another problem when comparing different wear rates *in vivo* is the way that this wear is normally expressed. When analysing wear over a period of time the wear rate is usually defined as mm/year. However, it is not necessarily the time *in situ* that determines the amount of wear of a particular joint but the number of cycles performed by the joint. As Schmalzried *et al* (1998) so simply put it - "wear is a function of use, not time".

In a study reported by Schmalzried and Callaghan (1999), with use of an electronic digital pedometer, the walking activity of 111 patients who had had a total joint replacement was measured. They found an average use of about 0.9 million cycles per year for each joint in the lower extremities. Moreover, there was a forty five fold difference in the range of gait cycles between the most and least active patients.

Derbyshire (1998) outlined even more problems when assessing the wear in total hip joints whether it be by radiographic measurements alone or by employing techniques such as the coordinate measurement machine (CMM) and the shadowgraph. He found that discrepancies arose due to the additional wear of the cylindrical portion of the Charnley acetabular cup and also due to the radial clearance of the joint. Neglecting the effect of the initial radial clearance when assessing the wear could result in a large overestimation of the wear volume, particularly at low wear depths. He concluded that it was imperative to measure the direction of wear (with respect to the cup face) as well as the depth of wear in order to obtain a true estimate of wear volume.

Many simulator and pin-on-plate studies have been performed to determine the wear of artificial joint materials. Table 2.4 summarises the results found by various workers.

Reference	Joint material	Machine	Testing conditions	Wear		
				Linear wear rate (mm/x10⁶ cycles)	Volumetric wear rate (mm³/x10⁶cycles)	Wear factor (mm³/Nm)
McKellop et al (1995)	32 mm Ø CoCr/UHMWPE	Simulator	Bovine serum		16	
Bigsby et al (1997)	32 mm Ø SS/UHMWPE Zirc/UHMWPE	Simulator	25% Bovine serum, CMM measurement		29.5 32.26	approx. 2×10^{-6}
Goldsmith and Dowson (1999)	22 mm Ø Zirc/UHMWPE	Simulator	25% Bovine serum, CMM measurement	0.016 (tunnelling eq.) 0.019 (CMM)	6.28	0.30×10^{-6}
McKellop (1981)	SS/UHMWPE CoCr/UHMWPE	Pin-on-plate	Bovine serum, Gravimetric		0.2 0.17	
Saikko (1993)	CoCr/UHMWPE Al₂O₃/UHMWPE Zirc/UHMWPE	Pin-on-plate	37°C, Distilled water, Gravimetric			0.1×10^{-6} 3.3×10^{-9} 2.6×10^{-9}

Table 2.4: Laboratory wear results of total hip replacement material pairings

McKellop *et al* (1995) tested 32 mm diameter CoCr against UHMWPE in a simulator which attempted to apply similar loading and motion cycles to that found *in vivo* although only through one axis of motion and load. The wear rates were found to be nearly constant throughout the period of testing at 16 mm^3/million cycles with bovine serum as the lubricant. The lower wear rates obtained from the simulator could be due to the lack of third body abrasion in this simplified situation.

Bigsby *et al* (1997) used a hip simulator with three axes of loading and motion lubricated with 25% bovine serum to obtain their values of wear rates for 32 mm diameter joints comparing stainless steel to zirconia for the femoral head material. They found the volumetric wear rates to be 29.5 and 32.26 mm^3/million cycles for zirconia and stainless steel femoral heads respectively ($k = 2 \times 10^{-6}$ mm^{3}N^{-1}m^{-1}). This difference was not found to be significant.

Using a ten station hip joint simulator with physiological loading and motion cycles, Goldsmith and Dowson (1999) tested 22 mm diameter zirconia on UHMWPE joints up to 7.27 million cycles. Twenty five per cent new born calf serum was used as the lubricant with 0.1 per cent sodium azide added. They found an initial relatively rapid penetration rate which was followed by a very low, steady, long term penetration rate after about 2 million cycles. The mean long term volumetric penetration rate was found to be 6.28 mm^3/10^6 cycles. The linear penetration rates were found to be 0.019 and 0.016 mm/10^6 cycles for direct measurement on a CMM and measurement deduced from the tunnelling expression respectively. The corresponding clinical wear factor was 0.30 x 10^{-6} mm^3/Nm.

Pin-on-plate studies have failed directly to reflect those measurements of wear determined both clinically and with the use of simulators, with most wear factors determined from this simple test being much lower than expected clinically. Wear rates from this type of test have been quoted at 0.2 mm^3/million cycles for stainless steel counterfaces and 0.17 mm^3/year for CoCr counterfaces (McKellop 1981). Saikko (1993) described widely varying wear rates from his ASTM standard pin-on-plate wear machine of 0.37 to 1.46 mg/million cycles for CoCrMo counterfaces (ave. $k = 1.0 \times 10^{-7}$ mm^{3}N^{-1}m^{-1}), 0.03 to 0.04 mg/million cycles for alumina counterfaces

(ave. $k = 3.3 \times 10^{-9}$ $mm^3N^{-1}m^{-1}$) and 0.02 to 0.04 mg/million cycles for zirconia counterfaces (ave. $k = 2.6 \times 10^{-9}$ $mm^3N^{-1}m^{-1}$).

Care must, however, be taken when comparing wear rates from different pin-on-plate tests as operating conditions vary from test to test and machine to machine, although a standard does exist for the conditions of such tests.

2.5.4 Failure of artificial hip joints

Modes of failure of artificial hip joints depend on the type of joint and over the years, as a problem has been overcome it has made way for further problems to expose themselves. Initially, in the McKee-Farrar metal-on-metal joints, the clearance between the femoral head and acetabular cup was made too small and loosening resulted from seizure of the two components. The clearance was enlarged and this seizure problem was virtually resolved (Semlitsch 1974). Component loosening was then found to be the principal mode of failure in these joints. This was thought to be due to the high fictional torques produced by this material pairing and so metal-on-metal joints were generally discarded in favour of the metal-on-UHMWPE joints.

Once operating room procedures were improved and the use of antibiotics became more widespread, failure of the metal-on-UHMWPE prostheses due to infection was virtually irradicated (Poss et al 1988). A new form of failure then became apparent as early fractures of the femoral stem in these types of prostheses became more frequent. With regard to this, Charnley increased the cross sectional area of the femoral stem in order to strengthen the stem to avoid fatigue failure and therefore abolish stem fracture. However, early loosening of the femoral stem then became more prevalent (Dall et al 1993). This combination of suboptimal design and poor cementing techniques has now been overcome and has given way to a new problem commonly found ten to fifteen years after implantation. This new mode of failure is known as 'particle disease'.

Follow-ups of the metal-on-UHMWPE prostheses highlighted the problem of component loosening which seemed to be due to localised loss of the bone at the bone-cement interface. This bone loss was attributed to the biological response to particles of PMMA and was subsequently termed 'cement disease'. In an attempt to solve this problem there developed an interest in cement-free prostheses. However, it was not long before the same problem of localised bone loss was discovered with the cementless prostheses thus invoking a name change to 'particle disease'.

2.5.5 Wear debris induced osteolysis

Most materials that are implanted have a reasonable level of biocompatibility in their bulk form, however adverse cellular and tissue reactions can occur in response to the wear particles. Willert and Semlitsch (1977) first suggested that it was the response of macrophages to wear debris which was an important cause of osteolysis and subsequent loosening. Osteolysis is defined as localised periprosthetic bone loss (Schmalzried *et al* 1992) and the process has been described well by Revell *et al* (1997). When wear debris is produced by the implant, whether it be from the articulating surfaces, the bone-cement interface, or any other source, the fibrous tissue layer surrounding the implant will try to expel these "foreign bodies". The body responds to different sized particles in a different way. This will be discussed in further detail later. If the particles are large (>5 μm) they are not phagocytosed but are surrounded by multinucleated giant cells (MNGC), if the particles are smaller (usually the case) they are engulfed by macrophages. It is not possible for the body to break down particles of UHMWPE and the macrophage and MNGC infiltrate release cytokines (chemical messages) which directly stimulate osteoclastic activity (and may inhibit osteoblast function) which leads to the resorption of bone and eventually to possible loosening of the implant. Radiologically, a lucent line can be seen around the implant caused by the fibrous tissue, which can be accompanied by pain and instability of the joint. UHMWPE particles have been found some distance from the articulating surfaces (Schmalzried *et al* 1992) in hips with and without cement. It is thought that these particles are dispersed by the joint fluid which flows according to the pressure gradients and therefore follows the path of least resistance.

Schmalzried *et al* (1992) defined the effective joint space, with the true limits being determined by how intimate the contact is between the prosthesis and the bone.

It has been found that the size of the wear particle influences the type of tissue reaction. Schmalzried *et al* (1992) using light microscopy and transmission electron microscopy looked at the distribution of polyethylene particles from both cemented and cementless hip prostheses and found particles of polyethylene within macrophages in all the hips they studied, MNGCs were rare and larger particles were found within these more often than within macrophages.

Howie *et al* (1993) performed *in vivo* studies on rats in which they examined the response to intra-articular injections of polyethylene wear particles. The particles were produced by a simple simulator which did not directly copy the joint loading or motion and were analysed by light microscopy to be mostly 15 μm and smaller Unfortunately the resolution of such microscopes does not allow particles of less than about 1 μm to be visualised. After injections of the particles into the knees of rats, sections were stained and examined by light microscopy. The knees, injected with the particles, showed areas of accumulation of macrophages and occasional MNGCs, large particles were located within the MNGCs whilst the smaller particles (<5 μm) were associated with a macrophage response. They therefore concluded that the size of the particle was an important determinant of the type of cellular response.

From a comparison of particle morphology between total hip replacements (THRs) and total knee replacements (TKRs) Schmalzried *et al* (1994) also came to the conclusion that particle size determined the cellular response. They found a consistent difference between the histology from THRs when compared with TKRs with respect to cell types and sizes of particles. The particles produced in THRs were much smaller in average size than those produced in TKRs, although this was assessed by light microscopy and therefore submicron particles were not clearly resolved. In THR pathology there was a predominance of macrophages with rare MNGCs whereas, in contrast, MNGCs were common in TKR pathology and the macrophages were both fewer and smaller in size.

Maloney *et al* (1995) looked at samples of soft tissue from around the femoral components of hip prostheses using light microscopy and scanning electron microscopy (SEM) and also found small particles to be associated with macrophages whilst the larger particles were found within MNGCs.

The results of *in vivo* and *in vitro* studies must be interpreted carefully as many have been performed with either commercially available particles or those developed in a simulator. These particles may not directly compare with those found in the body and indeed a lot of the studies have been performed using particles at least one order of magnitude larger than those found in the body. Also, the short term exposure to relatively large amounts of wear particles as used in animal studies may not necessarily reflect the response to the longer term problem of human joints.

Much work has been done in an attempt to define the sizes of the various particles produced by wear of total hip replacements. Lee *et al* (1992) used light microscopy to characterise the particles of polyethylene and both transmission electron microscopy (TEM) and light microscopy to characterise the metallic debris from failed cemented total hip replacements. They found the maximum dimension of the metallic particles to be within the range 0.6 μm to 1.8 μm whereas the polyethylene particles were 2 to 13 μm in size (8-13 μm maximum dimension). However, the resolution of light microscopy is such that particles less than 1 μm in size are not easily resolved.

The comparative study of TKRs and THRs performed by Schmalzried *et al* (1994) showed, using light microscopy, that in the twenty four failed THRs studied, a range of particle sizes from submicron to greater than 50 μm existed. The majority of the polyethylene particles were <1 μm with only a small fraction being greater than 10 μm and particles greater than 20 μm were rare.

Shanbhag *et al* (1994) examined debris from around uncemented Ti alloy hip prostheses using a scanning electron microscope (SEM). The UHMWPE debris was found to be either spheroids of 0.1 to 0.2 μm in diameter, fibrils typically 0.2 to 0.3

μm wide and up to 10 μm long or cigar shaped shards 20 to 200 μm long. The particle size distribution chart showed that about 92 per cent of the UHMWPE particles were less than 1 μm, they reported a mean of 0.53 ± 0.3 μm. Titanium particles were also found with a maximum dimension of between 10 and 400 μm.

Margevicius *et al* (1994) analysed specimens from the fibrous membrane surrounding total joint prostheses using light microscopy, SEM and an electrical resistance particle size analyser which had a lower limit of detection of 0.58 μm. They found the average mode diameter to be 0.63 μm, which was close to the lower limit of detection, with little difference in particle size distributions for the metal or polyethylene particles.

A study by Doorn *et al* (1996) compared polyethylene particles to metal particles using an SEM, although it was not clear whether the metal particles were from metal-on-metal origin or metal-on-plastic. The polyethylene particles were found to have a median size of 0.6 μm (range, 0.16 to 2 μm). The metallic particles were found to be in the range 0.1 to 400 μm (most less than 3 μm) and the problem of agglomeration of the wear particles leading to an overestimation of the true particle size was highlighted.

Wear particles from failed cementless hip prostheses were characterised by Maloney *et al* (1995) using light microscopy, SEM and an automated particle analyser similar to the one used by Margevicius *et al* (1994). Polarised light microscopy showed particles of polyethylene to be between 5 and 200 μm. Smaller particles were present that could not be characterised accurately by light microscopy, using the SEM these polyethylene particles were found to have a mean size of 0.5 ± 0.3 μm. More than 90 per cent of the polyethylene particles were less than 1 μm in size. Metallic particles were also characterised in the SEM and were found to have a mean size of 0.7 ± 0.3 μm. The particle analyser gave similar results to the SEM work even though the limit of detection in the former was 0.4 μm.

Kobayashi *et al* (1997) defined the particle size by the equivalent circle diameter (ECD); the diameter of the circle which has the same area as the measured feature. In total hip replacements, the most frequent polyethylene particle size was 0.4 μm and the majority of the particles were less than 1 μm.

Revell *et al* (1997) referred to some of his previous work in which he found the median ECD of retrieved polyethylene particles to be 0.82 μm and of metallic particles to be 0.47 μm.

It is clear from the above review of work that particles (both polyethylene and metallic) of less than 1 μm are commonly found in periprosthetic tissue and are therefore not visible by light microscopy. In addition, sectioning tissues in preparation for light microscopy may potentially alter the size and morphology of the wear particles. Any attempts at characterising wear particles that use light microscopy may lead to a gross overestimation of the mean particle size. It is therefore necessary to employ higher resolution methods such as examination by SEM. It is the maximum dimension of the wear particle that is the deciding factor on what type of tissue response will prevail and therefore a three dimensional method of characterisation would be preferable over the two dimensional SEM technique. Unfortunately, published work using such methods is relatively scarce, particularly for metallic particles and it must therefore be assumed that the majority of both metallic and polyethylene particles are less than 1 μm in size and will therefore stimulate a macrophage response within the body.

There is some controversy over whether, in fact, this osteolysis is indeed due to particulate debris or whether it is due to the movement of the prosthesis i.e. the opposing views of biological and mechanical loosening. The biological theory has been described in the previous pages; the tissue reactions to the wear particles resulting in osteolysis and subsequent loosening. The mechanical loosening theory suggests that mechanical factors, such as osteolysis caused by fluid pressure (Aspenberg and van der Vis, 1998) cause the joint to become loosened and then subsequent particle induced osteolysis will occur, the particles being the effect of the

loosening not the cause. There is substantial circumstantial evidence in support of the biological theory of loosening. Indeed, macrophages containing particulate debris have been found in association with osteolysis in well fixed, stable components (Howie *et al* 1993). Harris (1994) highlighted work by Charnley in conjunction with his metal-on-PTFE hip joint in which he discovered the 95 per cent failure rate to be due to particle induced osteolysis. This quick onset of osteolysis in the high wearing PTFE acetabular cups is surely in support of the biological theory of loosening. The now longer term particle induced osteolysis could be due to the lower wear of UHMWPE as compared with PTFE.

Aspenberg and Herbertsson (1996) performed several experiments to try to clarify the roles of particles and movement in bone resorption. They screwed titanium plates into the tibia of rats and allowed bone growth directly up to the titanium plate surface. They then determined the effects of particles of average size 4.7 ± 2.1 μm applied to the stable bone-metal interface, movement of the plate alone, movement and particles and particles in a stable fibrous interface. Histological examination showed no signs of bone resorption with the stable plate and application of particles. At six weeks of movement of the plate alone, only small areas of bone-plate contact were seen and an entire fibrous tissue membrane was formed around the plate. The effect of movement and particles was similar to that for movement alone but there was no obvious inflammatory reaction. The effect of particles in a stable fibrous interface was as follows: in the particle-free control specimens, most of the implants regained bone-to-metal contact, but this was not the case for those containing particles, although there was no obvious inflammatory reaction. Under all the conditions they tested, the response to the particles was more benign than that to the movement. The only situation that demonstrated the effects of the particles was in the fibrous tissue interface where the particles prevented the bone-to-metal ingrowth. They therefore concluded that the movement causes the formation of the fibrous tissue membrane and the particles may then prevent direct contact between the bone and implant. However, the lack of inflammatory response to the wear particles may be due to the short exposure time of the particles to the rats, also the size of particles used were larger than that previously found in the periprosthetic tissue and although particles of 5μm in size have been shown to induce a macrophage response (Howie

et al 1993), the speed and degree of this response may not be the same as the speed and degree of the response to the smaller particles (Green *et al* 1997). Also the crude method of application of polyethylene particles may not have allowed a dosage sufficient to cause macrophage response. Animal experiments should be interpreted with caution as the biological response of a rat may not be the same as that for humans with respect to the speed and degree of tissue response.

It has been reported that initial movement will hasten the onset of osteolysis, it will also increase the effective joint space as the prevention of migration of particles is dependent on the intactness of the cement-bone interface. This migration of particles will subsequently cause more particle induced osteolysis at sites distant to the articulating surfaces. It may therefore be concluded that both motion of the joint and the biological reaction to the particulate debris are important in the loosening of artificial hip joints. Further investigations must be undertaken to assess alternatives to the conventional prosthetic hip system in order to overcome these problems.

2.6 Hard bearing surfaces as an alternative

It has been suggested that osteolysis can be inhibited or even prevented by the action of certain drugs (Shanbhag *et al* 1997), however, there is not much literature on this subject and a daily prescription of drugs is not considered to be convenient or desirable by both doctors and patients alike. A realistic alternative to the high wearing conventional metal-on-UHMWPE prosthesis is the introduction of low wearing, hard bearing surfaces such as metal-on-metal or ceramic-on-ceramic.

It is hoped that the introduction of hard bearing surfaces into the prosthetic system will reduce the wear and therefore reduce the number of particles the body's immunological system has to cope with, therefore delaying the onset of osteolysis and producing a joint that will last the full duration of the patient's life. Both retrieval studies and laboratory studies have been performed on all metal joints in an attempt to assess the wear rates of such joints. Wear of metal-on-metal joints or ceramic-on-ceramic joints is usually assessed with a CMM by comparing the

geometry of the worn components to the expected geometry before implantation. However, it can be difficult to obtain an accurate estimate of the amount of wear in retrieved metal-on-metal or ceramic-on-ceramic prostheses because little or no information may be available on the original surfaces and geometry of the prostheses. Table 2.5 summarises the wear results of both metal-on-metal and ceramic-on-ceramic joints both *in vivo* and *in vitro*.

A retrieval study by McKellop *et al* (1996) found no significant difference between the linear wear rates for three different types of metal-on-metal joints when measured by a CMM. The McKee-Farrar, Muller and Ring prostheses gave mean linear wear rates for the femoral heads of 3.3, 5.2 and 5.9 µm/year respectively which equated to mean volumetric wear rates of 1.2, 2.3 and 3 mm^3/year respectively, this difference was significant (p = 0.02). The main range of clearances was 127-386 µm, with one exception at 1748 µm which gave particularly high wear and was not included in the calculations of mean wear rates.

A comparative study by Jacobsson *et al* (1996) looked at the survival of McKee-Farrar prostheses and Charnley prostheses over a twenty year period and found no major differences between the two different prostheses types. A survivorship analysis at twenty years *in situ* revealed 77 per cent of the McKee-Farrar joints and 73 per cent of the Charnleys to be clinically stable. Osteolytic lesions were more extensive in the Charnley prostheses.

Schmalzried *et al* (1996) found the wear in retrieved metal-on-metal joints to be unmeasurable using the shadowgraph technique but using a CMM reported the linear wear to be 0.09 mm at 21.3 years *in situ* (4.2 µm/year). Kothari *et al* (1996) determined the total volumetric wear rate also using a CMM to be about 5 mm^3/year.

Schmidt *et al* (1996) performed retrieval studies, simulator experiments and simple pin-on-disk experiments on all metal couplings. In the retrieval analyses he found the total wear rate for McKee-Farrar prostheses to be 12 µm/year and for the Muller metal-on-metal prostheses to be 4 µm/year, with a mean implantation period of 15

years. The wear rate tended to decrease with time *in situ* which he thought may be due to an initial high wear phase. The difference in wear rates experienced by the McKee-Farrar and Muller prostheses was attributed to the differences in material composition between the two prostheses. Wear factors of 2-3 x10^{-6} mm^{3}N^{-1}m^{-1} and 12-23 x10^{-6} mm^{3}N^{-1}m^{-1} were found for high and low carbon CoCrMo respectively in the pin-on-disk experiments. A biphasic wear pattern was observed for the Metasul CoCrMo/CoCrMo prosthesis in the hip simulator with an initial wear rate of 15-20 µm/year per component which fell after the first one to two million cycles to 5-10 µm/year per component. With this, there was a simultaneous drop in frictional torque from 3-4 Nm to 1-2 Nm. With excessive clearance, the wear rate remained at the high level throughout the test. The simulator wear rates were found to be two or three times higher than that found clinically.

In a brief review paper by Semlitsch (1993), the wear rates of CoCrMo against CoCrMo, stainless steel against polyethylene, CoCrMo against polyethylene, Al$_2$O$_3$ against polyethylene and Al$_2$O$_3$ against itself were reported to be 0.003-0.01 mm/year, 0.1 - 0.3 mm/year, 0.1-0.3 mm/year, 0.05-0.15 mm/year and 0.003-0.01 mm/year respectively. He also reported on some tests performed up to two million cycles on a hip simulator with a maximum load of 1585 N, a frequency of 0.5 cycles/sec and a lubricant of Ringer's Solution with 30 per cent bovine serum. Two different diameters of all metal (CoCrMo) bearing were tested; 28 mm and 32 mm and the wear rates were found to be 8 µm/year and 9 µm/year for both the femoral component and acetabular cup together. This was compared to the wear rate found clinically of 6 µm/year for both components.

Schmidt and Farrar (1996) assessed the wear in 22, 28 and 35 mm diameter all metal bearings (wrought CoCrMo) with a range of diametral clearances of 0.03 to 0.139 mm. These were each tested at least five times in a simulator with a peak load of 2000 N, a frequency 1.1 Hz and serum as the lubricant. The wear was measured gravimetrically. They found that at two million cycles the head size did not influence the wear: average wear 0.657 ±0.472 mm^3, 0.607 ± 0.260 mm^3 and 0.864 ± 0.434 mm^3 for the 22, 28 and 32 mm diameter joints respectively. They also tested a

metal-on-polyethylene combination and found the average wear at two million cycles to be 20.82 ± 3.84 mm^3.

Nine joints were tested in a hip simulator by Chan *et al* (1996). These were five low carbon wrought CoCrMo against itself and four high carbon cast CoCrMo against itself, both of 45 mm diameter and diametral clearances ranging from 89-198 μm and 10-630 μm respectively. The simulator applied a maximum load of 2100 N at a frequency of 1.13 Hz for 3 million cycles whilst lubricated in bovine calf serum. The wear was assessed gravimetrically. They found that the all metal joints exhibited biphasic wear. Initially the wear rate was high and then after about half a million cycles the wear rate dropped to a lower steady state value which was roughly the same for all joints (with the exception of the large clearance of 630 μm which persisted at the initial high wear rate for the duration of the test). For the low carbon wrought material, the initial high wear was 0.2-6 mm^3 for half a million cycles and then the low steady state wear rate continued at 0.25 mm^3/million cycles thereafter. A higher initial wear was observed for the high carbon cast alloys of 2-8 mm^3 for the first half million cycles which then dropped to 0.6 mm^3/million cycles thereafter. The wrought material gave lower wear than the cast and a small clearance resulted in lower wear than the larger clearances, this was also found in simulator studies by McKellop *et al* (1996), Schmidt *et al* (1996) and Medley *et al* (1997).

Medley *et al* (1996) noted the work done by Walker and Gold (1971) in which two different types of contacting geometry were found greatly to influence both the wear and friction of all metal joints. The early metal-on-metal joints had a geometry that permitted an equatorial contact between the head and the cup which led to high frictional torques and loosening, it is therefore desirable to have a polar contacting geometry. Medley believed it important to study the different diameters of bearings and different clearances to work towards an optimum design. A range of clearances were tested on a simulator for up to three million cycles in bovine serum. Measuring the wear gravimetrically, he found the biphasic wear pattern also observed by Chan *et al* (1996) and Schmidt *et al* (1996) where most wear rates decreased after 0.1 to 0.5 million cycles, however this behaviour was not observed in the joint with the largest clearance - the wear rate remained high for the duration of the test. This was

also observed by Scott and Schroeder (1997) and they concluded the optimum radial clearance in terms of wear for 28 mm diameter joints in 50% bovine serum to be 20-80 μm in which the wear at 1.5 million cycles was about 5 mg. Farrar and Schmidt (1997) found that as the clearance reduced, the wear reduced, however as the diametral clearance was reduced to 0.03 mm and below, the wear began to increase. They also found the biphasic wear pattern. At two million cycles for a diametral clearance between 0.033 and 0.139 mm with bovine serum as the lubricant, the wear was found to be 0.384 - 1.068 mm^3 in total.

Such wear quantification analyses on all ceramic bearings are scarce and often rely on follow up reports of all ceramic joints of sub optimal quality, i.e. those implanted before the introduction of the standards for ceramic production introduced in the late 1970's.

Winter *et al* (1992) reported a 25 per cent failure rate of 100 prostheses implanted for 12.2 years, the failure due to material related fractures or loosening of the socket or stem or both components. However, the joints in this study were implanted between 1974 and 1978 and are likely to be manufactured from a poorer quality alumina, with perhaps sub optimal design parameters such as too large a clearance.

The clinical and tribological performance of alumina-on-alumina prostheses implanted between 1976 and 1979 was studied by Boehler *et al* (1994). They found a survivorship of 83.8% at ten to fifteen years after implantation where failure was defined as radiographic loosening of the socket. They compared the wear rates of one stable and one loose implant and found that the loose joint wore significantly more than the stable joint (68 μm/year cf. 2.6 μm/year). These joints were, however, of a lower quality than today's standards.

Dorlot *et al* (1989) explained two different types of wear that may occur in all ceramic hip joints, normal wear and gross wear associated with grain excavation and disruption of the bearing surfaces. In a study of 20 hips retrieved for aseptic loosening of the socket (ave. implantation duration 54 months) he noted gross wear on 18 hips, most with verticalisation of the sockets. The gross wear observed was

always related either to verticalisation of the socket after loosening or to an incorrect positioning at surgery. The higher than normal contact stresses at the resulting peripheral contact of the socket were sufficient to nucleate subcritical cracks which led to gross wear. As long as these high contact stresses are avoided (i.e. through excellent sphericity or optimal clearance of the components, also through correct positioning at surgery) normal wear should be observed which can be less than 0.025 μm/year long term. Gross wear in this study was always due to incorrect positioning of the cup at surgery or due to loosening. It was never related to the material alone.

Sedel *et al* (1990) reported on a follow-up study over 2 to 11 years of 73, 32 mm diameter hips that were implanted between April 1977 and December 1986. They concluded through survival analysis that there was a 97.8 per cent chance of keeping the prosthesis at eight years. They found that catastrophic wear had been completely overcome by using good quality alumina and matched paired components which were ground together during the manufacturing process. Sedel *et al* (1994) reported a survival rate on a different series of all ceramic prostheses of 89.4 per cent at 10 years and *86.2 per cent at 11 years.*

A retrieval study by Walter (1992) on a series of all ceramic hip prostheses implanted between 1975 and 1982, determined the maximum wear rate for well positioned cases with loosened cups to be about 5 μm/year with a minimum of 0.025 μm/year. For well positioned cups without loosening, the maximum wear rate was 4 μm/year with a minimum of about the same as for the loosened case. For well positioned and well designed prostheses, an average wear rate for the heads was found to be 1.8 ± 1.9 μm/year and 2.1 ± 1.6 μm/year for cups. All wear rates exceeding 6.5 μm/year were found in those cases with rim wear or malalignment - these cases were not included in the calculations of average wear rates. From visual analysis of the surfaces, boundary lubrication was assumed to occur, however no attempt was made to verify this assumption. Simulator studies were also performed on all ceramic couplings manufactured from a higher quality material. For normal conditions the wear rate varied from 0.03 μm/year to 16 μm/year. A change in position of the

socket and varying clearances and sphericity deviations were found to greatly influence the wear.

Saikko and Pfaff (1998) performed simulator studies on all ceramic joints. The test frequency was 1.1 Hz and the maximum load was 3.5 kN. The tests were done at 37°C in distilled water. They found the wear of the ceramic components to be unmeasurable gravimetrically at up to five million cycles. The average friction factor was found to be 0.007 and they therefore concluded that the alumina-on-alumina joints exhibited low wear and friction under their testing conditions.

Reference	Joint description	Test description	Method of measurement	Mean wear		Wear factor (mm³/Nm)
				Linear wear rate (μm/year or equiv.)	Volumetric wear rate (mm³/year or equiv.)	
Semlitsch (1993)	m/m	None stated	Not stated	3 - 10		
	m/m			3 - 10		
	28 mm Ø m/m	Simulator, 30% BS)	Not stated	8		
	32 mm Ø m/m			9		
Walter (1992)	c/c	*In vivo*	Sphericity dev.	3.9		
	c/c	Simulator (not stated)	Gravimetric	0.03 - 16		
McKellop *et al* (1996)	McKee Farrar	Retrieval - femoral heads only	CMM	3.3	1.2	
	Muller			5.2	2.3	
	Ring			5.9	3	
Schmalzried *et al* (1996)	McKee Farrar	Retrieved	CMM	4.2		
Kothari *et al* (1996)	McKee Farrar	Retrieved	CMM		5	
Schmidt *et al* (1996)	McKee Farrar	Retrieved	CMM	12		
	Muller	Retrieved	CMM	4		
	Metasul	Simulator (30% BS)	Not stated	5-10		
	High Carbon m/m	Pin-on-disk (as above)	Not stated			2-3 x 10⁻⁶
	Low Carbon m/m	Pin-on-disk (as above)	Not stated			12-23 x 10⁻⁶
Chan *et al* (1996)	45 mm Ø	Simulator, Bovine serum	Gravimetric		0.25	
	Low Carbon m/m				0.6	
	High Carbon m/m					
Schmidt and Farrar (1996)	22 mm Ø m/m	Simulator, Bovine serum	Gravimetric		0.329	
	28 mm Ø m/m				0.304	
	35 mm Ø m./m				0.432	
Farrar and Schmidt (1997)	28 mm Ø m/m, Ø clearances 0.033 - 0.139 mm	Simulator, Bovine serum	Gravimetric		0.192 - 0.534	

Table 2.5: Summary of wear results for metal-on-metal and ceramic-on-ceramic combinations

Previous work has linked the degree of osteolysis directly to the volume of wear particles produced by the implant (Schmalzried *et al* 1992, Hall *et al* 1996 and Elfick *et al* 1998c). It would seem that all of the materials used in total hip replacements can induce a foreign body reaction and therefore osteolysis (Schmalzried *et al* 1994, Yoon *et al* 1998).

There is no doubt that the volumetric wear of all metal and all ceramic joints is about ten to one hundred times less the volumetric wear of the polyethylene component in the metal-on-plastic system, however, there is some concern over the particle size. The inflammatory response to wear particles also seems to be dependent on the size of the wear particles. For a given volume of UHMWPE particles the stimulatory effect *in vivo* decreases when particle size is larger than 7 μm or smaller than 0.3 μm (Green *et al* 1997). If the size of the metallic or ceramic particles is smaller than that of the polyethylene, then a greater number of particles will be produced for the same volumetric wear. However, the particle size of the metal particles would have to be at least an order of magnitude smaller than the polyethylene to produce an equal number of particles as found in the polyethylene joint. This has not been shown to be the case, indeed, the metallic particles have been shown to have approximately the same mean size as the benchmark polyethylene particles (Maloney *et al* 1995). Ceramic particles too have been found to have approximately the same size particles as polyethylene. Yoon *et al* (1998) found the mean size of the ceramic particles from an all ceramic joint using a scanning electron microscope to be 0.71 μm.

2.7 Aims of this work

The aim of this thesis is to report on an investigation into the tribology of hard bearing surfaces. The friction and lubrication regimes of CoCrMo against CoCrMo and alumina against alumina will be assessed in a hip function simulator and compared with those for conventional metal-on-UHMWPE joints. The wear performance of different compositions of CoCrMo on itself will be determined on a simple reciprocating pin-on-plate machine and a new design of pin-on-plate wear machine produced in accordance with the ASTM standard of 1982 with both reciprocating action and pin rotation will be discussed and validated.

3. Apparatus

3.0 Introduction

There are various types of machine to test material properties such as friction and wear. These range from materials screening devices such as the simple reciprocating pin-on-plate wear machines, where no attempt is made to match the full *in vivo* conditions accurately, to complex joint simulators.

3.1 Durham Hip Function Simulator

All frictional measurements performed and discussed in this thesis were undertaken on the Durham Hip Function Simulator No. 1, (Figure 3.1), originally commissioned by Roberts *et al* (1982). The simulator has also been described in detail elsewhere (Roberts *et al* 1982, Unsworth *et al* 1987, Unsworth *et al* 1988, Hall *et al* 1994 and Hall *et al* 1997).

Three main components made up the hip function simulator: the PC which was used for data analysis, the microprocessor which acquired data throughout the experimental run and controlled the load through a closed loop feedback system and the simulator which applied load and motion to the joint. The simulator comprised a low friction carriage into which the acetabular cup was positioned and an upper moving frame into which the femoral head was fixed. The prosthesis was therefore inverted relative to its position *in vivo*, (Figure 3.2). Briefly, a dynamic load was applied through the upper moving frame whilst subjecting the joint to a simple harmonic oscillatory motion in the flexion-extension plane. As the femoral component oscillated, the frictional torque created at the bearing surfaces was measured using a piezoelectric transducer. Tests were controlled by the operator via the PC. The simulator will be discussed in more detail in the following three sections; the loading system, the motion system and the measurement of frictional torque. The data acquisition and analysis system will then be discussed.
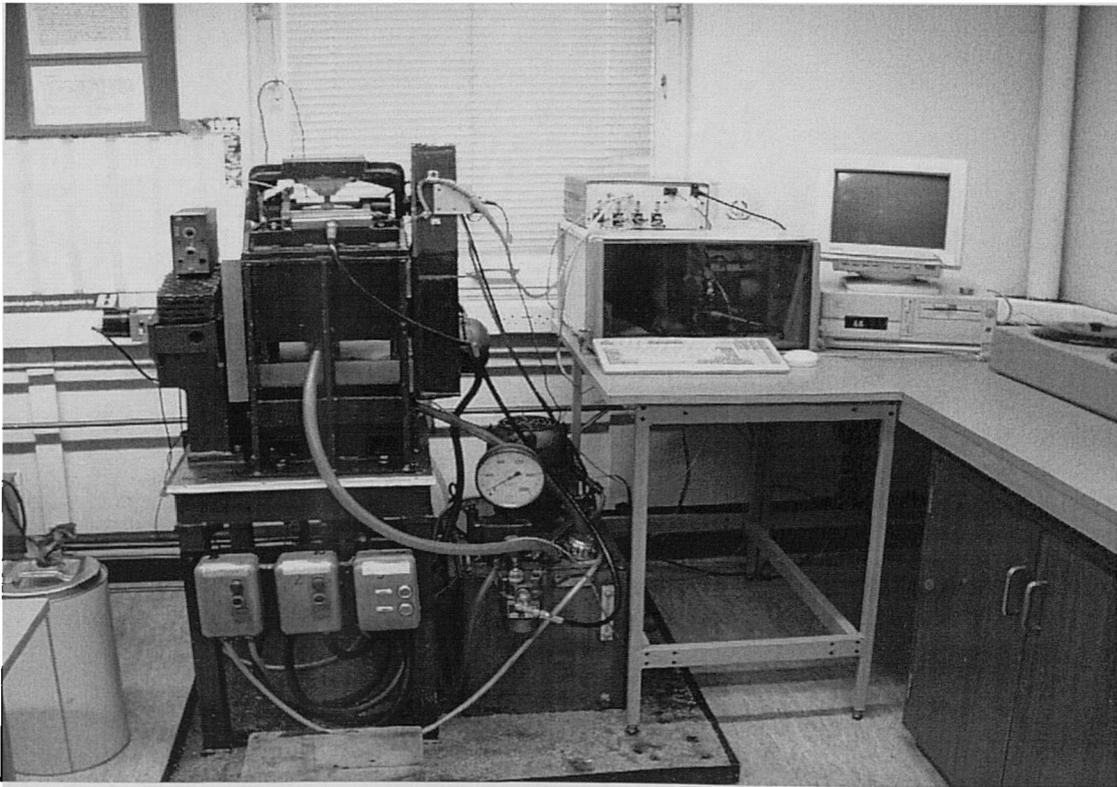
Figure 3.1: The Durham Hip Function Simulator
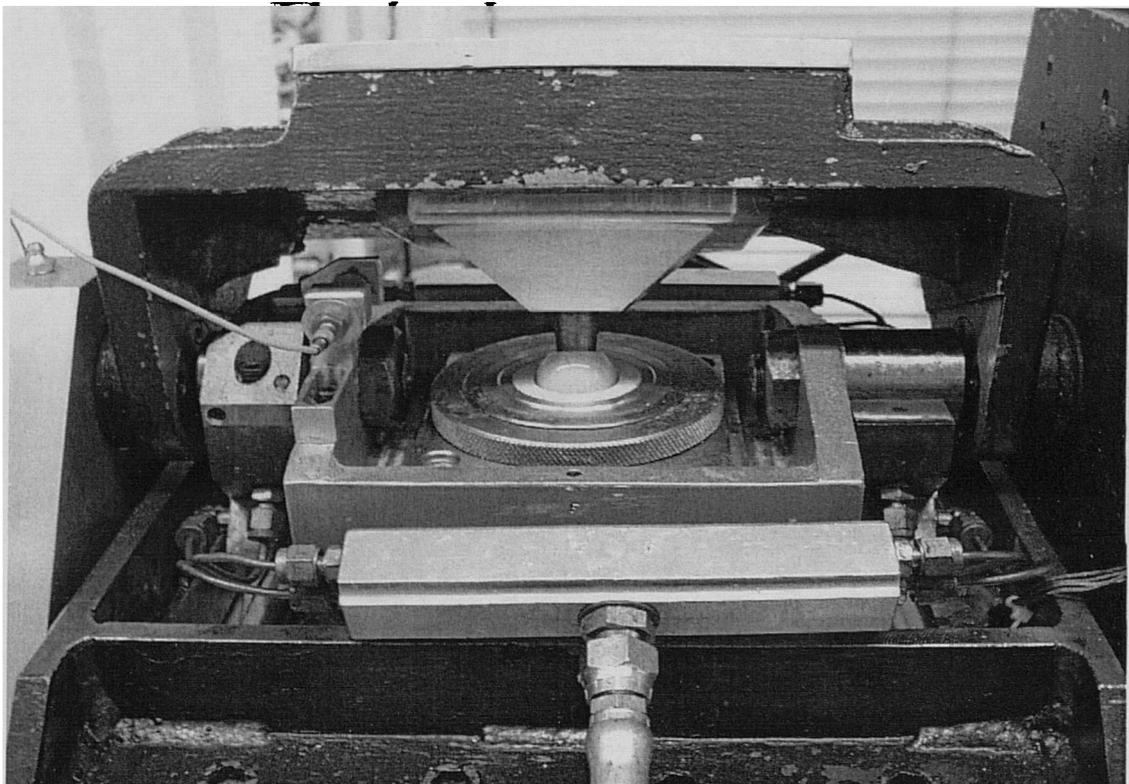
Figure 3.2: A prosthesis within the Durham Hip Function Simulator

3.1.1 The loading system

A servo hydraulic mechanism controlled by a PC via a microprocessor allowed a dynamic loading cycle to be achieved. The load was applied to the joints via a hydraulic actuator as a dynamic walking cycle with maximum and minimum loads normally set at 2000 N (2.7 x body weight - BW) and 100 N respectively. Figure 3.3 compares the simulator load cycle with that found by Paul (1966-67). Paul (1966-67) assessed joint loads by measuring external force actions transmitted to the leg and correlated these with photographic records. He found the maximum load applied to a hip joint during normal walking to be 3.9 x BW with peak loads at heel strike (HS) and toe off (TO). English and Kilvington (1979) measured human dynamic hip loads *in vivo* by incorporating strain gauges into the neck of a femoral prosthesis and found a peak load of 2.7 x BW and less evidence of the double peak loads found by Paul. Although the simulator loading cycle was simplified it did include the low load swing phase and high load stance phase.
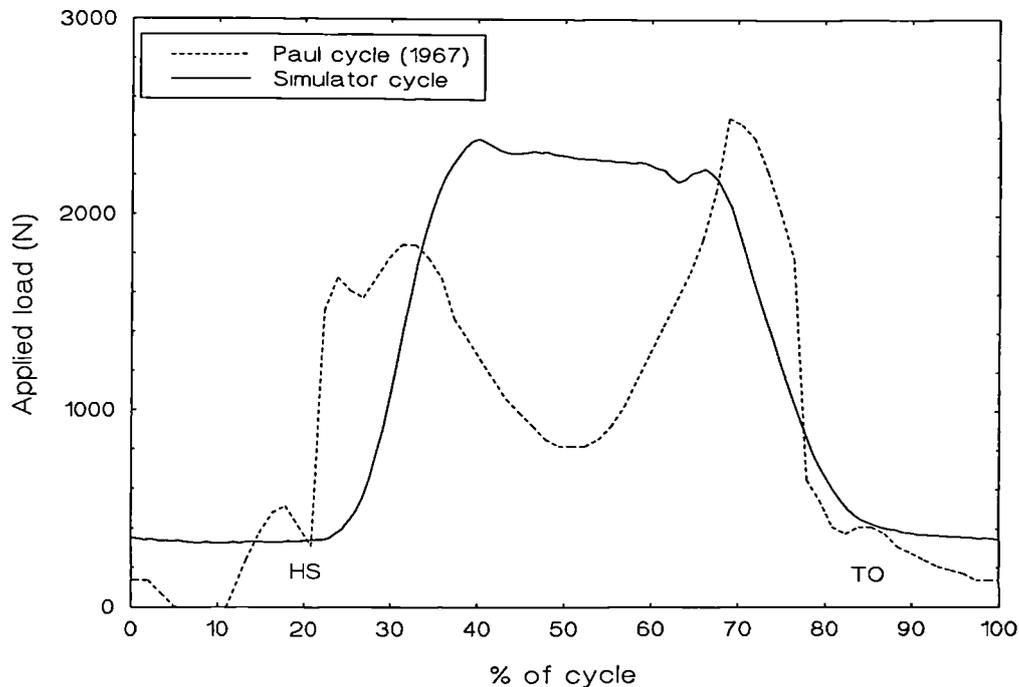
Figure 3.3: Comparison of loading cycles

Four miniature load cells (RDP, Model 13E) were positioned at the corners of the linear hydrostatic bearings. The applied load was measured continuously and the outputs from the four load cells were amplified by a strain gauge amplifier, summed and then converted from an analogue signal to a digital signal by an analogue to digital converter (ADC). This provided an output of the load at each sampling point and also acted as the feedback signal for the closed loop feedback system by which the load was regulated and maintained.

3.1.2 Motion system

A motor and variable speed transmission provided the drive for the simulator through a toothed belt. This was converted into simple harmonic oscillatory motion of the femoral head in the flexion-extension plane using a scotch yoke mechanism. The amplitude of the motion was set at 24° but could be adjusted by controlling the throw of the scotch yoke. The motion cycle applied by the simulator is compared with that found by Johntson and Smidt (1969) in Figure 3.4. The period of motion was 1.2 seconds. Throughout the cycle the angle of swing was measured by a potentiometer and these data were fed back to the microprocessor to give a value of position at each sampling point.
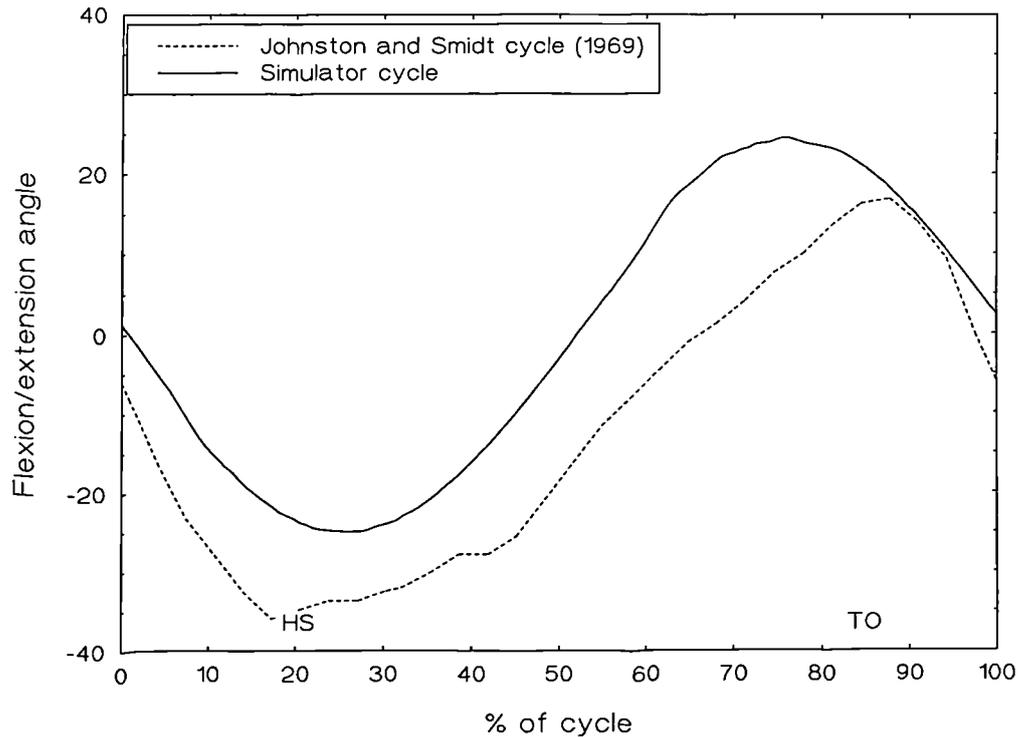
Figure 3.4: Comparison of motion cycles

3.1.3 Frictional measurement system

The acetabular cup was located in a low-friction carriage. This carriage was supported by two sets of externally pressurised bearings; two hydrostatic journal bearings which allowed rotation of the carriage in the sagittal plane and, underneath, two hydrostatic linear bearings which allowed some anterior-posterior and lateral translation. These bearings exhibited extremely low friction of the order of 10^{-4}, Unsworth (1978). The lower set of bearings acted to allow the joint to locate its own centre of rotation thereby preventing any misalignment in the anterior-posterior plane, whilst the other set of bearings provided an extremely low friction axis about which the acetabular carriage could rotate due only to the frictional torque generated by the surfaces of the joint. This also provided lateral alignment. The rotation was resisted by a Kistler piezoelectric transducer, this signal was amplified by a charge amplifier which was calibrated to measure the frictional torque produced. The analogue signal was converted to a digital signal by an ADC and then fed to the PC.

3.1.4 Elimination of errors

To obtain accurate measurements of friction it was necessary to have all the axes of rotation aligned i.e. that of the femoral head, upper moving frame, acetabular cup and acetabular carriage. The femoral head was aligned by measuring the exact height of the head in its holder and then extending it to its correct, aligned height using spacers. The cup was aligned using a setting up jig which reproduced the exact heights of the simulator. The height of the cup was adjusted by raising or lowering the cup holder within the jig prior to testing and then clamping it by means of a locking ring.

Any horizontal misalignment between the rotational axis of the acetabular carriage and acetabular cup which could not be eliminated *in situ* and hence would lead to an additional eccentricity torque, τ, was accommodated by performing two runs on each joint, one with the peak loading applied whilst the head was moving forwards in the cycle (normal run) and another with the peak loading applied whilst the head was moving backwards in the cycle (inverse run). These loading cycles each produced a torque T_f and T_b respectively from which the true torque was calculated (Equation 3.1)

$$T = \frac{|T_b| + |T_f|}{2}$$

(3.1)

This frictional torque was then converted to friction factor using Equation 2.4.

Calibrations of load, frictional torque and angular position were undertaken on the simulator at regular monthly intervals or after a prolonged period without testing. The load ADC and DAC from the four miniature load cells were compared to an external load cell, the frictional torque ADC output from the transducer to a known torque applied to the friction carriage by use of a loaded lever arm and the position ADC to an angular spirit level (see Appendix A).

Burgess (1996) performed a detailed analysis on the precision of Durham Hip Function Simulator no. 2 by assessing the errors in the load and friction measurement systems. By examining the instrument specifications such as ADC bit noise, load cell linearity and repeatability, strain gauge amplifier accuracy, transducer linearity and charge amplifier accuracy he was able to estimate the maximum error in the friction factors produced by the simulator. He found that for friction factor values of 0.1, 0.01 and 0.001 the corresponding errors in measurement would be 4.5%, 12% and 98% respectively. Thus, for the range of friction factors encountered with conventional metal-on-plastic joints (0.01 to 0.1) the simulator was found to have an acceptable accuracy with below 10% error. At a friction factor value of 0.001 and therefore an error of 98%, however, the resulting range of friction factors is 0 to 0.002. Therefore as the friction factors become lower than 0.01, the machine becomes considerably less accurate making trends more difficult to discern but still allowing low friction factors to be measured and therefore full fluid film lubrication to be identified. The Durham Hip Function Simulator No. 1 used equivalent instrumentation to Simulator No. 2 and therefore the analysis is the same.

3.1.5 Data acquisition and analysis

Each full run of the simulator consisted of 41 cycles. During the first, twenty-first and forty-first cycles the load, angular position of the femoral head and frictional torque were sampled and recorded 128 times and the data fed back to the PC via the Motorola 68020 microprocessor board which was built in house. Figure 3.5 shows a schematic representation of the simulator control system.
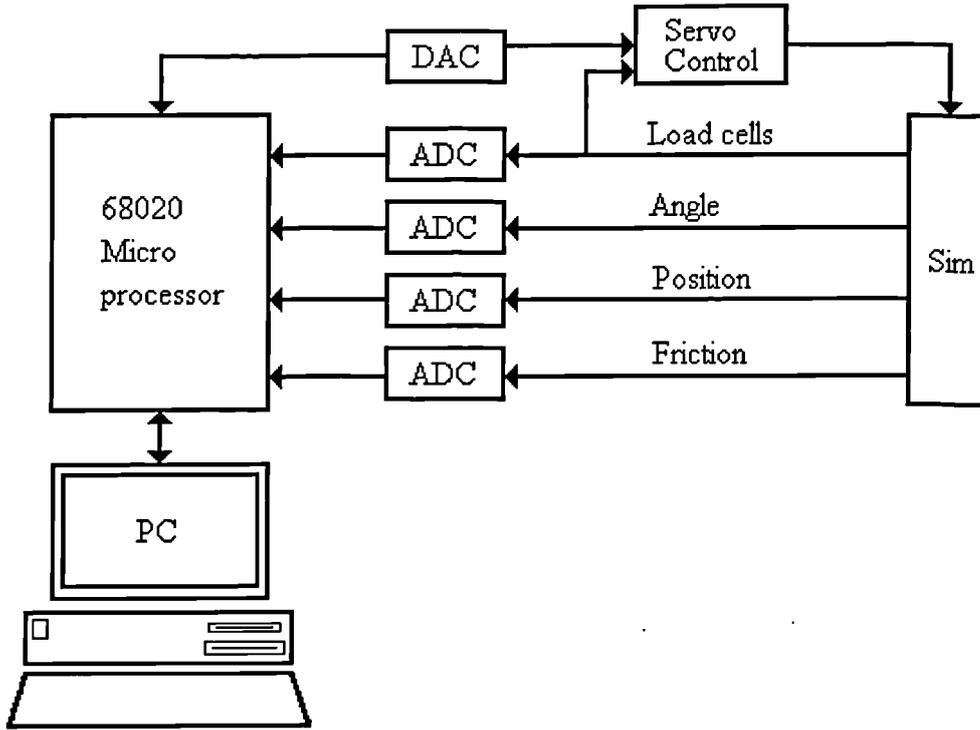
Figure 3.5: A schematic representation of the simulator control

After each run the PC was used to analyse the data using software developed by the University of Durham Microprocessor Centre. For the selected cycles, each encoder position, i, the applied load, L_i, the frictional torque, T_i and angle of swing, A_i were recorded in digital form and then converted to real physical units using the calibration coefficients. For each of the 128 sampling points the mean load, frictional torque and angle were calculated using Equations 3.2, 3.3 and 3.4 respectively. In order to combine the forward (normal) and backward (inverse) loading cycles it was necessary to accommodate the phase difference between the cycles (position i in the forward loading cycle was equivalent to position $i+64$ in the backward loading cycle, see Figure 3.6).

$$L_i = \frac{L_{fi} + L_{b(i+64)}}{2}$$

(3.2)

$$T_i = \frac{|T_{fi}| + |T_{b(i+64)}|}{2}$$

(3.3)

$$A_i = \frac{A_{fi} + A_{b(i+64)}}{2}$$

(3.4)

Similarly, the friction factor at each point in the cycle, f_i, can then be determined using Equation 3.5.

$$f_i = \frac{T_i}{R_h L_i}$$

(3.5)

Also, the entraining velocity at any point within the cycle, u_i, can be determined using Equation 3.6, where f was the frequency of the flexion-extension motion (0.83 Hz) and α the amplitude of motion (24°).

$$u_i = \left\{ \frac{\pi^2 \alpha}{180} f \cos\left(\frac{2\pi i}{128}\right) \right\} R_h$$

(3.6)

The Sommerfeld number was then calculated from Equation 3.7.

$$z_i = \frac{\eta u_i R_h}{L_i}$$

(3.7)

For each of the 128 sampling points the friction factor and Sommerfeld number were calculated. When analysing the data only 5 of the 128 sampling points from the 41st cycle were used. These points were taken at the position in the cycle corresponding to the stance phase of walking, i.e. high load and high velocity, this is shown graphically in Figure 3.7. The five points corresponded to encoder positions of 51.5, 57.5, 63.5, 69.5 and 75.5 for the forward loading cycle. At each of the five points the friction factor was determined using six points evenly distributed either side of the corresponding encoder position and averaging the resulting friction factors i.e. at point 51.5 the friction factors at points 49, 50, 51, 52, 53 and 54 were averaged and plotted at point 51.5. When calculating the means and standard deviations of a number of runs, the friction factor at encoder position 63.5 was taken for each test.
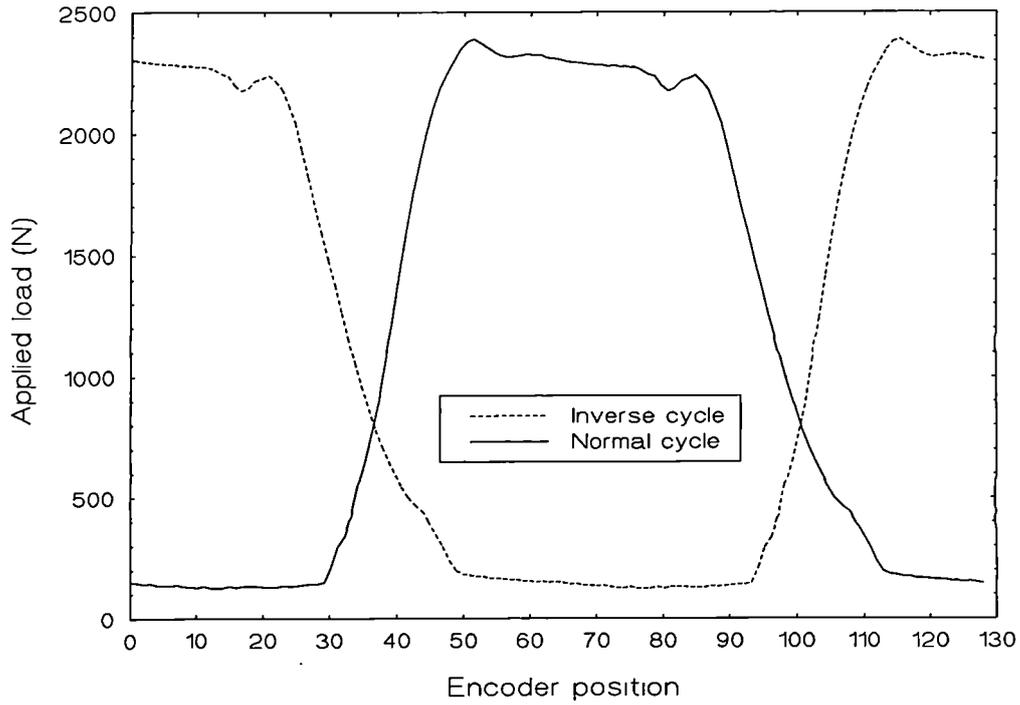
Figure 3.6: Normal and inverse loading cycles
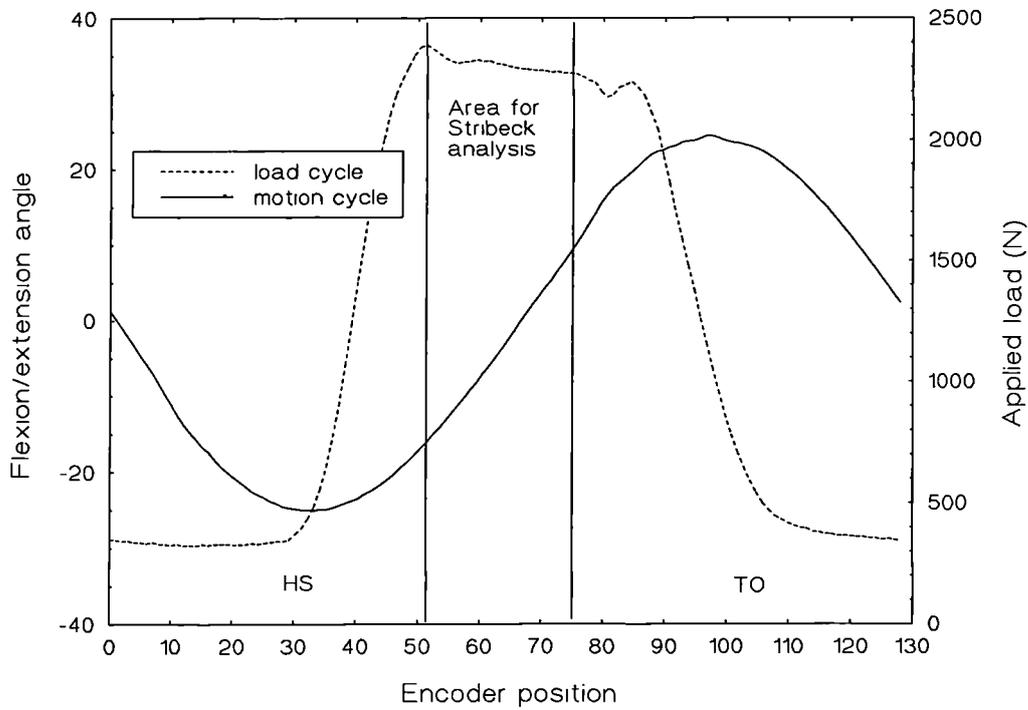
Figure 3.7: Simulator load and motion cycles showing area from which Stribeck results were taken

3.2 Pin-on-plate machine

Pin-on-plate machines represent a simple method to screen different combinations of materials for use in artificial joints. Unlike the hip function simulator, the pin-on-plate machine does not attempt to recreate the *in vivo* conditions which promote full fluid film lubrication. These machines assess the wear which will occur when two materials come into contact under similar sliding speeds and loads to those encountered in the body. The specimens are easier to manufacture than those for the simulator as they are just a simple pin and flat plate. This type of machine is therefore very useful in determining suitable material combinations for reduced wear, however, care must be taken when making comparisons with clinical results. It must be realised that the pin-on-plate apparatus offers crude material ranking only and any candidate materials should be tested in a simulator to determine wear prior to clinical trials. The pin-on-plate machine has been described in detail elsewhere (Stokoe 1990 and Joyce *et al* 1996).

The pin-on-plate wear machine consisted of an aluminium sledge reciprocating along two fixed parallel bars. Positioned on top of the sledge were the heated bed and the lubricant bath. The bed was heated by electrical resistors which subsequently heated the lubricant bath up to a temperature of $37^{\circ}C$, controlled by a thermocouple placed in the lubricant. The plates were fixed firmly within the lubricant bath by means of a plastic frame in which suitable locating holes were milled. The pins were held in stainless steel holders and supported on an arm, the pins were notched to allow adequate fixation within the holder and also to ensure correct orientation when replacing the pin after cleaning and weighing procedures. The loads were applied to the specimens via a lever arm mechanism. Level sensors allowed the lubricant to be maintained at an almost constant level and to be topped up when needed. An electronic counter was connected to the reciprocating sledge. The sledge was driven by a 125 W d.c. shunt motor, with the motor speed controlled using a variable voltage supply. Stroke length was altered by adjusting the crank radius of the drive shaft. A perspex cover was placed over the entire rig to act as a dust shield. Figure 3.8 shows the pin-on-plate machine.
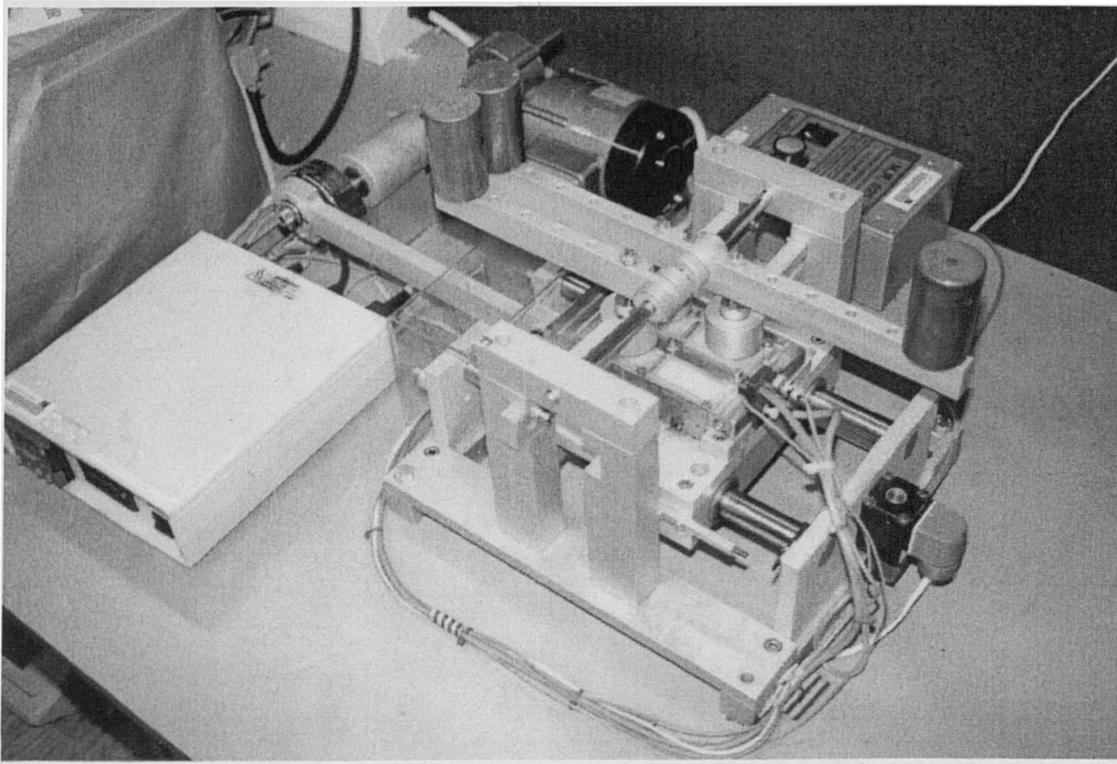
(a)
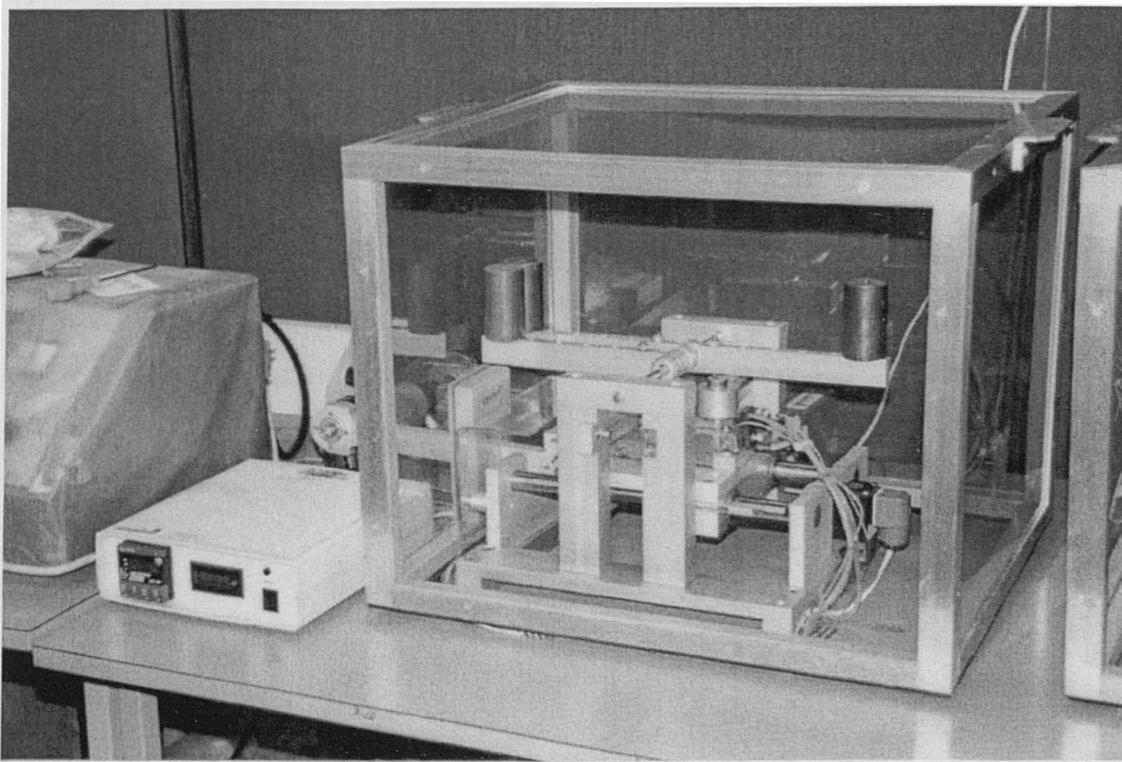
(b)

Figure 3.8 (a) and (b): The original pin-on-plate machine

3.3 Design of new pin-on-plate machine

A new design of wear machine was proposed which would comply with ASTM standard F732-82 (1982). The standard imposed restrictions on the pin specimens, the specimen chambers, the load, motion, sliding speed and the lubricant to be used in wear testing. Alterations which were needed to the original Durham pin-on-plate wear machine are detailed in the following section. For a multiple specimen machine, the specimens should be contained in individual isolated chambers to prevent cross contamination of wear debris. The machine should be designed to withstand a load of 225 N, in order to obtain physiological contact stress conditions. Specimens should be run at a sliding speed of 50 mms^{-1} and a stroke of 25 mm within a lubricant of filtered calf serum, however, the concentration of this serum was not specified.

In addition to the constraints set out in the ASTM standard, rotational motion was added to the pins. Previous work (Wang *et* al 1996 and Tipper *et al* 1999) has indicated that by simply adding a rotational element to the relative motion between the pin and plate specimens, results more in accordance with clinical wear factors can be obtained.

The new pin-on-plate machine was based on the existing four station reciprocating pin-on-plate machines at the Centre for Biomedical Engineering at the University of Durham. As with the existing machines, the sledge reciprocated along two fixed parallel hardened steel bars. The heated bed and stainless steel plate holder were positioned on top of this sledge. The plate holder consisted of six wells into which the plate specimens fitted exactly. The lubricant was contained within these individual wells and heated to a temperature of 37°C by resistors within the bed. This was controlled by a thermocouple. Only four of the stations were loaded, the remaining two were available to be used for soak control specimens. Initially, for validation purposes, only two of the four loaded stations incorporated rotation and reciprocating motion, the other two had reciprocating motion only. All four loaded pins were held in stainless steel holders. The holders were held in the pin arm, those pins with rotational motion were held within a polyacetyl bearing within the pin arm

and were not notched as correct pin orientation was not necessary in this situation. Level sensors made from platinum wire were attached to each loaded station to allow the lubricant to be maintained at an almost constant level. This was topped up at each station from a common reservoir. An additional smaller bath was incorporated into the plate holder for pin soak control specimens. A perspex cover with removable top and front panels was placed over the entire rig to prevent dust contamination from the atmosphere.

The new pin-on-plate wear machine was designed with a view to frictional measurement at a later stage, however, the initial requirement was for a statically loaded wear machine. Dead weights applied via a lever arm mechanism were chosen as the initial method of loading as alternatives such as pneumatic loading would be too complex and expensive for the simple application of static loads. The main area of the plate bed was, however, designed large enough to accommodate the incorporation of near friction free air bearings and pneumatic loading should this be required. Calculations were performed to determine the theoretical weights required to apply a given load to the pins via the lever arm.

Pin rotation was considered important but presented a more complex problem. Initially the requirements were for the application of internal/external rotation of the pin by ±10°, 90° out of phase with the reciprocating motion. This was to ensure that the motion was similar to that in the body resulting in crossing of the wear paths. A geared rack and pinion mechanism attached to the reciprocating plate holder could provide the internal/external rotation but it would not be easy to make this 90° out of phase. It could alternatively be achieved by stepper motors with computer control but this would increase the cost of the machine significantly, making this option unsatisfactory. Velocity vector calculations were performed to determine whether an easier solution was capable of providing crossing of the wear paths. The effect of three different situations on the wear vectors with respect to the pins were analysed. The first was internal/external rotation which was in phase with the reciprocating motion, that is the maximum pin velocity occurred at the same point as the maximum plate velocity. Secondly internal/external rotation which was 90° out of phase with the reciprocating motion was analysed. In this situation the zero pin

velocity at the point of change of direction occurred at the same time as the maximum velocity and therefore midpoint of the motion of the plate. Finally the effect of full rotation of the pin was analysed. The equations are shown below and for the full velocity vector analyses, please refer to Appendix B.

Internal/external rotation, in phase:

$$\tan\alpha = \frac{1.096R\cos\gamma}{78.5 - 1.096R\sin\gamma}$$
(3.8)

Internal/external rotation, out of phase:

$$\tan\alpha = \frac{1.096R\cos(7.2x)\cos\gamma}{78.5\sin(7.2x) - 1.096\cos(7.2x)\sin\gamma}$$
(3.9)

Full rotation:

$$\tan\alpha = \frac{\omega_{rot}R\cos(\omega_{rot}t)}{78.5\sin(\omega_{slid}t) - \omega_{rot}R\sin(\omega_{rot}t)}$$
(3.10)

Where α is the angle of the resultant velocity vector with respect to the pin, R is the radius on the pin at which the point was referenced, x is the sliding distance in the direction of reciprocating motion, ω_{rot} is the rotational angular velocity, ω_{slid} the angular velocity of the reciprocating motion, t the time and γ is as shown in Equation 3.11 below. When R is equal to the full pin radius, the angle of the resultant velocity vector is with respect to the periphery of the pin.

$$\gamma = \theta + \sin^{-1}(0.34\sin(3.6x))$$
(3.11)

where θ is the starting angle.

Figures 3.9 and 3.10 show the angle of the resultant velocity vector against position in cycle for both the internal/external rotation conditions. It is clear from these results that to avoid symmetry and therefore achieve crossing of the wear paths, pin rotation must be out of phase with the sliding action. As it would be difficult to incorporate an out of phase rotation vector with ±10° rotation, the velocity vector analysis for full rotation was considered in depth. Figures 3.11 and 3.12 show clearly that as long as:

$$T_{rot} \neq nT_{slid} \qquad\qquad\qquad (3.12)$$

then crossing of the wear paths will occur, where T_{rot} is the period of the pin rotation, T_{slid} is the period of the sliding motion and n is an integer or inverse of an integer. Velocity vector analysis was also performed for full rotation with respect to the plates. It was found that at some point in the cycle, full rotation would result in crossing of the wear paths. Therefore rotation was incorporated into the design of the new pin-on-plate machine in the form of full rotation. This could be achieved by simple, small and inexpensive motors.

Power requirements were calculated for the motors to be used for the pin rotation. These necessitated a maximum power of 6.25 W and torque of 0.31 Nm, for full calculations please refer to Appendix C. This was provided by a 65 r.p.m. variable speed, steel geared motor supplied by the RS catalogue.
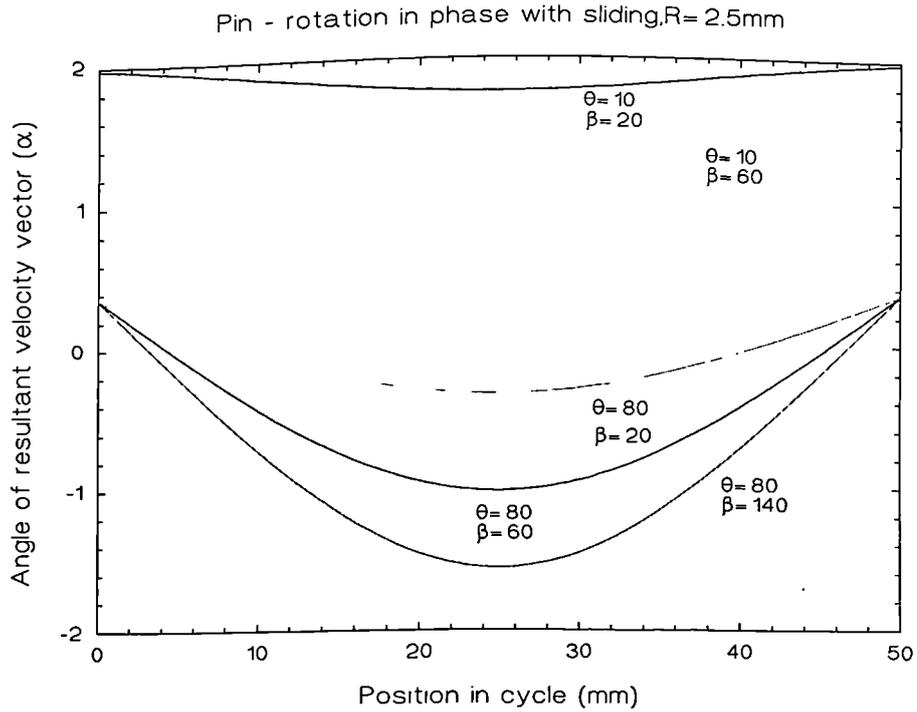
Figure 3.9: Velocity vector angle with respect to the pin (in phase with sliding)
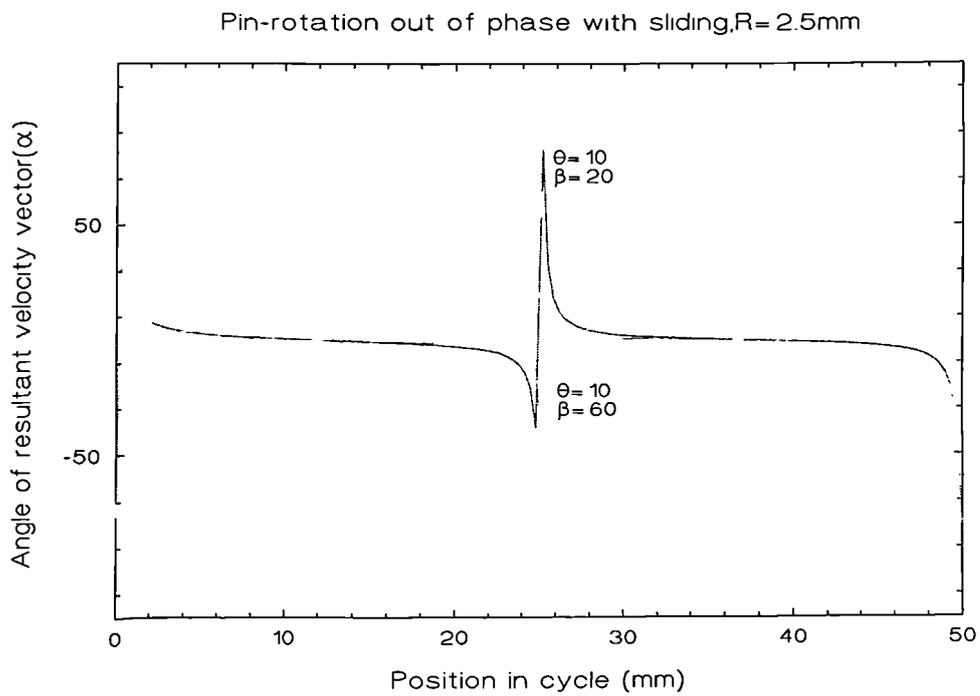
Figure 3.10: Velocity vector angle with respect to the pin (out of phase with sliding)

Pin-constant rotation ω= 2Π (same as sliding)

Time (Trot= 1s, Tslid= 1s)
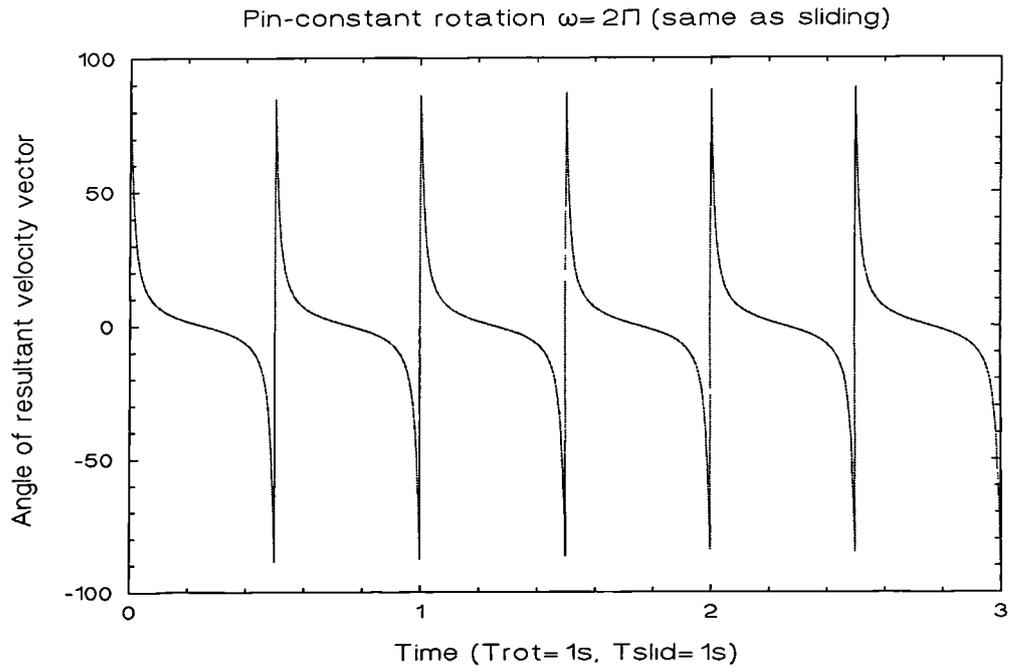
Figure 3.11: Velocity vector angle with respect to the pin ($T_{rot}=nT_{slid}$)

Pin - constant rotation, ω= 19.739rads-1

Time (Trot= 1/3.1416s, Tslid= 1s)
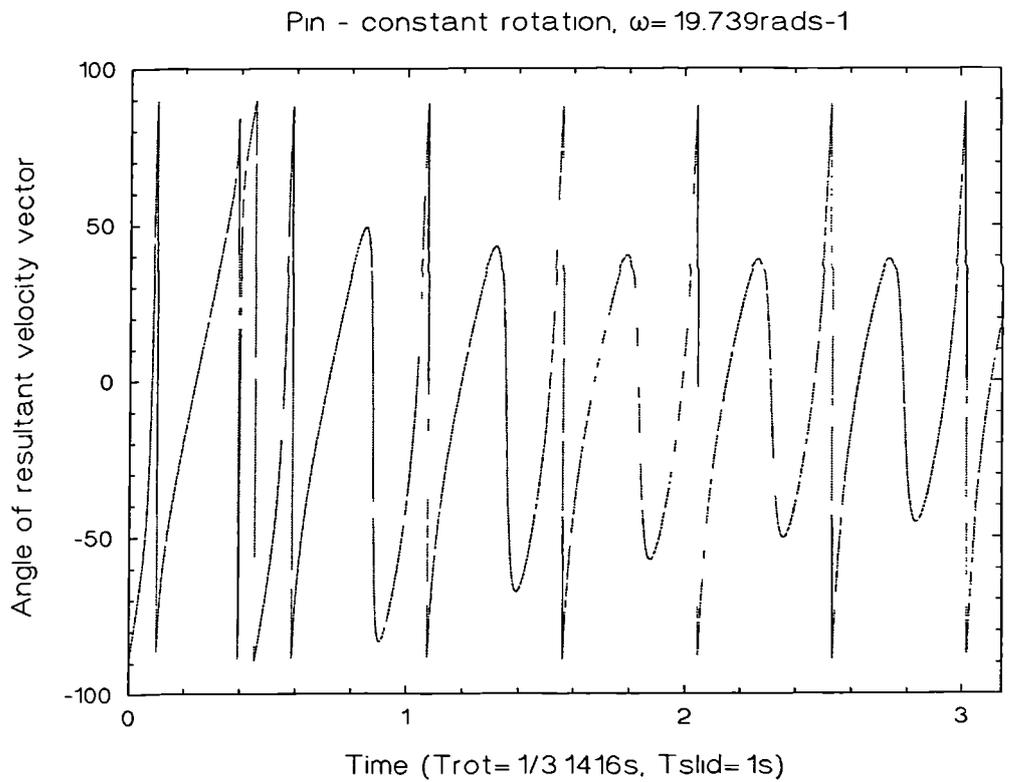
Figure 3.12: Velocity vector angle with respect to the pin ($T_{rot}\neq nT_{slid}$)

Calculations were also performed to determine the power requirements of the motor needed to provide the reciprocating motion of the plate bed. The higher load of 225N per station and the higher friction of metal/metal combinations would result in higher power and torque requirements than those provided by the existing motors and therefore a larger motor was needed. The maximum power required from the motor was calculated to be 73 W (see Figure 3.13) and the torque was calculated as 12 Nm. This was provided by a 0.18 kW, 14.9 Nm NECO, wound unfiltered, variable speed (max. speed 86 r.p.m.) d.c. motor, supplied by Laurance Scott and Electromotors Ltd. The full calculations can be found in Appendix D. The motor was mounted underneath the baseplate to conserve space.

Calculations were also performed to ensure that the deflections of the lever arms and fixed hardened steel parallel bars were minimal. (See Appendix E for details).

Once the apparatus was assembled, calibrations could be performed to assess the weight required to apply a given load to the pins via the lever arm mechanism. Firstly, known loads were applied directly onto the pin to calibrate the load versus displacement on the x-y plotter. Weights were then applied to the lever arm and the corresponding displacements on the x-y plotter measured. The displacements were then related via the initial calibrations to the actual loads. A graph of pin load versus weight on lever arm was then produced which could be referred back in order to reproduce any given load on the pin, see Figure 3.14. Linear regression analysis was applied to the curve and the equation of calibration was found to be:

$$required\ weight = (pin\ load - 0.554)/0.0369 \qquad (3.13)$$

The value determined from the above equation was compared with that calculated by theory. The difference in lever arm weights required for a given load between theory (785 g for a 40 N pin load) and practice (1069 g for a 40 N pin load) were attributed to friction within the apparatus.
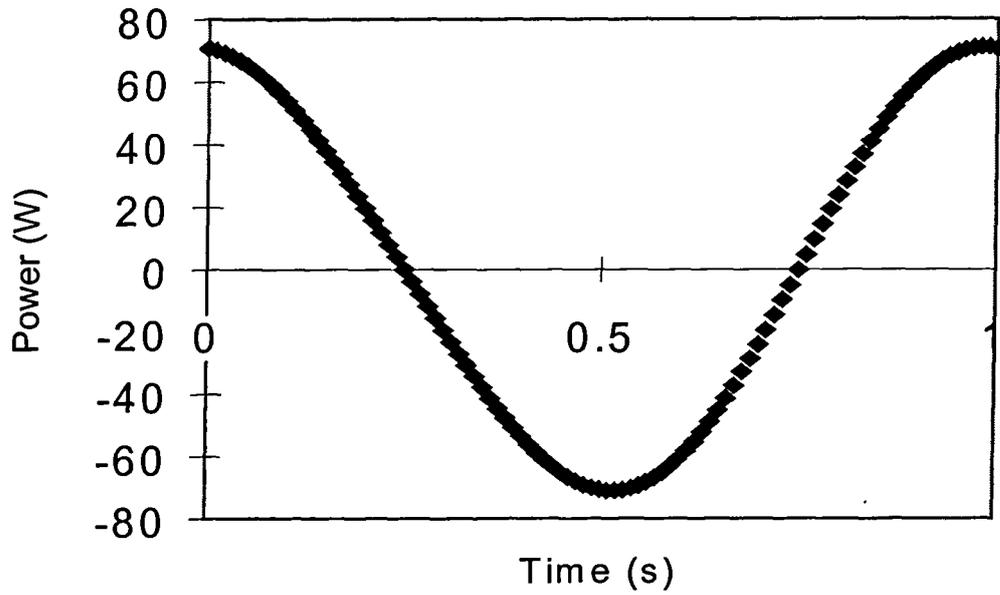
Figure 3.13: Power requirements for main motor throughout 1 second cycle
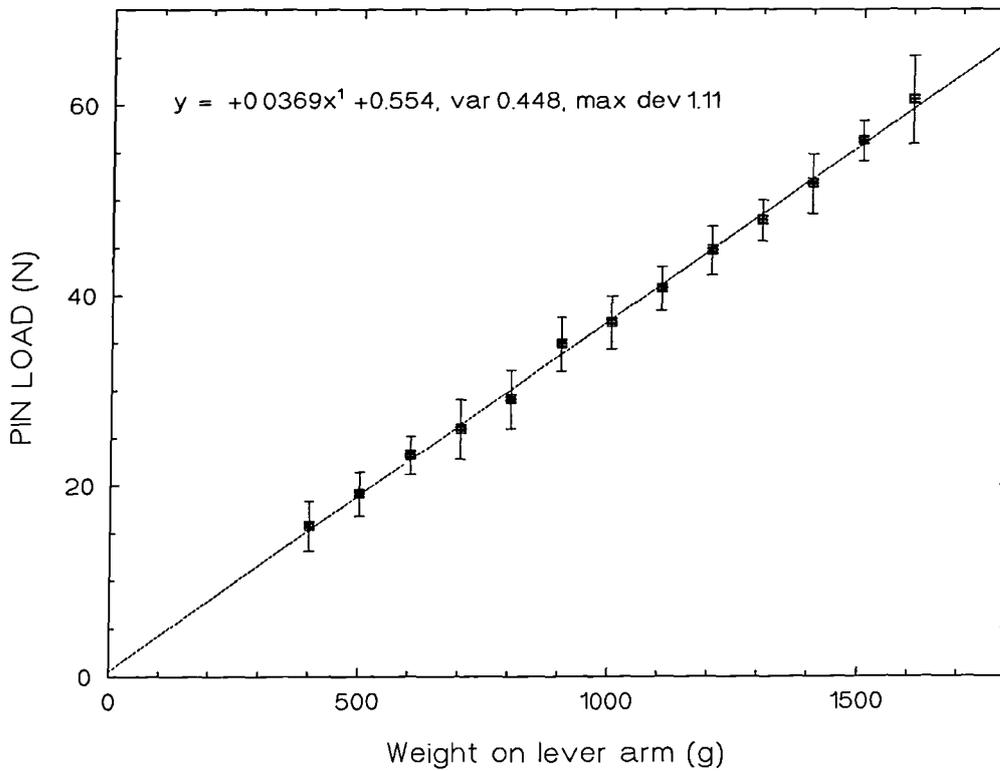
Figure 3.14: Lever arm load calibration

The full pin-on-plate assembly is shown in Figures 3.15 and 3.16.
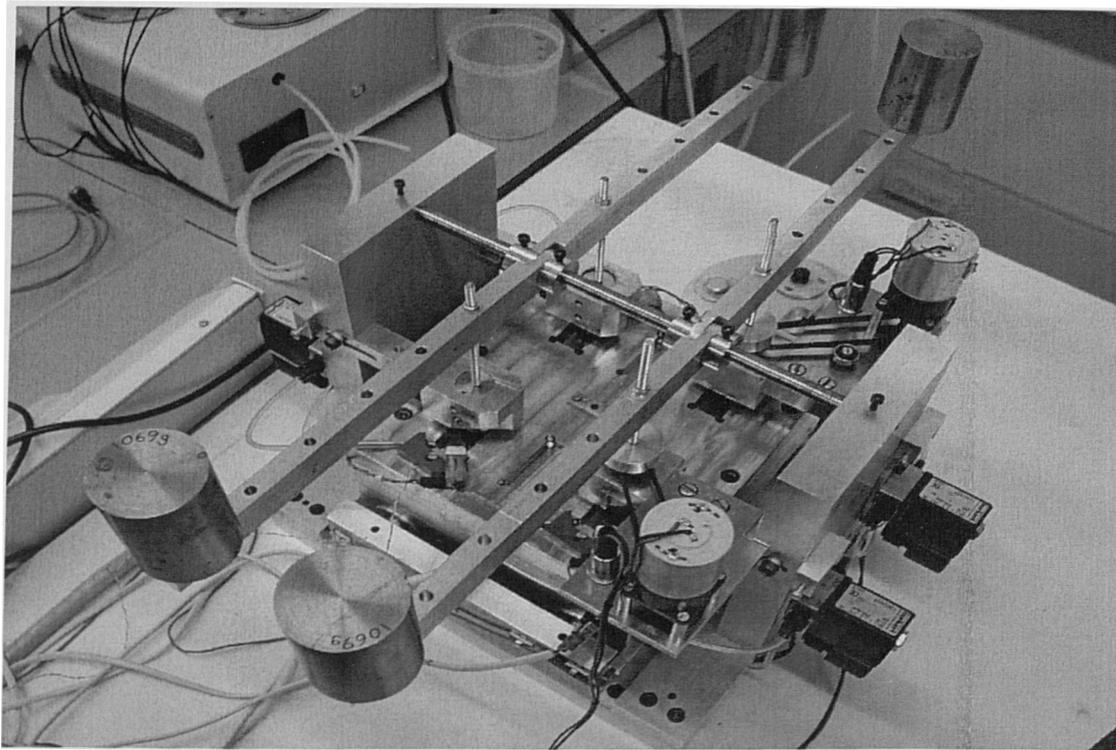
(a)
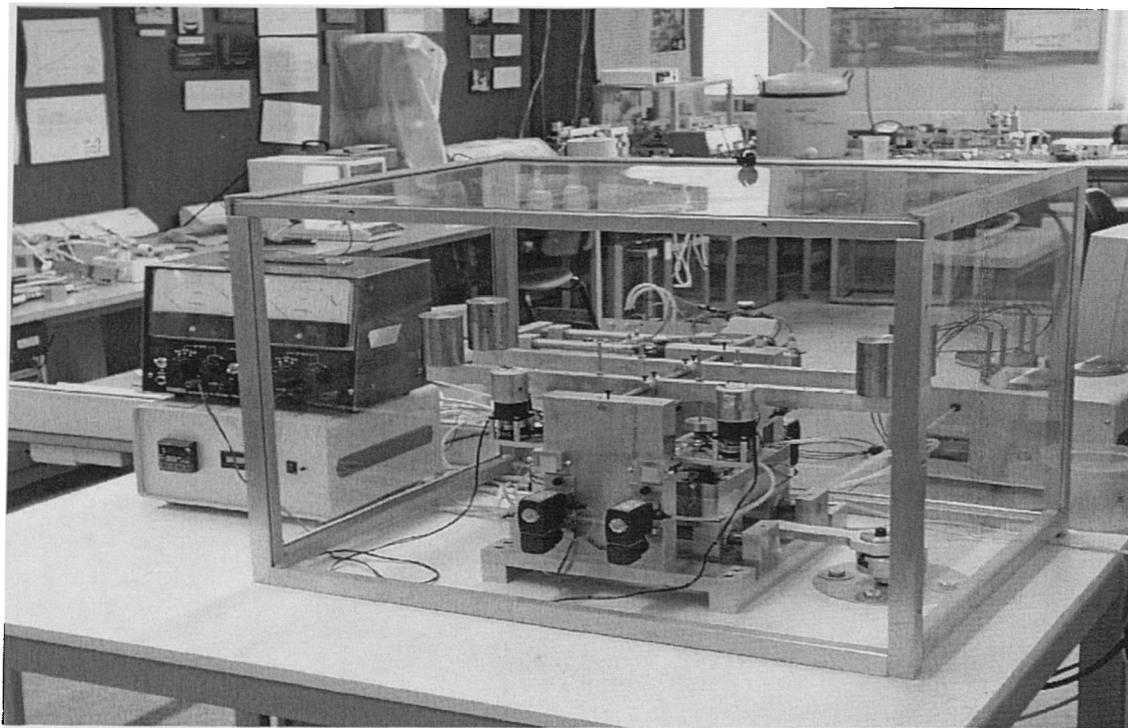
(b)

Figure 3.15 (a) and (b): The new pin-on-plate machine with rotation
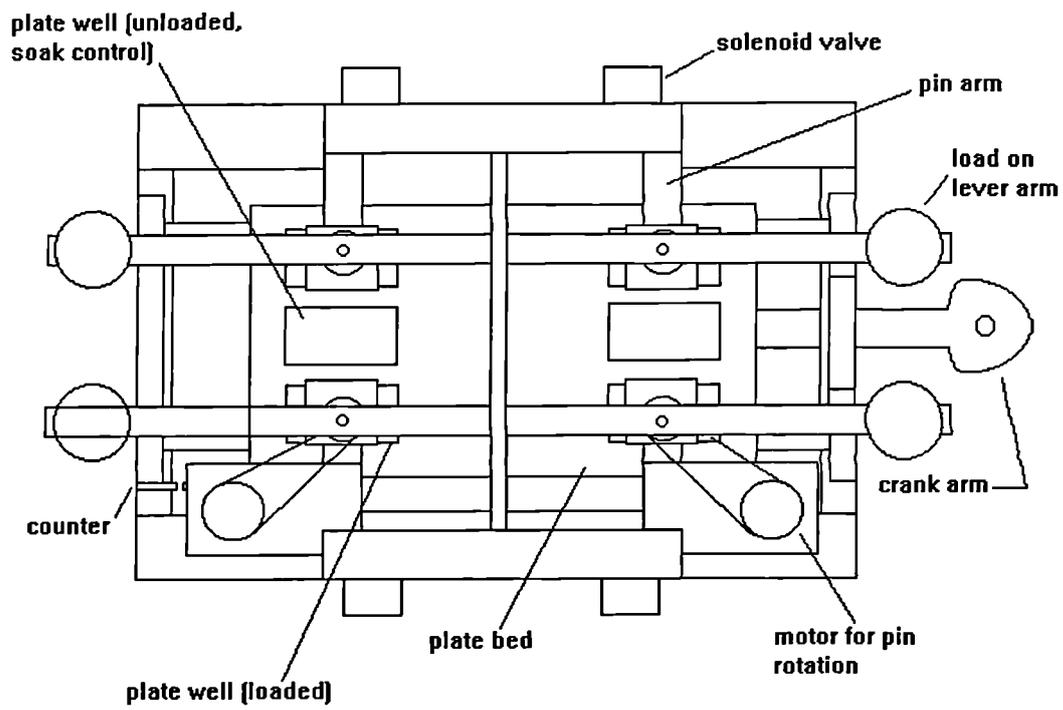
(a)
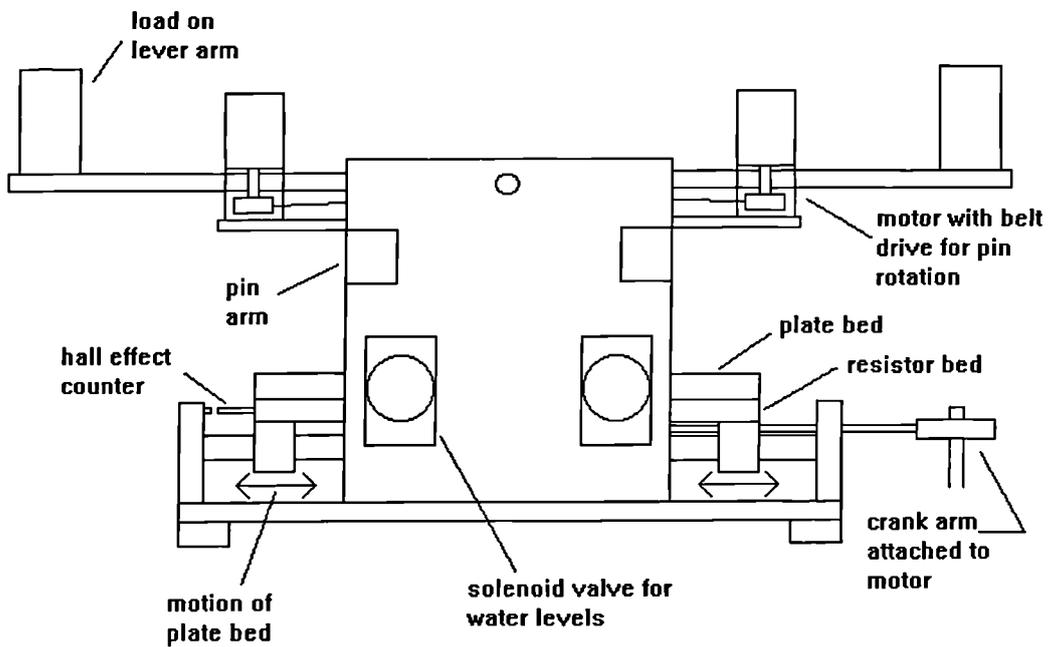
(b)

Figure 3.16 (a) and (b): Schematic representation of the new pin-on-plate machine

3.4 Surface measurements

Surface topography measurements were performed using a Zygo NewView 100 non-contacting 3D interferometric profilometer. The Zygo had a constant vertical resolution of less than one nanometer. The number of data points remained constant at 320 x 240 pixels and therefore the horizontal resolution varied with the size of the area of view which depended on the magnification of the chosen lens (see Table 3.1). In each case measurements of S_q, S_a and S_{sk} were taken.

Magnification	Area of view (μm)	Horizontal resolution (μm/pixel)
x10 lens	730 x 550	2.28
x20 (x10 lens with x2 zoom)	366 x 274	1.14
x40 lens	183 x 137	0.57

Table 3.1: Parameters for different magnifications on Zygo NewView profilometer

Further surface analyses were performed using a Zeiss Axiotech reflected light microscope.

For both the Zygo and the light microscope the true magnification was ten times the magnification of the objective lens.

4. Materials and Methods

4.0 Introduction

In order to achieve the best consistency possible; established test protocols were followed whenever possible - such as the Stribeck tests on the Durham Hip Function Simulator. Where this was not applicable, new protocols were designed and abided by to ensure standardisation of all test methods. *This enabled comparisons to be* made with a high level of confidence. The aim of these studies was to test the suitability of various designs of total hip replacements before clinical testing. Two main design parameters can be altered; the geometry of the contact and the material type. All friction measurements performed on the hard bearing surfaces (apart from the clearance tests) were also carried out on the conventional metal-on-plastic combination to allow direct comparisons between the alternative bearing surfaces and those in main use today - the "benchmark" joints.

4.1 Materials

4.1.1 Prostheses for friction testing

Friction tests were performed on metal-on-metal (low carbon, wrought CoCrMo alloy against itself), ceramic-on-ceramic (Al_2O_3 against itself) and metal-on-plastic (CoCrMo against UHMWPE) joints. All prostheses were of 28 mm diameter.

Twelve different clearances of metal-on-metal prostheses were available for testing ranging from 7 μm to 139 μm radial clearance (7, 10, 14, 17, 23, 29, 36, 45, 61, 83, 107 and 139 μm initial clearances). These were supplied by Biomet Merck Ltd.. Five ceramic-on-ceramic specimens were supplied by CeramTec, all of approximately the same radial clearance, 30 μm (26, 27.5, 29, 29.5 and 30 μm). The metal-on-plastic prostheses had a radial clearance of 0.2 mm. Three metal-on-plastic

joints were available for testing. The elastic moduli and Poisson's ratio for each material are shown in Table 4.1.

	CoCrMo (Blamey, 1993)	Al$_2$O$_3$ (Smallman and Bishop, 1995)	UHMWPE (Blamey, 1993)
E (Pa)	2.1 x 10^{11}	3.8 x 10^{11}	2.0 x 10^9
υ	0.3	0.23	0.4

Table 4.1: Material properties for different prosthesis materials

4.1.2 Pin-on-plate samples

Three different types of wrought CoCrMo/CoCrMo specimens were provided by Biomet Merck Ltd.; two high carbon materials (material A and material B) and one low carbon material (material C). Two plates of each material were provided along with two different pin configurations; flat ended (pin 1) and cylindrical ended with a radius of 50 mm (pin 2). The pin dimensions are shown in Figure 4.1. The CoCrMo samples had a density of 7970 kgm^{-3}.

Cross-linked polyethylene (XLPE) pins and plates were used as the samples for the validation of the new pin-on-plate machine. The XLPE samples had a density of 949 kgm^{-3}.

Further metal-on-metal samples were provided by Biomet Merck Ltd.; two pins and plates of the high carbon wrought CoCrMo alloy material A and two pins and plates of the low carbon wrought CoCrMo alloy material C. Each of the pins were flat ended.

5.0

⌀ 5.0

19.0

Flat ended pin
(all dimensions in mm)

R 50.0
(cylindrical)

5.0

⌀ 5.0

19.0

Cylindrical ended pin
(all dimensions in mm)
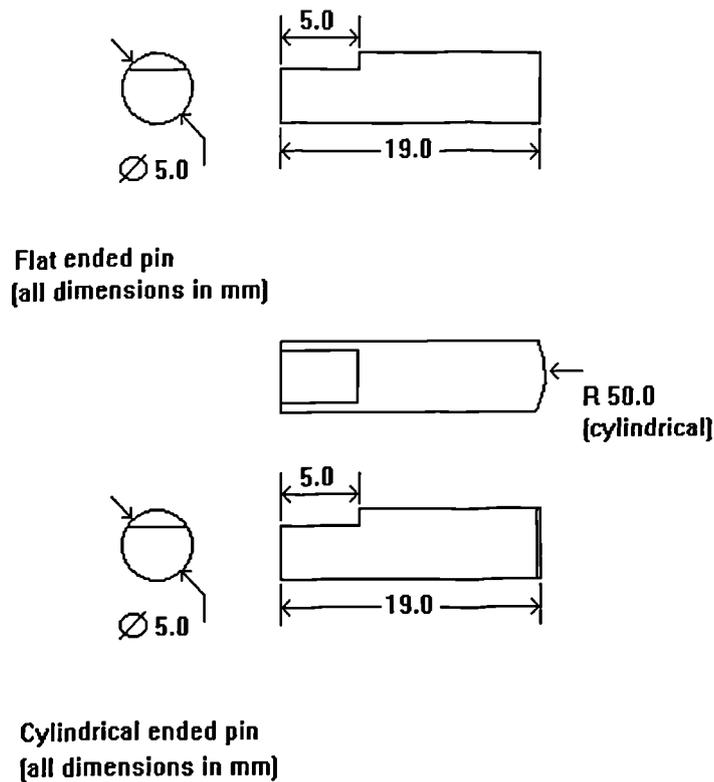
Figure 4.1: Pin dimensions

4.1.3 Lubricants

All viscosities were measured on the Ferranti-Shirley cone-on-plate viscometer MK3 at a shear rate of 3000 s^{-1} (as used by Unsworth *et al* 1987).

Aqueous solutions of carboxy methyl cellulose (CMC) were used as the lubricant at viscosities of 0.0047, 0.0123, 0.0333 and 0.154 Pa s. CMC fluids have been shown to have similar rheological properties to synovial fluid, i.e. they are shear-thinning, Cooke *et al* (1978). Tests were also run with distilled water (η=0.001 Pa s).

Silicone fluids were also used as a lubricant at viscosities of 0.0046, 0.00934, 0.048, 0.096, 0.4585, 0.971, 4.875 and 29.25 Pa s. Silicone fluids are Newtonian in nature over the range of shear rates tested; that is there is no variation in viscosity with shear rate. The fluids used were all Dow Corning 200 fluids.

The joints were also tested with new born calf serum. The serum was kept frozen until it was required and was tested at concentrations of 0, 8.3, 16.5, 24, 33, 50, 66 and 100 per cent at a viscosity of 0.0029 Pa s. The different concentrations were achieved by preparing CMC fluids to the same viscosity as 100 per cent filtered bovine serum. These constituents were then mixed by parts. One hundred per cent CMC fluids equated to 0% bovine serum. Fifty per cent bovine serum was also prepared to viscosities of 0.0011, 0.0024 and 0.0073 Pa s by adding CMC fluids of varying viscosities to 100% bovine serum. For the rest of the bovine serum tests, the bovine serum varied in viscosity leading to a viscosity of 0.0047 ± 0.0036 Pa s used in the remainder of the tests.

Tests were also undertaken with pooled, human synovial fluid taken from patients with arthritis (η = 0.0109 ± 0.0041 Pa s). Both the bovine serum (BS) and synovial fluid (SF) were tested filtered (1 μm filter, GF/B, Whatman, UK) and unfiltered.

The joints were cleaned thoroughly between tests with acetone and for those tests with a biological fluid as the lubricant with Gigasept also.

4.2 Methods

4.2.1 Simulator studies

The femoral head and acetabular components were mounted and aligned as described in Chapter 3. The procedure for performing a friction test on the Durham Hip Function Simulator is outlined below.

1. Place approximately 5 ml of chosen lubricant into the acetabular cup.
2. Place the acetabular component in the low friction carriage.
3. Place the femoral head into the upper moving frame.
4. Fasten the femoral head holder to the upper moving frame.
5. Run through the software batch file checking the filename to which the results are saved, the femoral head radius, the viscosity of the lubricant, the magnitude of the minimum and maximum loads, the loading cycle (normal or inverse) and the number of cycles recorded.
6. Turn the bearings and the load on.
7. To start the initial loading stage of the test press upper case P.
8. At the end of the initial loading stage you are prompted to press carriage return and then turn the motor on for the motion cycle.
9. At the end of the test you are once again prompted to press carriage return.
10. Stop the motor, load and bearings.
11. Remove the joint from the simulator and clean with acetone (for those tests with a biological fluid as the lubricant clean with Gigasept also).

Stribeck analysis was used to give an indication of the mode of lubrication in which friction factor, f, was plotted against Sommerfeld number, z. This, however, was only one type of test and other types of tests such as static loading tests to check for boundary lubrication were also carried out. Table 4.2 shows the different lubricants and loading cycles in each type of test performed on the Durham Hip Function Simulator.

Type of test	Joints tested	No. of runs performed	Min. load (N)	Max. load (N)	Lubricant(s)
Stribeck	m/m (all clearances)	2 4	100	2000	CMC (all η)
	c/c (all joints)	3			
	m/p (all joints)				
Stribeck	m/m (7, 14, 17, 29, 61, 139 μm)	3	100	2000	50% BS (all η)
	c/c (all joints)	2			
	m/p (all joints)	2			
Filtered & unfiltered	m/m (2 x 40 μm)	3	100	2000	100% BS & 100% SF
	c/c (all joints)	2			
	m/p (all joints)	2			
Static	m/m (3 x 40 μm)	2	1000[a]	1000[a]	CMC fluids and BS
	c/c (all joints)	2			
	m/p (all joints)	2			
To ffl	m/m (1 x 40 μm)	1	100	2000	Silicone fluids (all η)
	c/c (all joints)	1			
	m/p (all joints)	1			
% BS	m/m (2 x 40 μm)	3	100	2000	0, 8.3, 16.5, 24, 33, 50, 66, 100% BS
	c/c (all joints)	2			
	m/p (all joints)	3			
Long term	m/m (10, 23, 36, 45, 83, 107 μm)	2	100[b]	500[b] 1000[b] 1500[b] 2000[b]	100% BS

[a] These tests were also performed at 2000 N static load with both CMC fluids and BS and 500 N and 1500 N CMC fluids only.

[b] The long term friction tests consisted of at least 1000 cycles as opposed to the usual 41 cycle test. Only the normal run was conducted.

Table 4.2: Summary of friction simulator tests

For those tests where only one or two runs were performed, the data from each run is displayed on the graphs. For those tests with three or more runs the data is represented by the mean and standard deviation of all the runs.

4.2.2 Wear studies

Three different types of pin-on-plate tests were carried out. Firstly, simple sliding tests were performed on the existing machines to determine the effects of the two different pin configurations on the wear of three different compositions of CoCrMo (materials A, B and C). Each material composition was tested on a different machine to avoid cross contamination of the wear particles.

Tests using XLPE against itself were performed on the new wear machine to validate it against known results from the existing machines. The tests were carried out to the procedure outlined by an undergraduate final year project (Cartwright 1998). The aim of the undergraduate project was to investigate the influence of rotation on the wear process of XLPE/XLPE. Two stations applied reciprocating motion only, whilst the remaining two applied both reciprocation and rotation.

Finally, metal/metal samples were tested on the new machine to determine the effects of rotation on the wear of the metals. Reciprocation versus reciprocation plus rotation tests were carried out for metal/metal samples of material A and also material C.

The recommendations set out in the ASTM Standard Practice F 732-82 were followed with regard to the motion, sliding speed, lubricant and temperature. The pin-on-plate wear tests were carried out at a temperature of 37°C, at 60 r.p.m. with a 25 mm stroke resulting in a sliding speed of 50 mms^{-1}. A load of 40 N was applied vertically to each pin. Thirty per cent bovine serum with 0.2% sodium azide was used as the lubricant which was topped up with distilled water to counteract any loss

84

of fluid due to evaporation. Where applicable a constant rotation of approx. 60 r.p.m. was applied to the pins.

The wear was assessed gravimetrically. At least twice a week, the pin-on-plate samples were cleaned, weighed on a Mettler AE 200 balance (accurate to 0.1 mg) and the lubricant refreshed. The cleaning and weighing protocol is outlined below.

1. Turn the motor(s) off to stop the motion.
2. Turn the controller off.
3. Remove the loads from the lever arms.
4. Unscrew and remove the pin arms and then remove the pins.
5. Unscrew and remove the level and temperature sensor holder(s).
6. Syringe off any excess lubricant from the lubricant bath(s).
7. Remove the plates.
8. Clean the pins, plates and then machine itself with Gigasept and then acetone.
9. Weigh the pins and plates to the nearest 0.1 mg. Do this three times and then take an average.
10. Reassemble the wear machine and add the new lubricant.
11. Turn the controller on.
12. Start the motion once the lubricant temperature has reached 37°C.

The wear tests were performed up to at least four million cycles.

For the XLPE tests only, soak control specimens were also used which allowed any extra weight (and therefore reduction in apparent wear) due to fluid absorption to be accounted for. These specimens were placed in the wear machine, unloaded, under the same conditions as the loaded pins and plates. Before testing commenced, various cleaning protocols were tested to determined how the different types of cleaning affected the mass measurements of the XLPE samples. The samples were soaked in bovine serum for 66 hours. They were then dried with a cloth and weighed, cleaned with acetone and weighed, cleaned with Gigasept and then acetone and weighed and finally left for 30 minutes at ambient conditions and weighed. The method of cleaning was found to have no effect on the mass measurements.

4.2.3 Surface analysis measurements

Surface topography measurements were performed using the Zygo NewView 100 non-contacting 3D profilometer. At least five measurements of root mean square roughness, S_q were taken at random within the presumed contact zone of both the femoral head and the acetabular cup of each material combination. Also, at least five measurements of S_q were taken of the metal pins and plates of each material composition prior to wear testing. The initial metal-on-metal wear test specimens with sliding motion only were then analysed at the end of the full four million cycle test. However, for the second metal-on-metal wear test on the new machine the surface measurements were performed at regular one million cycle intervals until the end of the five million cycle wear test.

For the final wear tests of the metal pins and plates with rotation, further surface analyses were conducted at regular one million cycle intervals using the light microscope.

4.2.4 Protein gel technique

SDS-PAGE (sodium diodecyl sulphate - polyacrylamide gel electrophoresis; Laemmli 1970) was employed to determine the extent of protein adsorption to the various surfaces. This technique allows the polypeptide components of a protein mixture to be resolved based on their molecular weights and subsequently visualised. A specimen of each material was soaked in bovine serum for twenty four hours before the test. Firstly, the test samples were washed in distilled water, then in tris buffered saline solution (pH 7.4) and again in distilled water. This was done in order to get rid of any excess proteins within any lubricant not physically adsorbed to the surfaces. The samples were then put in separate resealable bags. One hundred microlitres of gel loading buffer, minus dye but containing detergent and reducing agent was then added to each specimen. Each sample was heated in a water bath at

60°C for ten minutes then transferred to an ultrasonic bath for ten minutes to aid protein extraction. As much of the buffer/protein solution was extracted from each sample as possible, put into marked tubes and then heated at 95°C for ten minutes to denature fully the proteins prior to electrophoresis. A small amount of dye was added to each sample to aid gel loading. Electrophoresis was performed using a Mini-PROTEAN II Cell (Bio-Rad) and 12.5% acrylamide, 0.33% N'N'-bio-methylene acrylamide and 0.35 mm thick gels. Low range protein standards (Bio-Rad) were also run on the gel to allow estimation of the molecular weight of the proteins and therefore help determine the identity of the proteins present. Following electrophoresis, the gels were stained to visualise the proteins using the Coomassie Brilliant Blue substitute East Stain (Zoion Research, Worcester, MA, USA) and supplied protocol. A control specimen of each material soaked for twenty four hours in distilled water was also tested with the above procedure. The protein gel technique was performed twice on each material sample.

5. Results

5.1 Friction

5.1.1 Stribeck analyses (CMC fluids)

5.1.1.1 Effect of clearance on friction of CoCrMo/CoCrMo joints

Stribeck analyses were performed on the metal/metal joints with CMC fluids as the lubricant. The general trend throughout the tests was a falling friction factor with increasing Sommerfeld number, indicative of a mixed lubrication regime. Figure 5.1 shows the common shape of Stribeck curve for these joints. Friction factors ranged from 0.34 at low viscosities of CMC fluids to 0.16 at higher viscosities. For those viscosities of CMC fluids within the physiological range, the friction factors produced were of the order of 0.28. Figures 5.2 to 5.6 show the variation in friction factor (runs 1 and 2 averaged) with radial clearance of the joint. Joint no. 3 (radial clearance of 14 µm) gave consistently low values of friction factor. In general friction factor did not seem highly dependent on clearance.
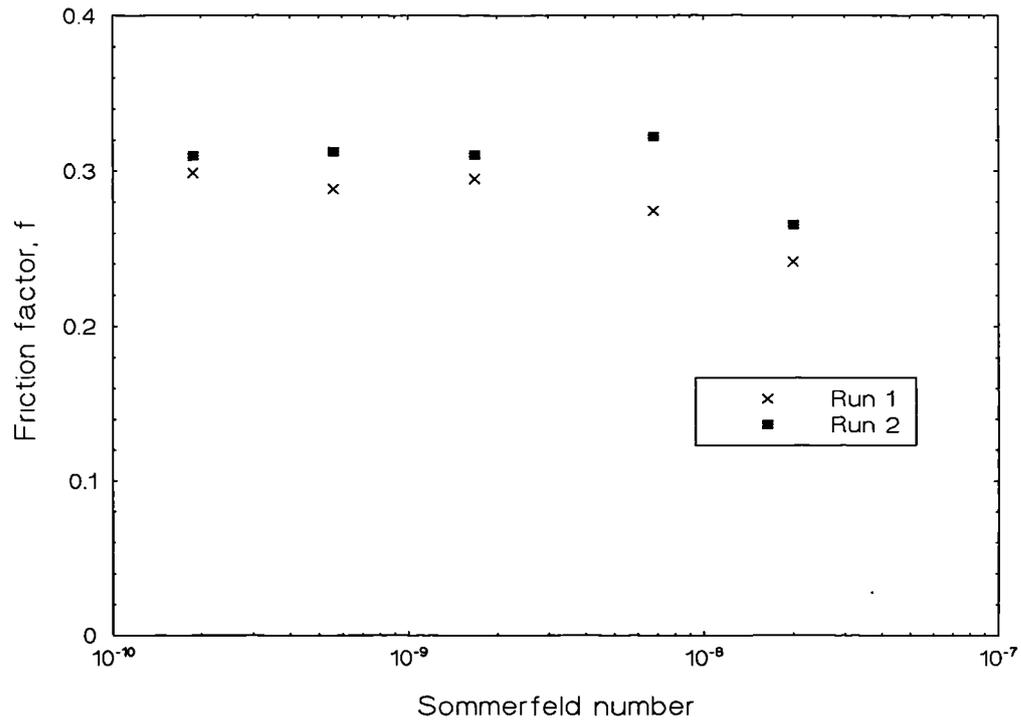
Figure 5.1: Typical Stribeck curve for metal/metal joint
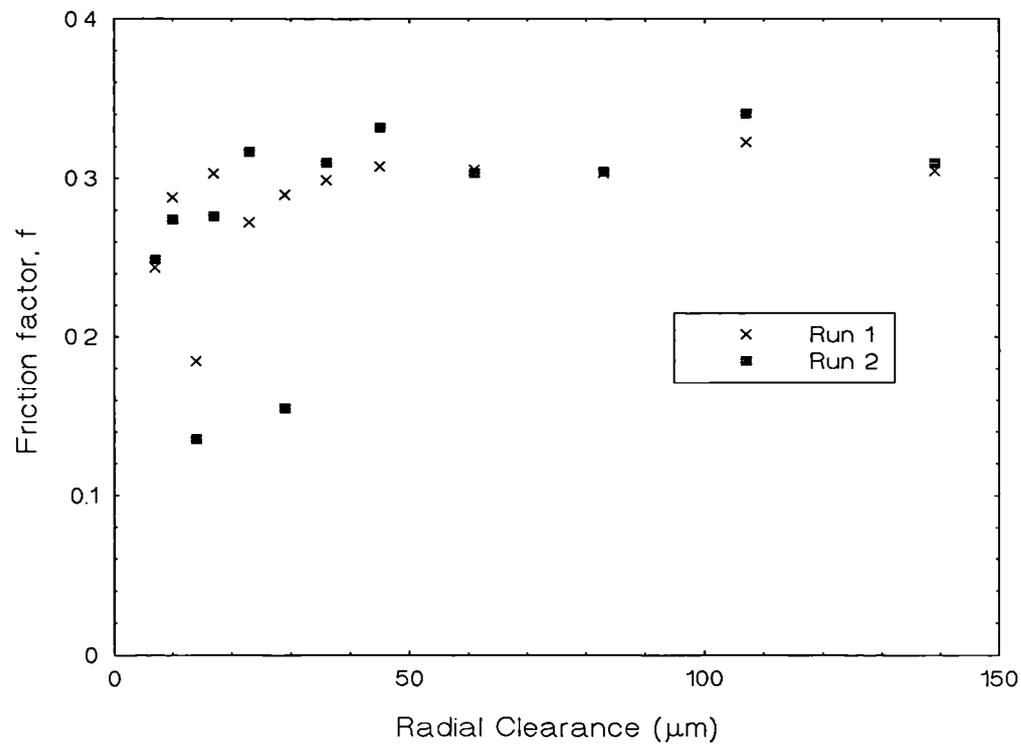
Figure 5.2: Friction factor vs. radial clearance at 0.001 Pa s (metal/metal)
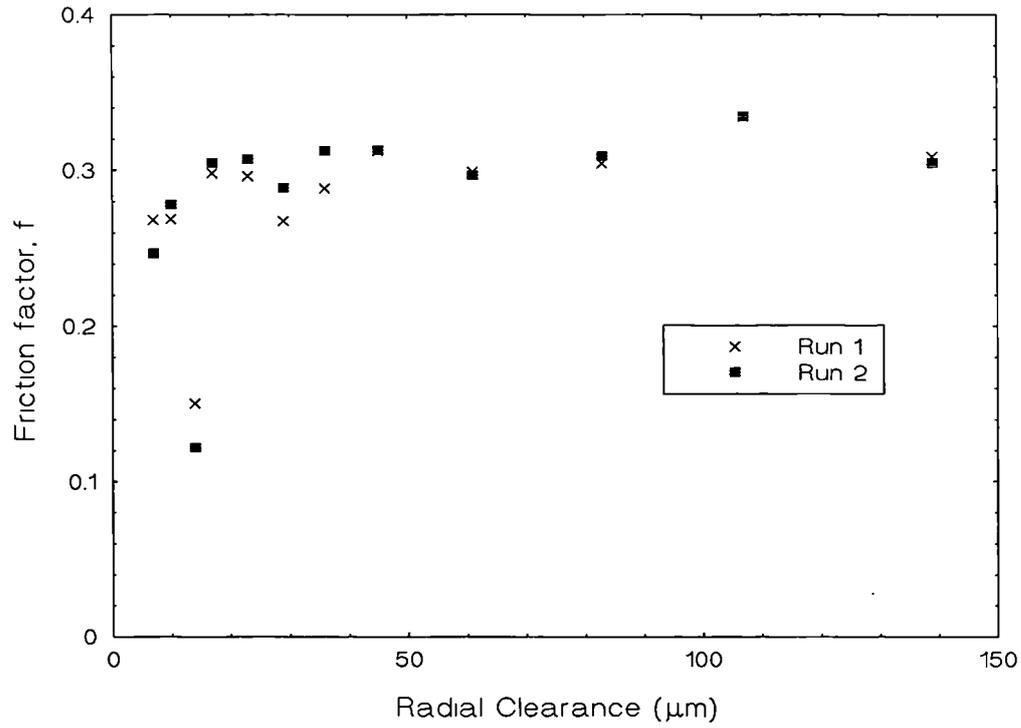
Figure 5.3: Friction factor vs. radial clearance at 0.003 Pa s (metal/metal)
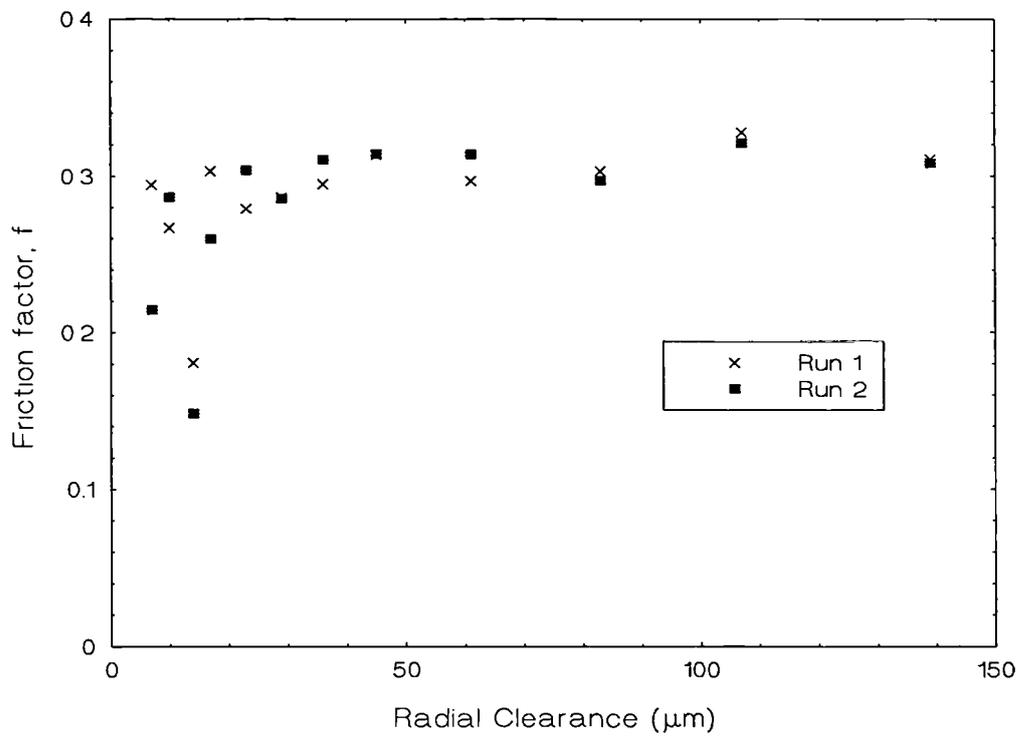
Figure 5.4: Friction factor vs. radial clearance at 0.009 Pa s (metal/metal)
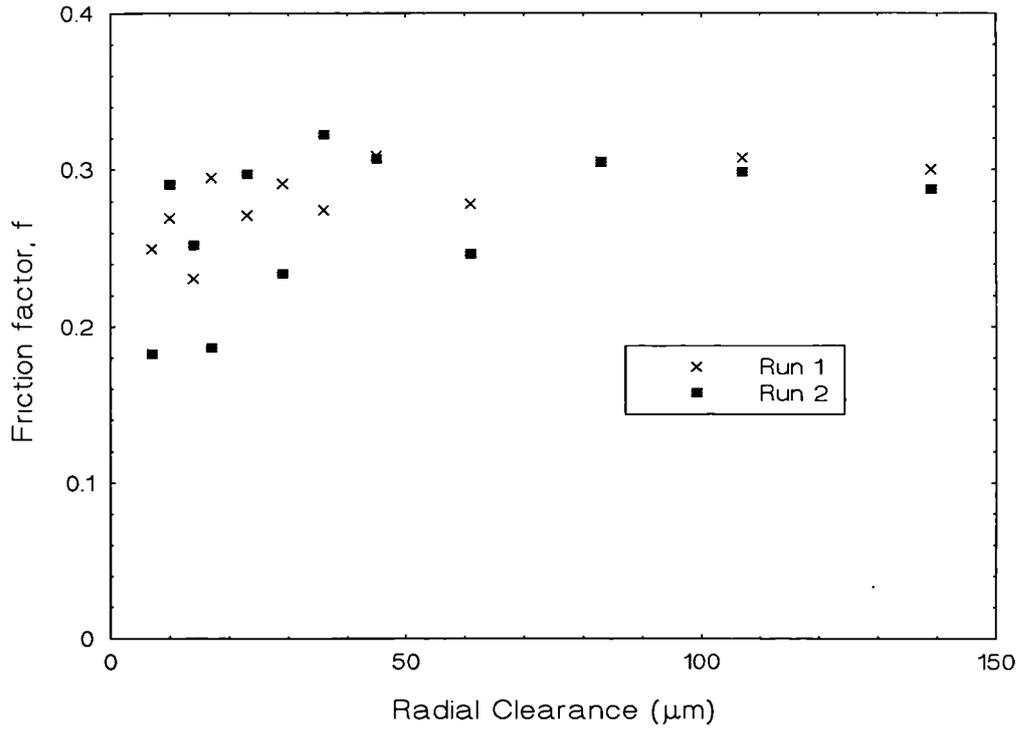
Figure 5.5: Friction factor vs. radial clearance at 0.0364 Pa s (metal/metal)
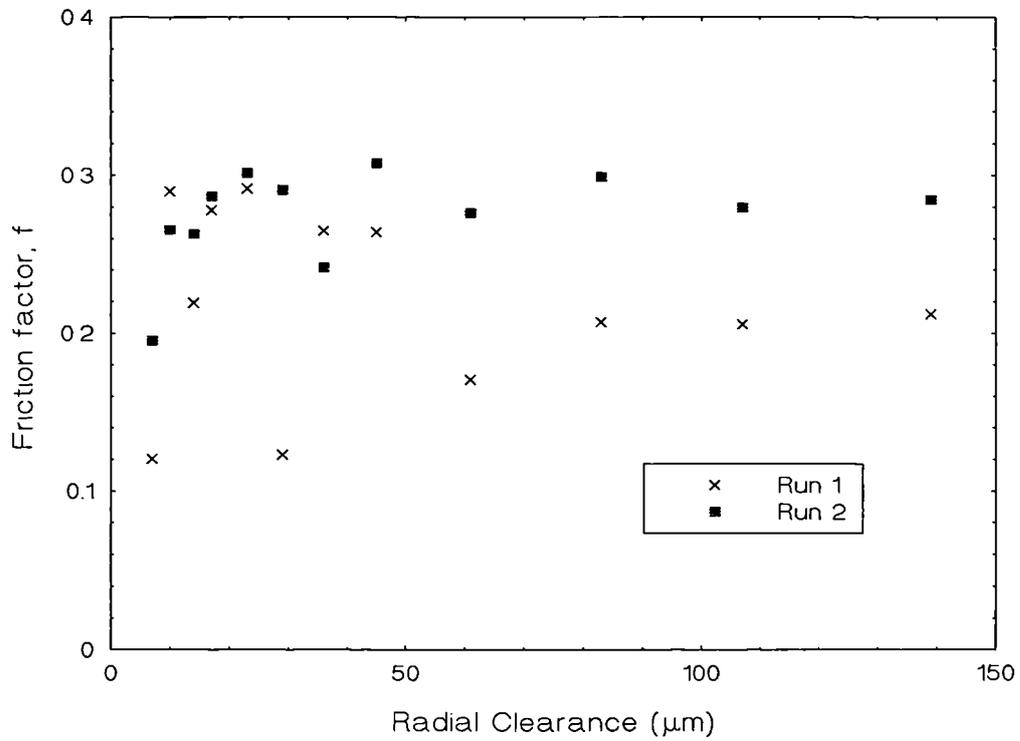
Figure 5.6: Friction factor vs. radial clearance at 0.108 Pa s (metal/metal)

A more thorough Stribeck analysis was performed on three CoCrMo/CoCrMo joints each of 40 μm radial clearance. Again, the general trend throughout these tests was a falling friction factor with increasing Sommerfeld number; indicative of a mixed lubrication regime. Figure 5.7 shows the Stribeck curve averaged over three runs. Friction factors were in the range 0.16 to 0.35 and for those viscosities within the physiological range the friction factors produced were of the order of 0.28.
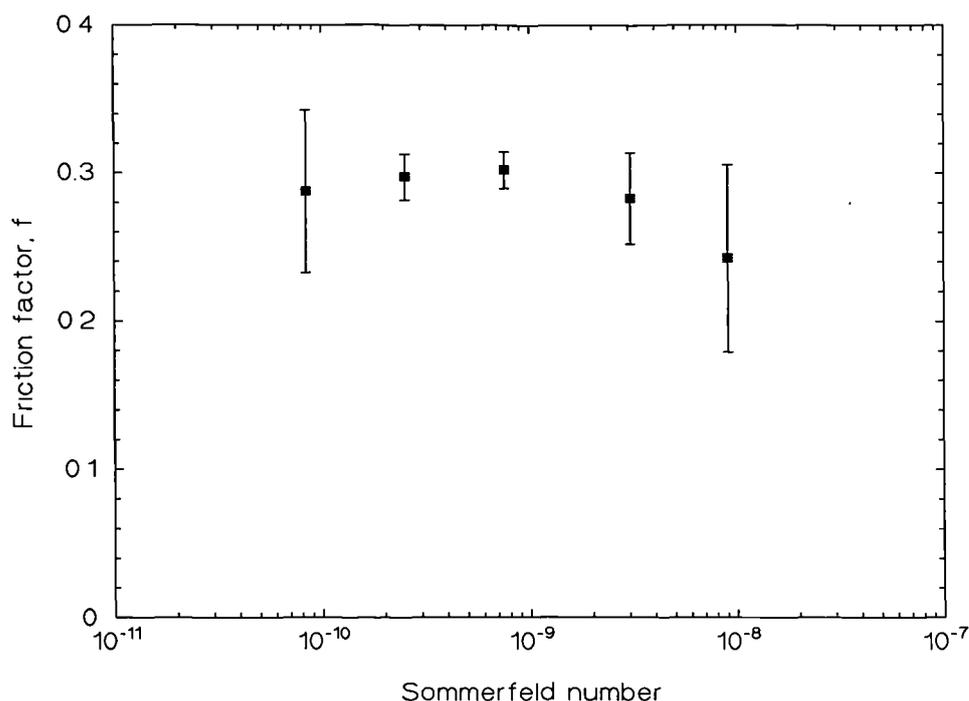
Figure 5.7: Stribeck curve for 40 μm radial clearance (metal/metal) joints

5.1.1.2 Al₂O₃/Al₂O₃ joints

5.1.1.2 Al_2O_3/Al_2O_3 joints

Stribeck analyses were carried out on the ceramic-on-ceramic joints with varying viscosities of CMC fluids and repeated four times for each joint. The results for these tests are shown in Figures 5.8 to 5.12. Plots of friction factor vs. radial clearance were also produced, however, it should be noted that there was very little variation in the radial clearance and therefore a trend is not readily discernible. Figure 5.13 shows an example of friction factor vs. radial clearance at 0.0123 Pa s, all other viscosities followed the same general trend.
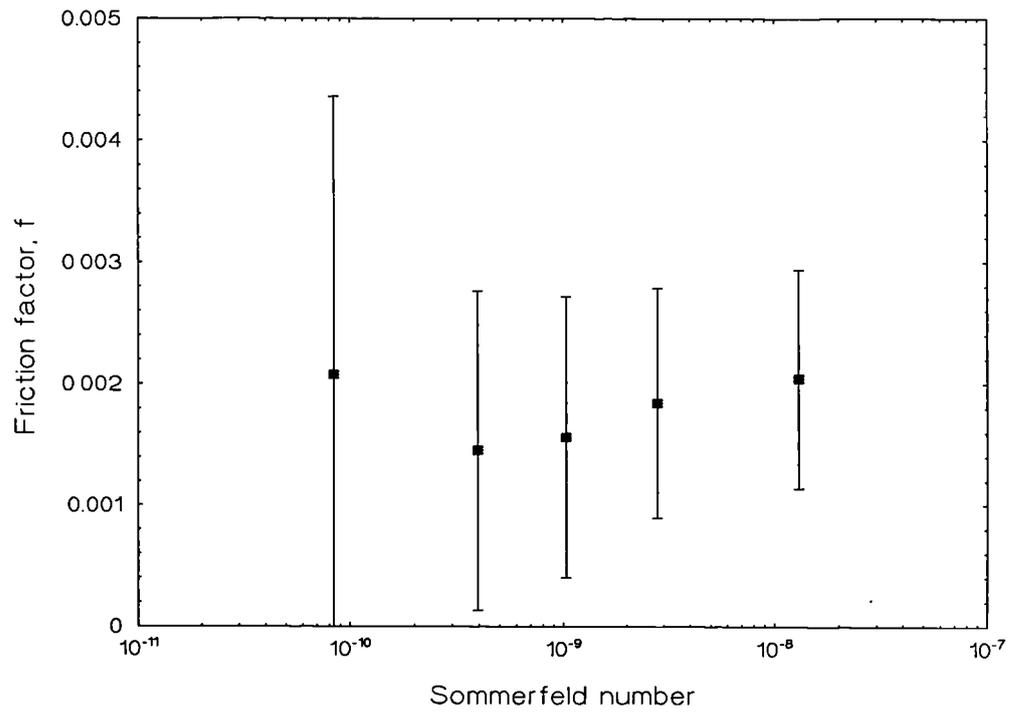
Figure 5.8: Stribeck plot for ceramic/ceramic joint no. 1, all four runs
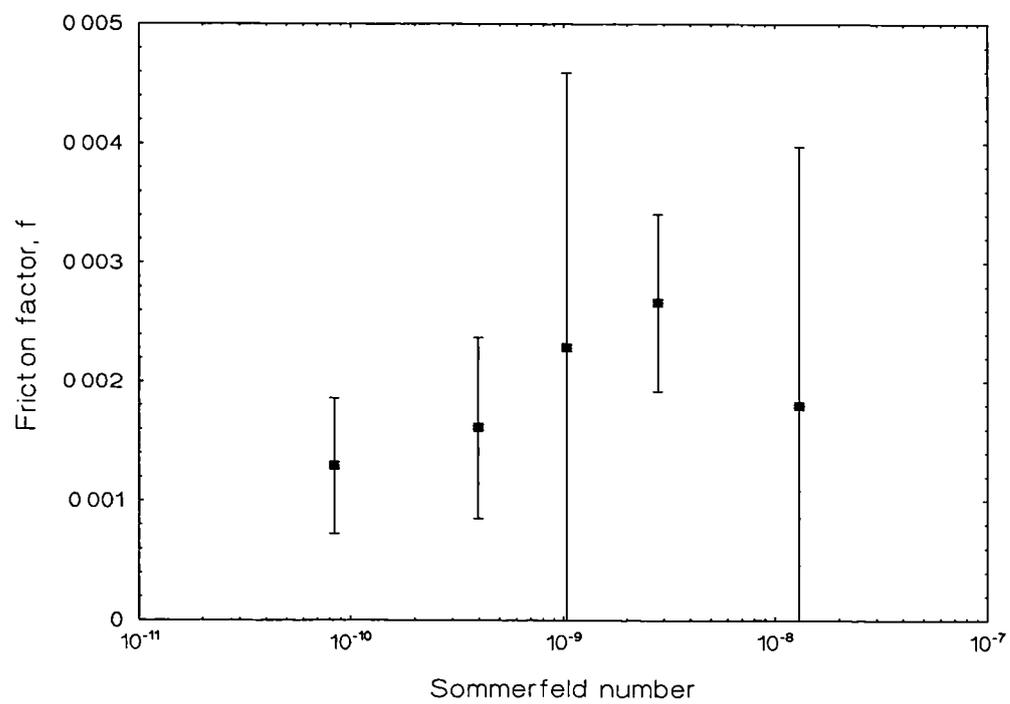
Figure 5.9: Stribeck plot for ceramic/ceramic joint no. 2, all four runs
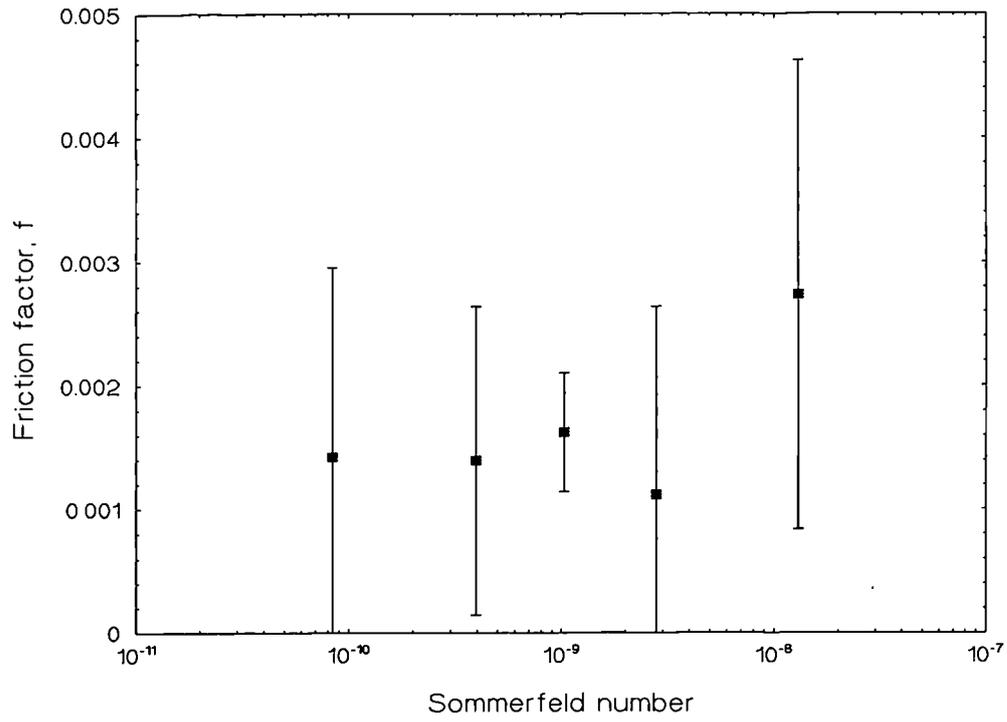
Figure 5.10: Stribeck plot for ceramic/ceramic joint no. 3, all four runs
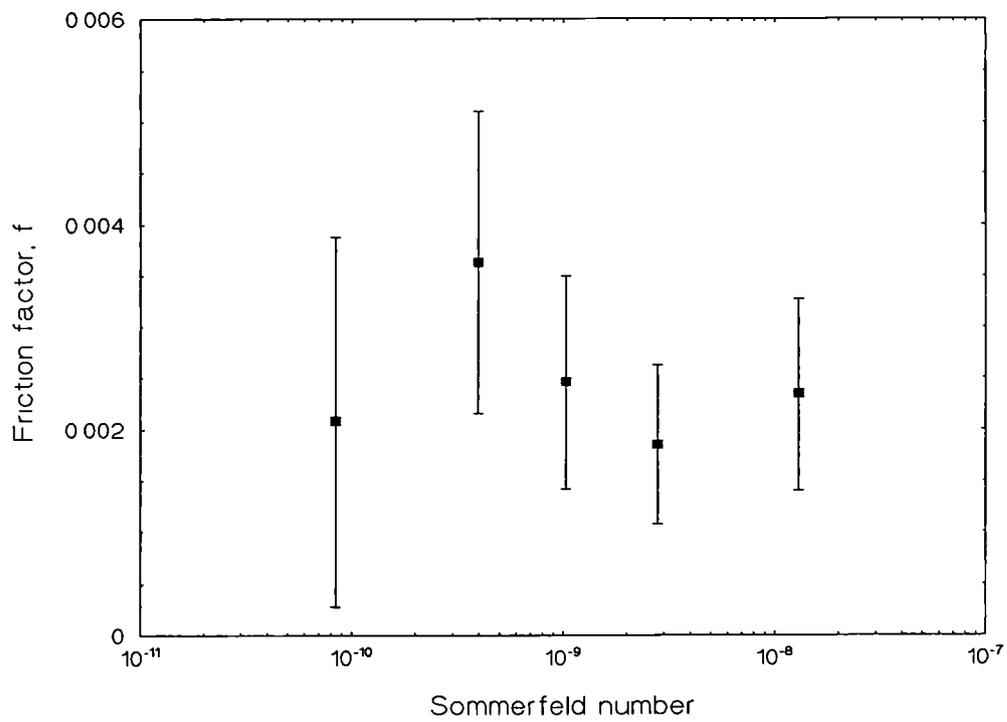
Figure 5.11: Stribeck plot for ceramic/ceramic joint no. 4, all four runs
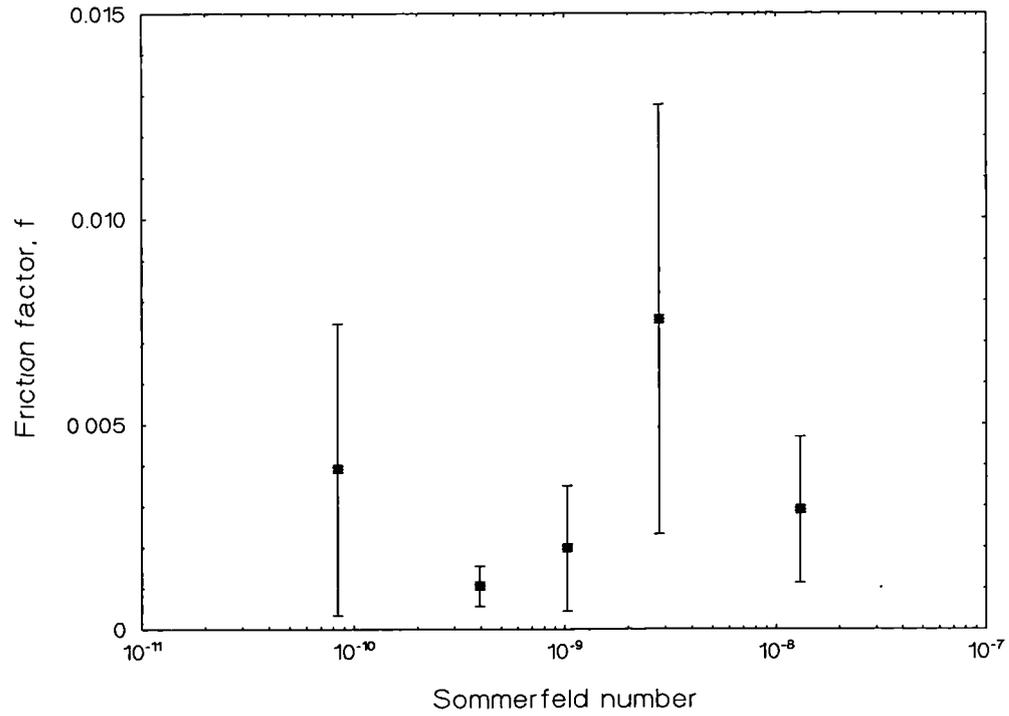
Figure 5.12: Stribeck plot for ceramic/ceramic joint no. 5, all four runs
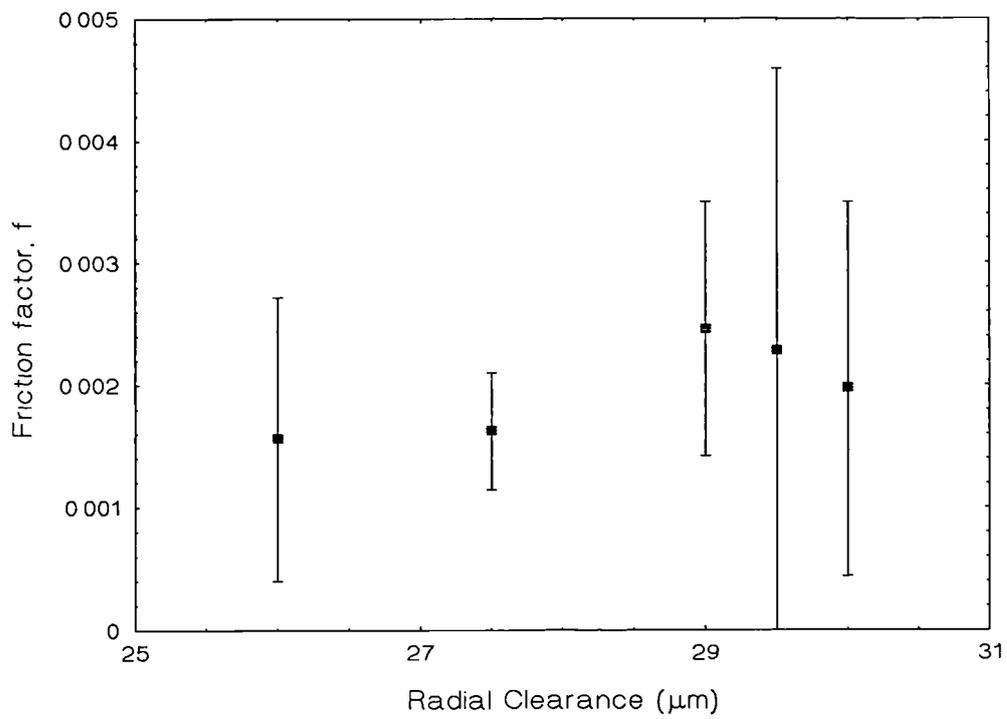
Figure 5.13: Friction factor vs. radial clearance at 0.0123 Pa s (ceramic/ceramic)

The results showed consistently low friction factors for all runs with all joints (0.001-0.01). The Stribeck plots showed an increasing friction factor with Sommerfeld number for the higher viscosities, indicative of a full fluid film lubricating regime. The friction factors produced were two orders of magnitude lower than those for the metal-on-metal joints. There seemed little difference in friction factor with clearance over the small range of clearances tested. Friction factor for CMC fluids within the physiological range of viscosities was of the order of 0.002.

5.1.1.3 CoCrMo/UHMWPE joints

Stribeck analyses were carried out on the metal/plastic joints with varying viscosities of CMC fluids and repeated three times on each joint. The results for these tests are shown in Figures 5.14 to 5.17.
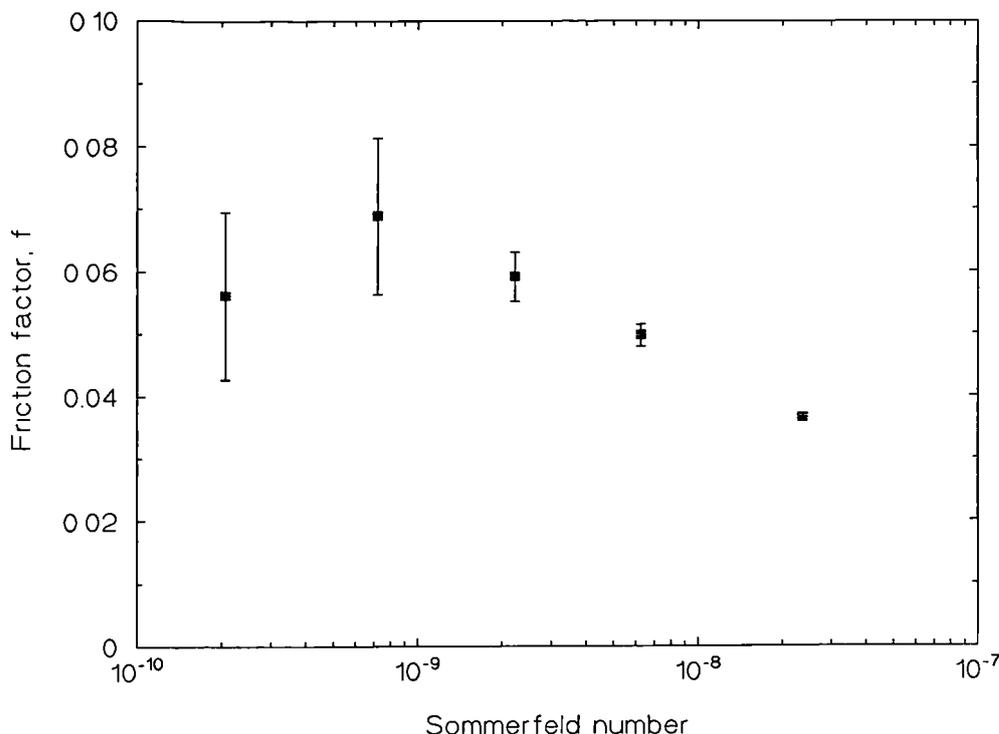
Figure 5.14: Stribeck plot for metal/plastic joint 1, all three runs
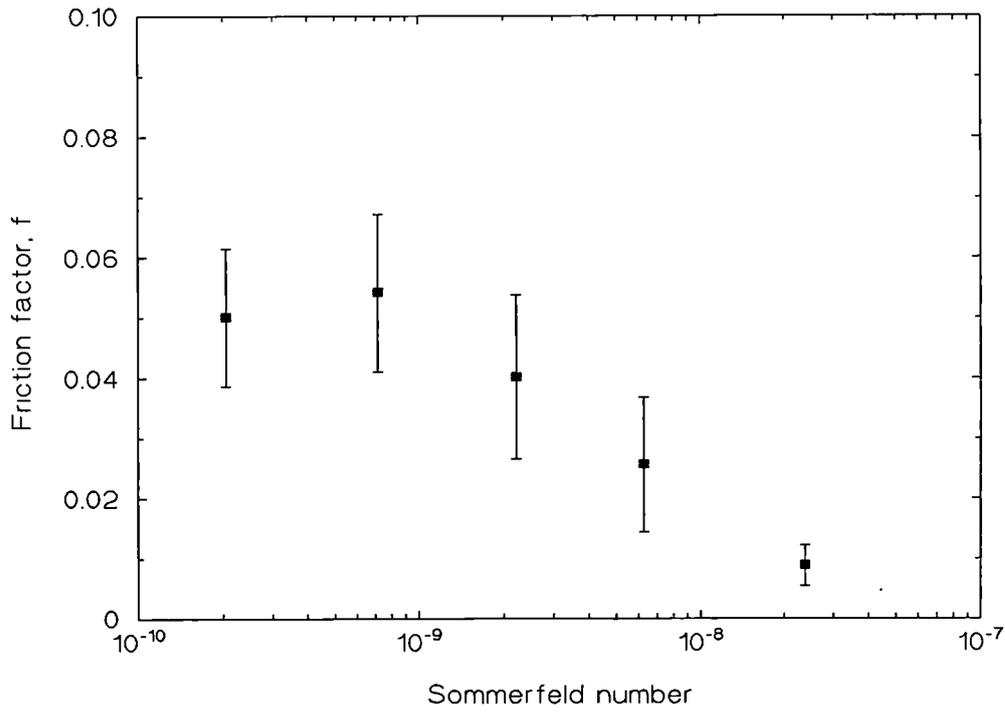
Figure 5.15: Stribeck plot for metal/plastic joint 2, all three runs
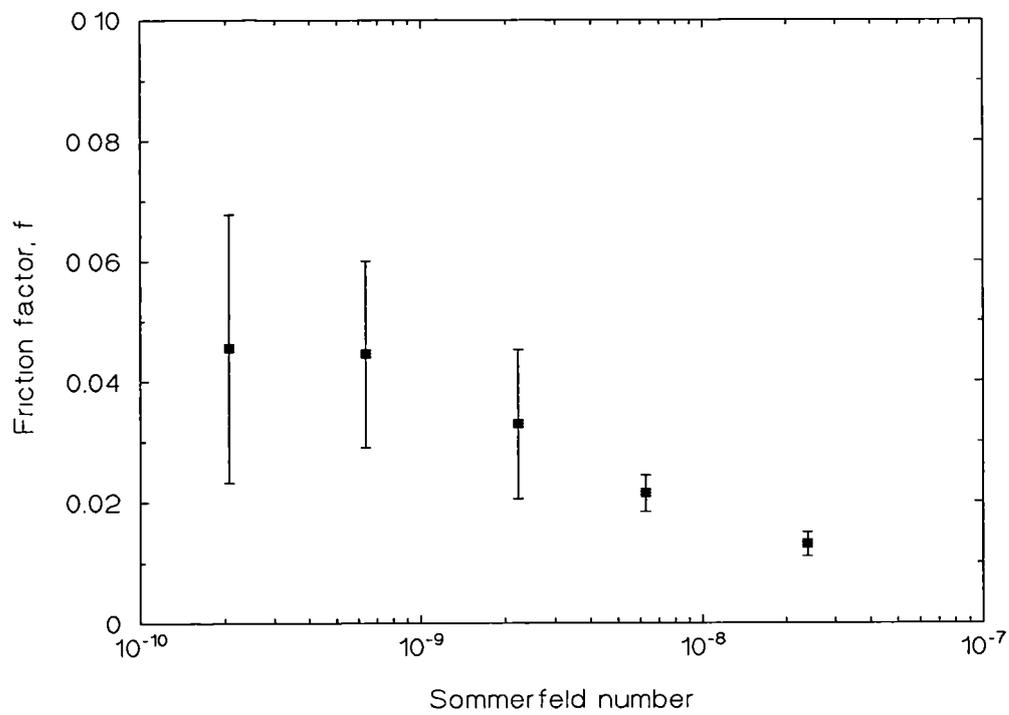
Figure 5.16: Stribeck plot for metal/plastic joint 3, all three runs
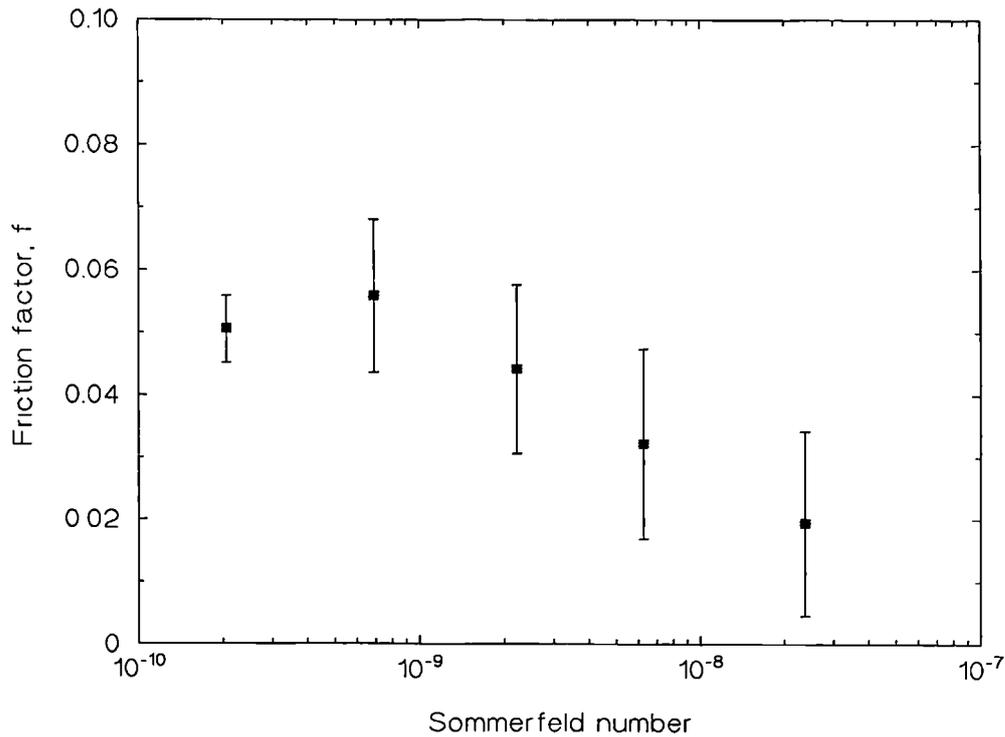
Figure 5.17: Stribeck plot for all metal/plastic joints, all runs

The Stribeck plots show a decreasing friction factor with increasing Sommerfeld number, indicative of a mixed lubrication regime. Friction factors were in the range 0.01-0.07 and for the viscosities of CMC fluids within the range expected for physiological fluids, the friction factors were of the order of 0.05.

5.1.2 Stribeck Analyses (50% bovine serum)

5.1.2.1 CoCrMo/CoCrMo

Tests were performed on a range of clearances using bovine serum of varying viscosities as the lubricant. These tests were performed three times on each joint. Figures 5.18 to 5.23 show the Stribeck curves for each joint, Figure 5.24 shows how friction factor varies with radial clearance. The tests show an almost constant friction factor with increasing Sommerfeld number, indicative of boundary/mixed

lubrication. Friction factors for the physiological range of viscosities were of the order of 0.15. The lowest radial clearance joint (5 μm) gave very high friction compared with the others (0.20 cf. 0.12). In general, as the radial clearance between the femoral head and acetabular cup increased friction factor decreased.
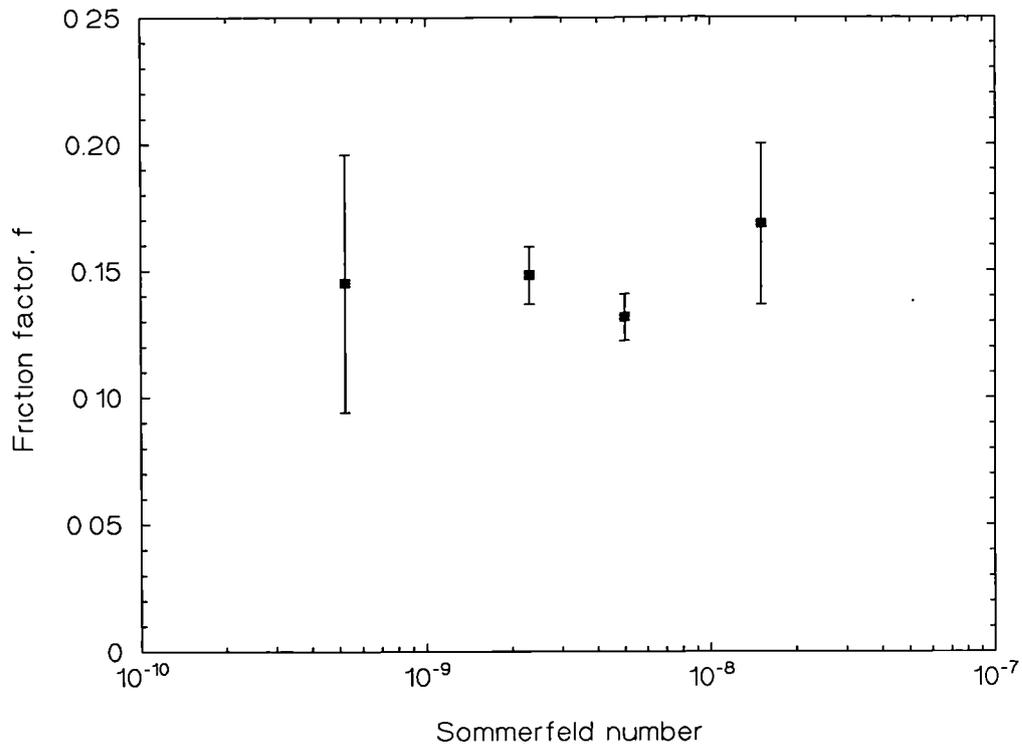
Figure 5.18: Metal C1/H13 (17 μm radial clearance) Stribeck curve for 50% bovine serum
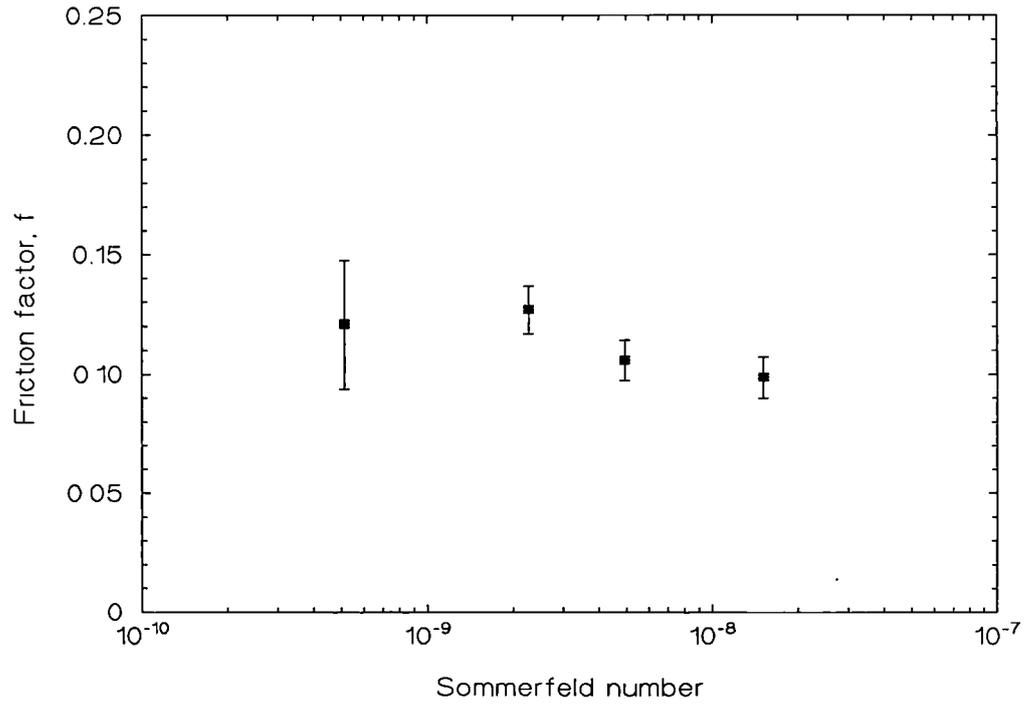
Figure 5.19: Metal C3/H15 (29 μm radial clearance) Stribeck curve for 50% bovine serum
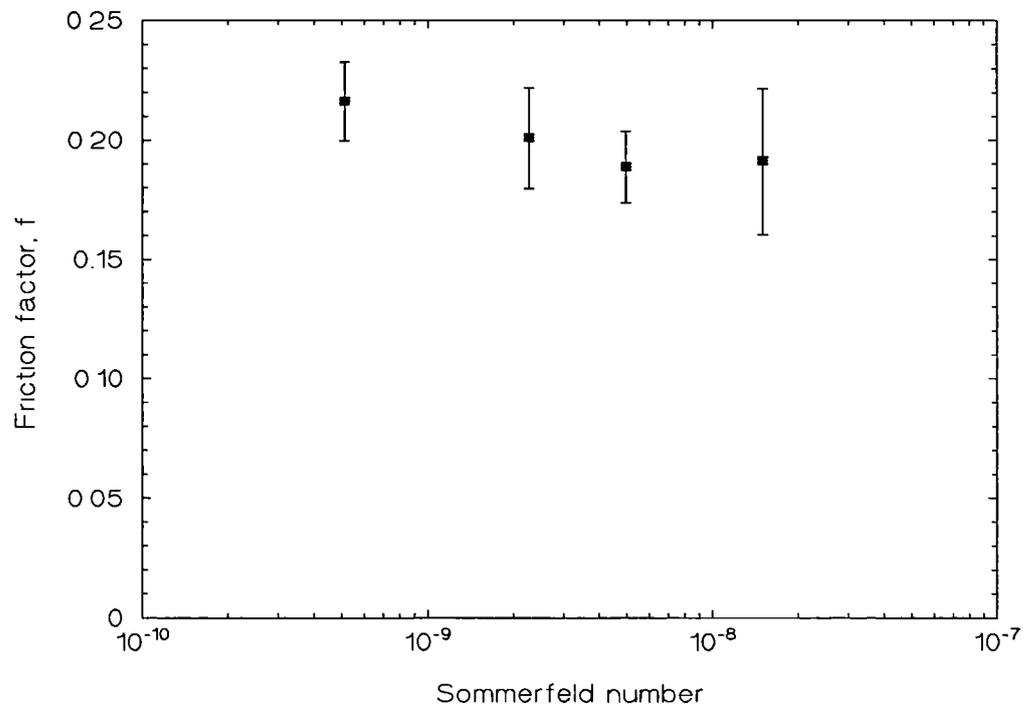
Figure 5.20: Metal C5/H17 (7 μm radial clearance) Stribeck curve for 50% bovine serum
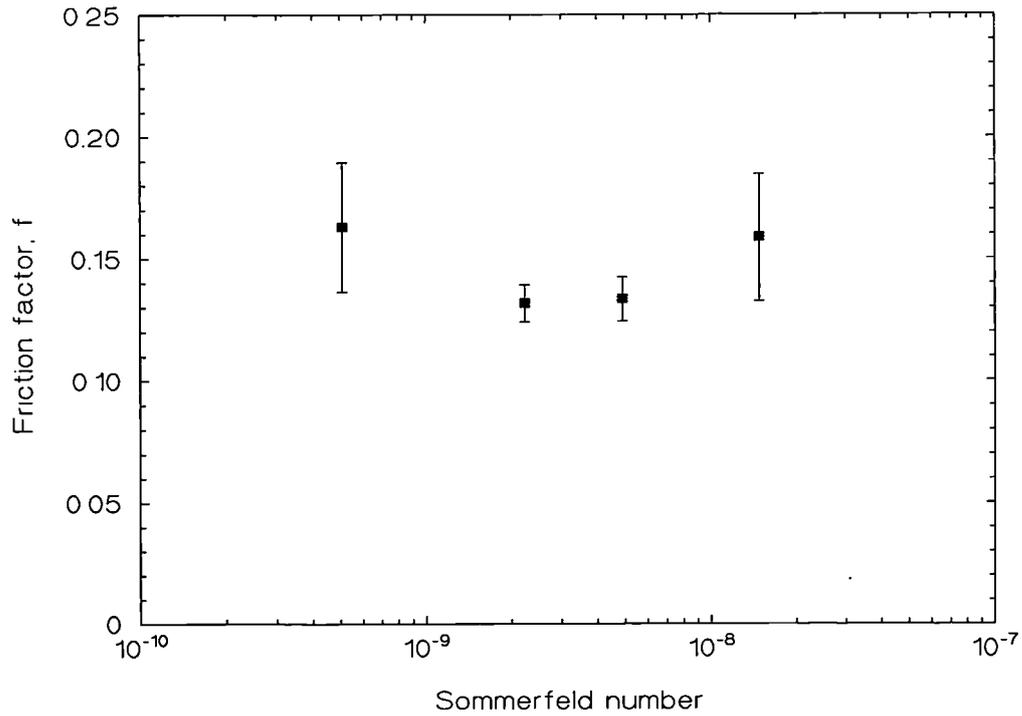
Figure 5.21: Metal C7/H19 (14 μm radial clearance) Stribeck curve for 50% bovine serum
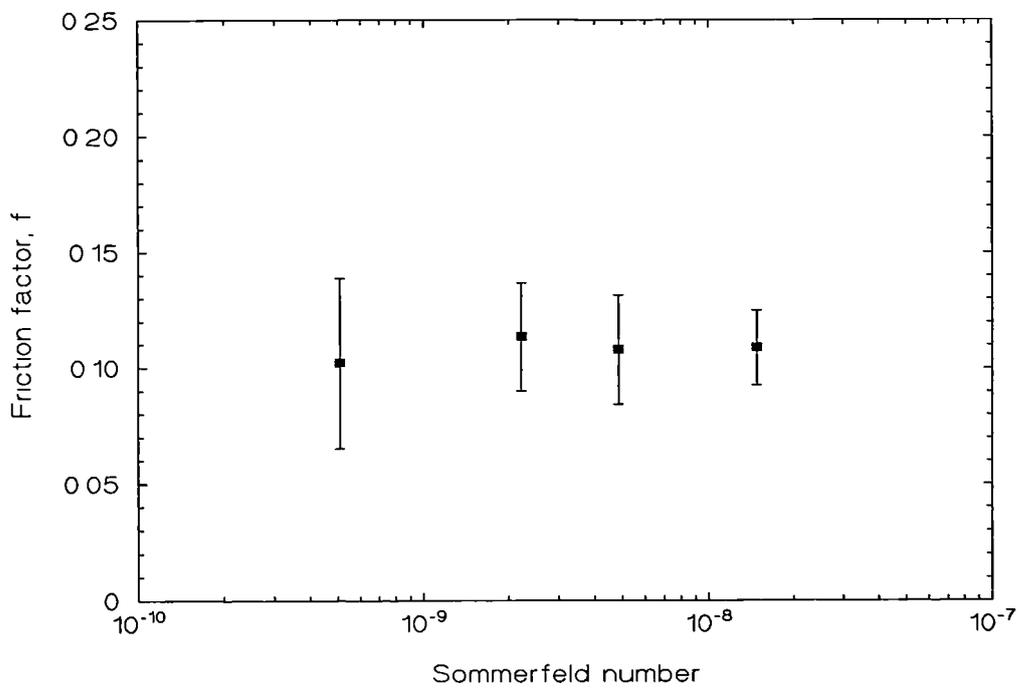
Figure 5.22: Metal C9/H21 (61 μm radial clearance) Stribeck curve for 50% bovine serum

101
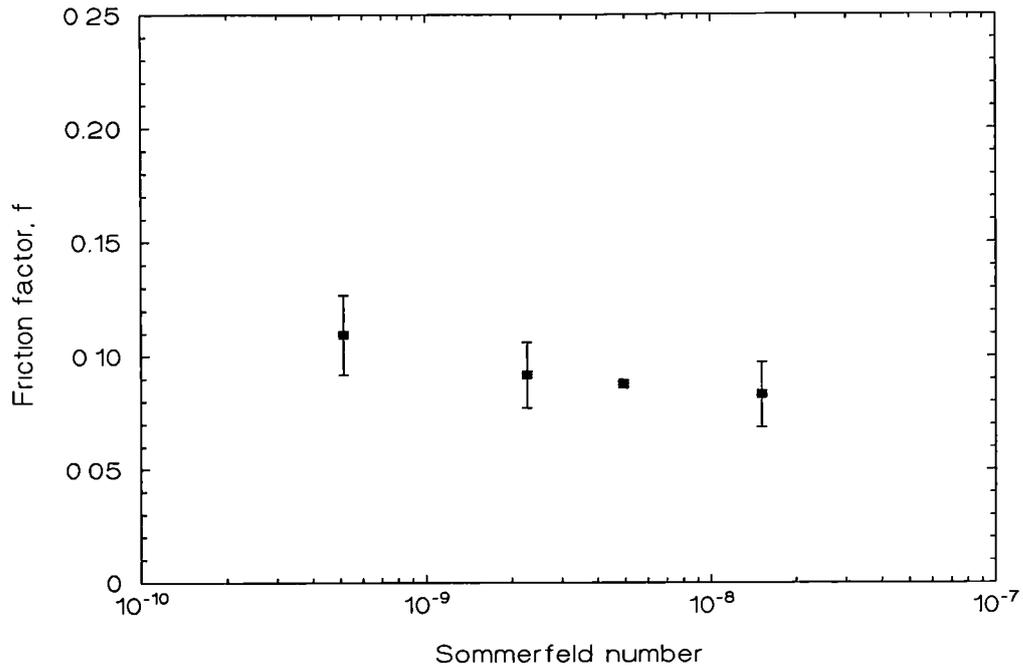
Figure 5.23: Metal C11/H23 (139 μm radial clearance) Stribeck curve for 50% bovine serum
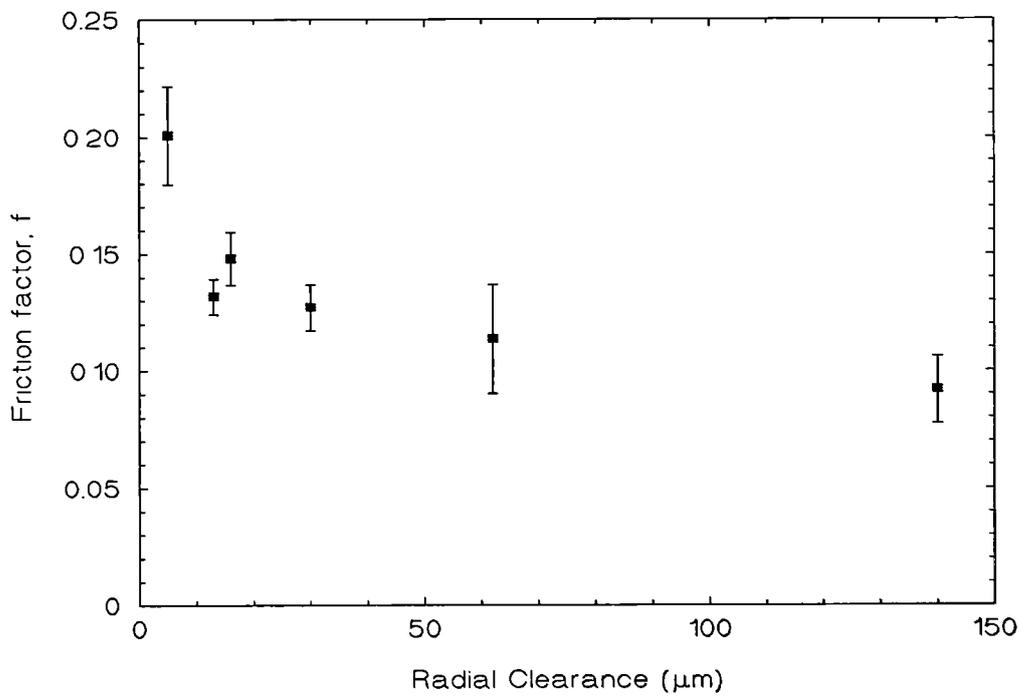
Figure 5.24: Friction factor vs. clearance for the metal/metal joints with 50% bovine serum at 0.011 Pa s

5.1.2.2 Al_2O_3/Al_2O_3

The five ceramic/ceramic joints were tested with varying viscosities of bovine serum, the tests were performed twice on each joint. The results are shown in Figures 5.25 to 5.30.
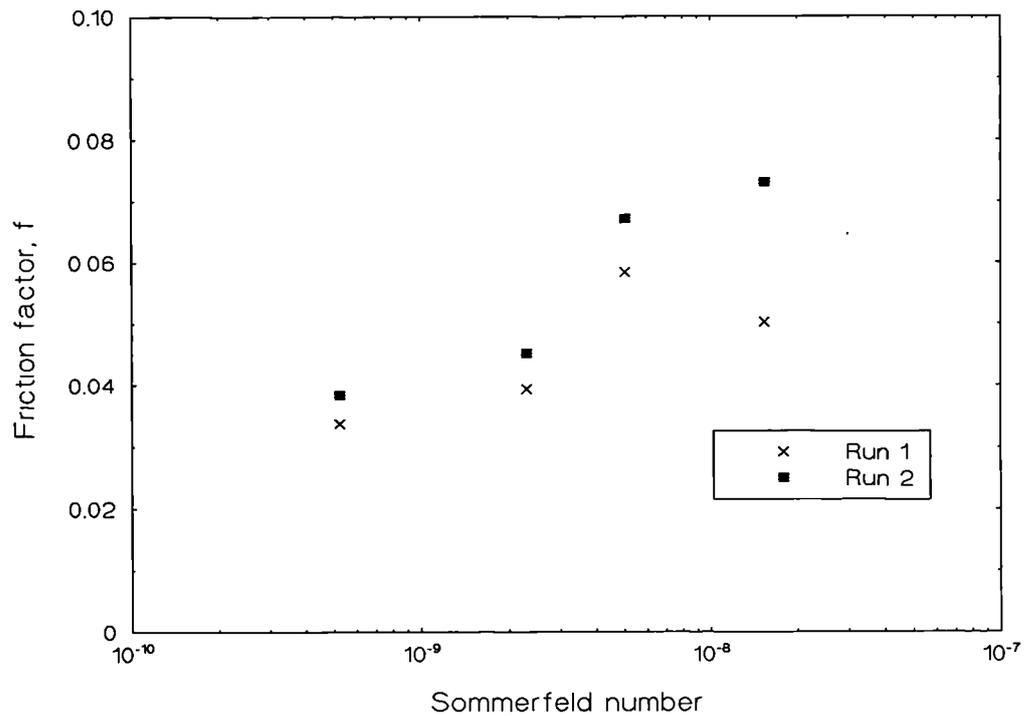
Figure 5.25: Ceramic/ceramic 1 Stribeck curve for 50% bovine serum
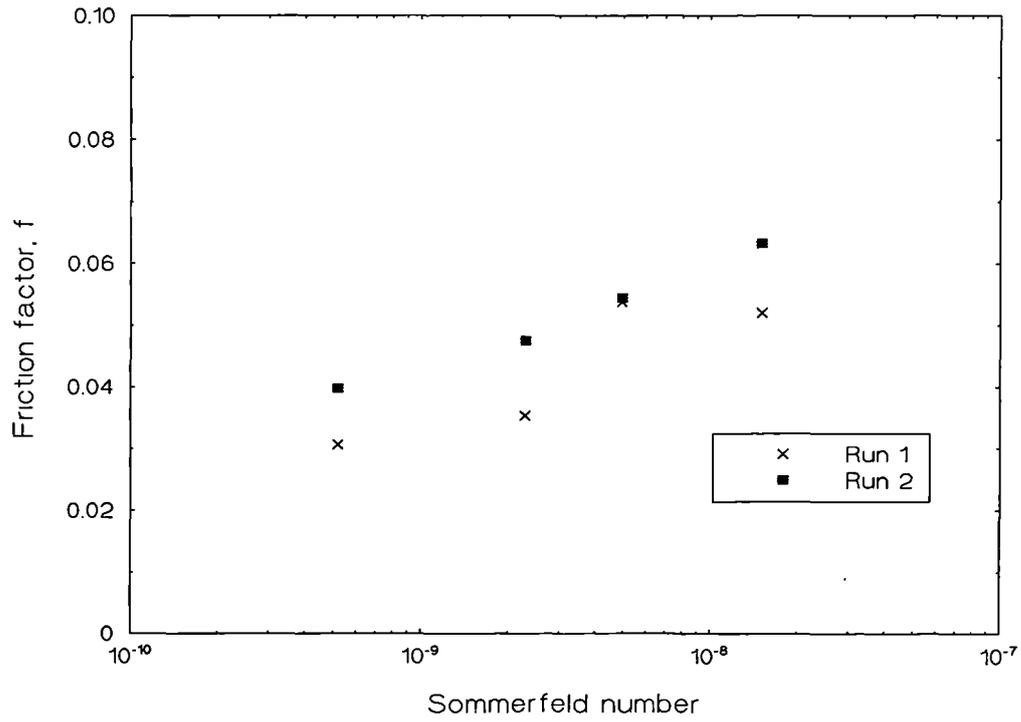
Figure 5.26: Ceramic/ceramic 2 Stribeck curve for 50% bovine serum
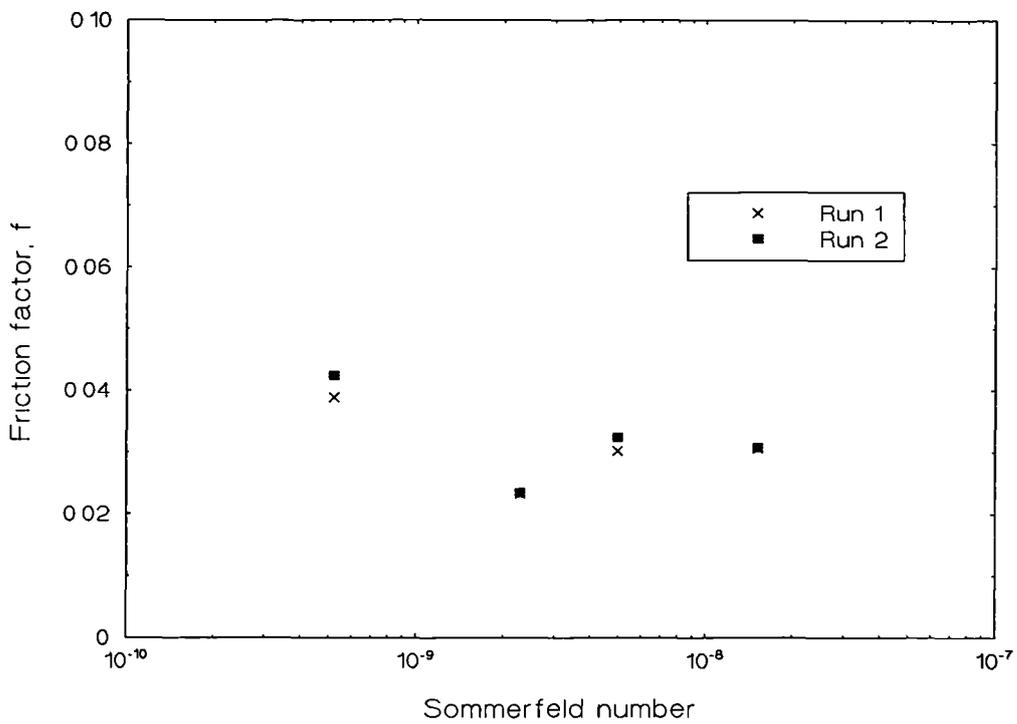
Figure 5.27: Ceramic/ceramic 3 Stribeck curve for 50% bovine serum
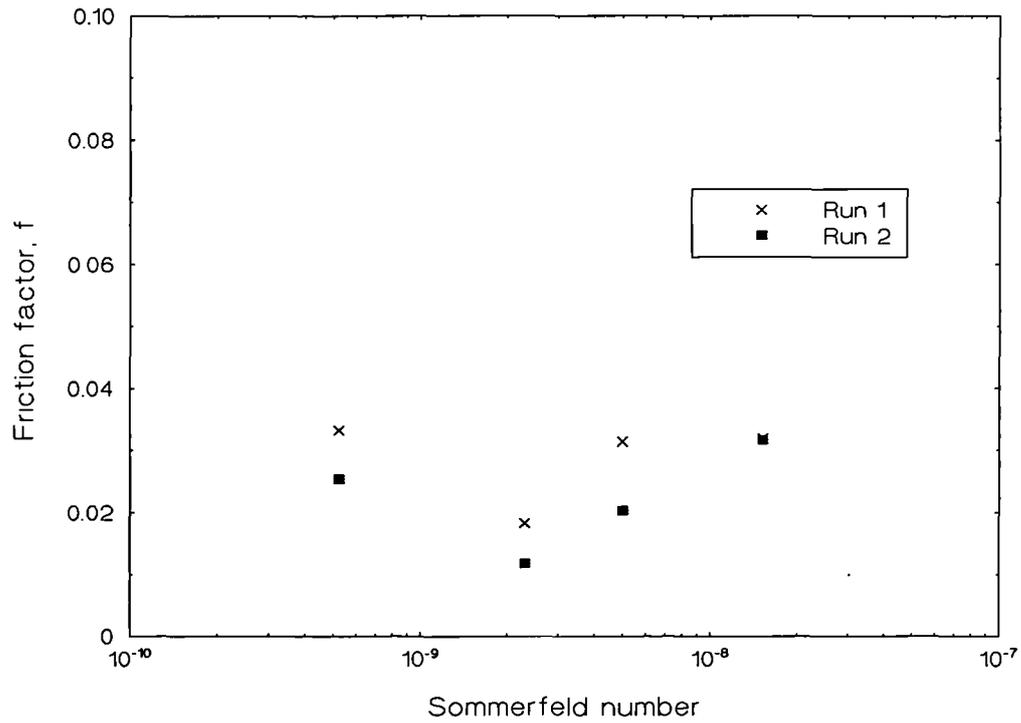
Figure 5.28: Ceramic/ceramic 4 Stribeck curve for 50% bovine serum
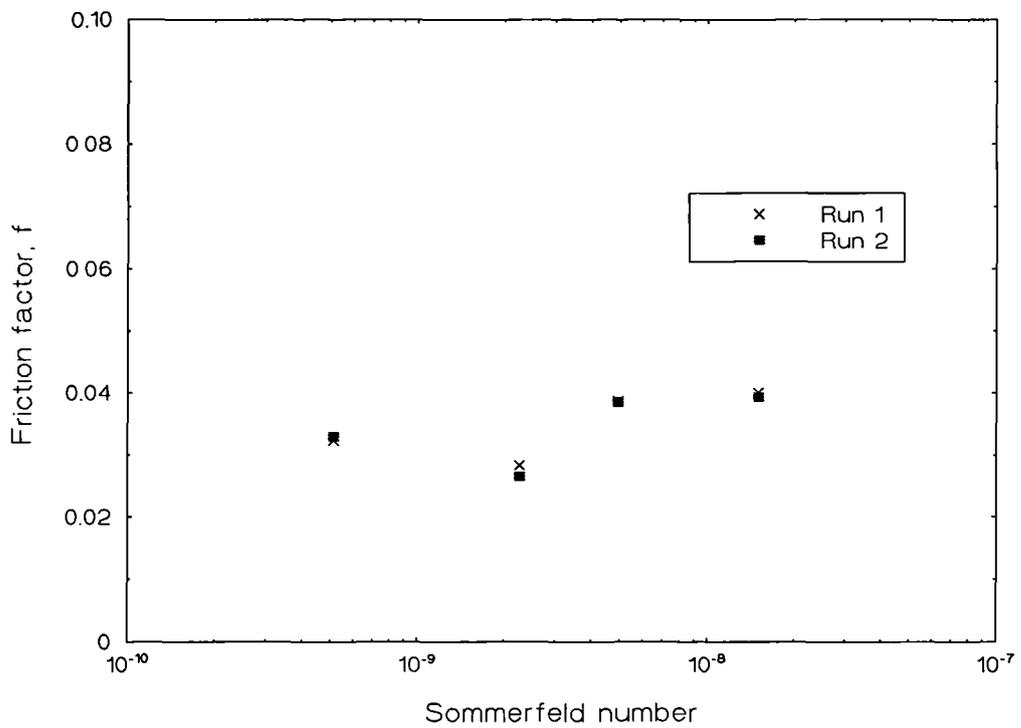
Figure 5.29: Ceramic/ceramic 5 Stribeck curve for 50% bovine serum
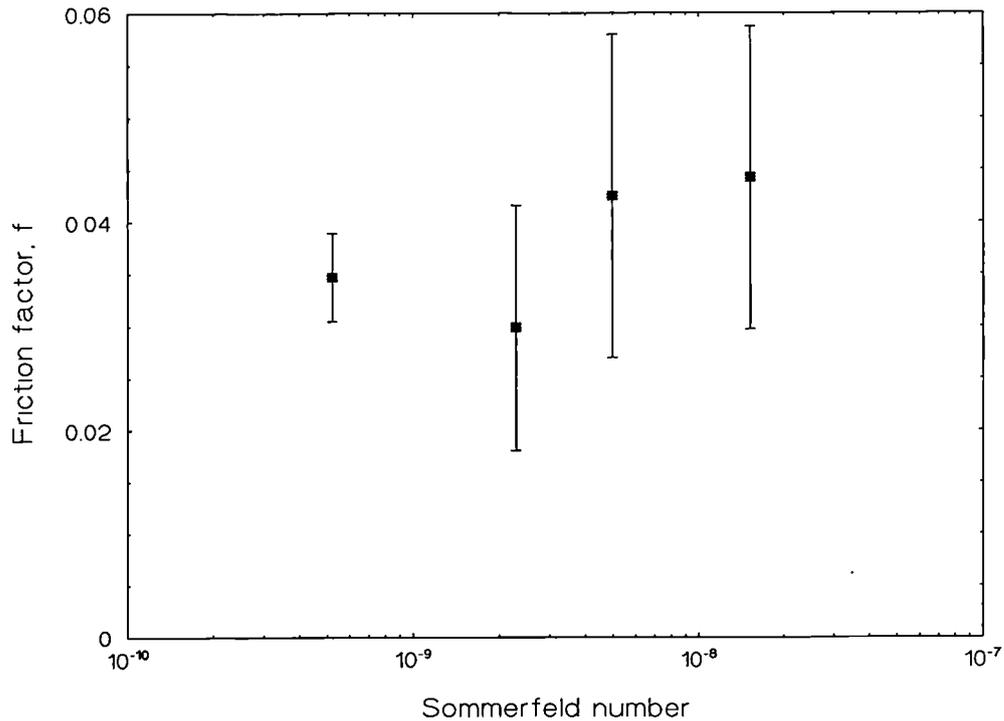
Figure 5.30: Ceramic/ceramic, all joints Stribeck curve for 50% bovine serum

The graphs showed a predominantly rising trend in friction factor with Sommerfeld number, usually related to a full fluid film lubricating regime, however, the friction factors of circa 0.02 to 0.07 are more indicative of a mixed lubrication regime. Friction factors for the physiological range of viscosities were of the order of 0.035.

5.1.2.3 CoCrMo/UHMWPE

The three metal/plastic joints were tested with varying viscosities of bovine serum, each joint was tested twice to produce the Stribeck plots shown in Figures 5.31 to 5.34.
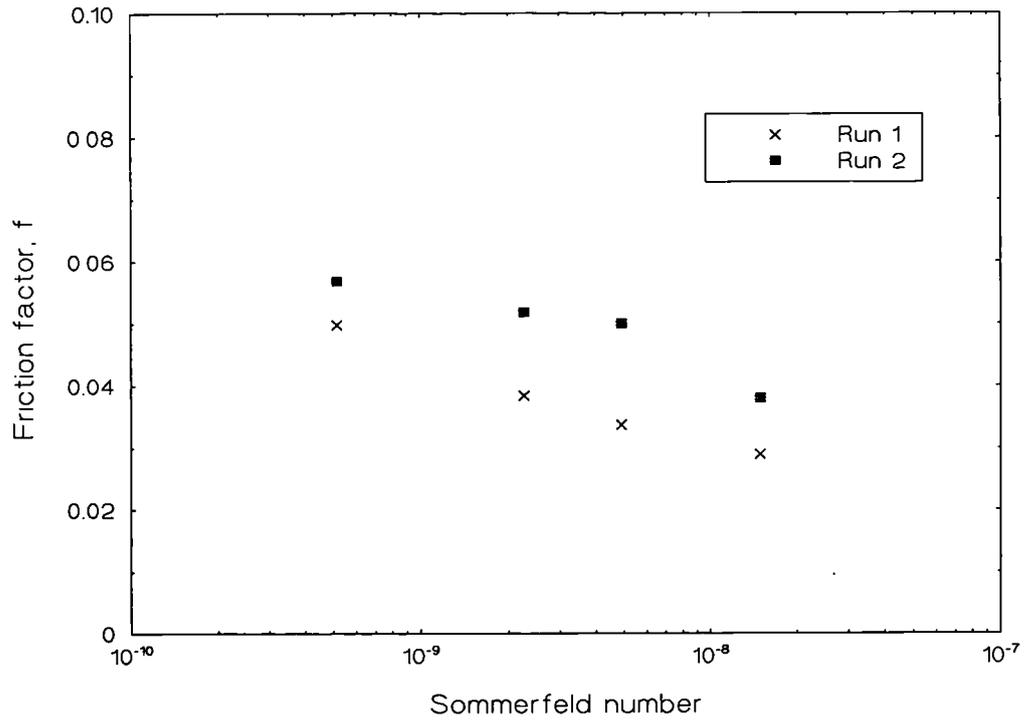
Figure 5.31: Metal/plastic 1 Stribeck curve for 50% bovine serum
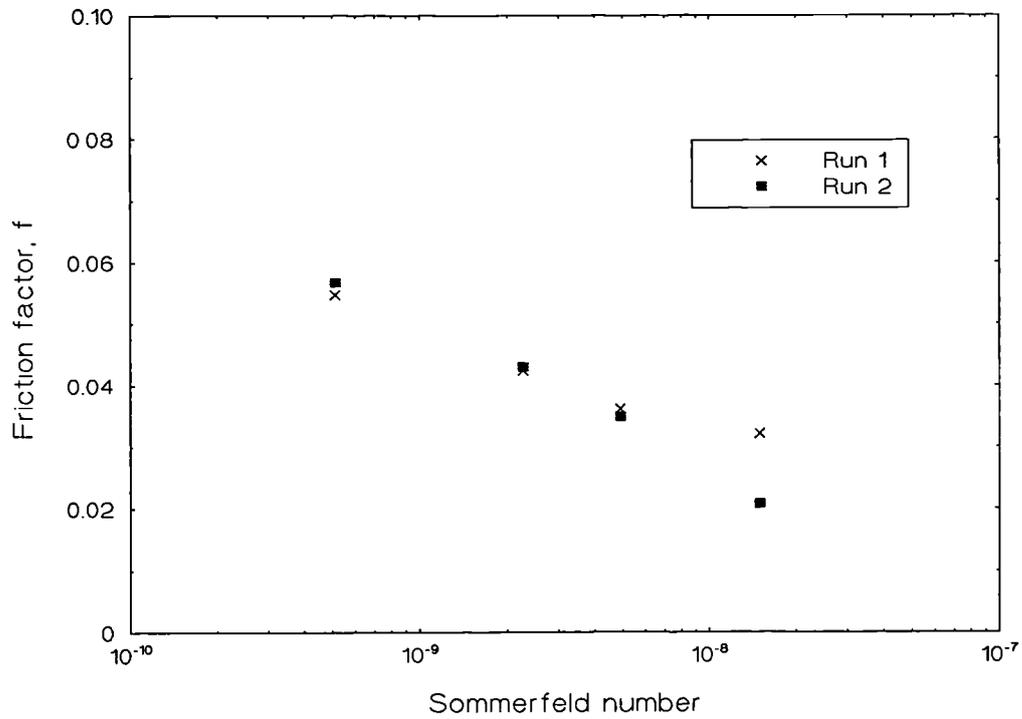
Figure 5.32: Metal/plastic 2 Stribeck curve for 50% bovine serum
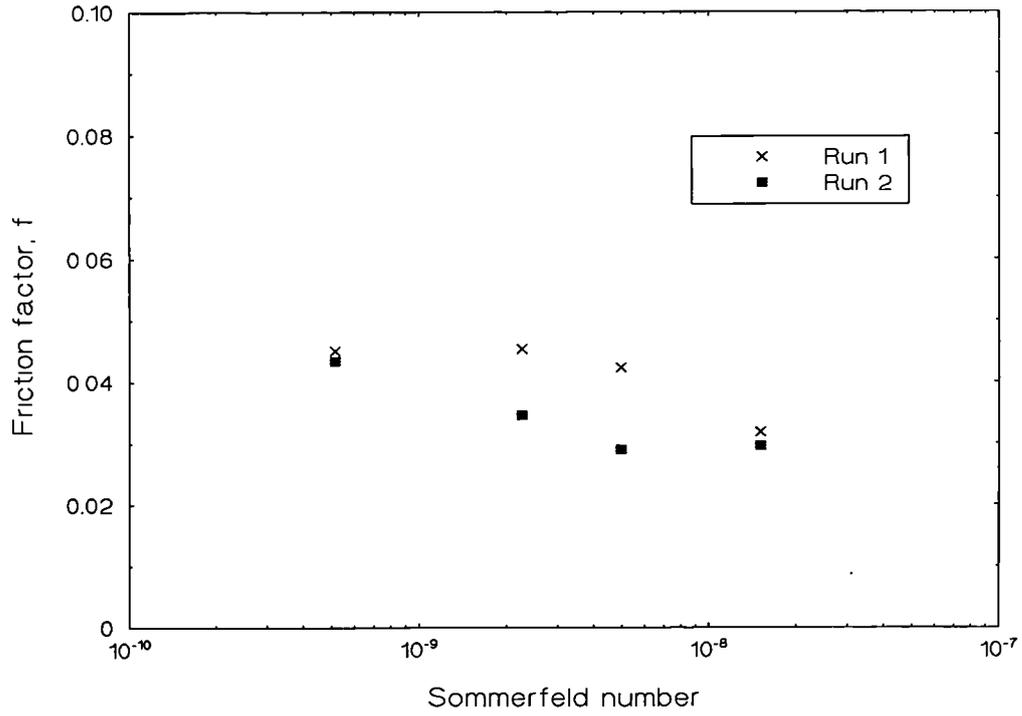
Figure 5.33: Metal/plastic 3 Stribeck curve for 50% bovine serum
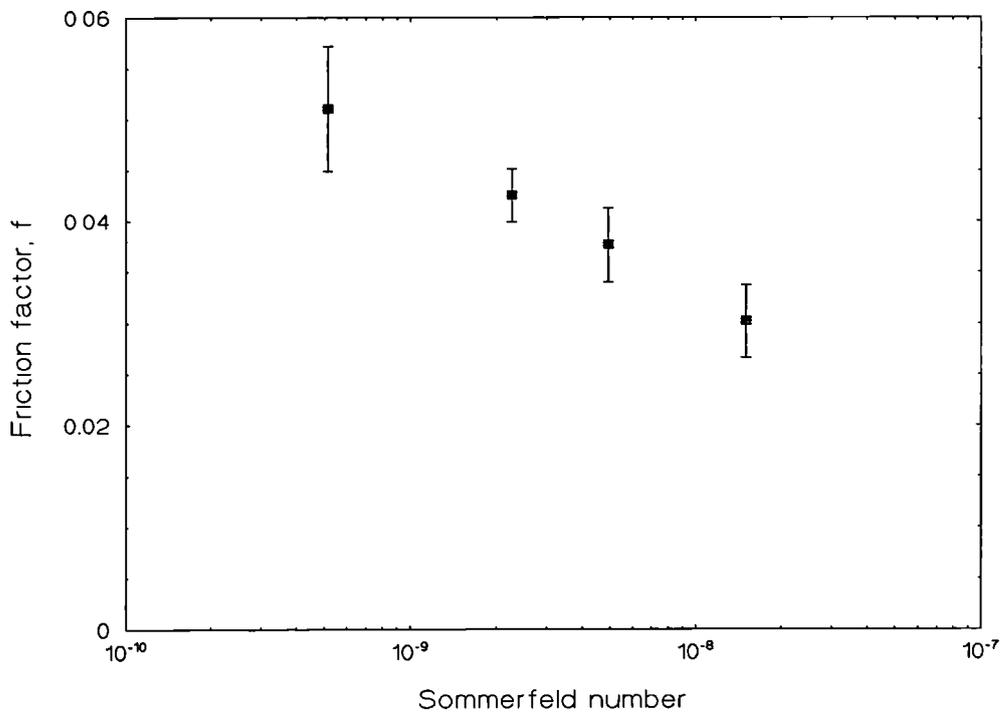
Figure 5.34: Metal/plastic, all joints Stribeck curve for 50% bovine serum

The falling friction factor with increasing Sommerfeld number was indicative of a mixed lubrication regime. The friction factor values were of the same order as those produced by the ceramic/ceramic joints when lubricated with different viscosities of bovine serum (circa 0.05 for the physiological range of viscosities).

5.1.3 Bovine serum vs. synovial fluid - filtered and unfiltered

5.1.3.1 CoCrMo/CoCrMo

Tests were performed to assess the effect on friction of both filtered (1 μm filter) and unfiltered bovine serum and synovial fluid. Three tests were performed on two joints, each of 40 μm radial clearance. Figure 5.35 shows the results of these tests (the friction factors for each joint were averaged together).
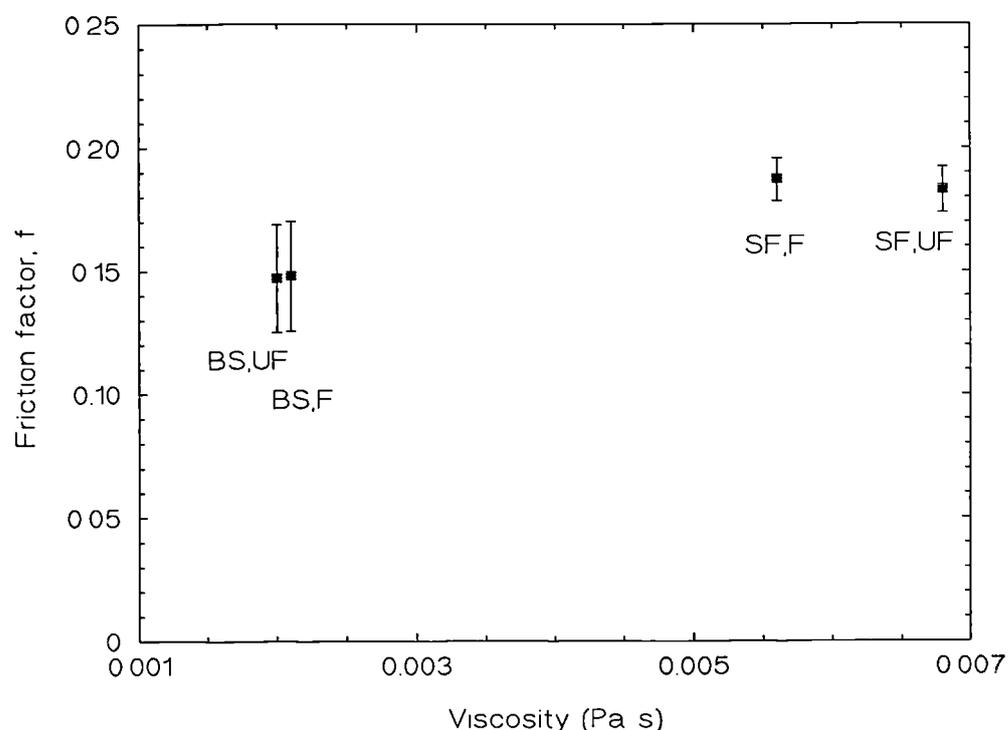
Figure 5.35: Filtered (F) and unfiltered (UF) bovine serum (BS) and synovial fluid (SF) (metal/metal)

There was little difference between the filtered and unfiltered samples of both bovine serum and synovial fluid. Bovine serum, however, gave a lower friction factor than synovial fluid. Compared with the values of friction factor for CMC fluids of equivalent viscosities to bovine serum and synovial fluid, the biological lubricants gave lower friction than the CMC lubricated tests (0.18 cf. 0.28).

5.1.3.2 Al_2O_3/Al_2O_3

Tests were also performed on the ceramic/ceramic joints with filtered and unfiltered bovine serum and synovial fluid, each of the five joints was tested twice. Unlike the metal-on-metal joints which showed a reduction in friction factor when lubricated with biological lubricants as opposed to CMC fluids, the ceramic-on-ceramic joints showed the opposite effect. Friction factor was increased by one order of magnitude when either bovine serum or synovial fluid were used as the lubricant (0.06 cf. 0.002). The results are shown in Figure 5.36.
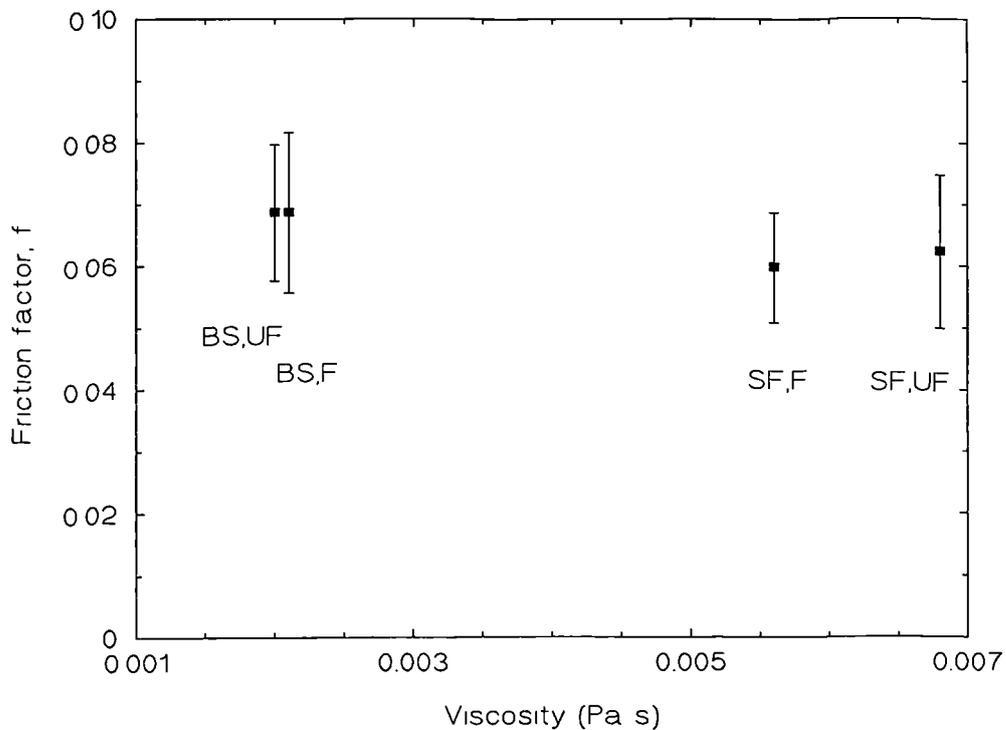
Figure 5.36: Filtered (F) and unfiltered (UF) bovine serum (BS) and synovial fluid (SF) (ceramic/ceramic)

Again, there was no difference between the friction factors produced with filtered and unfiltered lubricants. Also, little difference existed between the bovine serum and synovial fluid results.

5.1.3.3 CoCrMo/UHMWPE

Each of the three metal/plastic joints was tested twice with both filtered and unfiltered bovine serum and synovial fluid. The results are shown in Figure 5.37. The friction factors produced by the biological lubricants were slightly higher than those produced by CMC fluids of the same viscosity (0.06 cf. 0.05). The bovine serum gave slightly higher friction than the synovial fluid.
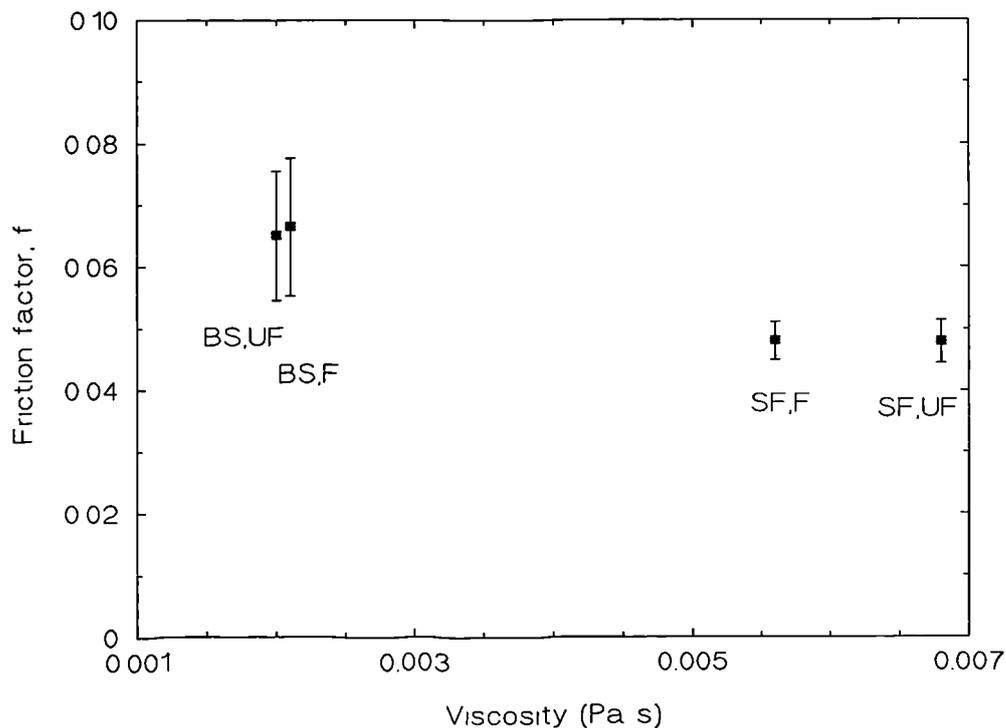
Figure 5.37: Filtered (F) and unfiltered (UF) bovine serum (BS) and synovial fluid (SF) (metal/plastic)

5.1.4 Static loading tests

Previous tests on both conventional joints and hard bearing surfaces suggested some boundary lubricating action when lubricated with biological fluids. To verify this, statically loaded tests were performed on the CoCrMo/CoCrMo joints, the Al_2O_3/Al_2O_3 joints and the CoCrMo/UHMWPE joints. Both bovine serum and synovial fluid were tested separately, using CMC fluids of equivalent viscosities to these biological fluids as the control fluid. Using a static load of 1000 N (i.e. a minimum and maximum load of 1000 N), the joints were tested under the normal and inverse loading conditions. The joints were then tested with a static load of 2000N. Each test was performed at least twice. The results are plotted as friction factor versus viscosity for all joint combinations.

Tests were also performed at static loads of 500 N and 1500 N with CMC fluids as the lubricant to determine the relationship between friction factor and load with these static loads.

5.1.4.1 CoCrMo/CoCrMo

The results of the static loading tests with biological fluids and CMC fluids at 1000 N and 2000 N are shown in Figures 5.38 and 5.39. Figure 5.40 shows the variation of friction factor with static load lubricated with CMC fluids. Three joints of the same radial clearance were tested twice. In each case the biological lubricants gave lower friction than the CMC tests, again, indicating some boundary lubricating action. There was no difference between the friction factors produced by the bovine serum and synovial fluid.
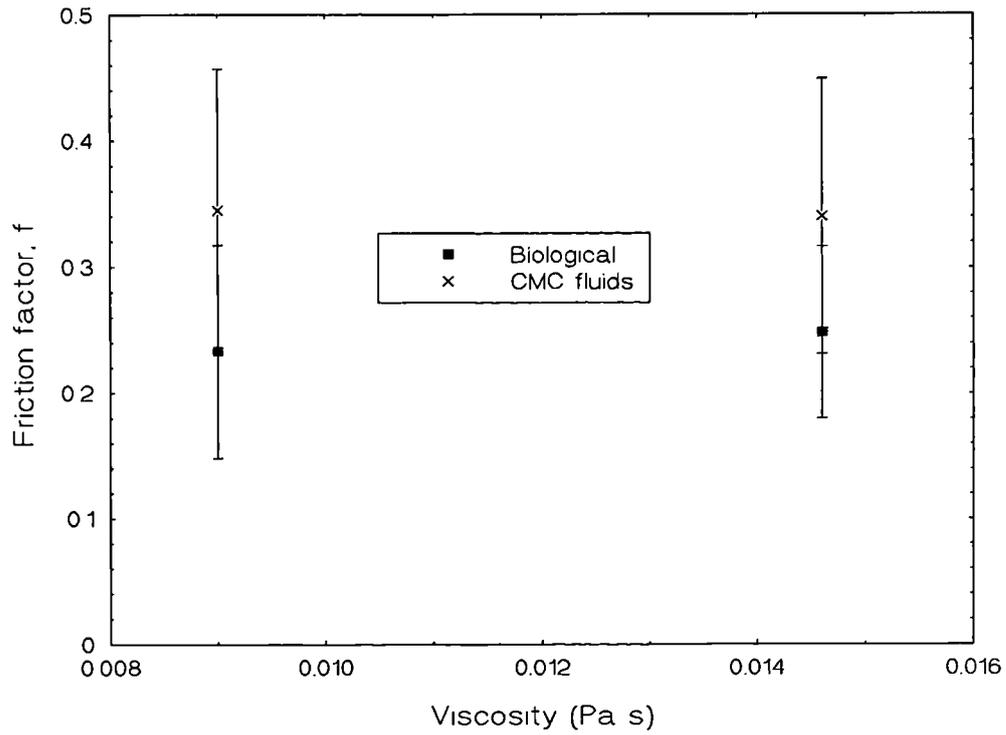
Figure 5.38: Static loading tests at 1000 N (metal/metal)
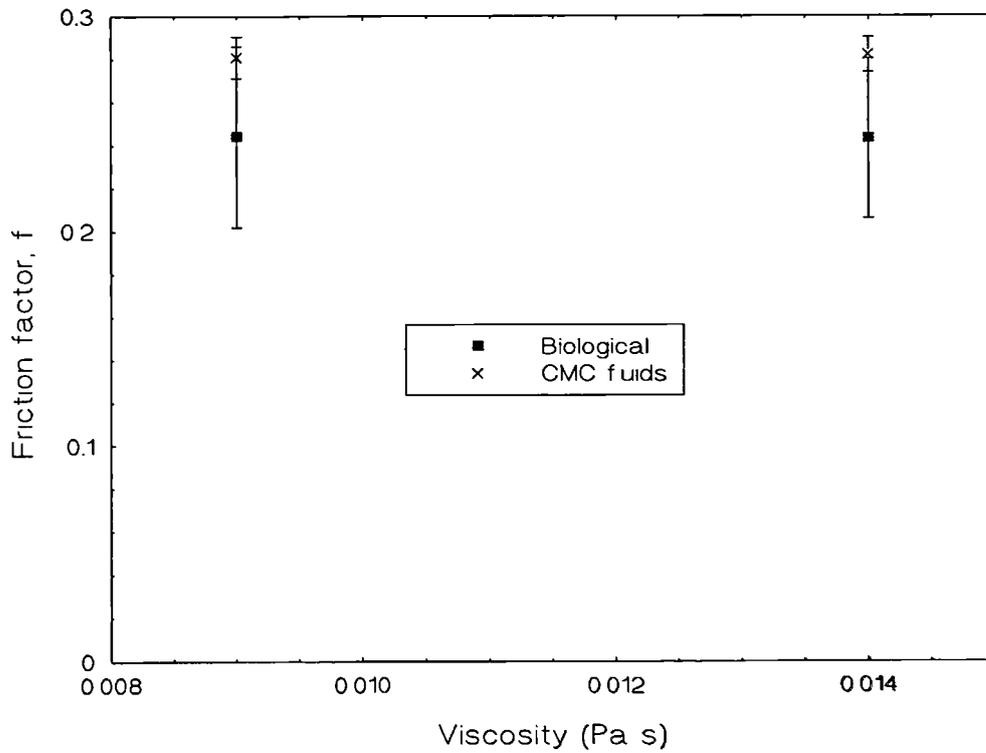
Figure 5.39: Static loading tests at 2000 N (metal/metal)
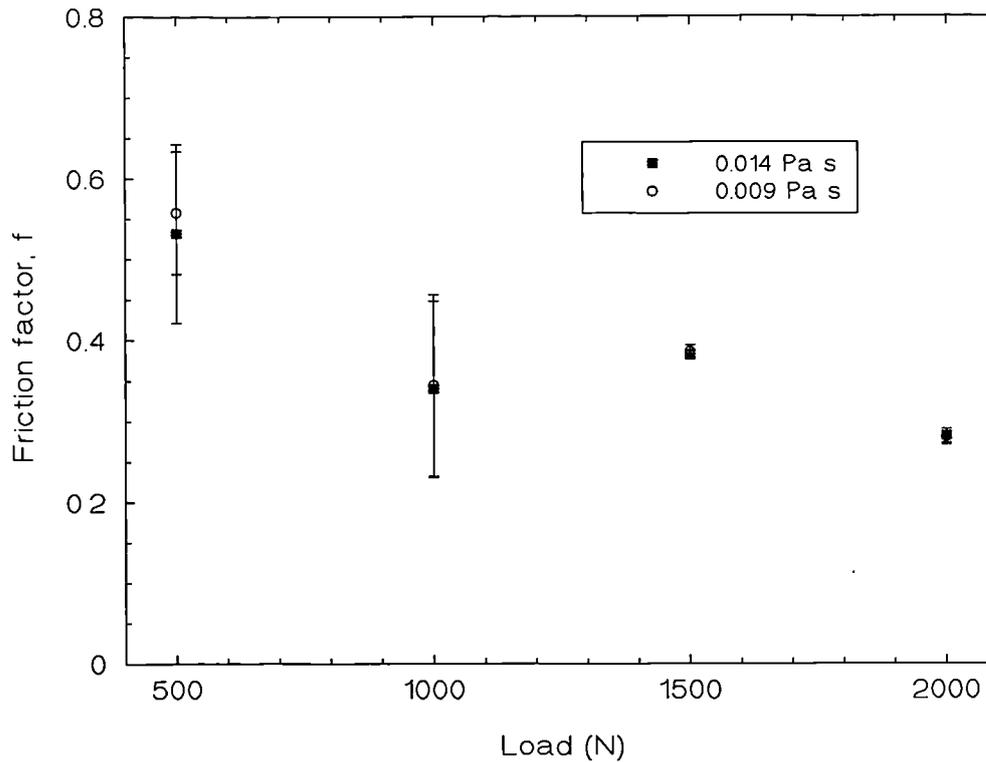
Figure 5.40: Friction factor versus load for static loading (metal/metal)

5.1.4.2 Al_2O_3/Al_2O_3

The results of the static loading tests with biological fluids and CMC fluids at 1000 N and 2000 N are shown in Figures 5.41 and 5.42. Figure 5.43 shows the variation of friction factor with static load for joints lubricated with CMC fluids. Five joints of the same radial clearance were tested twice. The biological lubricants gave significantly higher friction than the CMC fluids indicating some adverse boundary lubricating action. Again, little difference was observed in friction factor between bovine serum and synovial fluid.
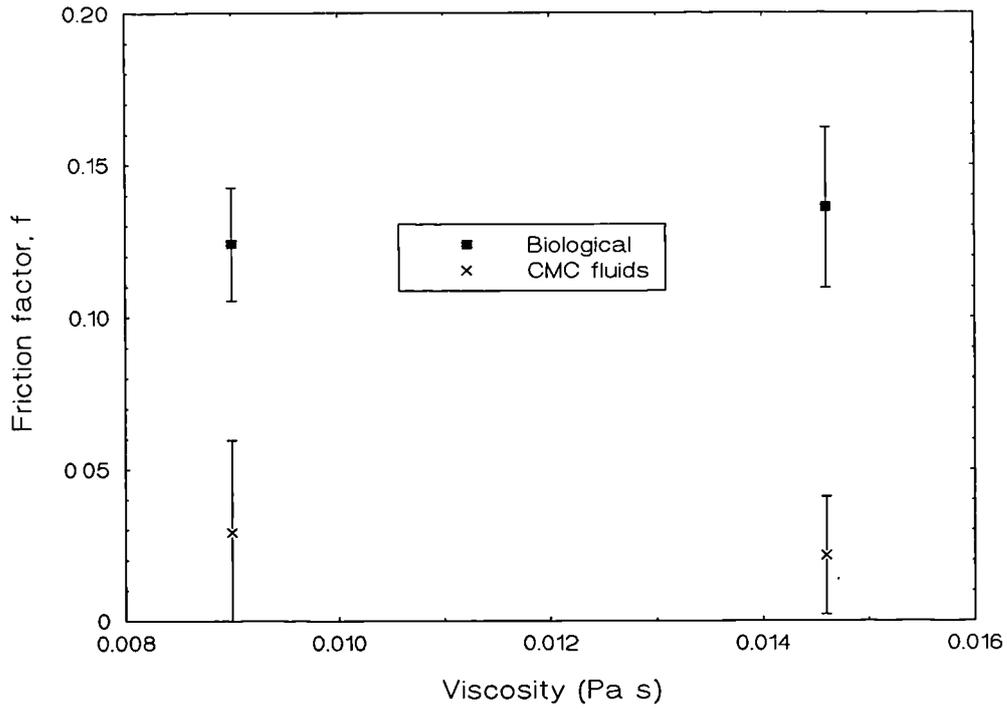
Figure 5.41: Static loading tests at 1000 N (ceramic/ceramic)
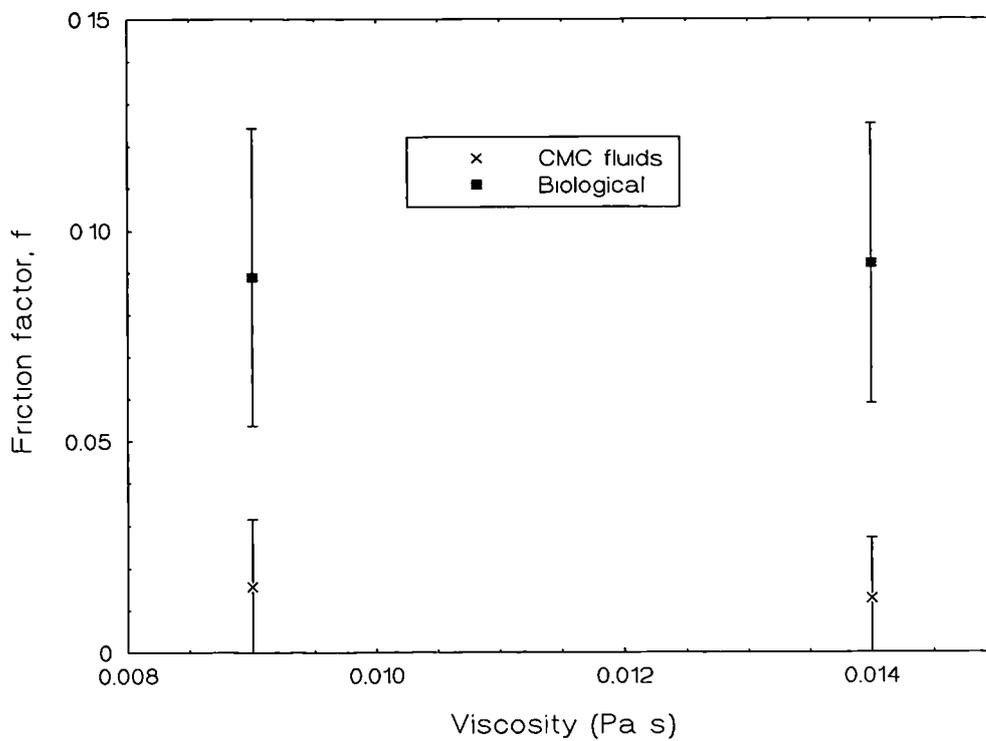
Figure 5.42: Static loading tests at 2000 N (ceramic/ceramic)
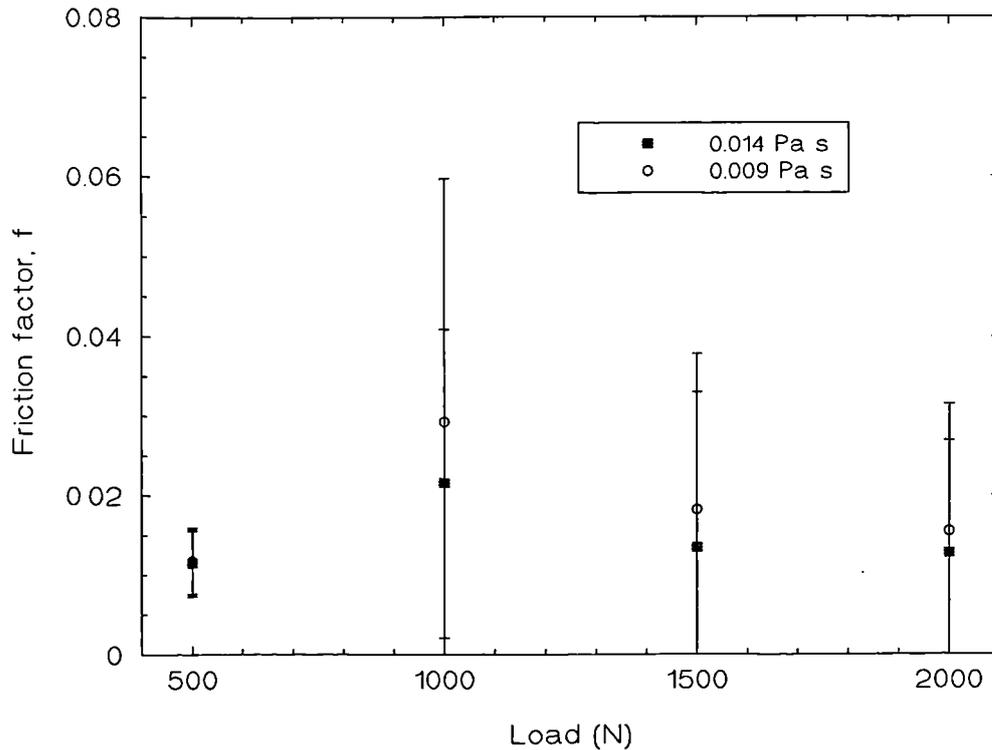
Figure 5.43: Friction factor versus load for static loading (ceramic/ceramic)

5.1.4.3 CoCrMo/UHMWPE

The results of the static loading tests with biological fluids and CMC fluids at 1000 N and 2000 N are shown in Figures 5.44 and 5.45. Figure 5.46 shows the variation of friction factor with static load lubricated with CMC fluids. Three joints of the same radial clearance were tested twice. In each case the biological lubricants gave slightly higher friction than the CMC fluids, indicating some adverse boundary lubricating action. There was little difference between the friction factors for both bovine serum and synovial fluid.
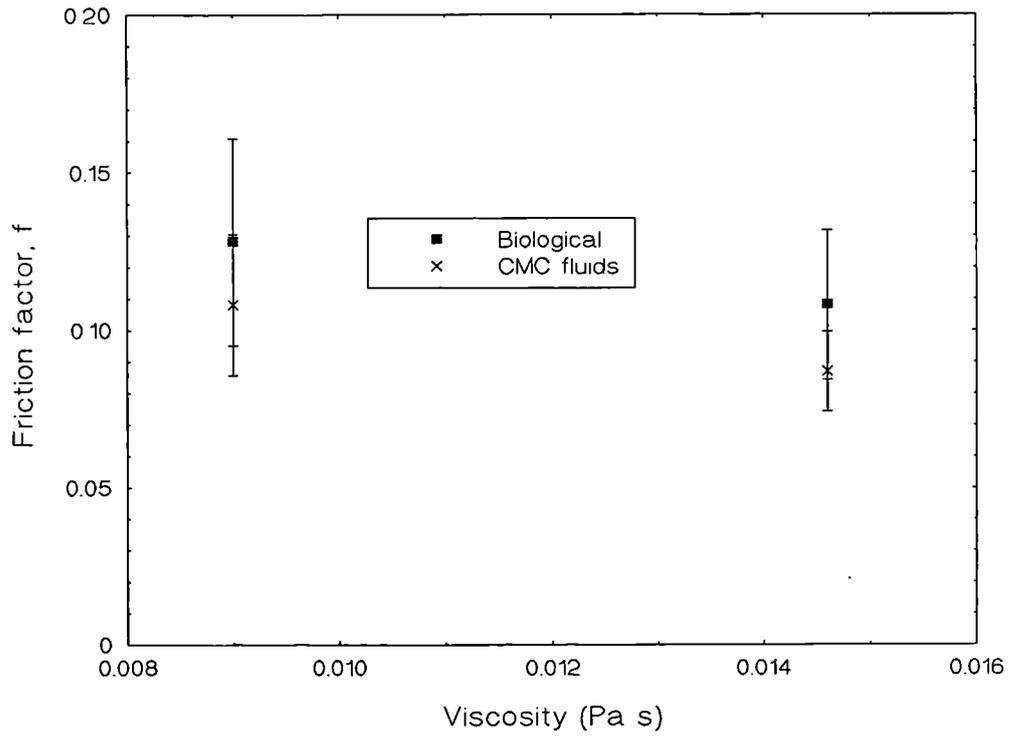
Figure 5.44: Static loading tests at 1000 N (metal/plastic)
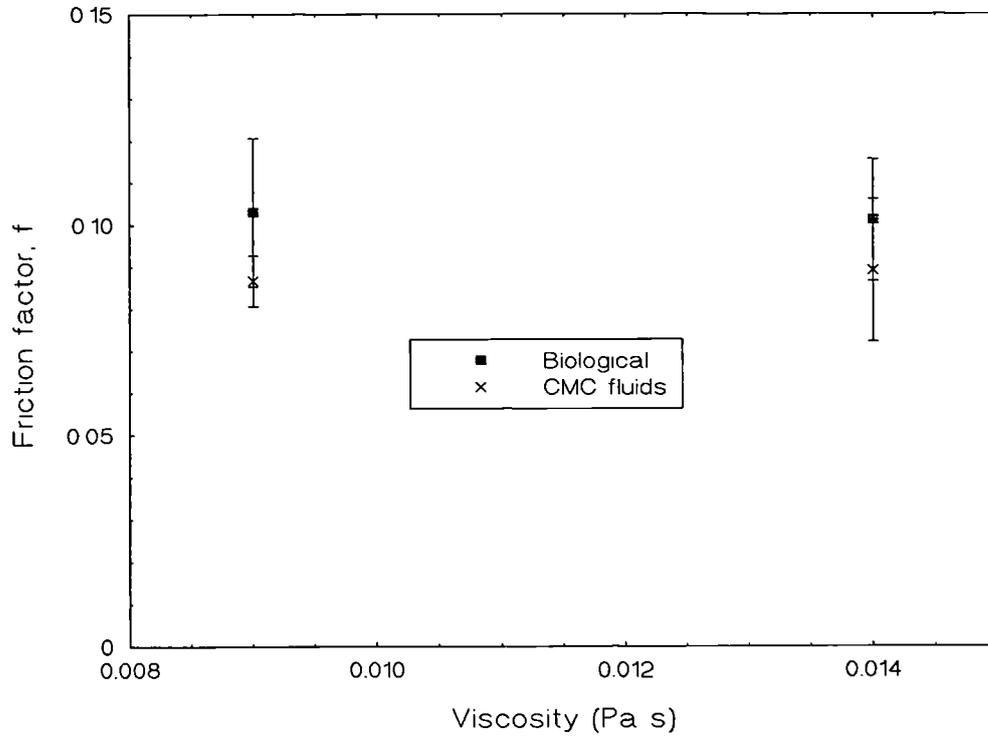
Figure 5.45: Static loading tests at 2000 N (metal/plastic)
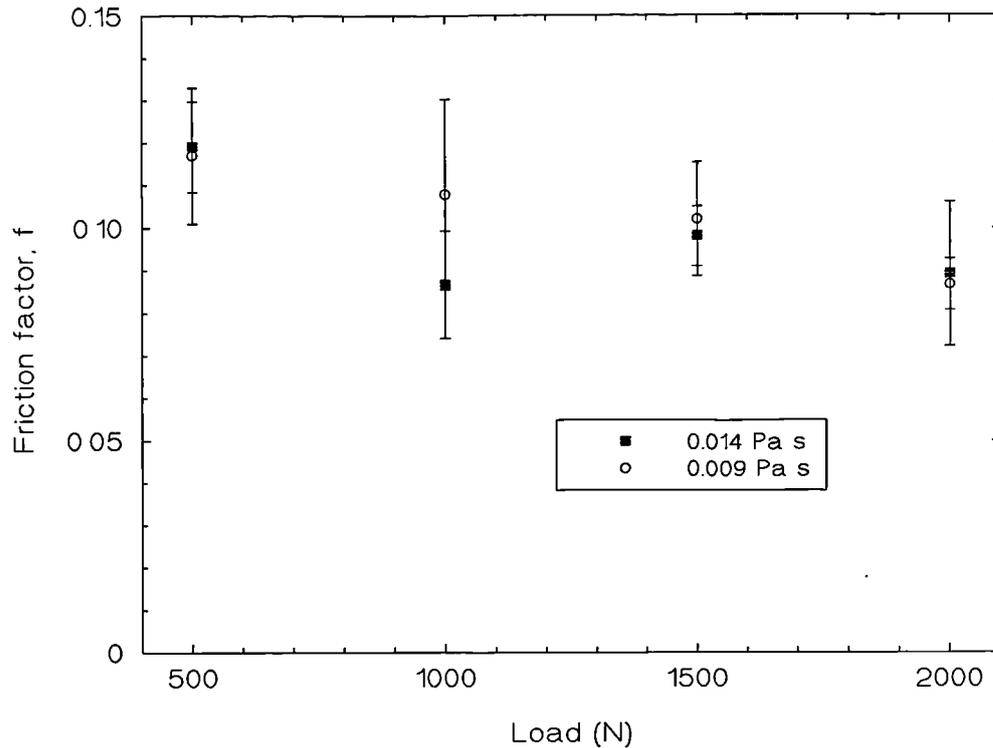
Figure 5.46: Friction factor versus load for static loading (metal/plastic)

5.1.5 Silicone fluids of high viscosities to promote full fluid film lubrication

Tests were performed with varying viscosities of silicone fluids (up to 29.25 Pa s) to determine at which viscosity the lubrication became full fluid film. These tests were carried out on all three conventional CoCrMo/UHMWPE joints, the five ceramic-on-ceramic joints and one of the CoCrMo/CoCrMo joints. It was not possible to test these fluids with more than the one metal-on-metal joint as the low viscosities of silicone fluids destroyed the metal surfaces leading to dramatic scratching, for this reason the higher viscosity fluids were tested first and only the three highest viscosities are shown for the metal-on-metal joints. The results are shown in the form of a Stribeck curve in Figure 5.47. Fluid film lubrication was apparent for viscosities greater than 0.971 Pa s for the metal-on-metal joints, 0.048 Pa s for the ceramic-on-ceramic joints and 0.459 Pa s for the metal-on-plastic joints.

118
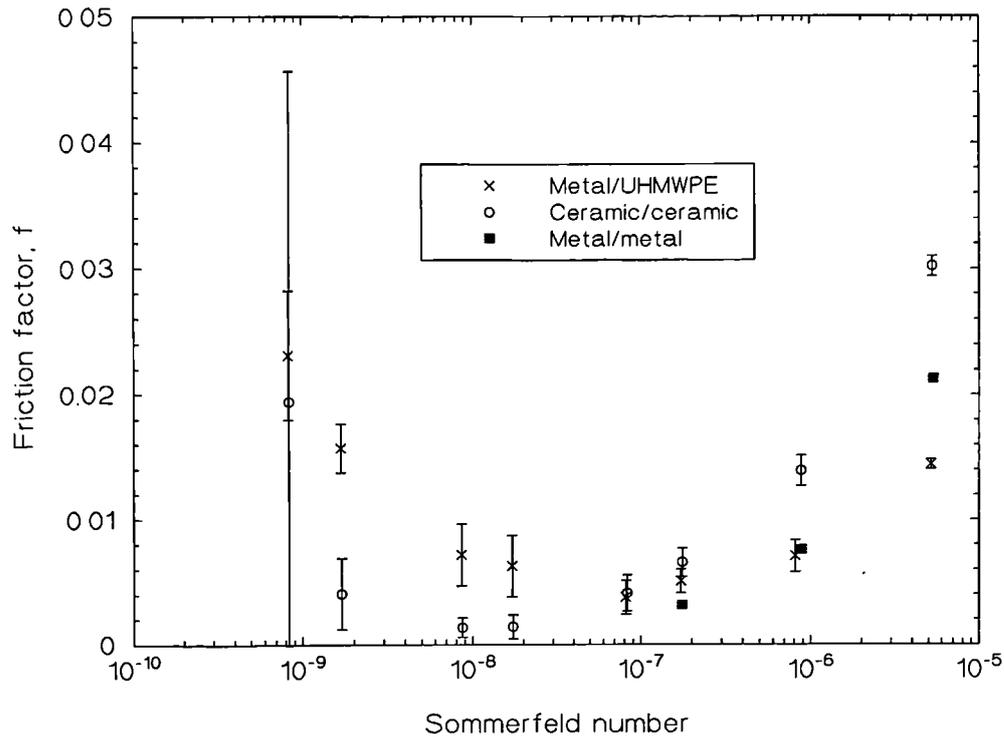
Figure 5.47: Stribeck plot for all material combinations with silicone fluids

5.1.6 Varying concentrations of bovine serum

Tests were performed on the two CoCrMo/CoCrMo joints, five Al_2O_3/Al_2O_3 joints and three CoCrMo/UHMWPE joints and repeated twice on the ceramic/ceramic joints and three times on the remaining joints. Single batch, new born calf serum was used as the lubricant at concentrations of 0%, 8.3%, 16.5%, 24% 33%, 50%, 66% and 100% at a viscosity of 0.0029 Pa s.

5.1.6.1 CoCrMo/CoCrMo

The metal-on-metal joints show a significant decrease in friction factor between 0% bovine serum and all other concentrations (Analysis of Variance (ANOVA); $p<0.03$), see Figure 5.48.
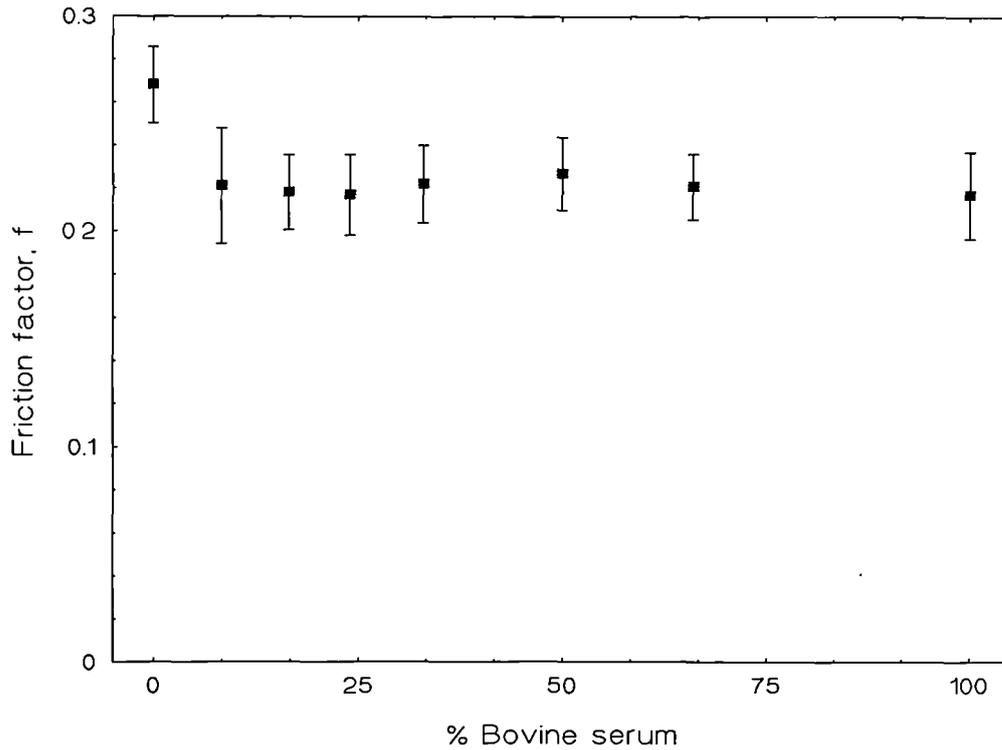
Figure 5.48: Friction factor vs. concentration of bovine serum for the metal-on-metal joints

5.1.6.2 Al_2O_3/Al_2O_3

Figure 5.49 shows the results for the ceramic-on-ceramic joints. Extremely low friction factors were encountered with 0% bovine serum as the lubricant, however, an immediate jump in friction factor occurred between 0% bovine serum and all other concentrations. This again was found to be statistically significant (ANOVA $p<0.001$).
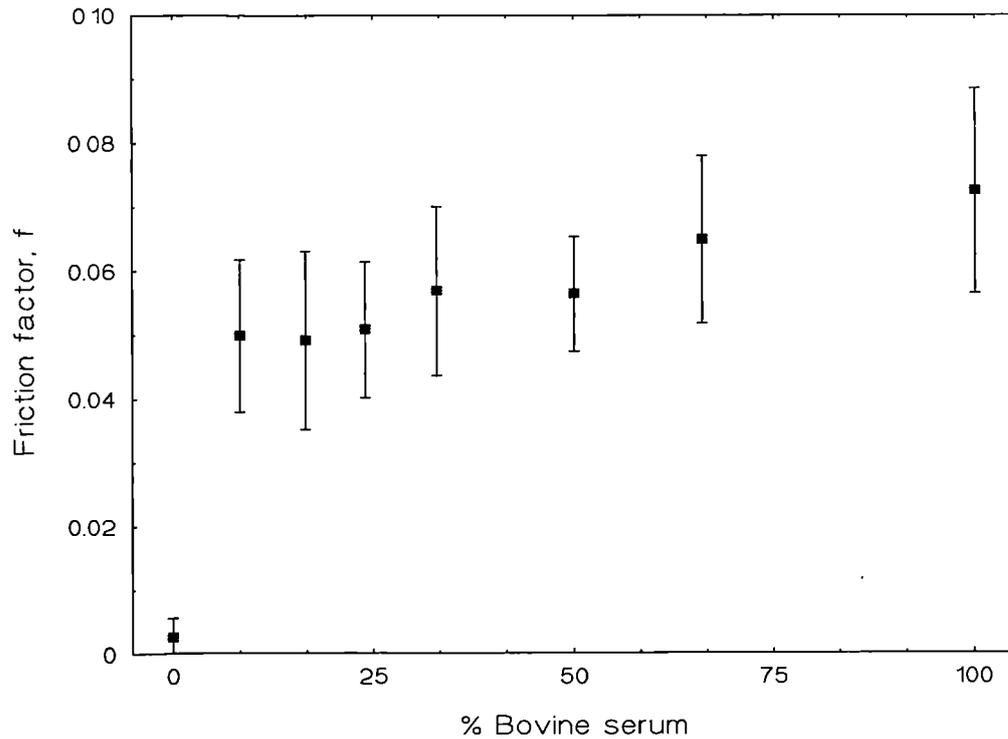
Figure 5.49: Friction factor vs. concentration of bovine serum for the ceramic-on-ceramic joints

5.1.6.3 CoCrMo/UHMWPE

Figure 5.50 shows the variation of friction factor with concentration of bovine serum for the metal-on-plastic coupling. There was an increase in friction factor with increasing concentration of bovine serum.
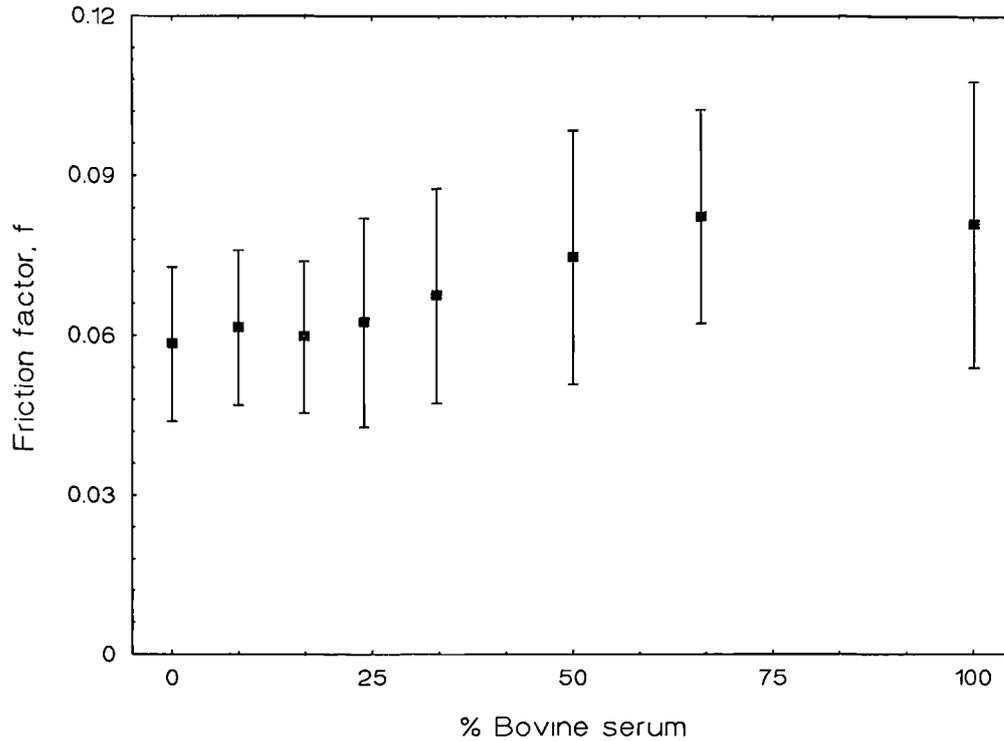
Figure 5.50: Friction factor vs. concentration of bovine serum for the metal-on-plastic joints

5.1.6.4 Friction factor ranking

Figure 5.51 shows the comparison of friction factors for all material combinations. This clearly shows that the metal-on-metal joints gave friction factors of one order of magnitude greater than any other material combination. This was shown to be statistically significant with the ANOVA test ($p<0.001$).

The ceramic-on-ceramic coupling gave friction factors of at least one order of magnitude less than all material combinations when employing solely CMC fluids as the lubricant ($p<0.001$). When bovine serum of any concentration was used as the lubricant the friction factors produced by the ceramic-on-ceramic joints were of the same order as those produced by the metal-on-plastic joints.
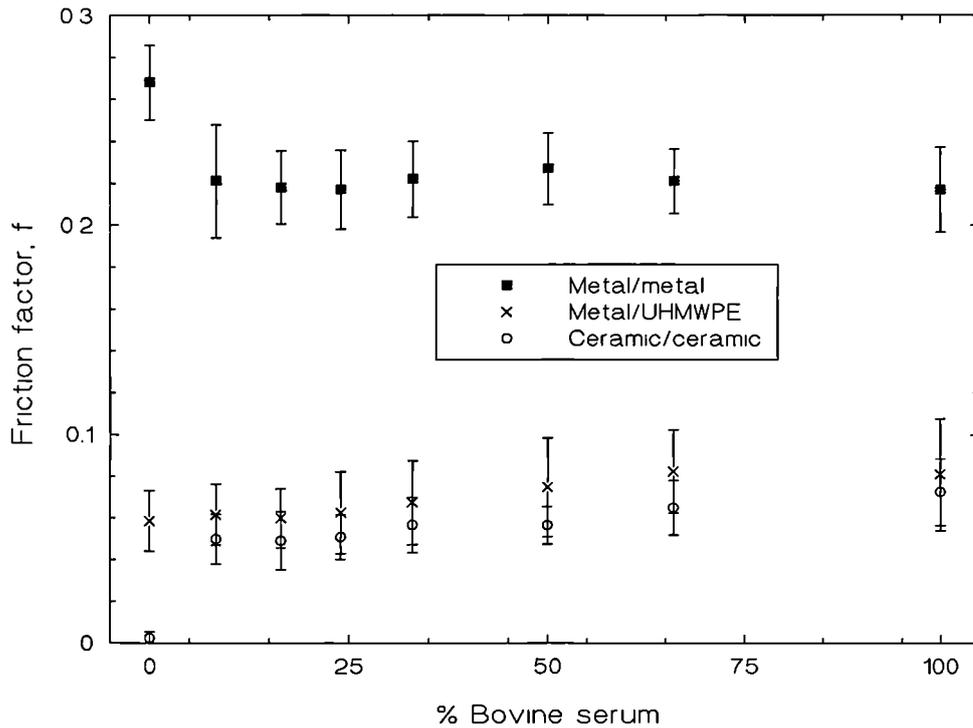
Figure 5.51: Friction factor vs. concentration of bovine serum, all material combinations

5.1.7 Long term friction tests on CoCrMo/CoCrMo joints

Six of the metal-on-metal joints were tested under long term friction conditions. One hundred per cent bovine serum was used for this series of tests at a viscosity of 0.0029 Pa s. It was anticipated that these tests would indicate how friction factor varies with time of testing.

The results are plotted in the form of friction factor against time, an example of which can be seen in Figure 5.52. The friction factor remained constant with time over the duration of each 1500 cycles. Friction factor also remained constant with load. It is important to establish that this graph is on a staggered time scale as only every 100th cycle was recorded. It is also important to point out the problem of eccentricity of these tests. In a full Stribeck analyses, a normal cycle is followed by an inverse cycle, by taking an average of these readings, any additional torque due to

the eccentricity of the femoral head in relation to the loading is eliminated. Due to time considerations, only the normal cycle was performed and therefore the frictional torques recorded could be distorted.
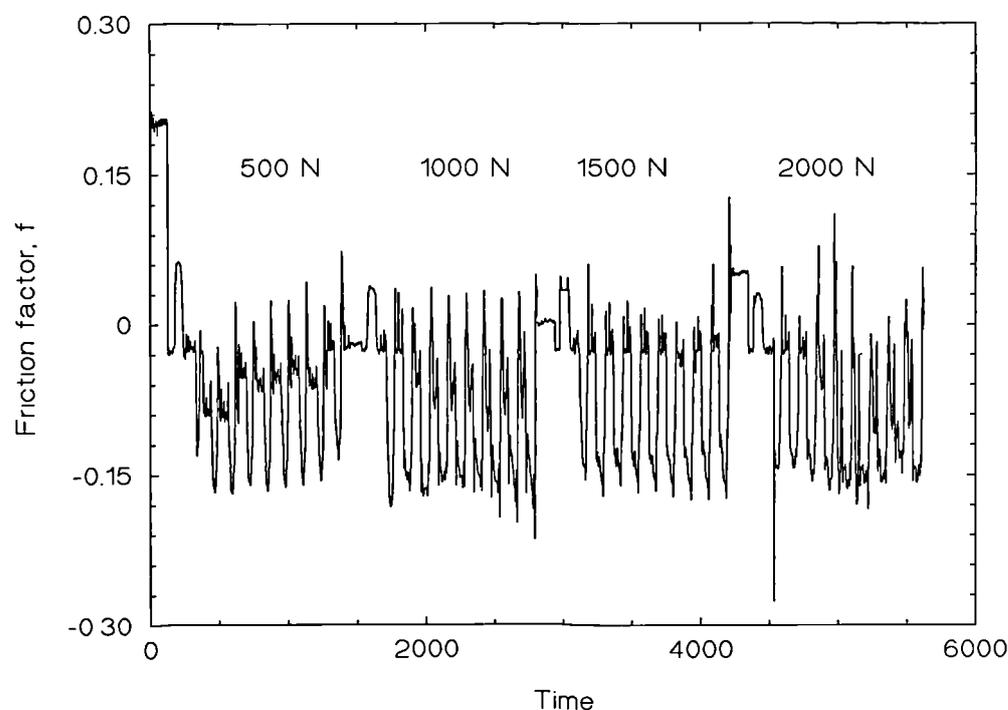
Figure 5.52: Friction factor versus time curve (C10/H22, run 1)

5.1.8 Summary of friction tests

The metal-on-metal joints gave friction factors of one order of magnitude greater than any other material combination except when lubricated in the full fluid film regime with high viscosities of silicone fluids. The ceramic-on-ceramic coupling gave friction factors of at least one order of magnitude less than all other material combinations when employing CMC fluids as the lubricant. When bovine serum of any concentration or synovial fluid were used as the lubricant the friction factors produced by the ceramic-on-ceramic joints were of the same order as those produced by the metal-on-plastic joints.

For the metal-on-metal combination at a clearance of 40 μm, comparing the values of friction factor for CMC fluids of equivalent viscosities to bovine serum and synovial fluid, the biological lubricants gave lower friction than the synthetic lubricants (0.18 cf. 0.28). Bovine serum gave slightly lower friction than synovial fluid. The ceramic-on-ceramic joints showed the opposite effect, friction factor was increased by one order of magnitude when either bovine serum or synovial fluid were used as the lubricant (0.07 cf. 0.002). Little difference existed between the bovine serum and synovial fluid friction results. Again, the friction factors produced for the metal-on-plastic joints were slightly higher when lubricated with biological lubricants rather than the synthetic lubricants (0.08 cf. 0.05), although the difference in friction factor was not nearly as large as for the ceramic-on-ceramic joints. The bovine serum gave slightly higher friction than the synovial fluid. Figure 5.53 shows the comparison of friction factors for each material combination with the different lubricants at equivalent viscosities.
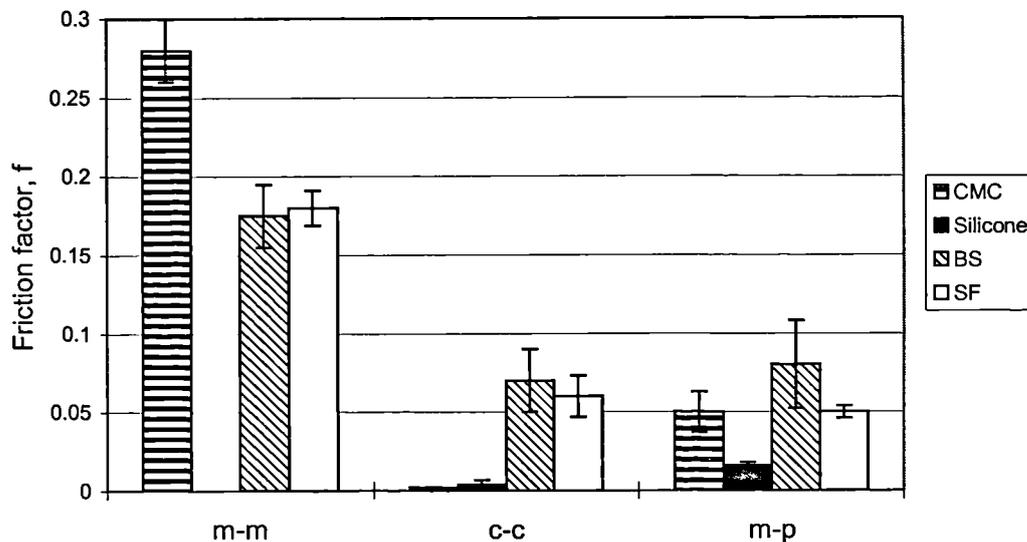
Figure 5.53: Comparison of friction factor for each material combination with each lubricant

5.1.8.1 Predicted lubrication modes

Table 5.1 shows the calculated minimum film thicknesses (equation 2.5) and predicted lubrication mode for each material combination. Although the predicted minimum film thicknesses were similar for both the all ceramic and all metal couplings, an important difference was observed for the dimensionless parameter, λ. The metal-on-metal joints exhibited a λ value of less than one, therefore suggesting a mixed lubrication regime whereas the ceramic-on-ceramic joints had a λ value of greater than 3 suggesting a full fluid film lubricating regime. This difference was due to the much lower surface roughness of the ceramic components. The CoCrMo/UHMWPE joint exhibited a λ value of less than one, suggesting, as would be expected, a mixed lubrication regime.

Femoral component	Acetabular component	Femoral S_{qh} (μm) (s.d.)	Acetabular S_{qc} (μm) (s.d.)	Predicted min. film thickness (eq. 2.5) (μm)	λ
CoCrMo	CoCrMo	0.008 (0.002)	0.08 (0.0365)	0.05	<1
Alumina	Alumina	0.003 (0.001)	0.01 (0.0063)	0.06	>3
CoCrMo	UHMWPE	0.04 (0.006)	1.29 (0.086)	0.09	<1

Table 5.1: Predicted lubrication modes (η=0.01 Pa s)

5.1.9 Protein gel technique

Figure 5.54 shows the results for the protein gel technique. All the materials were shown to have varying degrees of protein adsorbed onto the specimen surfaces. More protein was adsorbed onto the plastic and ceramic surfaces than the metal surface. One of the main proteins found on the surfaces was bovine serum albumin. The controls showed little or no protein adsorption for all material specimens.
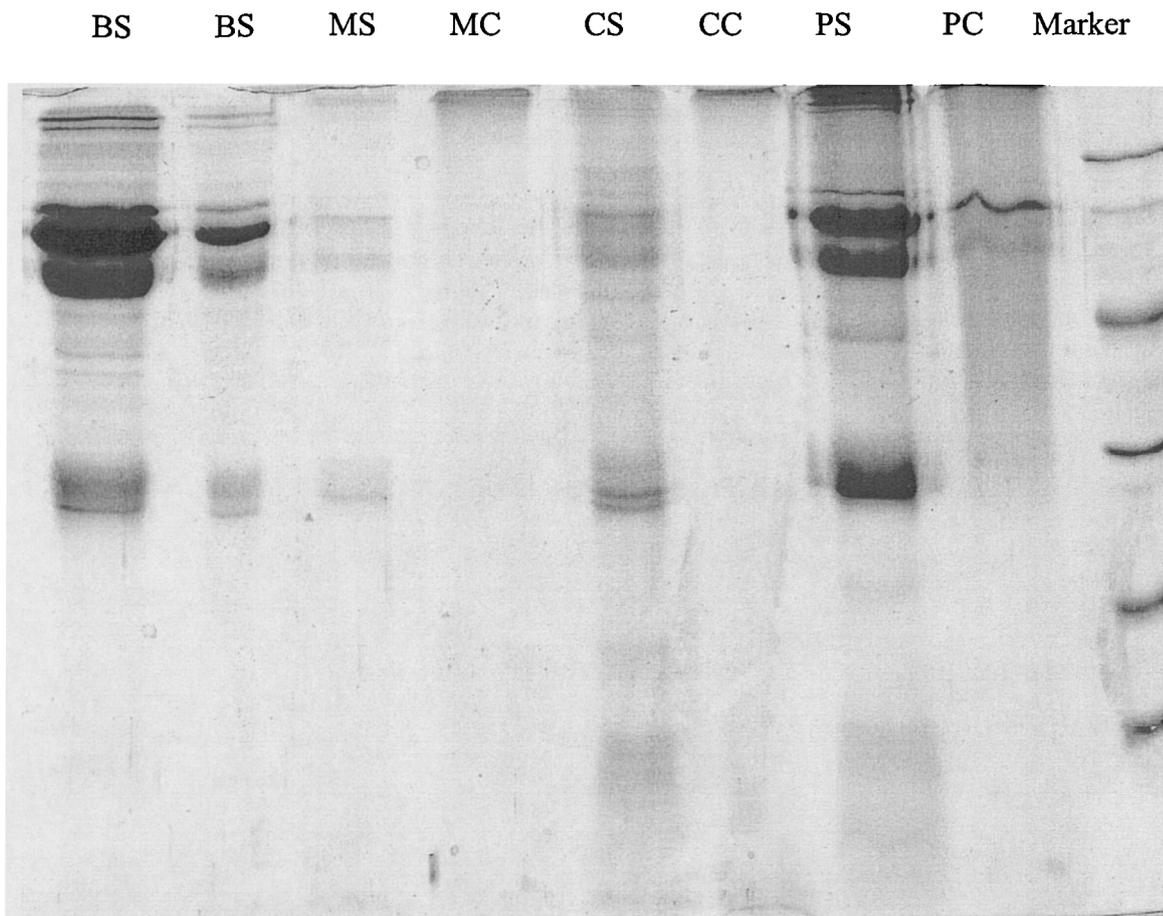
Figure 5.54: Protein gel technique results

(BS: bovine serum, MS: metal bovine serum sample, MC: metal control sample, CS: ceramic bovine serum sample, CC: ceramic control sample, PS: plastic bovine serum sample, PC: plastic control sample).

5.2 Wear

5.2.1 Initial metal/metal wear tests

Wear tests were performed on the existing pin-on-plate machines to determine the effects of two different pin configurations on the wear of three different compositions of CoCrMo.

The recommendations set out in the ASTM Standard Practice F 732-82 were followed with regard to the motion, sliding speed, lubricant and temperature. The motion was approximately sinusoidal, with a 25 mm stroke at a rate of 1 cycle per second producing an average sliding speed of 50 mm/s. At each station a load of 40N was applied with the use of lever arms. Bovine serum at a 30% concentration was used as the lubricant.

Three machines were used, each tested a specific material composition with two different pin configurations - a flat ended pin and a cylindrical ended pin. The final results of the wear tests are shown in Table 5.2. Two distinct wear factors could be distinguished for each sample and are described here as the primary wear phase and the secondary wear phase (see Figures 5.55 to 5.57). The secondary phase wear factor was usually lower than that of the primary wear phase.

Material	Wear factor (mm^3/Nm x 10^{-6})			
	Pin 1 (Flat ended)	Pin 2 (Cylindrical ended)	Plate 1	Plate 2
A (high carbon)	0.98/0.78	1.11/0.66	0.61/0.42	0.46/0.29
B (high carbon)	1.42/1.14	1.61/1.19	2.23/0.96	2.00/1.15
C (low carbon)	1.38/1.59	1.57/1.68	5.27/2.77	4.75/2.68

(primary wear phase/secondary wear phase)

Table 5.2: Wear factors for each material and pin configuration

The table above shows clearly that with respect to the plates:

Wear of A < Wear of B < Wear of C.

However, such a trend was not discernible for the pins as there was little difference between the pin wear of the three material compositions, although material A, again, gave the lowest wear. No difference was found between the two pin configurations on either the pin wear or the plate wear.
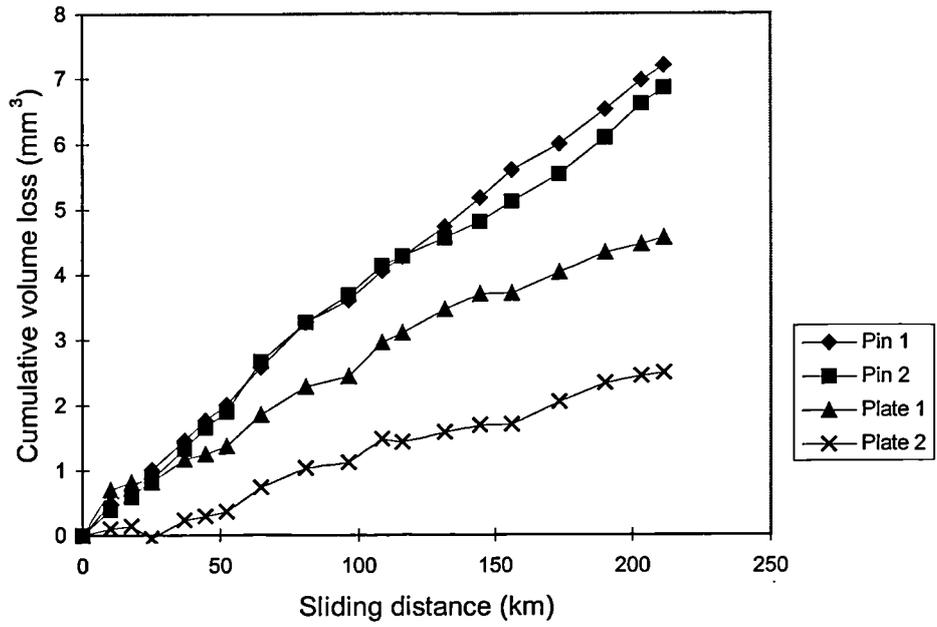
Figure 5.55 Volumetric wear vs. sliding distance for material A
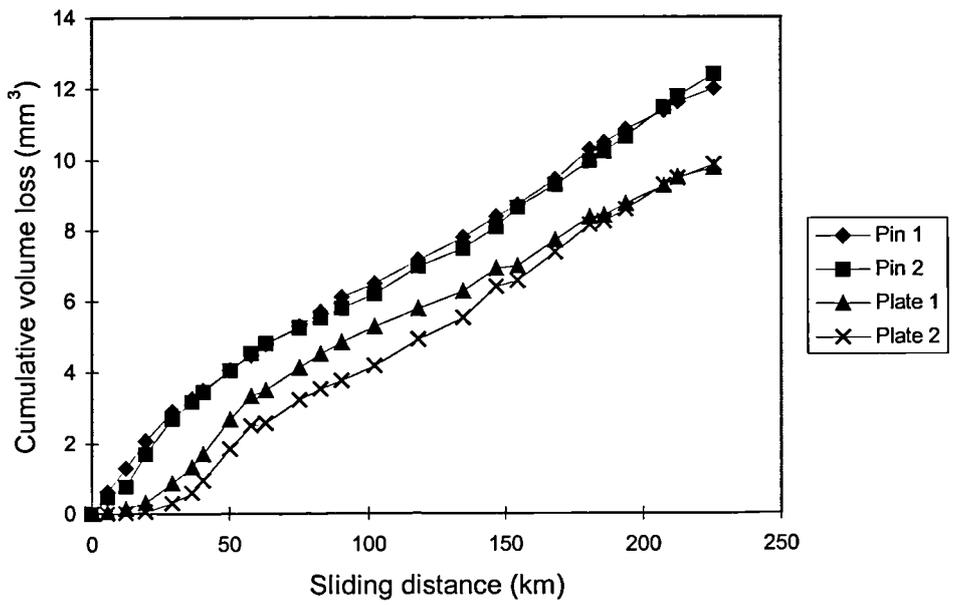
Figure 5.56 Volumetric wear vs. sliding distance for material B
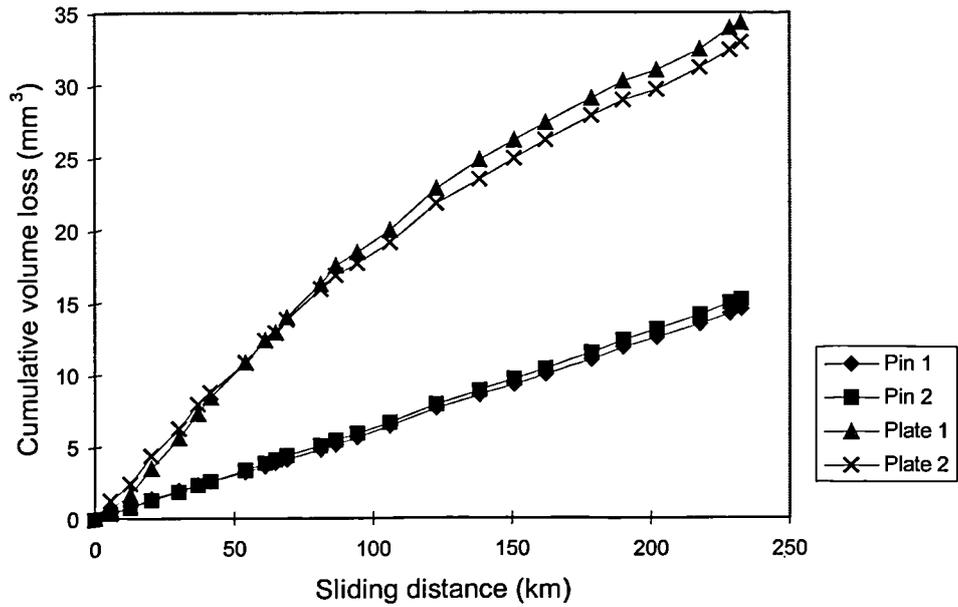
Figure 5.57 Volumetric wear vs. sliding distance for material C

Surface roughness measurements were taken both prior to testing and after the full duration of the test. Tables 5.3 to 5.5 compare the unworn and the worn surfaces for each material composition.

Component	S_a (μm)		S_q (μm)	
	Original	Worn	Original	Worn
Plate 1	0.149	0.624	0.201	0.774
Plate 2	0.133	1.006	0.188	1.264
Pin 1	0.0655	2.510	0.102	3.230
Pin 2	0.084	1.806	0.126	2.150

Table 5.3: Comparison of surface roughnesses for material A

Component	S_a (μm)		S_q (μm)	
	Original	Worn	Original	Worn
Plate 1	0.137	1.186	0.193	1.455
Plate 2	0.142	1.035	0.196	1.342
Pin 1	0.0695	1.231	0.118	1.487
Pin 2	0.066	1.068	0.102	1.312

Table 5.4: Comparison of surface roughnesses for material B

Component	S_a (μm)		S_q (μm)	
	Original	Worn	Original	Worn
Plate 1	0.145	0.886	0.196	1.150
Plate 2	0.094	1.084	0.143	1.361
Pin 1	0.0645	2.109	0.113	2.583
Pin 2	0.0845	1.341	0.126	1.709

Table 5.5: Comparison of surface roughnesses for material C

5.2.2 Validation of new wear machine - XLPE/XLPE

Tests using cross-linked polyethylene (XLPE) against itself were performed on the new wear machine to validate it against known results from the existing machines. The tests were carried out to the procedure outlined by an undergraduate final year project (Cartwright, 1998). Two stations applied reciprocating motion only, whilst the remaining two applied both reciprocation plus rotation.

A load of 40 N was applied vertically to the pin, 30% bovine serum was used as the lubricant at 37 °C. The reciprocating motion was set at 60 r.p.m. (1 Hz), with a stroke of 25 mm, thus giving an average sliding speed of 0.05 ms^{-1}. The rotational motion was also set at 60 r.p.m. Control pins and plates placed in the lubricant in the

same conditions as the test pins and plates were used to ensure any change of mass due to lubricant absorption could be accounted for.

The results are shown in Table 5.6 and are compared with those found previously (Cartwright, 1998), the average wear coefficients are shown in Table 5.7. Figures 5.58 and 5.59 show volumetric wear versus sliding distance for the duration of the wear test. The final wear coefficients were taken over the full duration of the test. The wear coefficients compare well with those found previously.

	Final wear factors (mm^3/Nm x 10^{-6})	
Sample	New machine	Existing machine
Plate 1 (rotation)	4.8	2.8
Plate 2 (rotation)	1.2	3.3
Plate 3	0.38	0.64
Plate 4	0.72	0.44
Pin 1 (rotation)	0.060	0.082
Pin 2 (rotation)	0.085	0.040
Pin 3	0.018	0.042
Pin 4	0.023	0.002

Table 5.6: Comparison of wear machine results

	Final average wear factors (mm^3/Nm x 10^{-6})	
Sample	New machine	Existing machine
Plate (rotation)	3.0	3.1
Plate	0.55	0.54
Pin (rotation)	0.073	0.061
Pin	0.021	0.022

Table 5.7: Comparison of average wear results
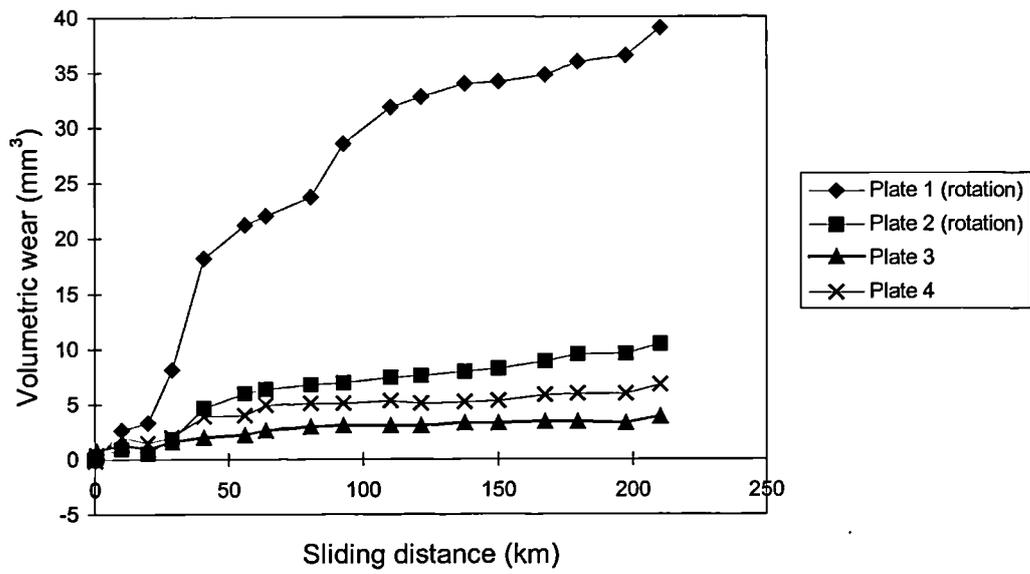
Figure 5.58: Volumetric wear vs. sliding distance for the XLPE plates
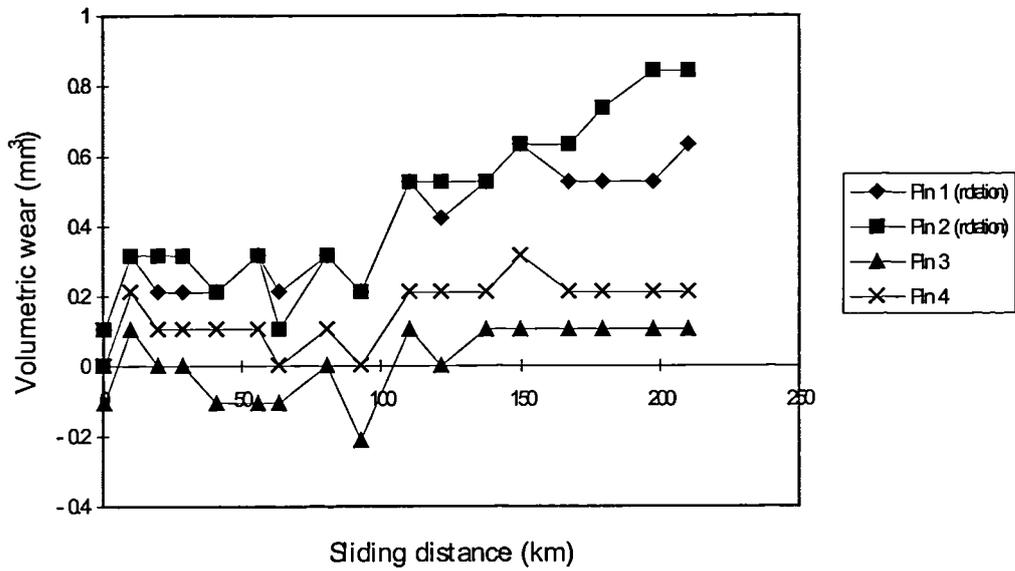
Figure 5.59: Volumetric wear vs. sliding distance for XLPE pins

5.2.3 Metal/metal wear tests - reciprocation plus rotation

Further tests were performed on the new wear machine to determine the effects of pin rotation on the wear of two different compositions of CoCrMo against itself (high carbon material A and low carbon material C). Two stations applied reciprocating motion only, one to material A the other to material C. Whilst the other two stations applied both reciprocation plus rotation, one to material A and the remaining station to material C.

The testing conditions were the same as those used in section 5.2.2. Control pins and plates were not necessary for the metal samples as fluid absorption would be negligible.

The results are shown in Table 5.8 and graphically in Figures 5.60 and 5.61. The final wear coefficients were taken over the full duration of the test.

Sample	Material	Wear factor (mm^3/Nm x 10^{-6})
Plate 1 (rotation)	C	0.61
Plate 2 (rotation)	A	0.063
Plate 3	A	0.22
Plate 4	C	4.5
Pin 1 (rotation)	C	0.55
Pin 2 (rotation)	A	0.78
Pin 3	A	0.53
Pin 4	C	1.9

Table 5.8: Wear factors for metal/metal samples with and without rotation
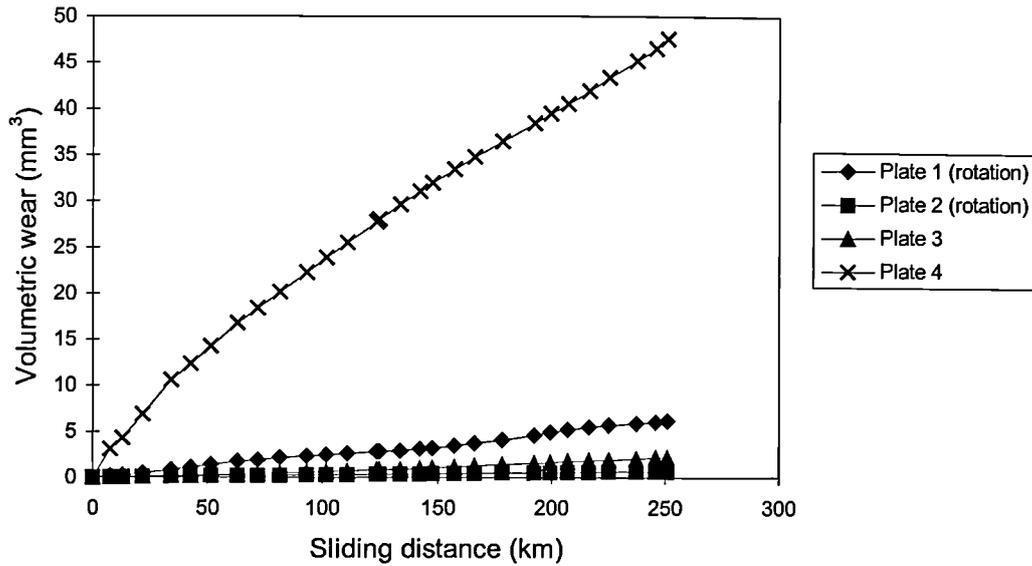
Figure 5.60: Volumetric wear vs. sliding distance for the CoCrMo plates
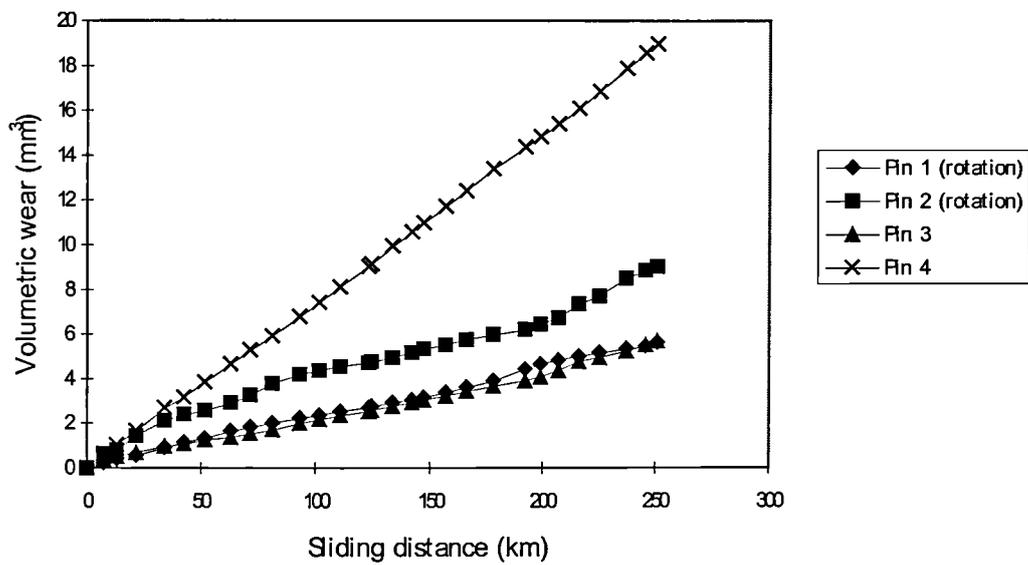
Figure 5.61: Volumetric wear vs. sliding distance for the CoCrMo pins

The wear coefficients (for simple reciprocating motion only) compare well with those found previously (section 5.2.1). See Table 5.9. For both the pins and the plates: Wear A < Wear C.

	Wear factor (mm^3/Nm x 10^{-6})	
Sample	New machine	Existing machine
Plate A	0.22	0.61/0.42
Pin A	0.53	0.98/0.78
Plate C	4.5	5.3/2.8
Pin C	1.9	1.4/1.6

(primary wear phase/secondary wear phase)

Table 5.9: Comparison of wear factors

Both pin and plate wear were drastically reduced when rotation was incorporated into the motion as well as reciprocation for material C. The plate wear of material A was also reduced significantly with both rotation and reciprocation, however, the pin wear remained about the same. The overall wear (that for both the pin and plate combined) was significantly reduced with added rotation for material C but remained approximately the same for material A.

Figures 5.62 to 5.65 show the variation of surface roughness over the duration of the test for material combinations C1, A2, A3 and C4 respectively. Measurements were taken every one million cycles.
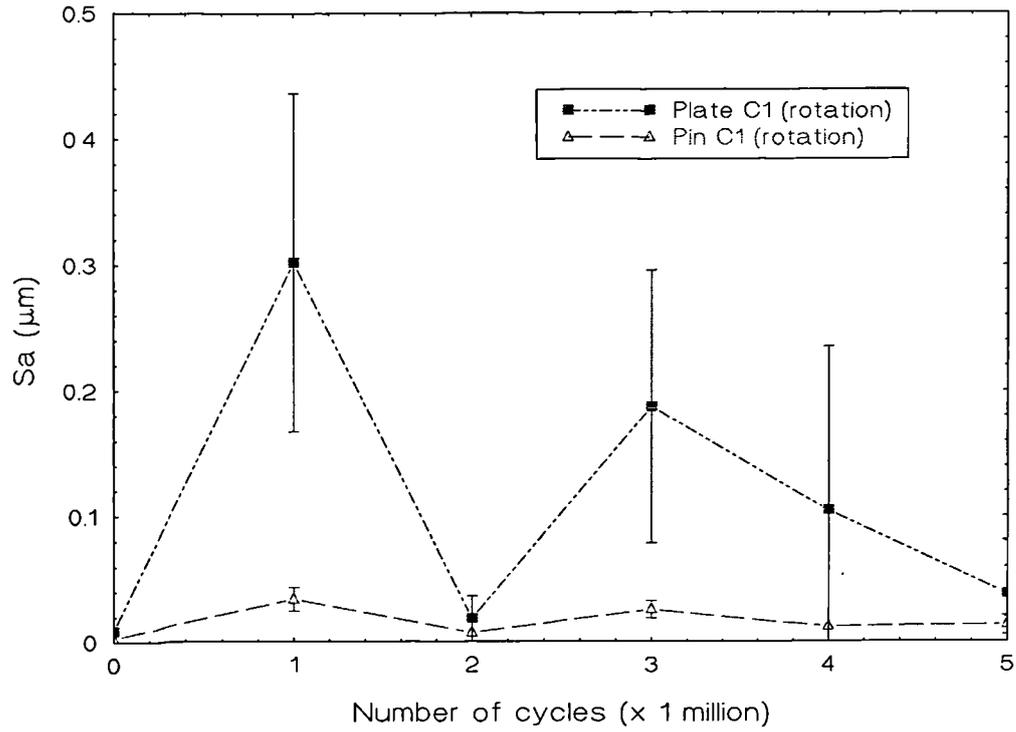
Figure 5.62: Change in surface roughness throughout duration of test (C1)
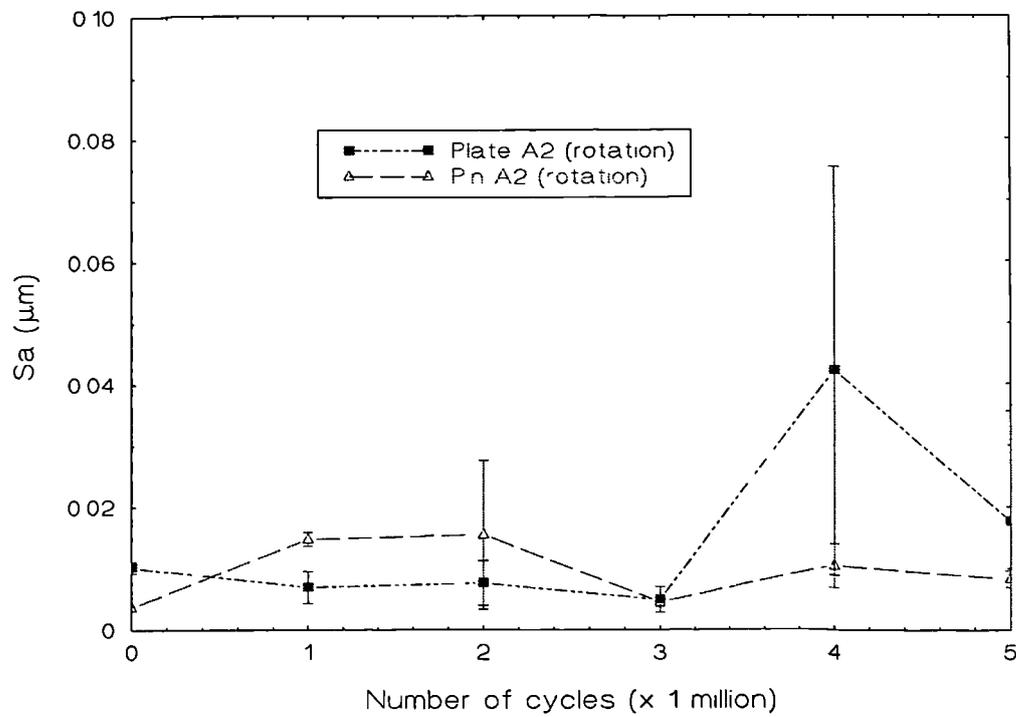
Figure 5.63: Change in surface roughness throughout duration of test (A2)
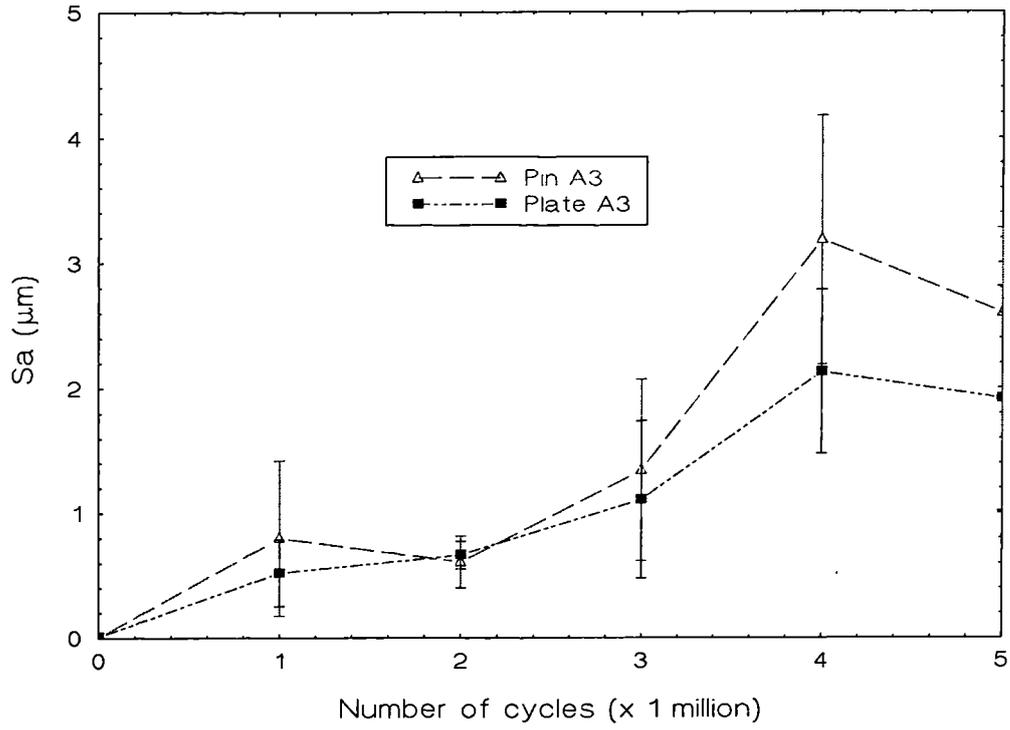
Figure 5.64: Change in surface roughness throughout duration of test (A3)
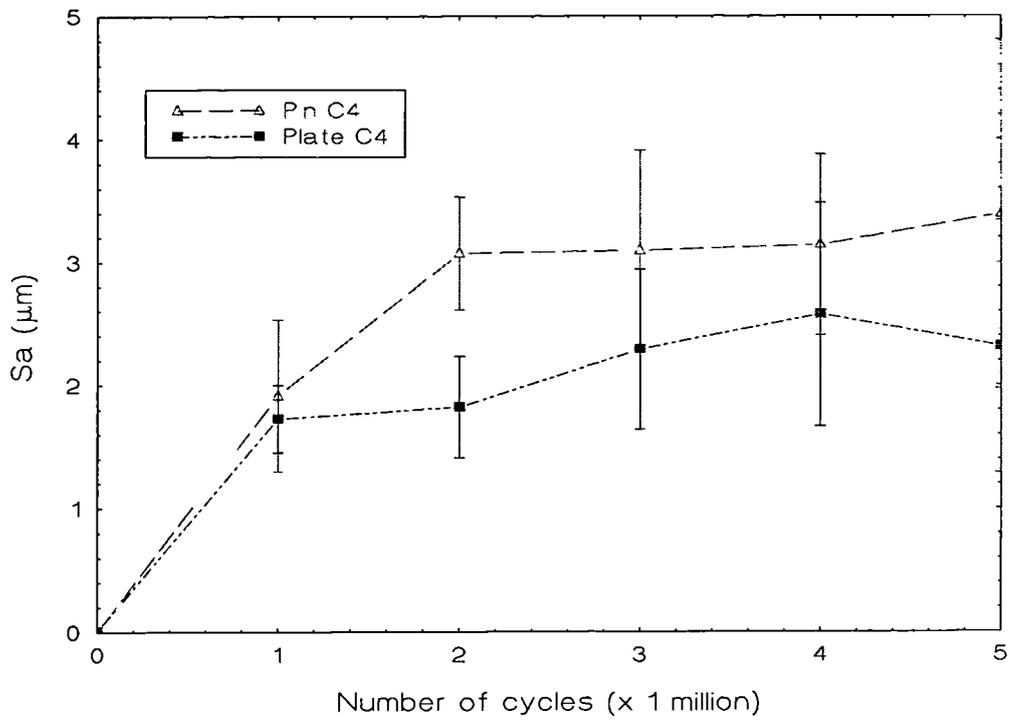
Figure 5.65: Change in surface roughness throughout duration of test (C4)

Initially, all the surface roughnesses were very similar and were all below the limits of surface roughness specified in the standard.

Once the wear had started there was little difference between the surface roughness measurements throughout the test for both pin C1 and A2 (i.e. the pins with rotation and reciprocation). Both pins remained very smooth to both the eye and in terms of surface roughness measurement. The wear tracks on the plates with rotation varied considerably throughout the duration of the test. The surface roughness measurements for both plate C1 and plate A2 also fluctuated throughout the tests. There were both highly polished areas and areas of light to moderate scratching seen on the plates. The position and amount of this scratching on the wear track varied during the course of the test.

As soon as the reciprocation motion started, the wear of both pins and plates A3 and C4 established as unidirectional scratching in the direction of motion. The surface roughness of the wear track increased with duration of sliding.

6. Discussion

6.0 Introduction

All the friction tests were consistent between runs. Friction measurement is far less time consuming than long term wear studies. It can give an indication of the mode of lubrication occurring within joint prostheses as the loading, motion and lubricating conditions can be well matched to physiological conditions. The lubrication mode can be determined not only from the magnitudes of the resulting friction factors but also from the use of a Stribeck plot. Although friction is not now thought of as being a major factor in the loosening of artificial hip joints (Mai *et al* 1996), low friction is still considered to be desirable as it will reduce the contribution to loosening of joints by fatigue.

6.1 Friction

6.1.1 Stribeck analyses (CMC fluids)

6.1.1.1 Effect of clearance on the friction of CoCrMo/CoCrMo joints

It was difficult to determine a trend between friction factor and radial clearance from the plots shown in Figures 5.2 to 5.6. However, the smaller radial clearances produced the lower friction factors. Using the lubrication theory of Hamrock and Dowson (1978), for low elastic modulus materials under fully flooded conditions where no assumptions were made about the pressure within the contact, it can be seen from Figure 6.1 that the smaller clearances result in larger film thicknesses.
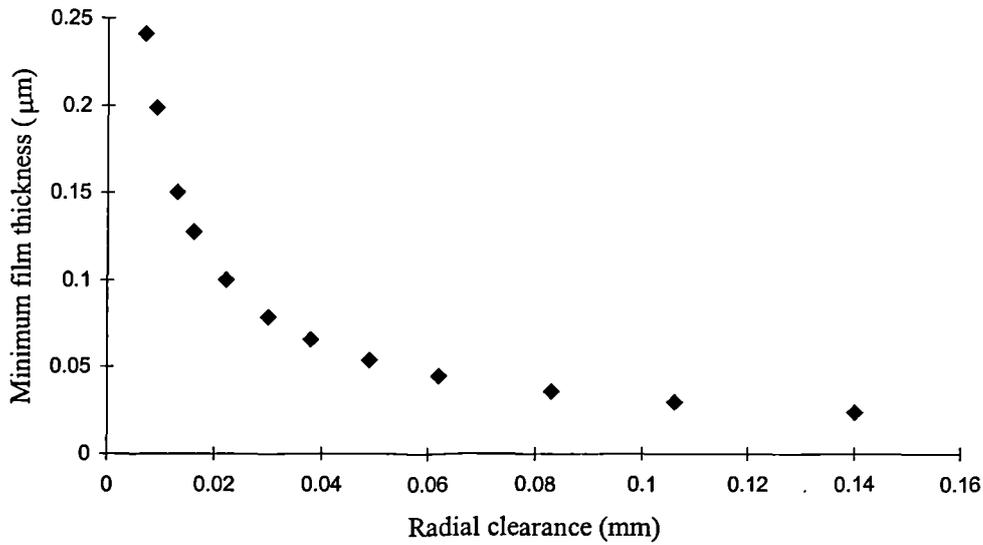
Figure 6.1: Minimum film thickness versus radial clearance

Figure 6.2 shows how the dimensionless load carrying capacity of a bearing depends on the ratio of the film thicknesses within the wedge, where h_i is the inlet film thickness and h_o is the minimum film thickness. The maximum load carrying capacity occurs when $h_i/h_o = 2.18$, the minimum coefficient of friction also occurs close to this value. Calculations were performed to determine how h_i/h_o varied with radial clearance. The results can be seen in Figure 6.3. The method of calculation is shown in Appendix F. The smallest radial clearance of 7 μm gave a ratio of 3.8.
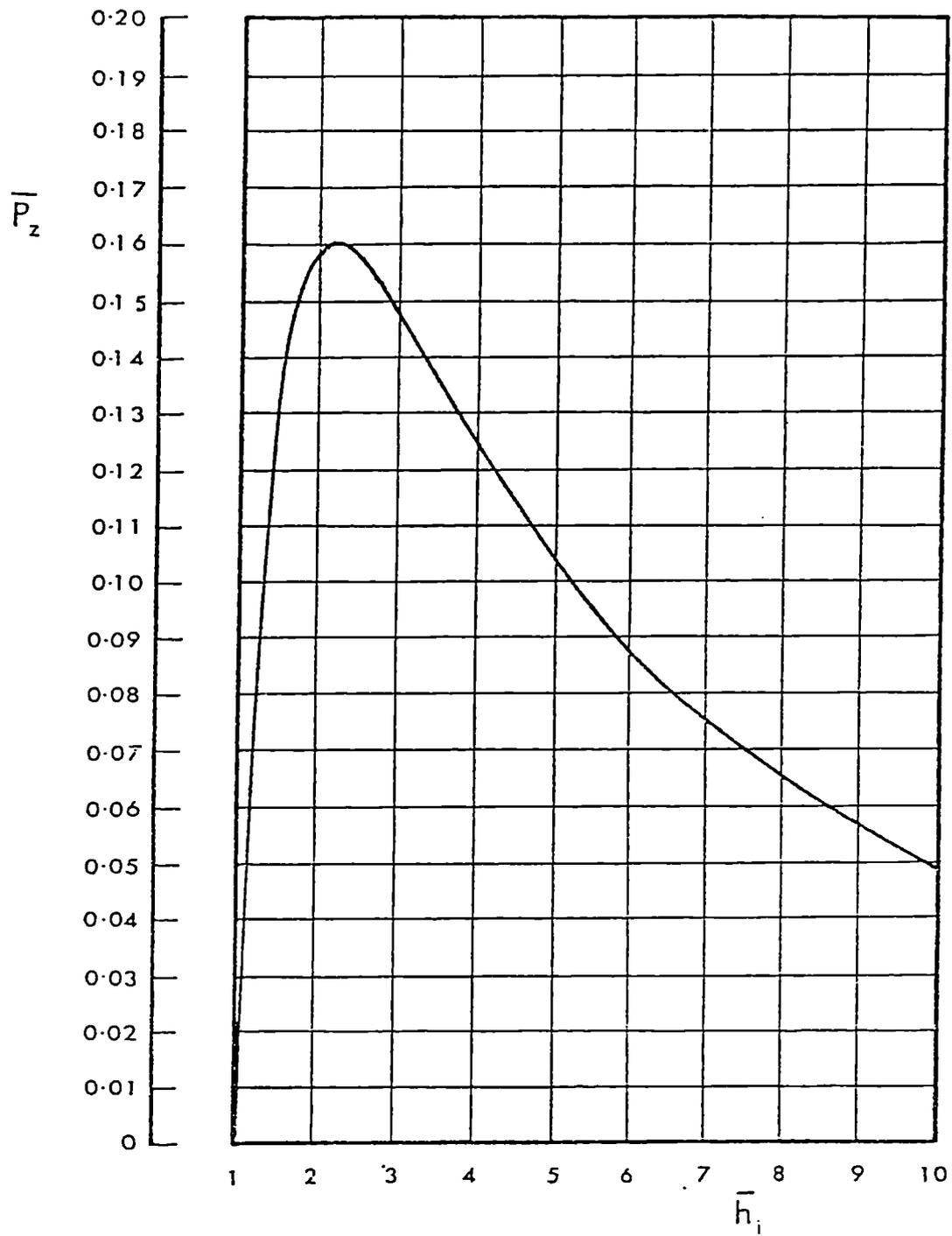
Figure 6.2: Dimensionless load carrying capacity versus ratio of heights in a wedge (from Dowson, Lecture notes in Tribology, Leeds University)
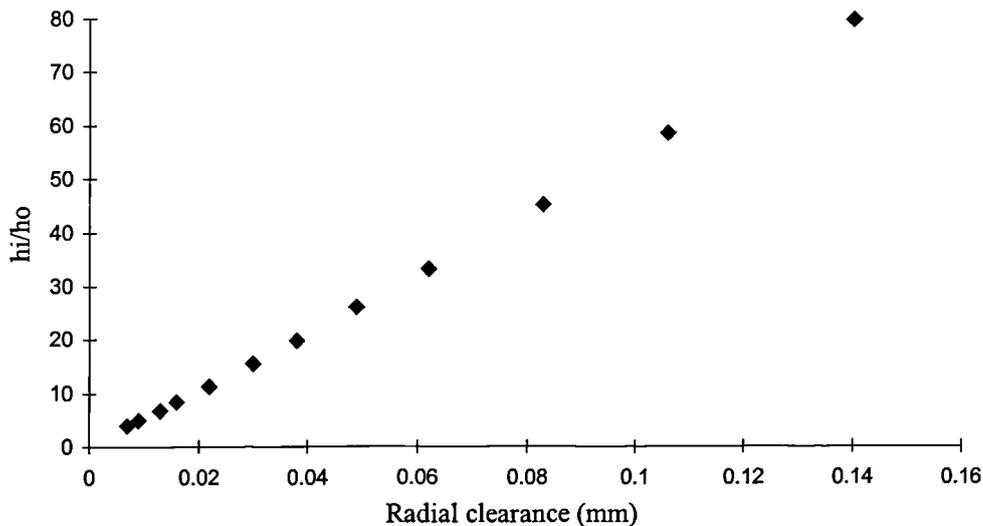
Figure 6.3: Ratio of heights in the wedge versus radial clearance

In addition to the differing radial clearances between the joints the metal-on-metal joints were not perfectly spherical. The clearances that have been stated were the average radial clearances but the polar radial clearances were somewhat different. This makes it even more difficult to discern a relationship between friction factor and clearance as any increase or decrease in friction factor may be due not only to the change in radial clearance but also to the differing sphericities of the joints. The out of roundness measurements of both the heads and the cups of the all metal joints were provided by Biomet Ltd.. These were determined on a Taly-Rond (out of roundness measuring machine) and are shown in Tables 6.1a and b. Three tests were carried out to produce these measurements, however, the errors involved with the measurements were not available from Biomet Ltd.. It is therefore difficult to rely on these values when determining any effect of sphericity on the friction factor.

Joint no 3 (14 μm radial clearance) gave consistently low values of friction factor throughout the tests. This may have been due to the sphericity of this particular joint. As well as the varying clearances and sphericity between joints, there was also a small variation in surface roughness between the joints. The surface roughness measurements were also provided by the sponsoring company and were taken with a Taly Surf (Table 6.1a and b). However, only one trace was taken. Four heads and

four cups were also tested on a Micromap 512 non-contacting optical profilometer prior to testing on the friction simulator. Each joint was tested at least twice. The measurements were found to differ from those taken on the Taly Surf (see Table 6.2). Joint no. 3 was not one of the joints tested. It is therefore not possible to conclude whether surface roughness played a role in the good lubricating properties of the 14 μm radial clearance joint.

Sample	R_a (μm)	Out of roundness (μm)
C1	0.04	2
C2	0.03	2
C3	0.04	2
C4	0.03	2
C5	0.01	2
C6	0.01	3
C7	0.02	2
C8	0.01	4
C9	0.01	2
C10	0.02	2
C11	0.01	2
C12	0.02	2

Table 6.1a: Roughness and out of roundness values of the metal cups (provided by Biomet Ltd.)

Sample	R_a (μm)	Out of roundness (μm)
H1	0.01	5
H2	0.01	5
H3	0.01	6
H4	0.01	3
H5	0.02	4
H6	0.01	5
H7	0.01	3
H8	0.02	4
H9	0.01	4
H10	0.01	3
H11	0.01	3
H12	0.01	4

Table 6.1b: Roughness and out of roundness values of the metal heads (provided by Biomet Ltd.)

	S_a (μm)	
Sample	Biomet (Taly Surf)	Micromap
C1	0.04	0.051
C2	0.03	0.012
C6	0.01	0.041
C12	0.02	0.027
H1	0.01	0.009
H2	0.01	0.009
H6	0.01	0.009
H12	0.01	0.010

Table 6.2: Comparison of surface roughness measurements

Large radial clearance   Small radial clearance
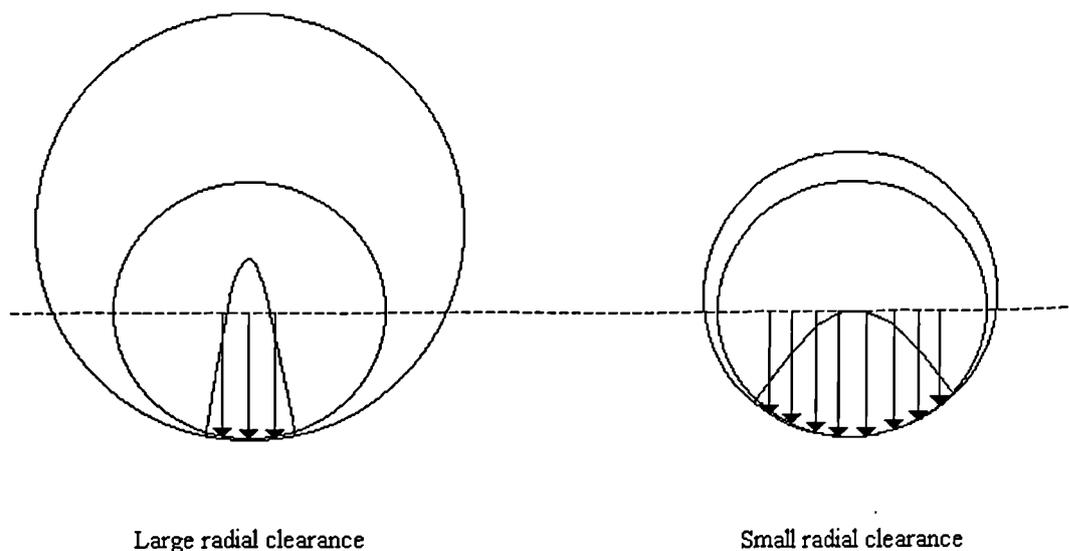
Figure 6.4: Magnitudes of frictional torques for a large and a small radial clearance

As the radial clearance increases the contact area reduces (becoming more like a point contact) and the maximum contact pressure increases. Gore *et* al (1981) theoretically determined the relationship between friction factor and coefficient of friction and found that the two closely approximated to each other and for a point contact the friction factor is equal to the coefficient of friction. As the contact geometry moves further away from a point contact (i.e. as the clearance is reduced) the friction factor will become increasingly different from the true coefficient of friction and has been found to always be larger than the coefficient of friction (for all reasonable pressure distributions). Therefore as the clearance gets smaller, the friction factor will become larger than the true coefficient of friction. Therefore, on the simulator, the smallest clearances would be expected to produce the larger friction factors due to this theory alone.

The lubrication mode of the metal-on-metal joints when lubricated with CMC fluids was mixed. The thin fluid film developed due to the viscosity of the lubricant (even at the higher viscosities) and the entraining velocities was not sufficient to separate

the rough metallic surfaces fully. Therefore contact of the metal asperities occurred resulting in relatively high friction (0.26). The subsequent frictional torques (circa 7 Nm) were still below those required to cause failure at the fixation interface, Andersson *et al* (1972). However, the torque measured by Andersson and colleagues was the torque that was required to remove a well fixed acetabular component by a single application. The high frictional torques developed by metal-on-metal bearing surfaces could therefore have implications in fatigue failure.

In all cases the second run gave higher friction than the first. The metal bearing surfaces became badly scratched immediately during testing increasing the surface roughness and therefore making full fluid film lubrication impossible (except, perhaps, at viscosities of lubricant well above the physiological level).

The friction in the metal-on-metal joints was due mainly to the contacting of the metal asperities with a very small proportion from the shearing of the lubricant film.

6.1.1.2 Al_2O_3/Al_2O_3 joints

The ceramic-on-ceramic joints produced extremely low values of friction factor for all lubricant viscosities. These friction factor values were within the high error range of the equipment (section 3.1.4). At a friction factor of 0.002 and an error margin of 98% the resulting range of friction factors is 0.001 to 0.003. It was therefore possible to conclude low friction (and almost definitely full fluid film lubrication) but caution must be used when discerning trends, and comparisons between other ceramic-on-ceramic joints were difficult.

The ceramic surfaces were initially very smooth (S_a = 0.002 and 0.003 for femoral and acetabular components respectively). Even after numerous tests there was no change in the topography of the bearing surfaces and no damage was evident by either the eye, microscope or the Zygo. The lubrication regime was approaching full fluid film for viscosities equivalent to physiological conditions. The thin film developed within the system was sufficient to separate the surfaces with minimal penetration by asperities. The very smooth surfaces of the ceramics and the

hydrophilic nature of the material were responsible for the superior lubricating properties of the ceramic-on-ceramic joints when lubricated with CMC fluids. As the friction was due mainly to the shearing of the lubricant it remained low during the tests and increased with lubricant viscosity.

6.1.1.3 CoCrMo/UHMWPE joints

Friction factors in metal-on-plastic joints have been measured for decades. The friction factors reported in this study are similar to those found previously (Walker and Gold 1973, Walker 1971, O'Kelly *et al* 1977, Unsworth 1978, O'Kelly *et al* 1979, Gore *et al* 1981, Unsworth *et al* 1994, Hall *et al* 1994, Hall *et al* 1997 and Elfick *et al* 1998a).

The frictional properties of this material combination are determined mainly by the plastic component. The lubrication mode was mixed and the majority of the friction was due to the shearing of the plastic (as this is the softer material) with a proportion due to shearing of the lubricant. Metal-on-plastic shearing creates less friction than the metal-on-metal shearing due to the way in which the surfaces bond. The elastic properties of the acetabular component of the metal-on-plastic joint also aid in the lubrication. In accordance with EHL theory the UHMWPE surface deforms under pressure, to a certain extent flattening out the asperities, resulting in less metal to plastic contact.

6.1.2 Stribeck analyses (50% bovine serum)

6.1.2.1 CoCrMo/CoCrMo

The friction factor in the metal-on-metal joints was slightly reduced when lubricated with 50% bovine serum as opposed to CMC fluids. The Stribeck plots indicated a boundary/mixed lubricating regime. It is suggested that the proteins present within bovine serum enhance the lubrication in metal-on-metal joints by adsorbing onto the surfaces. The joint surfaces are now encountering both shearing of the protein layers

and a small amount of shearing of the lubricating fluid along with some metal-on-metal rubbing. The resulting protein to protein rubbing creates less friction than the full metal-on-metal rubbing in the mixed lubrication regime in which these joints operate (Unsworth 1976, Unsworth 1978, Unsworth *et al* 1988, Unsworth 1991). The surface proteins present when using bovine serum as the lubricant may alter the contact conditions thus reducing naked asperity contact and thereby creating a less harsh environment in terms of adhesive wear.

Under high contact pressures we may expect these protein layers to be penetrated resulting in more pure metal-on-metal rubbing and an increase in friction factor. This, however, has not been found to be the case. The problems of determining any trend between radial clearance and friction factor have been discussed earlier. However, with 50% bovine serum, as the radial clearance gets larger and therefore the contact area reduces, the friction factor in turn reduces (see Figure 5.24). It could be the case that a greater contact pressure may result in a stronger bond between the protein layer and the metal substrate. There would therefore be less penetration of the metal through the protein layer resulting in reduced friction.

If the smallest clearance (7 μm) is ignored then there seems little dependence of friction factor on radial clearance. Let us consider two examples of clearance at 29 μm and 7 μm radial clearance respectively. The friction factors produced by the 29 μm radial clearance joint were 0.12 and 0.28 for 50% bovine serum and CMC fluids respectively. The sudden decrease in friction factor when lubricated with bovine serum is not as obvious in the 7 μm radial clearance case (0.2 cf. 0.25). If the difference between bovine serum and CMC fluids was as comparable in the 7 μm radial clearance case as it was for all other radial clearances then there would be no trend discernible between radial clearance and friction factor. The joints were repolished between the CMC tests and the bovine serum tests. The sphericity of the 7 μm radial clearance joint may have been altered during this process, as was the surface roughness. Therefore, again it is difficult to establish whether the change in friction factor was due to the clearance or another factor. Indeed, the fact that the metal-on-metal joints were repolished in between tests makes a direct comparison,

other than to note the reduction in friction factor with the bovine serum tests, between the separate CMC fluids tests and bovine serum tests impossible.

6.1.2.2 Al$_2$O$_3$/Al$_2$O$_3$

The friction factor produced by the ceramic-on-ceramic joints significantly increased when lubricated with 50% bovine serum as opposed to CMC fluids and the lubrication mode became mixed. It is suggested that this is due to the effects of the proteins contained within the bovine serum attaching to the bearing surfaces. Ceramic-on-ceramic joints work predominantly in the full fluid film lubricating regime when using CMC fluids which contain no proteins. The layer of protein adsorbed onto the ceramic surfaces may be sufficient to penetrate this fluid film leading to a predominantly mixed lubrication regime. It is hypothesised that the subsequent friction developed by this protein to protein rubbing is greater than that due to the shearing of the fluid film. Indeed, a recent study by Spikes (1996a) implied that "solid like" films of up to 20 nm thickness could be adsorbed onto the surfaces of materials. This would be sufficient to break down at least part of the fluid film in the ceramic-on-ceramic joints. Protein adsorption could also alter the surface properties of the material making the ceramic less hydrophilic reducing its lubricating capabilities.

The friction developed in the ceramic-on-ceramic joints was lower than that in the metal-on-metal joints when lubricated with bovine serum because the metal-on-metal joints not only exhibited protein to protein rubbing but metal-on-metal contact also. The ceramic-on-ceramic joints would also have a higher proportion of fluid film shearing.

As with the CMC tests there was no change in surface topography between tests with bovine serum therefore although the introduction of bovine serum as the lubricant significantly increased the friction in the joints no permanent surface damage was evident.

6.1.2.3 CoCrMo/UHMWPE

The metal-on-plastic joints operated in the mixed lubrication regime when lubricated with either CMC fluids or 50% bovine serum. These joints produced similar friction factors to the ceramic-on-ceramic joints when lubricated with bovine serum. Protein is, again, thought to be adsorbed onto the surfaces of both the metal and the plastic resulting in some protein to protein rubbing which will create the same friction as the protein to protein rubbing in the ceramic-on-ceramic joints. In this case, however, we also have metal-on-plastic contact as well as protein to protein (with a small proportion of the friction developed by the shearing of the lubricant film) leading to slightly higher friction than when lubricated with CMC fluids.

6.1.3 Bovine serum vs. synovial fluid - filtered and unfiltered

6.1.3.1 CoCrMo/CoCrMo

Synovial fluid produced slightly higher friction than bovine serum for the metal-on-metal joints. There was no difference between the filtered and unfiltered lubricants in either case.

Although the friction was increased slightly when synovial fluid was used as the lubricant instead of bovine serum, the friction was still lower than when lubricated with CMC fluids. Therefore, it can be assumed that the proteins in the synovial fluid have the same lubricating effects as those in the bovine serum.

The filtered lubricants were filtered with a 1 μm filter. A filter of this size would just remove foreign particles, such as small fragments of bone, it would not remove any proteins within the fluid or the hyaluronic acid chains. Indeed, there was little difference in viscosity between the filtered and unfiltered fluids. As the samples of both synovial fluid and bovine serum were relatively "clean" the filtering did not have much effect on the lubricating properties of the two fluids. When filtering the synovial fluid the viscosity seemed to reduce temporarily and then quickly thicken up

to its original viscosity. It is possible that the hyaluronic acid chains (which were originally curled up) disentangle and straighten as they pass through the filter with the aid of a vacuum pump. Once the chains were through the filter they then curled up again to their initial state.

6.1.3.2 Al_2O_3/Al_2O_3

There was no difference in friction between either synovial fluid and bovine serum or filtered and unfiltered lubricants with the ceramic-on-ceramic joints. It can, again, therefore be assumed that the proteins in the synovial fluid have the same effect on the friction as those in the bovine serum.

6.1.3.3 CoCrMo/UHMWPE

The synovial fluid was found to be a better lubricant in terms of friction than the bovine serum for the metal-on-plastic joints. No difference was found between filtered and unfiltered synovial fluid or bovine serum.

6.1.4 Static loading tests

6.1.4.1 CoCrMo/CoCrMo

There was no difference between synovial fluid and bovine serum when tested with a static load. However, the biological lubricants gave lower friction factor values than the CMC fluids. A static load was used to eliminate the squeeze film action and therefore to promote a boundary lubrication regime. The lower friction with the biological lubricants indicates an effective boundary film lubrication effect.

Friction factor, in general, decreased with increasing static load. As the bearing surfaces are pressed harder together the contact radius is effectively increased. Therefore the effective radius over which the torque is applied is decreased (see Figure 6.4). The observed reduction in friction factor with increase in static load

may therefore be an artefact of the experimental apparatus and not a true property of the joint. Although with metal-on-metal joints this effect will not be large due to the high elastic modulus of the material. The decrease in friction factor with increasing load is more likely to be due to the way in which the metal-on-metal asperities deform under load. According to Archard (1953), for the multiple asperity model of elastic and plastic contact respectively:

$$a_t \propto L^{4/5} \qquad\qquad\qquad (6.1)$$

$$a_t \propto L \qquad\qquad\qquad (6.2)$$

where a_t is the true area of contact and L is the applied load. As frictional torque is directly proportional to the true area of contact and the friction factor is directly proportional to the frictional torque and inversely proportional to the load, a relationship between friction factor and load can be deduced.

$$f \propto L^{-1/5} \qquad\qquad\qquad (6.3)$$

The above equation is for purely elastic contact, for plastic contact friction factor is independent of load. Metal-on-metal contact, depending, among other things, on the loading conditions will be mainly elastic with some plastic contact. Therefore the exponent should be between -1/5 and 0. A curve was fitted to Figure 5.40 and the exponent was found to be -1/2.5. The protein layer may be affecting this.

6.1.4.2 Al_2O_3/Al_2O_3

There was no difference between synovial fluid and bovine serum when tested with a static load. As has been the case throughout the tests with the ceramic-on-ceramic joints, the biological lubricants gave significantly higher friction than the CMC fluids of the same viscosities. Because the squeeze film action has been eliminated it is possible to conclude that the addition of proteins in the lubricant has an adverse

effect on the friction due to the boundary lubricating mechanism which operates in this case.

As with the metal-on-metal joints, a trendline was fitted to Figure 5.43 and the experimental results were compared with Archard's theory. The contacting conditions in an all ceramic joint would be expected to be elastic and therefore the friction factor would be expected to vary with load in the same way as for the metal-on-metal joints. This was not found to be the case, however, as friction factor was found to be almost independent of load in accordance with the theory of plastic contact. Again, the layer of adsorbed proteins may have altered these contacting conditions.

6.1.4.3 CoCrMo/UHMWPE

Again, no difference was found between synovial fluid and bovine serum when tested with static loads. The biological lubricants gave slightly higher friction than the CMC fluids indicating adverse boundary lubricating action.

Friction factor was found to be dependent on load to the power of -1/5. If Archard's single asperity model is applied then it can be deduced that friction factor, for elastic contact should be proportional to load to the power of -1/3 and should be independent of load for plastic contacting conditions. The contact in a metal-on-plastic joint will be mainly plastic with some elastic contact. The exponent should, therefore, be between 0 and -1/3.

6.1.5 Silicone fluids to full fluid film lubrication

In general the friction factors produced in the prostheses were lower when lubricated with silicone fluids than when lubricated with CMC fluids. Silicone fluids are Newtonian in nature at these shear rates. Therefore as the fluid is sheared the viscosity will remain the same. CMC fluids, however, are shear thinning and therefore as the shear rate increases the viscosity of the fluid decreases. At the high

shear rates encountered in the simulator, the actual viscosity of the CMC fluids will be reduced and therefore the friction factor will be increased when working in the mixed lubrication regime. However, the lower viscosities of silicone fluids severely scratched the surfaces of the metal-on-metal joints resulting in a high friction. Not only that but substantial metallic debris was found within the lubricant after only 41 cycles in the friction simulator. This severe scratching of the metal-on-metal joints has been found by other workers (Dowson, personal communication).

Fluid film lubrication was achieved with all material combinations but only the ceramic-on-ceramic joints operated in the full fluid film regime at the lower end of the viscosity range. At the higher viscosities when each material combination was operating in the full fluid film lubricating regime there was a difference in friction factor between material combinations. This was due to the different contact geometries between the hard bearing surfaces and the conventional joints. The minimum film thickness was larger in the conventional joints than the metal-on-metal and ceramic-on-ceramic joints thus reducing the friction for the same viscosity of lubricant when in the full fluid film regime.

6.1.6 Varying concentrations of bovine serum

6.1.6.1 CoCrMo/CoCrMo

There was a significant difference in friction factor between 0% bovine serum and all other concentrations of bovine serum (i.e. between CMC fluids and bovine serum). The addition of proteins reduced the friction within the joints. This seemed to have an immediate effect regardless of the concentration of proteins within the lubricant. Once proteins were added, little effect on the friction was apparent with any subsequent increase in the protein concentration.

It could be that, for the metal-on-metal joints, the adsorption rate of proteins onto the joint surfaces saturated almost immediately and therefore the resulting friction with 8.3% bovine serum was the same as that for 100% bovine serum. This would

explain why no further difference in friction was observed as the concentration of the bovine serum was increased.

6.1.6.2 Al₂O₃/Al₂O₃

An immediate significant rise in friction factor occurred with the ceramic-on-ceramic joints when proteins were added to the lubricant. As the concentration of the proteins increased the friction also increased slightly. The introduction of proteins in the lubricant resulted in a break-down of the fluid film. As more proteins adhere to the surfaces of the ceramics the effective roughness further increases therefore penetrating the fluid film more with subsequently more protein to protein rubbing, less proportion of shearing of the lubricant and higher friction.

6.1.6.3 CoCrMo/UHMWPE

As the protein content of the lubricant was increased so did the friction but the effect was not as pronounced for the metal-on-plastic joints as was the decrease in friction for the metal-on-metal joints or the increase in friction for the ceramic-on-ceramic joints.

6.1.6.4 Friction factor ranking

For the CMC fluids the metal-on-metal joints gave higher friction than the metal-on-plastic joints which in turn gave higher friction than the ceramic-on-ceramic joints. When using 100% bovine serum as the lubricant the metal-on-metal joints again gave the highest friction with the metal-on-plastic and ceramic-on-ceramic joints giving similar but much lower friction.

Figure 5.51 clearly shows the difference in friction factor between the metal-on-metal, ceramic-on-ceramic and metal-on-plastic joints. The all ceramic joints gave consistently low values of friction factor with the CMC fluids. This friction was one order of magnitude lower than the friction developed within the metal-on-plastic joints which, in turn, was one order of magnitude lower than the all metal

combination. Even with bovine serum the friction produced in the all metal joints was one order of magnitude greater than that for the all ceramic joints or the conventional metal-on-plastic joints.

At 100% bovine serum, the metal-on-plastic joints and the ceramic-on-ceramic joints gave approximately the same friction factors. This may be due to the protein adsorption onto the surfaces being saturated therefore resulting in an equivalent amount of almost pure protein to protein rubbing with only a small amount of friction due to shearing of the lubricant film alone. The metal-on-metal friction was higher because, although some protein to protein rubbing existed, there may still be some metal-on-metal rubbing which creates very high friction. The proteins may not adhere as strongly to the metal surfaces resulting in more penetration of the protein layer in the all metal joints than the ceramic-on-ceramic or metal-on-plastic joints.

The concentrations of proteins within 100% bovine serum have been compared with those within 100% synovial fluid (normal). One hundred per cent synovial fluid can be equated to approximately 30% bovine serum in terms of protein content (Davies, 1967 and Geigy Scientific Tables). Although few protein analyses have been performed on diseased synovial fluid, fluid from joints with rheumatoid arthritis was found to have a higher content of proteins than normal synovial fluid (Geigy Scientific Tables). Therefore as the concentration of bovine serum is increased up to 100%, there are more proteins present in the fluid than there would be should synovial fluid be used as the lubricant. This is borne out by the fact that, for both the ceramic-on-ceramic and metal-on-plastic joints, the friction factors produced when synovial fluid was used as the lubricant were lower than those produced with the higher concentrations of bovine serum. The friction factor for the metal-on-metal joints, once protein had been added, did not alter considerably with concentration of bovine serum. The metal-on-metal joints produced the same friction with synovial fluid and for all concentrations of bovine serum above zero.

6.1.7 Long term friction tests on CoCrMo/CoCrMo joints

The long term friction tests were performed twice on selected joints and the friction was highly consistent between runs. The friction factor in the metal-on-metal joints did not seem to vary considerably with time. This is unlike that found by Schmidt *et al* (1996) and may be due to the differences between the loading and motion cycles applied in this study and in the study by Schmidt and colleagues. The Hip Function Friction Simulator used in this study only applied one axis of load and motion. Initial scratching of the metal surfaces in the direction of motion occurred as soon as the motion was started thus giving high friction. The scratching did not appear (by either the naked eye or through a microscope) to get better or worse with time. It has been shown by Tipper *et al* (1999) that by adding a second or third axis of motion the wear and lubricating conditions within the bearing can be affected. The joints tested by Schmidt *et al* (1996) were tested in a simulator with more than one axis of motion therefore affecting the way the scratches occur on the surface and therefore the way in which the frictional torque was developed over time. The hip simulator with more than one motion axis is more likely to reflect physiological conditions and therefore how friction factor may vary with time *in situ*.

Throughout the long term friction tests the bovine serum was replenished by adding more lubricant at regular intervals. If this were not the case then there may have been an increase in friction factor over time due to proteins being rubbed off the surface or being degraded.

Friction factor was also independent of load. An increase in the contact pressure may break down the protein layer and therefore produce more naked metal-on-metal asperity rubbing and subsequently higher friction. This was not found to be the case for loads up to 2000 N.

6.1.8 Overview

Friction factors for the metal-on-metal and metal-on-plastic joints in CMC fluids and bovine serum were found to be similar to those found previously by other workers (Walker and Gold 1973, Walker 1971, Unsworth 1976, O'Kelly *et al* 1977, Unsworth 1978, O'Kelly *et al* 1979, Gore *et al* 1981, Unsworth *et al* 1988, Unsworth 1991, Semlitsch 1993, Unsworth *et al* 1994, Hall *et al* 1994, Schmidt *et al* 1996, Hall *et al* 1997, Elfick *et al* 1998a). The friction factors for the ceramic-on-ceramic joints in CMC fluids were also similar to those found by other workers when tested in other water-based lubricants, Saikko and Pfaff (1998). However, other studies have found the friction within ceramic-on-ceramic joints to be up to one order of magnitude higher than those found in this study, Walter (1992).

The metal-on-metal joints that were supplied for friction testing were of the low carbon material composition, type C. However, material A, the high carbon material, was subsequently chosen as the material for the clinical trials due to the much lower wear rates of the high carbon CoCrMo against itself compared with the low carbon CoCrMo against itself. It was not possible to obtain a joint of the high carbon material to test on the friction simulator and therefore the frictional properties of this material were not established.

When using CMC fluids as the lubricant, the metal-on-metal and the metal-on-plastic joints were found to operate in the mixed lubrication regime with both a falling friction factor with increasing Sommerfeld number and a λ value of less than one. The mixed lubrication regime was also found to be acting within these joints when bovine serum was used as the lubricant.

The ceramic-on-ceramic joints, however, reacted differently to the change of lubricant. When using CMC fluids or silicone fluids as the lubricant the ceramic-on-ceramic joints were shown to have full fluid film lubrication where the surfaces are separated completely by a thin film of lubricant. This was indicated by both an increasing friction factor with increasing Sommerfeld number and by demonstrating

a λ value of more than three. When bovine serum was employed as the lubricant the friction in the ceramic-on-ceramic joints increased significantly and the lubrication regime moved from being full fluid film to being mixed. The ceramic surfaces used in total hip replacements have a very low roughness value which aids the lubrication as a thinner film is needed to separate the surfaces. Not only this but ceramics have much better wettability than both metals and plastics, Davidson (1991). The contact angles for these surfaces are shown in Table 6.3. The lower the surface contact angle and hence higher the wettability, the more hydrophilic in nature the surfaces are which aids in lubrication.

Material	Contact angle
CoCrMo	60°
Al_2O_3	30°
UHMWPE	100°

Table 6.3: Contact angle of distilled water on different polished, flat surfaces (from Davidson, 1991)

When considering the effect that a boundary lubricant, such as protein, has on the friction of a bearing it is useful to look at the ratio of the different types of contact. With a non-boundary lubricant such as CMC fluids, the friction (μ) produced by a material combination is made up of the friction produced by the contacting of the "dry" asperities (μ_{dry}) and that produced by the shearing of the fluid film (μ_{fl}), i.e.

$$\mu = \mu_{dry} + \mu_{fl} \tag{6.4}$$

However, when a boundary lubricant is introduced the friction factor will be decreased if $\mu_b < \mu_{dry}$. Where μ_b is the friction produced at the boundary lubricated asperity contact. The boundary lubricant may, however, also increase the real contact area by filling in asperity voids and because $\mu_b > \mu_{fl}$ this will increase the friction. Now we have:

$$\mu = \mu_b + \mu_{fl} \tag{6.5}$$

so the friction now depends on the ratio of the boundary film contact to the shearing of the fluid film. In mixed lubrication this may either increase or decrease the friction depending on the difference between μ_{dry} and μ_b. In the case of the ceramic-on-ceramic joints which operated in the full fluid film regime when lubricated with a non-boundary lubricating fluid, the friction will be increased as $\mu_b > \mu_{fl}$. This may, however, benefit the wear of such joints and also the start up friction.

It has been suggested that calcium phosphate deposits from the bovine serum can adsorb onto the surfaces of prosthesis materials (McKellop and Clark 1984) thus altering the friction within these joints. The introduction of ethylenediaminetetra-acetic acid (EDTA) into the bovine serum will inhibit the formation of calcium phosphate coatings. A small number of friction tests were performed on all the material combinations with bovine serum and 5 μM EDTA to determine whether in fact it was these calcium deposits that were causing the changes in friction encountered when using bovine serum as the lubricant. The results showed only a small change in friction when EDTA was added to the lubricant. Therefore protein can still be assumed to be the dominant factor in altering the friction in different material combinations, although there may be a small effect due to calcium phosphate deposits.

CMC fluids are non-Newtonian and therefore shear thinning in nature, as are both synovial fluid and bovine serum. The shear rate at which these fluid viscosities were measured was lower than that applied by the simulator at the position in the cycle where the friction was recorded. It is assumed that the viscosity at the shear rate at which the joints were tested is slightly reduced in all cases. This would have no effect on the shape of the Stribeck plot but would shift it to the left if the correct viscosities were used in the calculation of Sommerfeld number.

6.1.9 Protein gel technique

Proteins were found to be adsorbed onto all of the material combinations tested (this was found in both of the tests performed). The intensity of the protein band on the gel in the protein gel technique is indicative of the amount of protein that is adsorbed onto the material surface. Therefore it can be concluded that for each material the main protein that is found on the surfaces is bovine serum albumin and that the ceramic and plastic materials adsorb more protein than the metal. The second protein that is seen to bind onto the surfaces of the prosthesis materials is expected to be a mixture of γ and β globulins.

6.2 Wear

6.2.1 Initial metal/metal wear tests

The wear factors produced by both the high carbon and low carbon metal samples were similar to those found by Schmidt *et al* (1996) and Tipper *et al* (1999) for similar materials. The two wear phases exhibited by these pin-on-plate tests have been shown by many other workers (Schmidt *et al* 1996, Chan *et al* 1996, Medley *et al* 1996 and Farrar and Schmidt 1997). In most cases the secondary phase wear factor was significantly lower than the primary phase wear factor. In all cases the wear produced by the pin-on-plate apparatus is far greater than that found both clinically and by wear simulators. This is unlike those results for metal-on-polyethylene samples where pin-on-plate studies produce much lower wear than that found clinically (McKellop 1981 and Weightman and Light 1985).

The high carbon material wore considerably less than the low carbon material, Schmidt *et al* (1996) and Tipper *et al* (1999) also found this. Figure 6.5 shows the total wear factors for both the pins and the plates of the three material compositions, in all cases the secondary phase wear factors were used. The lower wear in the high

carbon material was due to its greater distribution of the wear resisting carbides. The hard carbide particles increase the surface hardness of the metal and hence the resistance against plastic deformation. Adhesive wear is the main form of wear when one metal slides against another. There is usually a very good bond between the carbide and the metal matrix reducing the occurrence of adhesive wear at these contacts.
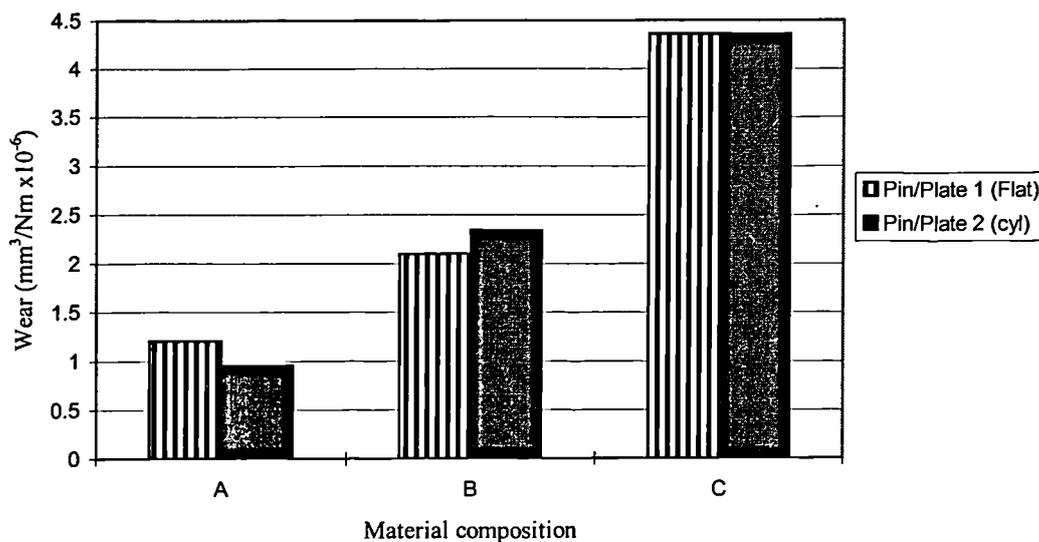
Figure 6.5: Total wear factors for each material composition

There was no difference between the wear of the cylindrically ended pin and the flat ended pin either with respect to the pin or the plate (Figure 6.5). Therefore there was no benefit on the wear with the introduction of the wedge in the cylindrically ended pin. Calculations were performed to determine the ratio of the heights in the wedge (see Appendix F). This ratio was found to be incredibly large and therefore not at all beneficial (see Figure 6.2).

Previous studies by various authors have found the wear factors for metals and ceramics against UHMWPE (in a lubricant of bovine serum) to be one or even two orders of magnitude lower than the results found here for metal-on-metal samples. (McKellop 1981, Weightman and Light 1985, Kumar *et al* 1991 and Cooper *et al* 1993). However, metal-on-metal joints produce far less wear than metal/ceramic-on-plastic joints clinically.

The simple reciprocating pin-on-plate tests apply more rigorous loading conditions to the metal samples than is normally found in the body. This results in much higher wear rates than found clinically for metal-on-metal joints. However, this is not the case for metal-on-plastic joints. During simple reciprocating motion between metal and UHMWPE samples the polyethylene molecular chains will align themselves which will result in a reduction in the wear compared to that found clinically - the opposite effect to that found with the all metal samples. Because of the way the wear rates of different materials react to this kind of test it is impossible to compare directly the wear rates found from a simple reciprocating pin-on-plate machine for different material combinations. Indeed, simple reciprocating pin-on-plate machines should only be used (with caution) to compare wear rates of similar material combinations e.g. high and low carbon metals.

Care should always be taken when comparing the wear factors of materials with those found by different workers as the testing conditions are unlikely to be the same. Discrepancies lie in the sliding speed, stroke length, loading conditions and perhaps most importantly lubricant. Although a standard does exist for the testing conditions in a pin-on-plate machine this, unfortunately, seems rarely abided by.

6.2.2 Validation of new wear machine - XLPE/XLPE

The addition of rotational motion to the reciprocating pin-on-plate machine resulted in a significant increase in the wear of XLPE against itself. For both reciprocation alone and rotation plus reciprocation the pin wear was minimal and most of the wear resulted from the plate. The wear of the plate with rotation was five times that without rotation. The results compare almost perfectly with those found by Cartwright (1998). As a validation exercise this series of tests was entirely successful.

The increase in wear with added rotation is what would be expected. Although XLPE chains are cross linked, some orientation of the polyethylene molecular chains

will still occur when only one direction of motion is applied. Therefore when rotation and reciprocation motion is applied to the XLPE samples the alignment of the polyethylene chains does not occur and the wear is increased. The difference in the wear between pure sliding conditions and that with added rotation for XLPE should not be as large as that for UHMWPE but nevertheless will still occur.

6.2.3 Metal/metal wear tests - reciprocation plus rotation

The addition of the rotational motion to material C (low carbon) significantly reduced the wear. This effect on material A (high carbon), however, was far less pronounced than in material C. The plate wear reduced but the pin wear was not significantly changed. Tipper *et al* (1999) also found that the introduction of a second axis of motion to metal-on-metal wear samples decreased the wear of the low carbon content material significantly but not that of the high carbon content material. Overall the wear order is specified below and can be seen in Figure 6.6.

Wear of A (with rotation) = Wear of A < Wear of C (with rotation) < Wear of C
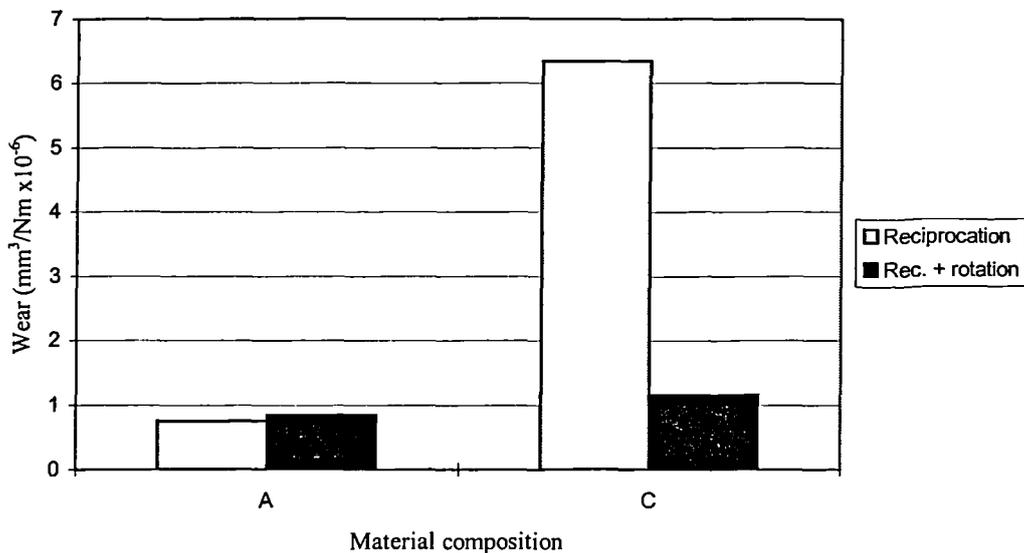
Figure 6.6: Total wear of the metal-on-metal pins and plates with and without rotation

Therefore although the addition of rotation decreased the wear of material C dramatically, it did not decrease it below the wear of material A with reciprocating motion alone (1.15×10^{-6} mm^3/Nm cf. 0.75×10^{-6} mm^3/Nm). Material A is therefore the best in terms of wear.

It is hypothesised that the reduction in wear factor with the addition of rotational motion is due to the self healing properties of the metal surfaces. With reciprocation alone the metal surfaces are scratched in the direction of sliding. When rotation is added some of the "built up edge" surrounding the scratch (because the metal is ductile) may be folded back into the wear track making it less likely to become an abrading asperity but also making it less likely to be removed as a wear particle. Multidirectional polishing of metals in this type of test has also been discussed by Tipper *et al* (1999).

The simple reciprocation tests compared well with those on the existing machines (Table 5.6). However, there was less evidence of a biphasic wear pattern.

When calculating the wear factors only the reciprocating sliding distance was taken into account, no alteration was made to the sliding distance due to the rotation of the pin in those tests which incorporated both reciprocation and rotational motion. This is a somewhat simplified method of calculating the wear factor. Calculations were performed to determine what effect, if any, the rotation had on the overall sliding distance (see Appendix G). It was shown that rotation increased the average sliding distance (depending on which position on the pin the calculations were performed with respect to, the sliding distance was either increased or decreased) but only by a factor of about 2.1%. It was therefore deduced that using the reciprocating sliding distance in the calculations of wear factor was, indeed, a good approximation to the sliding distance.

7. Conclusions

This study has presented a thorough investigation into the friction of various material combinations. Perhaps the most interesting aspect of the results is the effect of the additions of protein into the lubricant on the friction of artificial joints, particularly the ceramic-on-ceramic joints. The ceramic coupling was shown to be the lowest friction combination when tested with synthetic lubricants. For these lubricants the theoretical predictions of lubrication mode correlate well with experimental data. However, these predictions are less appropriate with biological fluids as the lubricant as both the viscosity of the bulk lubricant along with the adsorbed films of protein affect the lubricating conditions. Indeed, the friction in the ceramic-on-ceramic joint was increased considerably when lubricated with these fluids.

It is clear that the levels of friction factor encountered in artificial joints depends on the lubricant, whether it be CMC fluids, silicone fluids, synovial fluid or bovine serum. Friction factor also depends, albeit in some cases only slightly, on the concentration of bovine serum used. This highlights the need for standardisation of the lubricants used in both friction testing and in wear tests. Protein adsorption may, however, have benefits on the wear of such prostheses. Under loading conditions where the fluid film may break down, such as the stance phase of walking, lubrication may be in the boundary regime. Any resulting asperity contact may be reduced by this protein layer, resulting in reduced wear of the bearing surfaces.

A new wear machine complying to the ASTM standards was designed, tested and validated. From this it was concluded that the high carbon CoCrMo was a better material in terms of wear than the low carbon CoCrMo. It was also concluded that the addition of rotational motion to the simple reciprocating pin-on-plate machine reduced the wear in metal-on-metal samples more closely to that found clinically. The pin-on-plate machine with rotation is therefore considered to be a more accurate method of comparing the wear of different material combinations than the simple reciprocating machines. It is also considered to be a cheap and simple solution for comparing these material combinations before testing them on simulators that more accurately match the loading and motion cycles within the body.

8. Recommendations for future research

Further frictional tests and also wear tests, should be performed on metal-on-metal and ceramic-on-ceramic prostheses to determine the effects of altering the surface roughness and also the sphericities of the joint components. The effect of radial clearance on the friction of ceramic-on-ceramic joints should also be investigated.

The concentration of bovine serum is an important variable in the friction of total hip prostheses. Pin-on-plate and simulator studies should be performed on all material combinations to determine the effect of varying the concentration of bovine serum on the wear of such prostheses.

The interactions of the proteins present within bovine serum and synovial fluid with the surfaces of prosthesis materials needs to be further investigated. It may be possible to identify the proteins using, for example, X-ray photoelectron spectroscopy (XPS). The effects of these proteins on both the friction and wear of material combinations must be determined to provide a more thorough understanding of the tribology of prostheses, particularly ceramic-on-ceramic joints. Studies should be performed using isolated components of synovial fluid and bovine serum to determine the individual effects of these on the friction and wear of both hard bearing surfaces and conventional joints.

9. References

Amstutz, H. C. and **Grigoris, P.** Metal on metal bearings in hip arthroplasty. *Clin. Orthop. Rel. Res.*, 1996, **329S**, S11-S33.

Andersson, G. B. J., Freeman, M. A. R. and **Swanson, S. A. V.** Loosening of the cemented acetabular cup in total hip replacement. *J. Bone Jt Surg.*, 1972, **54B**, 590-599.

Archard, J. F. Contact and rubbing of flat surfaces. *Journal of Applied Physics*, 1953, **24**, 8, 981-988.

Aspenberg, P. and **Herbertsson, P.** Periprosthetic bone resorption: particles versus movement. *J. Bone Jt Surg.* 1996, **78-B**, 4, 641-646.

Aspenberg, P. and **van der Vis, H.** Fluid pressure may cause periprosthetic osteolysis. *Acta. Orthop. Scand.*, 1998, **69**, 1, 1-4.

ASTM F732-82. Standard practice for reciprocating pin-on-flat evaluation of friction and wear properties of polymeric materials for use in total joint prostheses. *Annual Book of ASTM standards*, 1982, **13.01**, 263-269.

Bankston, A. B., Faris, P. M., Keating, E. M. and **Ritter, M. A.** Polyethylene wear in total hip arthroplasty in patient-matched groups. *J. Arthrop.*, 1993, **8**, 3, 315-322.

Bigsby, R. J. A., Hardaker, C. S. and **Fisher, J.** Wear of ultra-high molecular weight polyethylene acetabular cups in a physiological hip joint simulator in the anatomical position using bovine serum as a lubricant. *Proc. Instn. Mech. Engrs*, 1997, **211**, 265-271.

Blamey, J. M. Improved tribology and materials for a new generation of hip prosthesis. 1993, Ph.D. Thesis, School of Engineering, University of Durham.

Boehler, M., Knahr, K., Plenk, H., Walter, A., Salzer, M. and **Schreiber, V.** Long-term results of uncemented alumina acetabular implants. *J. Bone Jt Surg.* 1994, **76-B**, 1, 53-59.

Briscoe, B. Wear of polymers: an essay on fundamental aspects. *Tribology International*, August 1981, **4**, 231-243.

Burgess, I. C. Tribological and mechanical properties of compliant bearings total joint replacements. PhD Thesis, 1996, University of Durham.

Burwell, J. T. and **Strang, C. D.** On the empirical law of adhesive wear. *J. Appl. Phys.* 1952, **23**, 18-28.

Callaghan, J. J., Forest, E. E., Olejniczak, J. P., Goetz, D. D. and **Johnston, R. C.** Charnley total hip arthroplasty in patients less than fifty years old. *J. Bone Jt Surg.* 1998, **80-A**, 5, 704-714.

Cartwright, T. The effect of rotation on the wear of cross-linked polyethylene (XLPE). Final year project for MEng, 1998, University of Durham.

Cates, H. E., Faris, P. M., Keating, E. M. and **Ritter, M. A.** Polyethylene wear in metal-backed acetabular cups. *J. Bone Jt Surg.* 1993, **75-B**, 2, 249-253.

Chan, F. W., Bobyn, J. D., Medley, J. B., Krygier, J. J., Yue, S. and **Tanzer, M.** Engineering issues and wear performance of metal on metal hip implants. *Clin. Orthop. Rel. Res.*, 1996, **333**, 96-107.

Charnley, J. The lubrication of animal joints. *IMechE Symposium on Biomechanics*, London 1959, 12-22.

Charnley, J. and **Kamangar, A.** The optimum size of prosthetic heads in relation to the wear of plastic sockets in total replacement of the hip. *Med. Biol. Engng.*, 1969, 7, 31-39.

Cooke, A. F., Dowson, D. and **Wright, V.** The rheology of synovial fluid and some potential synthetic lubricants for degenerate synovial joints. *J. Engng. in Medicine.*, 1978, 7, 66-72.

Cooper, J. R., Dowson, D. and **Fisher, J.** The effect of transfer film and surface roughness on the wear of lubricated ultra-high molecular weight polyethylene. *Clin. Mater.*, 1993, 14, 295-302.

Cudworth, C. J. and **Higginson, G. R.** Friction of lubricated soft surface layers. *Wear*, 1976, 37, 299-312.

Dall, D. M., Learmonth, I. D., Solomon, M. I., Miles, A. W. and **Davenport, J. M.** Fracture and loosening of Charnley femoral stems. *J. Bone Jt Surg.* 1993, 75-B, 2, 259-265.

Davidson, J. A. Phenomena related to adhesive and oxidation abrasive wear and friction of metal orthopaedic implant bearing surfaces. Ph.D. Dissertation, 1991, Orthopaedic Research Department, Memphis, TN.

Davies, D. V. Properties of synovial fluid. *Proc. Instn. Mech. Engrs*, 1967, 181, 25-28.

Deeley, Friction. T. E. Stanton publ. Longmans, Green & Co. London. 1923.

Derbyshire, B. The estimation of acetabular cup wear volume from two-dimensional measurements: a comprehensive analysis. *Proc. Instn. Mech. Engrs*, 1998, 212, 281-291.

Dintenfass, L. Lubrication in synovial joints: a theoretical analysis. *J. Bone Jt Surg.* 1963, **45-A**, 6, 1241-1255.

Doorn, P. F., Campbell, P. A. and **Amstutz, H. C.** Metal versus polyethylene wear particles in total hip replacements. *Clin. Orthop. Rel. Res.*, 1996, **329S**, S206-S215.

Dorlot, J.-M., Christel, P. and **Meunier, A.** Wear analysis of retrieved alumina heads and sockets of hip prostheses. *J. Biomed. Mater. Res.: Applied Biomaterials*, 1989, **23**, A3, 299-310.

Dowson, D. Modes of lubrication in human joints. *Proc. Instn. Mech. Engrs*, 1966-67, **181**, Part J, 45-54.

Dowson, D., Wright, V., Unsworth, A. and **Gvozdanovic, D.** An overall view of synovial joint lubrication. *Ann. Rheum. Dis.* 1975, **34**, 94-97.

Dowson, D. and **Wallbridge, N. C.** Laboratory wear tests and clinical observations of the penetration of femoral heads into acetabular cups in total replacement hip joints. I. Charnley prostheses with polytetraflouroethylene acetabular cups. *Wear*, 1985, **104** (3), 203-215.

Dowson, D. and **Jin, Z-M.** Micro-elastohydrodynamic lubrication of synovial joints. *J. Engng. in Medicine.*, 1986, **15**, 2, 63-65.

Dowson, D. Thin films in tribology. In: Dowson, D. *et al*, eds. Thin films in tribology. *19th Leeds - Lyon Symposium*. Amsterdam, Elsevier Science., 1993, 1.

Elfick, A. P. D., Hall, R. M., Pinder, I. M. and **Unsworth, A.** The frictional behaviour of explanted PCA hip prostheses. *Proc. Instn. Mech. Engrs*, 1998a, **212**, 395-397.

Elfick, A. P. D., Hall, R. M., Unsworth, A. and Pinder, I. M.   Tribological performance of the PCA total hip replacement.   *J. Bone Jt Surg.*, 1998b, **80-B**, Sup III,

Elfick, A. P. D., Hall, R. M., Pinder, I. M. and Unsworth, A.   Wear in retrieved acetabular components: effect of femoral head radius and patient parameters.   *J. Arthrop.*, 1998c, **13**, 291-295.

Elloy, M.   Simulator testing of joint prostheses: the need for realistic simulator testing.   SERC/IMechE Annual Expert Meeting on *Failure of Joint Prostheses*, Bournemouth, 1993, 79-82.

English, T. A. and Kilvington, M.   In vivo records of hip loads using a femoral implant with telemetric output (a preliminary report).   *J. Biomed. Eng.* 1979, **1**.

Farrar, R. and Schmidt, M. B.   The effect of diametral clearance on wear between head and cup for metal on metal articulations.   *43rd Annual Meeting, ORS, San Fransisco, California*, February 1997, **12**.

Fein, R. S.   Are synovial joints squeeze-film lubricated?   *Proc. Instn. Mech. Engrs*, 1966-67, **181**, Part J, 125-128.

Fisher, J.   Wear of ultra high molecular weight polyethylene in total artificial joints. Current Orthopaedics-Biomechanics Masterclass, 1994.

Geigy Scientific Tables.   J. R. Geigy S. A., Basle, Switzerland, 1970, seventh edition.

Goldsmith, A. A. J. and Dowson, D.   A multi-station hip joint simulator study of the performance of 22 mm diameter zirconia - ultra-high molecular weight polyethylene total replacement hip joints.   *Proc. Instn. Mech. Engrs*, 1999, **213**, 77-90.

Gore, T. A., Higginson, G. R. and Kornberg, R. E. Some evidence of squeeze-film lubrication in hip prostheses. *J. Engng. in Medicine.*, 1981, **10**, 89-95.

Green, T. R., Matthews, J. B., Wroblewski, B. M., Fisher, J. and Ingham, E. Polyethylene particles of a "critical size" are necessary for the induction of cytokines by macrophages *in vitro*. Presented at the Spring Meeting of the British Orthopaedic Research Society, March 1997.

Greenwood, J. A. and Williamson, J. B. P. Contact of nominally flat surfaces. *Proc. Roy. Soc. (London)*, 1966, **295**, A, 300-319.

Hall, R. M., Unsworth, A., Wroblewski, B. M. and Burgess, I. C. Frictional characterisation of explanted Charnley hip prostheses. *Wear*, 1994, **175**.

Hall, R. M., Unsworth, A., Craig, P. S., Hardaker, C., Siney, P. and Wroblewski, B. M. Measurement of wear in retrieved acetabular components. *Proc. Instn. Mech. Engrs*, 1995, **209**, 233-242.

Hall, R. M., Unsworth, A., Siney, P. and Wroblewski, B. M. Wear in retrieved Charnley acetabular sockets. *Proc. Instn. Mech. Engrs*, 1996, **210**, 197-207.

Hall, R. M., Siney, P. D., Unsworth, A. and Wroblewski, B. M. Friction in explanted prostheses. *Brit. J. Rheum.*, 1997.

Hall, R. M., Siney, P., Unsworth, A. and Wroblewski, B. M. The association between rates of wear in retrieved acetabular components and the radius of the femoral head. *Proc. Instn. Mech. Engrs*, 1998a, **212**, 321-326.

Hall, R. M., Siney, P., Craig, P. S., Unsworth, A. and Wroblewski, B. M. Discrepancy between penetration depths derived from radiographic and direct measurement of acetabular components. *Proc. Instn. Mech. Engrs*, 1998b, **212**, 57-64.

Hamrock, B. J. and **Dowson, D.** Elastohydrodynamic lubrication of elliptical contacts for materials of low elastic modulus I-Fully flooded conjunction. *J. Lubrication. Technol.*, 1978, **100**, 236-245.

Hamrock, B. J. Fundamentals of fluid film lubrication. 1994, McGraw-Hill, Singapore.

Hardy, W., B and **Doubleday, I.** Boundary lubrication - the paraffin series. *Proc. R. Soc. London Ser. A.*, 1922, **100**, 25-39.

Hardy, W. B. and **Bircumshaw, I.** Boundary lubrication - plane surface and the limitations of Amonton's law. *Proc. Roy. Soc. Lond.*, 1925, **A109**, 1-27.

Harris, W. H. Osteolysis and particle disease in hip replacement: a review. *Acta. Orthop. Scand.*, 1994, **65**, 1, 113-123.

Hernandez, J. R., Keating, E. M., Faris, P. M., Meding, J. B. and **Ritter, M. A.** Polyethylene wear in uncemented acetabular components. *J. Bone Jt Surg.* 1994, **76-B**, 2, 263-266.

Higginson, G. R. Elastohydrodynamic lubrication in human hip joints. *J. Engng. in Medicine.*, 1978, **7**, 1, 35-41.

Holm, R. Electric contacts. 1946, Almqvist and Wiksells, Stockholm.

Howie, D. W., Vernon-Roberts, B., Oakeshott, R. and **Manthey, B.** A rat model of resorption of bone at the cement-bone interface in the presence of polyethylene wear particles. *J. Bone Jt Surg.*, 1988, **70-A**, 257-263.

Howie, D. W., Manthey, B., Hay, S. and **Vernon-Roberts, B.** The synovial response to intraarticular injection in rats of polyethylene wear particles. *Clin. Orthop. Rel. Res.*, 1993, 352-357.

Hutchings, I., M. Tribology - friction and wear of engineering materials. 1992, Edward Arnold, London.

Isaac, G. H., Wroblewski, B. M., Atkinson, J. R. and **Dowson, D.** A tribological study of retrieved hip prostheses. *Clin. Orthop. Rel. Res.*, 1992, **276**, 115-125.

Jacobsson, S-A., Djerf, K. and **Wahlström, O.** 20-year results of McKee-Farrar versus Charnley prosthesis. *Clin. Orthop. Rel. Res.*, 1996, **329S**, S60-S68.

Jin, Z. M., Dowson, D. and **Fisher, J.** Analysis of fluid film lubrication in artificial hip joint replacements with surfaces of high elastic modulus. *Proc. Instn. Mech. Engrs*, 1997, **211**, 247-256.

Johnson, K. L., Greenwood, J. A. and **Poon, S. Y.** A Simple theory of asperity contact in elastohydrodynamic lubrication. *Wear*, 1972, **19**, 91-108.

Johnston, R. C. and **Smidt, G. L.** Measurement of the hip joint motion during walking. *J. Bone Jt Surg.* 1969, **51-A**, 6, 1083-1094.

Jones, E. S. Joint lubrication. *Lancet*, 1936, **1**, 1043-1044.

Joyce, T.J., Ash, H. E. and **Unsworth, A.** The wear of cross-linked polyethylene against itself. *Proc. Instn. Mech. Engrs*, 1996, **210**, 11-16.

Kabo, J. M., Gebhard, J. S., Loren, G. and **Amstutz, H. C.** In vivo wear of polyethylene acetabular components. *J. Bone Jt Surg.* 1993, **75-B**, 2, 254-258.

Kingsbury, A. A new oil testing machine and some of its results. *Trans. ASME.*, 1903, **24**, 143-160.

Kobayashi, A., Bonfield, W., Kadoya, Y., Yamac, T., Freeman, M. A. R., Scott, G. and Revell, P. A. The size and shape of particulate polyethylene wear debris in total joint replacements. *Proc. Instn. Mech. Engrs*, 1997, **211**, 11-15.

Kothari, M., Bartel, D. L. and Booker, J. F. Surface geometry of retrieved McKee-Farrar total hip replacements. *Clin. Orthop. Rel. Res.*, 1996, **329S**, S141-S147.

Kumar, P., Oka, M., Ikeuchi, K., Shimizu, K., Yamamuro, T., Okumura ,H. and Kotoura, Y. Low wear rate of UHMWPE against zirconia ceramic (Y-PSZ) in comparison to alumina ceramic and SUS 316L alloy. *J. Biomed. Mater. Res.*, 1991, **25**, 813-828.

Laemmli, U. K. Cleavage of Structural Proteins during the Assembly of the Head of Bacteriophage T4. *Nature*, 1970, **227**, 680-685.

Lancaster, J. K. Friction and wear. In: *Polymer science*, 1972, Jenkins, A. D. (ed), North-Holland Publishing Company, Ch 14, 959-1046.

Lancaster, J. K. Material-specific wear mechanisms: relevance to wear modelling. *Wear*, 1990, **141**, 159-183.

Lee, J-M., Salvati, E. A., Betts, F., DiCarlo, E. F., Doty, S. B. and Bullough, P. G. Size of metallic and polyethylene debris particles in failed cemented total hip replacements. *J. Bone Jt Surg.*, 1992, **74-B**, 3, 380-384.

Little, T., Freeman, M. and Swanson, A. Experiments on friction in the human hip joint. *Lubrication and Wear in Joints*, 1969, Sector, London, 110-114.

Livermore, J., Ilstrup, D. and Morrey, B. Effect of femoral head size on wear of the polyethylene acetabular component. *J. Bone Jt Surg.*, 1990, **72-A**, 518-528.

Mai, M. T., Schmalzried, T. P., Dorey, F. J., Campbell, P. A. and Amstutz, H. C. The contribution of frictional torque to loosening at the cement-bone interface in Tharies hip replacements. *J. Bone Jt Surg.*, 1996, 78-A, 4, 505-511.

Maloney, W. J., Smith, R. L., Schmalzried, T. P., Chiba, J., Huene, D. and Rubash, H. Isolation and characterisation of wear particles generated in patients who have had failure of a hip arthroplasty without cement. *J. Bone Jt Surg.*, 1995, 77-A, 9, 1301-1310.

Margevicius, K. J., Bauer, T. W., McMahon, J. T., Brown, S. A. and Merritt, K. Isolation and characterisation of debris in membranes around total joint prostheses. *J. Bone Jt Surg.*, 1994, 76-A, 1664-1675.

McKellop, H. Wear of artificial joint materials II twelve-channel wear-screening device: correlation of experimental and clinical results. *J. Engng. in Medicine.*, 1981, 10.

McKellop, H. A. and Clark, I. C. Functional behaviour of orthopaedic biomaterials. Volume II: Applications (Eds P. Ducheyne and G. Hastings), 1984, Ch. 3, CRC Press, Boca Raton.

McKellop, H. A., Campbell, P., Park, S-H., Schmalzried, T. P., Grigoris, P., Amstutz, H. C. and Sarmiento, A. The origin of submicron polyethylene wear debris in total hip arthroplasty. *Clin. Orthop. Rel. Res.*, 1995, 311, 3-20.

McKellop, H., Park, S. H., Chiesa, R., Doorn, P., Lu, B., Normand, P., Grigoris, P. and Amstutz, H. In vivo wear of 3 types of metal on metal hip prostheses during 2 decades of use. *Clin. Orthop. Rel. Res.*, 1996, 329S, S128-S140.

Medley, J. B., Chan, F. W., Krygier, J. J. and Bobyn, J. D. Comparison of alloys and designs in a hip simulator study of metal on metal implants. *Clin. Orthop. Rel. Res.*, 1996, 329S, S148-S159.

Medley, J. B., Krygier, J. J., Bobyn, J. D., Chan, F. W., Lippincott, A. and Tanzer, M. Kinematics of the MATCO hip simulator and issues related to the wear testing of metal-metal implants. *Proc. Instn. Mech. Engrs*, 1997, **211**, 89-99.

Müller, M.E. The benefits of metal-on-metal total hip replacements. *Clin. Orthop. Rel. Res.*, 1995, **311**, 54-59.

O'Kelly, J., Unsworth, A., Dowson, D., Jobbins, B. and Wright, V. Pendulum and simulator for studies of friction in hip joints. Evaluation of Artificial Hip Joints. Biological Engineering Society. 1977.

O'Kelly, J., Unsworth, A., Dowson, D., and Wright, V. An experimental study of the friction and lubrication in hip prostheses. *J. Engng. in Medicine.* 1978, **7**.

O'Kelly, J., Unsworth, A., Dowson, D., Hall, D. A. and Wright, V. A study of the role of synovial fluid and its constituents in the friction and lubrication of human hip joints. *J. Engng. in Medicine.* 1979, **8**, 3, 153-159.

Palacios-Carvajal, J., Palacios-Cabezas, J. and Palacios-Cabezas, P. The reason for failures of hip prostheses. *Orthopaedics International Edition*, 1996, **4**, 11-16.

Paul, J. P. Forces transmitted by joints in the human body. *Proc. Instn. Mech. Engrs*, 1966-67, **181**, Part J, 8-15.

Poss, R., Brick, G. W., Wright, R. J., Roberts, D. W. and Sledge, C. B. The effects of modern cementing techniques on the longevity of total hip arthropasty. *Orthopedic Clinics of North America*, 1988, **19**, 3, 591-598.

Rabinowicz, E. Friction and wear of materials. 1965, Wiley, New York.

Revell, P. A., AL-Saffar, N. and Kobayashi, A. Biological reaction to debris in relation to joint prostheses. *Proc. Instn. Mech. Engrs*, 1997, **211**, H2, 187-199.

Reynolds, O. On the theory of lubrication and its application to Mr. Beauchamp Tower's experiments, including an experimental determination of viscosity of olive oil. *Philos. Trans. Roy. Soc. London. Ser. A.*, 1886, **177**, 157-234.

Roberts, B.J., Unsworth, A. and **Main, N.** Modes of lubrication in human hip joints. *Annals of the Rheumatic Diseases*. 1982, **41**, 217-224.

Saikko, V. Wear and friction properties of prosthetic joint materials evaluated on a reciprocating pin-on-flat apparatus. *Wear*, 1993, **166**, 169-178.

Saikko, V. and **Pfaff, H-G.** Low wear and friction in alumina/alumina total hip joints. *Acta. Orthop. Scand.*, 1998, **69** (5), 443-448.

Schmalzried, T. P., Jasty, M. and **Harris, W.H.** Periprosthetic bone loss in total hip arthroplasty. *J. Bone Jt Surg.*, 1992, **74-A**, 849-863.

Schmalzried, T. P., Jasty, M., Rosenberg, A. and **Harris, W. H.** Polyethylene wear debris and tissue reactions in knee as compared to hip replacement prostheses. *Journal of Applied Biomaterials*, 1994, **5**, 185-190.

Schmalzried, T.P., Peters, P.C., Maurer, B.T., Bragdon, C.R. and **Harris, W.H.** Long-duration metal-on-metal total hip arthroplasties with low wear of the articulating surfaces. *J Arthroplasty*, 1996, **11**, 322-331.

Schmalzried, T. P., Dorey, F. J. and **McKellop, H.** The multifactorial nature of polyethylene wear in vivo. *J. Bone Jt Surg.* 1998, **80-A**, 8, 1234-1242.

Schmalzried, T. P. and **Callaghan, J. J.** Current concepts review: wear in total hip and knee replacements. *J. Bone Jt Surg.* 1999, **81-A**, 1, 115-136.

Schmidt, M., Weber, H. and Schön, R. Cobalt chromium molybdenum metal combination for modular hip prostheses. *Clin. Orthop. Rel. Res.*, 1996, **329S**, S35-S47.

Schmidt, M. B. and Farrar, R. Effect of diameter on the wear of metal on metal hips. 1996, 38.

Scott, R. A. and Schroeder, D.W. The effect of radial mismatch on the wear of metal on metal hip prostheses: A hip simulator study. *43rd Annual Meeting, ORS, San Fransisco, California*, February 1997, 764.

Sedel, L., Kerboull, L., Christel, P., Meunier, A. and Witvoet, J. Alumina-on-alumina hip replacement: results and survivorship in young patients. *J. Bone Jt Surg.* 1990, **72-B**, 4, 658-663.

Sedel, L., Nizard, R. S., Kerboull, L. and Witvoet, J. Alumina-alumina hip replacement in patients younger than 50 years old. *Clin. Orthop. Rel. Res.*, 1994, **298**, 175-183.

Semlitsch, M. Technical progress in artificial hip joints. *J. Engng. in Medicine.* 1974, **3**, 4, 10-19.

Semlitsch, M. CoCrMoC metal/metal articulation as a solution to the problem of wear of hip joint replacements. SERC/IMechE Annual Expert Meeting on *Failure of Joint Prostheses*, 28-30 November 1993, 40-45.

Shanbhag, A. S., Jacobs, J. J., Glant, T. T, Gilbert, J. L., Black, J. and Galante, J. O. Composition and morphology of wear debris in failed uncemented total hip replacement. *J. Bone Jt Surg.* 1994, **76-B**, 1, 60-67.

Shanbhag, A. S., Hasselman, C. T. and Rubash, H. E. Inhibition of wear debris mediated osteolysis in a canine total hip arthroplasty model. *Clin. Orthop. Rel. Res.*, 1997, **344**, 33-43.

Simon, S. R., Paul, I. L., Rose, R. M. and **Radin, E. L.** "Stiction-friction" of total hip prostheses and its relationship to loosening. *J. Bone Jt Surg. 57-A*, 1975, **No.2**.

Smallman, R. E. and **Bishop, R.J.** Metals and materials: science, processes, applications. 1995, Butterworth-Heinemann Ltd., Oxford.

Spikes, H. Mechanisms of boundary lubrication. *10th International Colloquium*, 1996a, 1737-1751.

Spikes, H. Mixed lubrication - an overview. *10th International Colloquium*, 1996b, 1713-1735.

Stokoe, S. M. A finger function simulator. PhD Thesis, 1990, University of Durham, 164-170.

Sychterz, C. J., Moon, K. H., Hashimoto, Y., Terefenko, K. M., Anderson, C. and **Bauer, T. W.** Wear of polyethylene cups in total hip arthroplasty. *J. Bone Jt Surg.*, 1996, **78-A**, 8, 1193-1200.

Tabor, D. Fiction - the present state of our understanding. *J. Lubrication. Technol.*, 1981, **103**, 169-179.

Tallian, T. E., Chiu, Y. P., Huttenlocher, D. F., Kamenshine, J. A., Sibley, L. B. and **Sindlinger, N. E.** Lubricant films in rolling contact of rough surfaces. *ASLE Trans.*, 1964, **7**, 109-124.

Tallian, T. E. The theory of partial elastohydrodynamic contacts. *Wear*, 1972, **21**, 49-101.

Tanner, R. I. An alternative mechanism for the lubrication of synovial joints. *Phys. Med. Biol.*, 1966, **11**, 1, 119-127.

Tipper, J. L., Firkins, P. J., Ingham, E., Fisher, J., Stone, M.H., and Farrar, R. Quantitative analysis of the wear debris from low and high carbon content cobalt chrome alloys used in metal on metal total hip replacements. *Journal of Materials Science: Materials in Medicine,* 1999, **10**, 353-362.

Unsworth, A., Dowson, D., and Wright, V. The frictional behaviour of human synovial joints - part I: Natural joints. *Trans. A.S.M.E. J. Lubrication. Technol.,* 1975, July, 369-376.

Unsworth, A., Dowson, D., Wright, V. and Koshal, D. The frictional behaviour of human synovial joints - part II: Artificial joints. *Trans. A.S.M.E. J. Lubrication. Technol.,* 1975, July, 377-382.

Unsworth, A., Dowson, D. and Wright, V. Some new evidence on human joint lubrication. *Ann. Rheum. Dis.,* 1975, **34**, No. 4, 277-285.

Unsworth, A. Friction and lubrication of artificial hip joints. *Ann. Rheum. Dis.* 1976, **35**, 539-541.

Unsworth, A. The effects of lubrication in hip joint prostheses. *Phys. Med. Biol.,* 1978, **23**, 253-268.

Unsworth, A., Pearcy, M. J., White, E. F. T. and White, G. Soft layer lubrication of artificial hip joints. *Proc. Instn. Mech. Engrs,* 1987, 715-724.

Unsworth, A., Pearcy, M. J., White, E. F. T. and White, G. Frictional properties of artificial hip joints. *J. Engng. in Medicine.,* 1988, **17**, 101-104.

Unsworth, A. Tribology of human and artificial joints. *J. Engng. in Medicine.,* 1991, **205**, 163-172.

Unsworth, A., Hall, R. M., Burgess, I. C., Wroblewski, B. M., Streicher, R. M. and Semlitsch, M. Frictional resistance of new and explanted artificial hip joints. International Tribology conference - AUSTRIB December 1994.

Walker, P. S. Friction of internal artificial joints. *J. Engng. in Medicine.*, 1971, **1**. 123-130.

Walker, P.S. and Gold, B. L. The tribology (friction, lubrication and wear) of all-metal artificial hip joints. *Wear*, 1971, **17**, 285-299.

Walker, P.S. and Gold, B. L. Comparison of the bearing performance of normal and artificial human joints. *J. Lubrication. Technol.*, July 1973, 333-339.

Walter, I. A. On the material and the tribology of alumina-alumina couplings for hip joint prostheses. *Clin. Orthop. Rel. Res.*, 1992, **282**. 31-46.

Wang, A., Stark, C. and Dumbleton, J. H. Mechanistic and morphological origins of ultra-high molecular weight polyethylene wear debris in total joint replacement prostheses. *Proc. Instn. Mech. Engrs*, 1996, **210**, 141-155.

Weightman, B. and Light, D. A comparison of RCH 1000 and Hi-Fax 1900 ultra-high molecular weight polyethylene. *Biomaterials,* 1985, **6**, 177-183.

Wells, H. M. and Southcombe, J. E. The theory and practice of lubrication: the germ process. *J. Soc. of Chem. Ind.*, 1920, **39**, 51T-60T.

Willert, H. G. and Semlitsch, M. Reactions of the articular capsule to wear products of artificial joint prostheses. *J. Biomed. Mater. Res.*, 1977, **11**, 157-164.

Winter, M., Griss, P., Scheller, G. and Moser, T. 10 year to 14 year results of a ceramic hip prosthesis. *Clin. Orthop. Rel. Res.*, 1992, **282**. 73-80.

Wroblewski, B. M., McCullagh, P. J. and **Siney, P.D.** Quality of the surface finish of the head of the femoral component and the wear rate of the socket in long-term results of the Charnley low-friction arthroplasty. *Proc. Instn. Mech. Engrs*, 1992, **206**, 181-183.

Wroblewski, B.M. and **Siney, P. D.** Charnley low-friction arthroplasty in the young patient. *Clin. Orthop. Rel. Res.*, 1992, **285**, 45-47.

Wroblewski, B. M. and **Siney, P.D.** Charnley low-friction arthroplasty of the hip - long term results. *Clin. Orthop. Rel. Res.*, 1993, **292**.

Yoon, T. R., Rowe, S. M., Jung, S. T., Seon, K. J. and **Maloney, W. J.** Osteolysis in association with a total hip arthroplasty with ceramic bearing surfaces. *J. Bone Jt Surg.* 1998, **80-A,** 10, 1459-1468.

APPENDICES

Appendix A: Calibration of the Durham Hip Function Simulator

A.1 Load calibration

- Plug the digital load cell into the mains and leave to warm up.

- Position the upper moving frame to the centre of its movement.

- Place the square metal plate in the acetabular carriage.

- Place the load cell in the acetabular carriage on top of the metal plate.

- Bolt the top plate onto the upper moving frame as you would the femoral head holder.

- Check the calibration of the load cell by switching the meter to the up position. The output should read 4378.

- Switch the meter to the down position which should read zero with no load.

- Go through the usual procedure to set up the simulator software.

- From **c:_sim_v60** DOS prompt, type **fs** and then load m48sim20 from the simulator disc. Type **run** to go to the main simulator menu. Choose SETUP.

- Turn on the load and the bearings.

- Tighten up the top plate (if necessary).

- Starting with the load at zero, increase the load (in increments of about 200 N) by using the ↑ and ↓ arrow keys. NB. there is a delay between the request and the response so adjust the load slowly and carefully.

- At each increment press ↵ and type in the true value of load from the output of the load cell. Press ↵ again.

- Once the load reaches (approx.) 2000 N, come down in steps of 200 N until at zero.

- Save the setup information by typing S and then select EXIT from the main simulator menu. **Control+C** will return the screen to the DOS prompt.

- The information that was saved from the setup procedure will have been recorded in a file named setup.dat.   Copy setup.dat to a coded filename such as l181095a.dat, where 'l' represents a load calibration, followed by the date.

- Type **ep** to access easyplot and open the calibration file you have just created by going to ADD and then typing the filename.

- Two curves should be plotted on the same axes, the required load and the measured load. To plot the load calibration go into TOOLS, select DEFINE DATA and type **xpyppyppppppppp**.

- To determine the load calibration coefficients go to TOOLS, select CURVE FIT and choose option 1 and $y = ax + b$. Position the line equation by the appropriate curve. Repeat for the second curve. The upper curve is the ADC calibration and the lower the DAC calibration.

- Label the graph using the same coded name as before, then go to FILE and SAVE as codedfilename.sav.

- Go to FILE, select QUIT and type **y** to exit easyplot.

- Update the calibration coefficients in the calibration files.

A.2 Friction calibration

- Turn the bearings on.

- Fasten the friction calibration bar to the acetabular carriage with two screws.

- Hang the weight holder on the hook and counterbalance with a weight on the opposite end of the bar.

- Go through the usual procedure to set up the simulator software.

- From **c:_sim_v60** DOS prompt, type **fs** and then load m48sim20 from the simulator disc. Type **run** to go to the main simulator menu. Choose SETUP.

- Position the switch on the charge amplifier to RESET and then flick it back to OPERATE.

- Apply weights to the hanging weight holder at increments of 200 g and up to a maximum of 2.6 kg and then back down to zero.

- At each increment press ⏎ and type in the true mass that has been applied. Press ⏎ again.

- In between applying each weight increment, remove all the weight from the holder, position the switch on the charge amplifier to RESET and then again to OPERATE.

- Save the setup information by typing **S** and then select EXIT from the main simulator menu. **Control+C** will return the screen to the DOS prompt.

- The information that was saved from the setup procedure will have been recorded in a file named setup.dat. Copy setup.dat to a coded filename such as f181095a.dat, where 'f' represents a friction calibration, followed by the date.

- Type **ep** to access easyplot and open the calibration file you have just created by going to ADD and then typing the filename.

- The friction calibration should then be plotted by going into TOOLS, selecting DEFINE DATA and then typing **yppppppppxp**. This will produce a graph of friction in grams against ADC units.

- To convert grams to a frictional torque in Nmm, go to EDIT, select XFORM and type **y = y*9.81*0.3168**, where 9.81 is the gravitational constant and 0.3168 is the torque arm from the transducer to the applied load divided by 1000 to give the correct units.

- To determine the friction calibration coefficients go to TOOLS, select CURVE FIT and choose y = ax + b. Position the line equation by the curve.

- Label the graph using the same coded name as before, then go to FILE and SAVE as codedfilename.sav.

- Go to FILE, select QUIT and type **y** to exit easyplot.

- Repeat the above procedure with the calibration bar fitted the other way to calibrate in both tension and compression.

- Update the calibration coefficients in the calibration files.

A.3 Angle calibration

- Position the upper moving frame to the centre of its movement.
- Bolt the top plate onto the upper moving frame as you would the femoral head holder.

- Using the angular spirit level measure the maximum angular extension in each direction i.e. flexion and extension. The maximum angular extension should be 24° and even on both sides.

- Use the adjustable spanner to rotate the head holder to one extreme of motion. Take the reading of the angle and then move the angle by about 5°. Do this over the full range of angles i.e. 24° to -24°.

- At each increment press ⏎ and type in the true angle. Press ⏎ again. Make sure to enter the correct sign with extension towards the back being -ve and towards the front being +ve.

- Save the setup information by typing **S** and then select EXIT from the main simulator menu. **Control+C** will return the screen to the DOS prompt.

- The information that was saved from the setup procedure will have been recorded in a file named setup.dat. Copy setup.dat to a coded filename such as a181095a.dat, where 'a' represents an angle calibration, followed by the date.

- Type **ep** to access easyplot and open the calibration file you have just created by going to ADD and then typing the filename.

- The angle calibration should then be plotted by going into TOOLS, selecting DEFINE DATA and then typing **yppppppppppppppppxpp**.

- To determine the angle calibration coefficients go to TOOLS, select CURVE FIT and type **y = a*sin(b*x+c)+d**. You will be prompted to input suggested values of a, b, c and d so input the values of these found from the previous calibration. Position the line equation by the curve.

- Label the graph using the same coded name as before, then go to FILE and SAVE as codedfilename.sav.

- Go to FILE, select QUIT and type **y** to exit easyplot.

- Update the calibration coefficients in the calibration files.

Appendix B: Velocity vector analysis

B.1 Velocity vector analysis - in phase

Figure B.1: Reciprocating motion of a particle on the pin
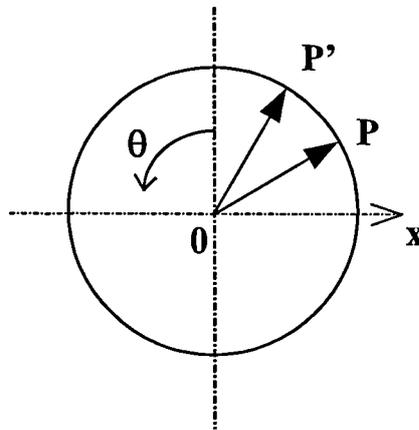
One reciprocating motion: P to P' to P

From simple harmonic motion:

$$v_{rot} = v_o \sin\left(\frac{\pi x}{d}\right)$$

Where v_{rot} is the rotational velocity, v_o is the maximum velocity, x is the horizontal sliding distance, d is the stroke length in the direction of sliding ($d = 25$ mm) and π radians = 180°.

$$\therefore \quad v_{rot} = v_0 \sin(7.2x)$$

Horizontal component, v_{rotH}:

A particle undergoes motion defined by γ. γ is defined with respect to Ox and gives the position of the particle with respect to Ox. Let θ be the starting position (i.e. at angle P_{ox}) and β be the amount of oscillation (0° to 20° to 0°).

$$\gamma = \theta + \beta$$

$\therefore$ $\sin\gamma$ gives the horizontal component.

β is a function of the translational motion and will be at a maximum when $x = 25$ mm.

Need: $\sin\gamma = \sin(\theta + \beta)$

$$\beta = \sin^{-1}(0.34\sin(3.6x))$$

Where 0.34 is a scaling factor to give $\beta = \pm 10°$max. (sin20°).

$$\therefore \quad \gamma = \theta + \sin^{-1}(0.34\sin(3.6x))$$

thus

$$-\sin\gamma = -\sin(\theta + \sin^{-1}(0.34\sin(3.6x)))$$

leading to the horizontal component of the velocity vector, v_{rotH} :

$$v_{rot_H} = -v_0\sin(7.2x)\sin\gamma$$

where v_0 is the maximum velocity for the rotational motion.

Vertical component, v_{rotV}:

$$v_{rot_V} = v_0 \sin(7.2x)\cos\gamma$$

Maximum velocity for rotational vector, v_0:

$$\beta = \beta_0 \sin(\omega t)$$

where β_0 is the maximum displacement ($\beta_0 = \dfrac{10\pi}{180}$), t is the time, 1s and ω is the angular velocity, 6.28 rads^{-1}.

$$\dot{\beta} = \beta_0 \omega \cos(\omega t)$$

$\cos(\omega t)$ is a maximum at 1:

$$\dot{\beta}_0 = 1.096 \text{ rads}^{-1}$$

$$v = \dot{\beta}R$$

$$\therefore \quad v_0 = 1.096R$$

where R is the radius on the pin at which the point is referenced.

Combined motion (sliding plus rotation):

After resolving v_{rot} into both horizontal and vertical components:

$$v_{total_H} = v_{slid} + v_{rot_H}$$

$$v_{total_V} = v_{rot_V}$$

where v_{slid} is the sliding velocity.

Giving the angle of resultant velocity vector:

$$\tan \alpha = \frac{v_{rot_V}}{v_{slid} + v_{rot_H}}$$

where

$$v_{slid} = v_{slid_0} \sin(7.2x)$$

where v_{slid0} is the maximum sliding velocity and is calculated below:

$$x = x_0 \sin(wt)$$

where $x_0 = 12.5$ mm and $\omega = 6.28$ rads^{-1}.

$$\dot{x} = v_{slid} = x_0 \omega \cos(\omega t)$$

Again, $\cos(\omega t)$ is a maximum at 1,

$$\therefore \quad v_{slid0} = 78.5 \text{ mms}^{-1}.$$

Giving Equation 3.8 of this thesis.

B.2 Velocity vector analysis - out of phase

The proof is as for in phase, however v_{rot} now becomes:

$$v_{rot} = v_0 \cos(7.2x)$$

Thus leading to Equation 3.9 of this thesis.

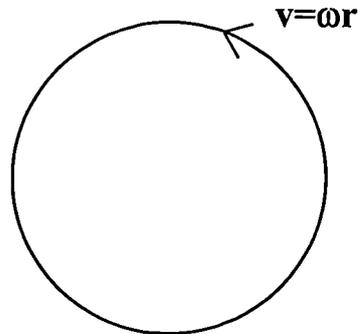## B.3 Velocity vector analysis - full rotation

Figure B.2: Full rotation

$$v_{rot_H} = -\omega_{rot} R \sin(\omega_{rot} t)$$

$$v_{rot_V} = \omega_{rot} R \cos(\omega_{rot} t)$$

$$v_{slid} = 78.5 \sin(\omega_{slid} t)$$

Giving Equation 3.10, of this thesis, where ω_{rot} is the angular rotational velocity, ω_{slid} is the angular sliding velocity and R is the radius at the point of reference.

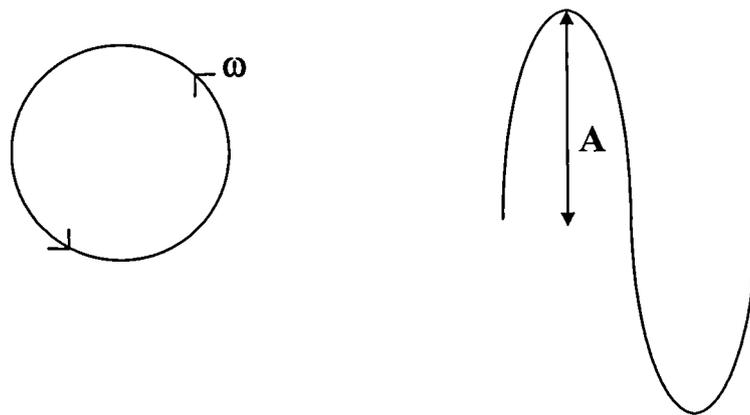# Appendix C: Power calculations for motors providing pin rotation

Figure C.1: Motion of full rotation

$$P = Fv$$

Where P is the power, F is the force and v is the velocity of rotation.

$$F = m_r a + \mu N$$

Where m_r is the mass of the pin and its holder (0.085 kg), a is the acceleration of the pin rotation, μ is the coefficient of friction at the pin/plate interface (0.5) and N is the normal load applied to the pin (250 N).

Due to simple harmonic motion:

$$x = A \sin(\omega t)$$

$$v = A\omega \cos(\omega t)$$

and

$$a = -A\omega^2 \sin(\omega t)$$

where A is the amplitude of motion (0.0025 m), ω is the angular velocity (20 rads^{-1} maximum) and t is the time.

Therefore:

$$F = -m_r A \omega^2 \sin(\omega t) + \mu N$$

and

$$P = -m_r A^2 \omega^3 \sin(\omega t) \cos(\omega t) + \mu N A \omega \cos(\omega t)$$

$$[\sin(\omega t) \cos(\omega t)]_{max} = 0.5$$

and

$$[\cos(\omega t)]_{max} = 1$$

Giving:

$$P_{max} = -\frac{m_r A^2 \omega^3}{2} \pm \mu N A \omega$$

Using the values given in the text we can deduce:

$$P_{max} \le 6.25 \text{ W}$$

Since

$$T = \frac{P}{\omega}$$

where T is the torque required to turn the pin,

$$T \le 0.31 \text{ Nm}$$

Appendix D: Power calculations for motor providing reciprocating motion
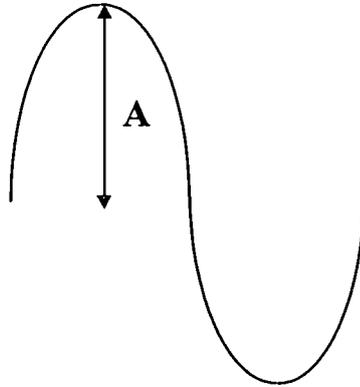
Figure D.1: Motion of motor providing reciprocation

$$P = Fv$$

Where P is the power, F is the force and v is the velocity of rotation.

$$F = m_p a + \mu N$$

Where m_p is the mass of the plate bed (12 kg), a is the acceleration of the plate reciprocation, μ is the coefficient of friction at the pin/plate interface (0.5) and N is the normal load applied to the plate bed (225 N x 4 = 900 N).

Due to simple harmonic motion:

$$x = A\sin(\omega t)$$

$$v = A\omega\cos(\omega t)$$

and

$$a = -A\omega^2 \sin(\omega t)$$

where A is the amplitude of motion (0.025 m), ω is the angular velocity (6.28 rads^{-1}) and t is the time.

Therefore:

$$F = -m_p A\omega^2 \sin(\omega t) + \mu N$$

and

$$P = -m_p A^2 \omega^3 \sin(\omega t) \cos(\omega t) + \mu N A \omega \cos(\omega t)$$

$$[\sin(\omega t)\cos(\omega t)]_{max} = 0.5$$

and

$$[\cos(\omega t)]_{max} = 1$$

Giving:

$$P_{max} = -\frac{m_p A^2 \omega^3}{2} \pm \mu N A \omega$$

Using the values given in the text we can deduce:

$$P_{max} \le 71.57 \text{ W}$$

Since

$$T = \frac{P}{\omega}$$

where T is the torque required to move the plate,

$$T \leq 11.4 \text{ Nm}$$

Appendix E: Deflections of wear machine components

E.1 Deflections of the lever arms
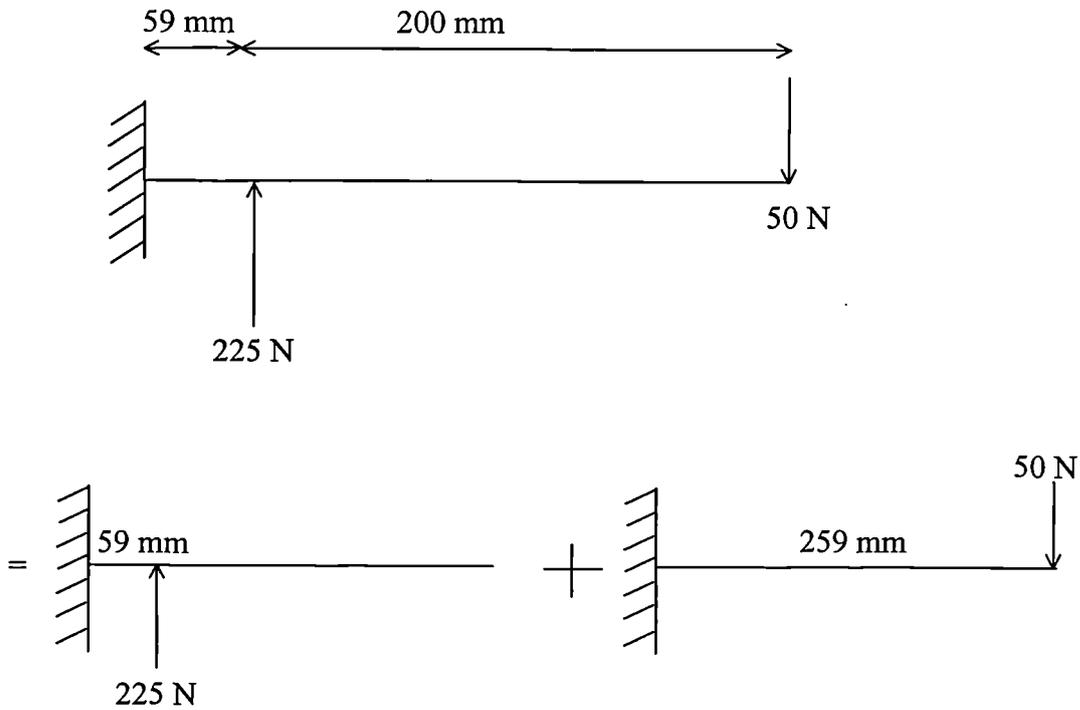
Figure E.1: Deflections of lever arms

$$v = \quad -\frac{WL^3}{3EI} \qquad + \qquad -\frac{WL^3}{3EI}$$

$$v = \quad 0.014 \text{ mm} \qquad + \qquad 0.26 \text{ mm}$$

$$\therefore \qquad v < 0.3 \text{ mm}$$

E.2 Deflections of the fixed hardened steel parallel bars

Figure E.2: Deflections of fixed hardened steel parallel bars

Vertically:

$$R_A + R_B = 260 + 260$$

$$\Rightarrow \quad R_A = 260 \text{ N}$$

$$R_B = 260 \text{ N}$$

Moments about B:

$$R_A L - P_1(L-a) - P_2(L-b) - M_A + M_B = 0$$

$$\Rightarrow \quad -M_A + M_B = 0$$

$$\therefore \quad M_A = M_B$$

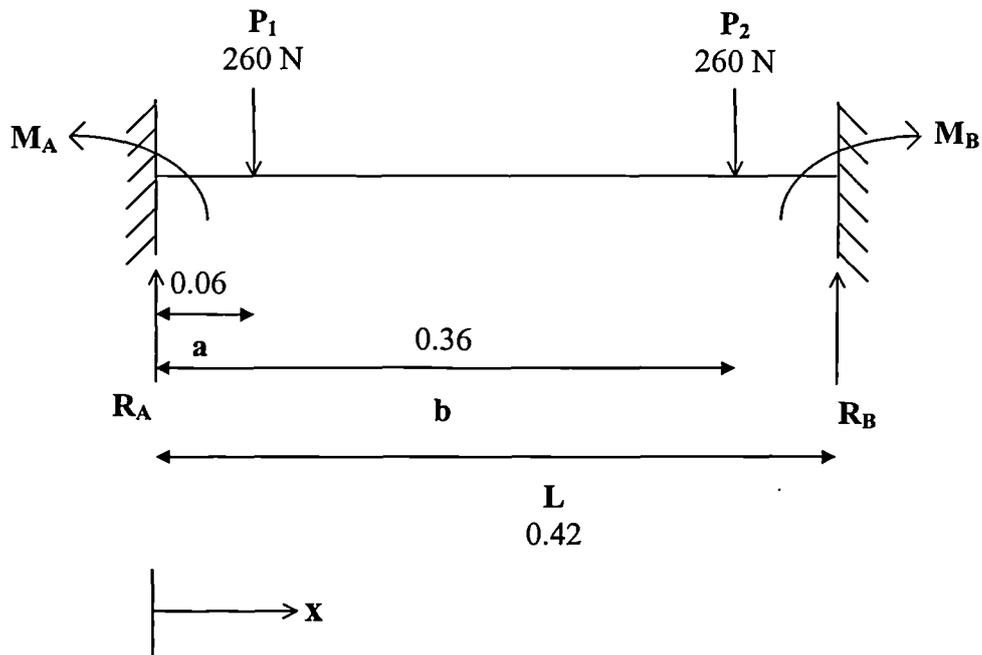$$EI\frac{d^2v}{dx^2} = -R_Ax + P_1(x-a) + P_2(x-b) + M_A$$

Where E is the elastic modulus of the material, I is the second moment of area and v is the deflection.

$$EI\frac{d^2v}{dx^2} = -260x + 260(x-0.06) + 260(x-0.36) + M_A$$

Integrating:

$$EI\frac{dv}{dx} = -130x^2 + 130(x-0.06)^2 + 130(x-0.36)^2 + M_A + C_1$$

$$EIv = -43.3x^3 + 43.3(x-0.06)^3 + 43.3(x-0.36)^3 + M_A\frac{x^2}{2} + C_1x + C_2$$

where C_1 and C_2 are constants of integration.

Boundary conditions:

@ $x = 0$, $v = 0$, $\frac{dv}{dx} = 0$

@ $x = L$, $v = 0$, $\frac{dv}{dx} = 0$

$\Rightarrow$ $C_1 = C_2 = 0$

Substituting:

$$0 = -43.3L^3 + 43.3(L-0.06)^3 + 43.3(L-0.36)^3 + M_A\frac{L^2}{2}$$

$\Rightarrow$ $M_A = 13.37$ Nm

$M_B = 13.37$ Nm

The maximum deflection will be at $x = \dfrac{L}{2}$, i.e. at $x = 0.21$ m. Leading to:

$EIv = -0.10584$ N

where E is 70×10^9 Nm^2 and I is shown below.

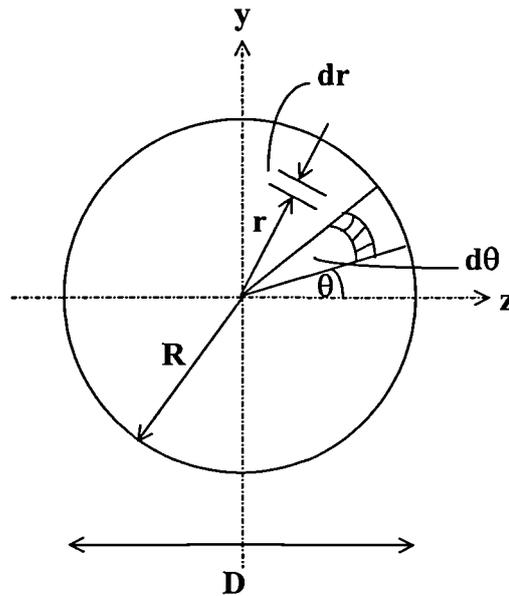Figure E.3: Calculation of second moment of area

$dA = r d\theta dr$

Second moment of element about axis zz:

$(r \sin \theta)^2 r d\theta dr$

Integrate between $0 \leq \theta \geq 2\pi$

$I_z = \int_0^{2\pi} (r \sin \theta)^2 r d\theta dr = \pi r^3 dr$

For a solid circle:

$$I_z = \int_0^R \pi r^3 \, dr$$

$$\therefore \qquad I_z = \frac{\pi R^2}{4} = \frac{\pi D^4}{64}$$

Leading to:

$$v = \frac{-3.08 \times 10^{-11}}{D^4}$$

For $D = 20$ mm, $v = 0.2$ mm.

Therefore $D \geq 20$ mm for minimal bending.

Stresses:

$$\frac{M}{I} = \frac{\sigma}{y}$$

Where M is the bending moment of the beam and σ is the stress.

$M_{max} = 260 \times 0.06 = 15.6$ Nm

$D = 20$ mm

$$y_{max} = \frac{D}{2} = 10 \times 10^{-3} \text{ m}$$

σ_y, the yield stress of the material, is 300 MPa

$$\therefore \qquad \sigma = 20 \text{ MPa}$$

and since $\sigma <<< \sigma_y$ the bars will not yield under the given loads.

Appendix F: Calculation of ratio of heights in a wedge

F.1 Metal-on-metal joints
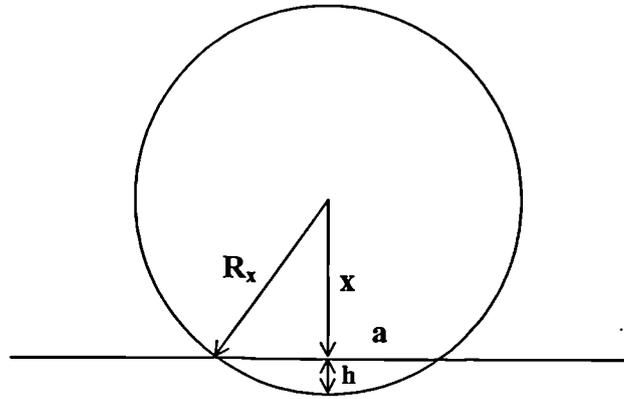
Figure F.1: Calculation of ratio of heights in a wedge

The minimum film thickness, h_0, was calculated for the metal-on-metal joints at each radial clearance using the theory by Hamrock and Dowson (1978) and Equations 2.8, 2.9 and 2.10. Here u was taken as 0.015 ms^{-1}, η as 0.01 Pa s, E' as 2.3 x 10^{11} and L as 2000 N. Further values used for this analysis are given in Table F.1.

From Figure F.1 it is clear to see that:

$$h = R_x - x$$

and

$$x = \left(R_x^2 - a^2 \right)^{0.5}$$

where a is the contact radius and is given by:

$$a = \left(\frac{LR_x}{E'} \right)^{\frac{1}{3}}$$

The inlet film thickness h_i, is determined by the equation below.

$$h_i = h + h_0$$

Resulting in the graph shown in Figure 6.3 for ratio of heights in a wedge versus radial clearance for the metal-on-metal joints.

F.2 Cylindrically ended pin

Using the equations above, with a value of R_x of 0.05 m, u of 0.05 ms^{-1}, η of 0.003 Pa s, E' of 2.3 x 10^{11} and a contact radius, a, of 0.0025 m, the value h_i/h_0 is found to be 23810.52.

Cup radius (mm)	Head radius (mm)	R_x (m)	Clearance (mm)	h_0 (μm)	a (m)	x (mm)	h (m)	h_i (m)	h_0/h_i
13.965	13.949	12.17486	0.016	0.127276	0.004729	12.17486	9.18E-07	1.05E-06	8.215778
13.968	13.919	3.967767	0.049	0.053681	0.003254	3.967766	1.33E-06	1.39E-06	25.86085
13.971	13.941	6.492324	0.03	0.078431	0.003835	6.492323	1.13E-06	1.21E-06	15.43988
13.983	13.945	5.131393	0.038	0.065436	0.003546	5.131392	1.22E-06	1.29E-06	19.71913
13.985	13.978	27.92605	0.007	0.241193	0.006237	27.92605	6.96E-07	9.38E-07	3.88723
13.987	13.978	21.72337	0.009	0.19878	0.005736	21.72336	7.57E-07	9.56E-07	4.809215
14.004	13.991	15.07154	0.013	0.15001	0.005078	15.07153	8.55E-07	1.01E-06	6.701791
14.005	13.983	8.901451	0.022	0.100005	0.00426	8.90145	1.02E-06	1.12E-06	11.19389
14.027	13.965	3.159469	0.062	0.045044	0.003016	3.159467	1.44E-06	1.48E-06	32.96473
14.04	13.957	2.360919	0.083	0.035992	0.002737	2.360917	1.59E-06	1.62E-06	45.08381
14.066	13.926	1.399165	0.14	0.024058	0.002299	1.399163	1.89E-06	1.91E-06	79.51813
14.092	13.986	1.859346	0.106	0.029946	0.002528	1.859345	1.72E-06	1.75E-06	58.37435

Table F.1: Values used in the calculations for Figure 6.2

Appendix G: Calculation of the additional sliding distance due to the rotational motion on the pin
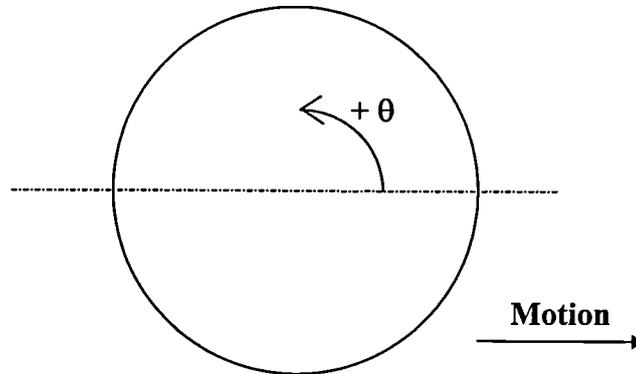

Figure G.1: Relative position of theta0 (θ)

A computer programme was developed to calculate the additional sliding distance on any point of the pin due to the additional rotational motion on the pin. The computer programme is outlined below.

```
#include <stdio.h>
#include <math.h>
#include <graph.h>


struct PT {
        float x,y;
        } ;



struct PT pos(float A,float r,float theta,float theta0,float ratio)
{
struct PT t;
```

```
theta0 *= 3.14159 / 180.0 ;
theta  *= 3.14159 / 180.0 ;


t.x = A*sin(theta) + r*cos(theta*ratio+theta0);
t.y =    0    + r*sin(theta*ratio+theta0);


return t ;
}


void draw( struct PT pt ,float A ,float r , int mode )
{
int x,y;


x = 320 + pt.x*310/(A+r) ;
y = 175 - pt.y*165/(r) ;


if( mode == 0 ) _moveto( x, y ) ;
else _lineto( x, y ) ;


}


FILE *fp ;


main()
{
float A = 0.0125 ;
float r = 0.0025 ;
float r0 = 0.0025 ;
float theta,theta0=-90.0 ;
struct PT pt,ptold ;
int i;
int color ;
float distance,dx,dy;
```

```c
float ratio = 1.05 ;

fp = fopen("results","w");

_setvideomode(_ERESCOLOR) ;

color = 1 ;

theta0 = -90 ;
/* for(theta0 = - 90 ; theta0 < 275 ; theta0 += 45 ) */
for( r = 0 ; r <= 0.00251 ; r += 0.00025 )
        {
        _setcolor(color);
        ptold = pos( A , r , 0 , theta0 , ratio ) ;

        draw( ptold , A ,r0 , 0 ) ;

        distance = 0 ;
        for( theta = 1 ; theta <= 360 ; theta++ )
                {
                pt = pos( A , r , theta , theta0 , ratio ) ;
                draw( pt , A , r0 , 1 ) ;
                dx = pt.x - ptold.x ;
                dy = pt.y - ptold.y ;
                distance += sqrt( dx*dx + dy*dy) ;
                ptold = pt ;
                }

        fprintf(fp,"%7.5f %f\n",r,distance) ;

        color++ ;
        if( color > 7 ) color = 1;
        }
```

```
scanf("%d", &i);
}
```

Where r is the radius on the pin, A is the amplitude of reciprocation and *ratio* is the ratio of the frequency of rotation to the frequency of reciprocation.

It was found that different points on the pin travelled different distances, at starting position theta0 (θ on Figure G.1) equals -90° the maximum distance is travelled and the minimum distance travelled is at a starting angle of 90°. Values of sliding distance per cycle were calculated across the pin radius at both the maximum and minimum sliding distance positions for a frequency ratio of 1.05. These are shown in Table G.1.

r (m)	Maximum sliding distance (m)	Minimum sliding distance (m)
0.00000	0.050000	0.050000
0.00025	0.051111	0.048989
0.00050	0.052292	0.048056
0.00075	0.053524	0.047184
0.00100	0.054796	0.046369
0.00125	0.056101	0.045604
0.00150	0.057435	0.044887
0.00175	0.058795	0.044215
0.00200	0.060176	0.043587
0.00225	0.061576	0.043001
0.00250	0.062993	0.042455

Table G.1: Maximum and minimum sliding distances across the radius of the pin

Taking an average sliding distance across the pin radius and then between the maximum and minimum positions, a difference of 2.1% was found between the true average sliding distance per cycle (0.05105 m) and the reciprocating sliding distance per cycle (0.05 m). Therefore the values used for sliding distance in Chapter 5 are

slightly underestimated values and the true wear factor would be slightly lower than quoted.

List of publications from this work

Scholes, S. C., Hall, R. M., Unsworth, A. and **Scott, R.** The effects of material combination and lubricant on the friction of total hip prostheses. *J. Bone Jt. Surgery,* 1997, 79-B, Supp IV, 464.

Scholes, S. C., Hall, R. M., Unsworth, A. and **Scott, R.** The effect of material combination on the friction of total hip prostheses with varying concentrations of bovine serum. *ISTA '97, San Diego, California,* 1997, 150.

Scholes, S. C., Unsworth, A., Hall, R. M. and **Scott, R.** The effects of material combination and lubricant on the friction of total hip prostheses. *The Institution of Engineers Australia, Austrib '98, Tribology at Work, Brisbane,* 1998, 311-315.

Scholes, S. C. and **Unsworth, A.** Comparison of friction and lubrication of different hip prostheses. *Proc. Instn. Mech. Engrs.,* In Press.

Scholes, S. C., Unsworth, A., Hall, R. M. and **Scott, R.** The effects of material combination and lubricant on the friction of total hip prostheses. *Wear,* In Press.

Unsworth, A., Scholes, S. C., Smith, S. L., Elfick, A. P. D. and **Ash, H. E.** Tribology of replacement hip joints. Accepted for *26th Leeds-Lyon Tribology Symposium,* 1999.